

**From form to flow: reconstructing the life posture and  
hydrodynamics of iconic Ediacaran taxa**

by

©Daniel Pérez-Pinedo

A thesis submitted to the School of  
Graduate Studies in partial fulfilment  
of the requirements for the degree of  
Doctor of Philosophy (manuscript style)

Department of Earth Sciences  
Memorial University of Newfoundland

May 2025

St. John's, Newfoundland

A mis amigos.

Nada es lindo ni arrogante  
en tu porte, ni guerrero,  
nada fiero  
que aderece su talante.

Brotas derecha o torcida  
con esa humildad que cede  
sólo a la ley de la vida,  
que es vivir como se puede.

Antonio Machado

# Abstract

The Ediacaran successions of Newfoundland include some of the oldest macroscopic candidate metazoans. These fossils are preserved as two-dimensional near-census assemblages on deep-marine volcanoclastic sediments beneath tuffites. The communities, dominated by the frondose morphogroups Rangeomorpha and Arboreomorpha, were traditionally interpreted as consisting primarily of erect taxa that had been felled and aligned by paleocurrents, alongside some randomly oriented reclining forms. However, in the absence of sedimentological evidence, paleocurrent direction has been inferred from fossil orientation, despite the unresolved posture of many of these organisms in life.

This PhD focuses on the Melrose Surface near the Catalina Dome of the Discovery UNESCO Global Geopark, which provides sedimentological evidence for current direction in the form of current ripples and cross-lamination. This site offers a unique opportunity to reconstruct the life position and orientation of Ediacaran taxa relative to sedimentologically-determined paleocurrents. An integrative approach has been employed herein, combining different strategies detailed in three papers:

1. Taphonomic reinterpretation of the genus *Charniodiscus*: by examining the taphonomic clues of the type material *C. concentricus*, this taxon was reconstructed as a conical bifoliate erect/recumbent frond, distinguishing it from reclining arboreomorphs such as *C. procerus* (present in the surface), which shows consistently extraordinary stem preservation across stratigraphic units.
2. Clustering algorithms on *Fractofusus misrai* orientations: using novel statistics based on modified polythetic and monothetic clustering techniques adapted to circular variables,

preferential orientation trends oblique to the paleocurrent were identified in the population of *F. misrai* from the Melrose Surface.

3. Computational Fluid Dynamics (CFD) over *Fractofusus misrai*: turbulent flows were modeled to understand the hydrodynamic phenomena associated with highly detailed reconstructions *F. misrai*. The preferential orientations found on the Melrose Surface result from a balance between maximizing aspect ratio for feeding efficiency and reducing current-induced drag.

This work presents an integrative approach based on taphonomy, statistics, and CFD to reconstruct the position of Ediacaran taxa and the currents they lived in. The papers challenge the assumed erect position for all arboreomorphs and the random orientation for reclining rangeomorph taxa. This thesis advocates for interpreting fossils as reclining flat, responding rheotropically to paleocurrents, unless evidence supports otherwise.

## General summary

The Ediacaran rocks of the Bonavista Peninsula in Newfoundland record some of the earliest complex—possibly animal—life forms on Earth, predating the Cambrian explosion by 30 million years. These immobile, soft-bodied marine creatures are preserved in sedimentary rocks, that were once deep-sea floors, by burial under volcanic ash. Traditionally these frond-like Ediacaran organisms have been depicted as part of marine gardens with most living upright in the water column, eventually being felled and aligned by paleocurrents. Only a few were interpreted as having lived flat on the seafloor, unaffected by currents, and thus preserved in random orientations. A lack of physical sedimentological evidence for current directions has led to inferences concerning paleocurrent direction being mainly based on fossil orientations, which relies on the questionable assumption of erect body postures for almost all taxa.

This study focuses on the newly described Melrose Surface of the Catalina Dome on the Bonavista Peninsula. This site is important because paleocurrent directions are evidenced by sedimentological features, eliminating the need to resort to fossil orientation. We propose different approaches to reconstruct the life positions of Ediacaran organisms and their associated marine currents: firstly, fossil preservation was investigated to determine whether organisms were erect or reclining; secondly, statistical methods were applied to identify orientation trends in reclining organisms previously thought to be randomly oriented; and lastly, computational simulations were employed to recreate the marine currents in which these organisms lived.

The findings of this study, based on the way the fossils are preserved, challenge traditional interpretations, by showing that some fossils that were previously believed to have lived erect in the water column are more likely to have reclined on the seafloor. Additionally, contrary to previous work, preferred orientations of the reclining organisms were documented, suggesting they

grew in specific orientations responding to marine currents. These orientations are likely a result of trying to optimize nutrient access while maintaining their physical stability. We propose that Ediacaran organisms should be interpreted as having lived reclined flat on the seafloor, in the manner that they were preserved, unless there is evidence to the contrary.

## Coauthorship and copyright statement

I declare that the thesis herein presented is substantially my own work except where otherwise indicated. This study contains three chapters, ch.2-4, that have been published in international peer-reviewed scientific journals. Therefore, these chapters are presented as published papers in which Daniel Pérez-Pinedo is the main author. Several colleagues have contributed considerably and have therefore been granted co-authorships. The detailed information about each author contribution is detailed herein:

Chapter 2: Conceptualization, D.P-P., and D.M; methodology, D.P-P., and D.M; investigation, DP.-P., C.M., R.T., R.N., and D.M; figures, D.P-P., and C.M; project administration, D.P-P., and D.M; writing, D.P-P., with editorial input by C.M., R.T., R.N., and D.M; funding acquisition, D.M.

Chapter 3: Conceptualization, D.P-P., J.N., and D.M; methodology, D.P-P; formal analysis, D.P-P; software, D.P-P; investigation, DP.-P., and D.M; figures: D.P-P., G.P., C.M; validation, D.P-P; data curation, D.P-P., G.P., and J.M; project administration, D.P-P., and D.M; writing, D.P-P. with editorial input by J.N., G.P., C.M., R.T., and D.M; funding acquisition, D.M.

Chapter 4: Conceptualization, D.P-P., R.N., J.N., and D.M; methodology, D.P-P and R.N; formal analysis, D.P-P; software D.P-P., investigation, D.P-P., J.N., and D.M; figures: D.P-P., and R.N; software, D.P.-P; validation, D.P-P; project administration, D.P.-P., and D.M., writing, D.P.-P. with editorial input by J.N., and D.M; funding acquisition, D.M.

Intellectual contributions to the thesis by coauthors and colleagues considerably enhanced the study, complementing the primary work of the first author. Editorial contributions were aimed to improve readability and conciseness of the thesis. The project was supported by a Discovery

Grant #RGPIN-2018-04880 from the Natural Sciences and Engineering Research Council of  
Canada to D.M.

## Acknowledgements

I extend my heartfelt gratitude to my supervisors, Dr. Duncan McIlroy and Dr. Rod Taylor, for their unwavering trust and support. Their humane and respectful treatment has made me feel valued and considered throughout this journey. They have provided me with a sense of security and taught me to confidently stand by my work. Above all, I am deeply thankful for their companionship, knowing I always had someone to listen and assist me when needed. I would also like to express my appreciation to Suzanne Dufour, and her role as an examiner, Hilary Corlett, Bruce Colbourne, Edith and Nev Samson, and my @MUNPaleobiology colleagues for their dedication and willingness to support me in various aspects of my PhD journey.

A mis abuelos, Miguel y Julia, y a los poetas de España, que hicimos nuestros y trajeron la pasión a mi vida.

A mis padres, Pedro y Maite, que me educaron en libertad y justicia y me enseñaron el mundo.

A mi mujer, Jenna, que me sostiene con sencillez y alimenta mis ganas de vivir.

# Table of contents

<b>Abstract</b> .....	iii
<b>General summary</b> .....	v
<b>Co-authorship and copyright statement</b> .....	vii
<b>Acknowledgments</b> .....	ix
<b>Table of contents</b> .....	x
<b>List of figures</b> .....	xiv
<b>List of tables</b> .....	xxii
<b>List of appendices</b> .....	xxiii
<b>Chapter 1 – Introduction</b> .....	1
1.1 The Ediacaran Biota .....	1
1.2 The Avalon Assemblage.....	4
1.2.1 Geological context of the Avalon Assemblage in Newfoundland.....	4
1.2.2 The Rangeomorpha and the Arboreomorpha.....	8
1.3 Avalonian paleoecology.....	10
1.3.1 Community structure.....	11
1.3.2 Feeding strategies.....	12
1.4 Palaeocurrents and body posture.....	14
1.4.1 Felling of erect fronds.....	14
1.4.2 <i>Fractofusus</i> as a randomly oriented recliner.....	17
1.5 Thesis objectives and integrative methodology.....	19
1.6 Thesis structure and summary.....	20
1.7 References.....	23

**Chapter 2 - *Charniodiscus* and *Arborea* are separate genera within the Arboreomorpha:**

**using the holotype of *C. concentricus* to resolve a taphonomic/taxonomic tangle.....41**

Abstract.....43

2.1 Introduction.....44

    2.1.1 Preservation in the Avalon Assemblage.....47

    2.1.2 Previous taphonomic/morphological consideration of the *Charniodiscus concentricus* holotype.....50

    2.1.3 Historical reasoning for a multifoliate *Charniodiscus concentricus*.....52

2.2 A new taphonomic understanding of the *Charniodiscus concentricus* holotype.....53

2.3 Evidence for *Charniodiscus* being a collapsed sub-conical structure.....56

2.4 Systematic paleontology.....57

2.5 Mode of life of *Charniodiscus concentricus*.....62

2.6 Paleobiological model of *Charniodiscus*.....65

    2.6.1 Taxonomic consideration of other *Charniodiscus* species.....67

2.7 Conclusion.....69

2.8 Data availability and statement.....71

2.9 Author contribution.....71

2.10 Funding.....71

2.11 Acknowledgements.....71

2.12 References.....72

**Chapter 3 - Frond orientations with independent current indicators demonstrate the**

**reclining rheotropic mode of life of several Ediacaran rangeomorph taxa.....81**

Abstract.....83

3.1 Introduction.....	84
3.1.1 Geologic setting.....	87
3.1.2 Historical paleobiological interpretation.....	90
3.1.3 Surface Assemblage.....	90
3.2 Materials and methods.....	93
3.2.1 Quantitative variables.....	95
3.2.2 Circular variables.....	97
3.3 Results.....	104
3.4 Discussion.....	109
3.5 Conclusion.....	117
3.6 Acknowledgements.....	119
3.7 Declaration of competing interest.....	119
3.8 Data availability statement.....	120
3.9 References.....	120

**Chapter 4 - Hydrodynamic insights into the paleobiology of the Ediacaran rangeomorph**

<b><i>Fractofusus misrai</i></b> .....	134
Abstract.....	135
4.1 Introduction.....	136
4.2 Results.....	141
4.2.1 Meshing parameters of the computational domain and the <i>F. misrai</i> <i>geometry</i> .....	141
4.2.2 Velocity field and flow recirculation patterns.....	141
4.2.3 Drag force.....	144

4.3 Discussion.....	144
4.3.1 Feeding strategies.....	147
4.3.2 Orientation and drag.....	152
4.3.3 Ecological role and paleobiology.....	155
4.4 Conclusion.....	156
4.5 Limitations of the study.....	158
4.6 Star Methods.....	158
4.6.1 Key resources table.....	158
4.6.2 Resource availability.....	158
4.6.3 Method details.....	159
4.6.4 Quantification and statistical analysis.....	164
4.7 Supplemental information.....	164
4.8 Acknowledgements.....	164
4.9 Author contribution.....	165
4.10 Declaration of interest.....	165
4.11 References.....	165
<b>Chapter 5 – Conclusion.....</b>	<b>176</b>
<b>Appendix A – Supplementary material from Chapter 3.....</b>	<b>179</b>
<b>Appendix B – Supplementary material from Chapter 4.....</b>	<b>264</b>

# List of figures

## Chapter 1

**Fig. 1.1:** Fossil plate of iconic Ediacaran rangeomorphs and arboreomorphs. A) *Charnia* sp. (MUN Surface, Catalina Dome in the Bonavista Peninsula). B) Opposing *Charnia* sp. (Catalina area, Bonavista Peninsula). C) *Pectinifrons abyssalis* (Mistaken Point Formation at Mistaken Point Ecological Reserve). D) *Fractofusus misrai* (E Surface, Mistaken Point Ecological Reserve). E) *Charniodiscus spinosus* (E Surface, Mistaken Point Ecological Reserve). D) *Charniodiscus procerus* (E Surface, Mistaken Point Ecological Reserve). *Fr*: *Fractofusus*. *Br*: *Bradgatia*. All scale bars 1 cm but C 5cm.....3

**Fig. 1.2:** General preservation model. A) Living benthic community consisting of an indeterminate reclining frond, *Fractofusus misrai*, and an indeterminate erect frond. B) Burial of community and sealing of the new sediment by new colonization of microbial matground (green). Decay of *F. misrai* and erosion of the frondose section of the indeterminate erect frond. C) Decay of the microbial mat forming a pyritic veneer in the sole of the burying bed (yellow). Resistant tissues from the indeterminate recliner leave a positive relief with underlying sediments moving up casting the top surface of the organism. Gravitational movement from the overlying sediments to cast the void left by the ventral impressions of *F. misrai* and the holdfast of the indeterminate erect frond producing a negative epirelief of the bottom surface. Figure modified from and inspired by Kenchington (2015), MacGabhann et al. (2019), and @paleobiome.....7

**Fig. 1.3:** Branching architecture of Ediacaran fronds. Rangeomorphs including Rangida (A, B), typified by *Rangia* and *Avalofractus*, and Charnida (C, D, E), illustrated by *Beothukis*, *Trepassia*, and *Charnia*. F) Arboreomorphs exemplified by *Arborea arborea*. DU: Displayed and unfurled. DF: Displayed and furled. RF: Rotated and furled. D: Dorsal. V: Ventral. Figure modified from

and inspired by Narbonne et al. (2009); Brasier et al. (2012), and Dunn et al. (2019).....10

**Fig. 1.4:** Submarine hydrodynamic processes thought to be relevant in the preservation of the Ediacaran organisms of the Avalon Assemblage. A) Conceptual diagram showing a downslope turbidity current (dark blue), and orthogonally-directed contour currents parallel to the slope (light blue). B) Frondose organisms in a recumbent position by the action of contour currents and pelagic deposition of ash. C) Tuffaceous turbidity current felling and preserving Ediacaran fronds. Figure modified from and inspired by Fonesu et al. (2020); Vixseboxse et al. (2021), and A. Reimann.....17

## Chapter 2

**Fig. 2.1:** Map of some of the most relevant Avalonian fossil assemblages (black circles). A) General map of Newfoundland, Atlantic Canada. B) Detail of the Avalon and Bonavista Peninsulas. C) General map of the United Kingdom. D) Detail of England.....45

**Fig. 2.2:** Casts of relevant *Charniodiscus* species. A) *C. concentricus* holotype (LEIUG 2383) from Charnwood Forest, UK. B,C) *C. procerus* and *C. spinosus* respectively from the upper part of the Mistaken Point Formation (E Surface) at Mistaken Point, Newfoundland. Jesmonite cast of field specimens. D,E) *C. longus* cast (SAM P13777) and *C. arboreus* (*Arborea*) cast (OUMNH AW.00043/p) respectively from Ediacara, South Australia. Scale bars 3 cm. Not retrodeformed.....46

**Fig. 2.3:** Preservation of the holotype of *C. concentricus* (LEIUG 2383) from Charnwood Forest, UK. A) Differential branch folding; underfolded (orange), overfolded (yellow), outfolded (blue and purple) and infolded (green). B) Interpretive drawing of the fossil showing features preserved

in different bedding planes; main bedding plane (yellow), above bedding plane (brown), and non-fossiliferous sediment (dotted brown pattern). Scale bar 3 cm. Not retrodeformed.....49

**Fig. 2.4:** Preservation style observed in Ediacaran organisms in Avalonia. A) Felling of an undetermined erect stemmed frond. B) Transversal cut of the felled frond preserved between the underlying volcanoclastic siltstone and the overlying tuffite; close-up shows features preserved in positive and negative reliefs and smothered matground. C) Resulting reliefs in the underlying volcanoclastic siltstone and their counterparts in the tuffaceous layer.....52

**Fig. 2.5:** Taphonomic stop-motion model of the holotype of *C. concentricus* showing different branch folding. A–C) Underfolding of proximal-most branches. A–I) Infolding of distal-most branches. D–I) Outfolding of bottom-right and central branches. F–I) Overfolding of bottom-left branches.....55

**Fig. 2.6:** *Charniodiscus procerus* from the so-called “Seilacher’s Corner”, upper part of the Mistaken Point Formation (E Surface) at Mistaken Point, Newfoundland. A) Cast. B) Basal disc, stem and flat basal section of the branches meeting the central axis at ~90° in orange; apical section of the branches showing pronounced curvature in red. Scale bars 3 cm. Jesmonite cast of field specimen. Not retrodeformed.....60

**Fig. 2.7:** *Charniodiscus* sp. from the Mistaken Point Formation (D Surface) at Mistaken Point, Newfoundland. A) Field photography of the specimen. B) Stem and flat basal section of the branches meeting the central axis at ~90° in orange; apical section of the branches showing pronounced curvature in red. Scale bars 3 cm. Field photography. Not retrodeformed.....61

**Fig. 2.8:** *Charniodiscus* sp. from Spaniard’s bay, Newfoundland. A) Overlying siltstone. B) Collapsed sub-conical frond preserved in sandstone. C) Cross section view. D) Underlying siltstone. Scale bar 1 cm. Field photography. Not retrodeformed.....65

### Chapter 3

**Fig. 3.1:** Ediacaran fossils from the Melrose Surface. A) *Fractofusus misrai*. B) *Pectinifrons abyssalis*. C) *Bradgatia* sp.. D) *Primocandelabrum* sp.. E) *Charniodiscus* sp. Scale bars, A, C–E 1 cm, B 3 cm.....86

**Fig. 3.2:** Location of the Melrose Surface in the Fermeuse Formation at Melrose, on the southern portion of the Catalina Dome, in the Discovery UNESCO Global Geopark. A) General map of Newfoundland, Atlantic Canada. Scale bar, 200 km. B) Detail of the Avalon and Bonavista Peninsulas. C) Geologic map of Catalina area and stratigraphic column.....87

**Fig. 3.3:** Climbing current ripples and corresponding cross-lamination used as physical sedimentological evidence to infer paleocurrent direction at the Melrose Surface. Paleocurrent direction: 102° SE. Note wavy bedding partly coincident with the cleavage.....89

**Fig. 3.4:** Sedimentary log through interbedded siltstones and thin ripple cross-laminated sandstones, including the fossiliferous Melrose Surface, on the southern portion of the Catalina Dome in the Discovery UNESCO Global Geopark. I) Slumped silty sandstones with weakly erosive base. II) Upward-thinning and upward-fining succession with ripple cross-laminated sandstones. III) Thinning and fining. Upward-fining siltstone and thin sandstone beds with wavy bedding. IV) Siltstone with thin sandstones and two black siltstones; some ripple cross- lamination. Vfs, very fine sand; fs, fine sand; ms, medium sand; cs, coarse sand.....94

**Fig. 3.5:** Composite figure showing: A) logarithmic transformation of size-frequency distributions of *Fractofusus misrai* with Gaussian curve overlapping for illustrative purposes; B) Bayesian information criterion (BIC) results for univariate data (width and length measured in centimeters) (E and V for equal and unequal variance, respectively); C), BIC results for bivariate data. Model parameterizations: EII, spherical, equal volume; VII, spherical, unequal volume; EEI, diagonal,

equal volume, and shape; VEI, diagonal, varying volume, equal shape; EVI, diagonal, equal volume, varying shape; VVI, diagonal, varying volume and shape; EEE, ellipsoidal, equal volume, shape, and orientation; EEV, ellipsoidal, equal volume and shape; VEV, ellipsoidal, equal shape; VVV, ellipsoidal, varying volume, shape, and orientation. Biologically realistic models assume ellipsoidal distributions (see Fraley and Raftery [2007] and Darroch et al. [2013] for more information).....96

**Fig. 3.6:** Preliminary exploration of *Fractofusus misrai* orientation. A) Bayesian information criterion (BIC) results for orientation under 180° and corresponding rose plot with angular histogram. B) BIC results for orientation over 180° and corresponding rose plot with angular histogram. E and V for equal and unequal variance, respectively.....99

**Fig. 3.7:** Circular statistical analysis of *Fractofusus misrai* under 180°. A) Modified parallel coordinate plot (PCP) with corresponding medoids reflecting the two-cluster solution with proposed Gower’s distance and Ward’s method. B) G1 values of Caliński-Harabasz pseudo F-statistic. In red (circle) the selected two-cluster solution. C) Dendrogram of cluster solution, green dashed line (top) for the selected two-cluster solution and red dashed line (bottom) for a potential three-cluster solution.....102

**Fig. 3.8:** Circular statistical analysis of *Fractofusus misrai* over 180°. A) Modified parallel coordinate plot (PCP) with corresponding medoids reflecting the two-cluster solution with proposed Gower’s distance and Ward’s method. B) G1 values of Caliński-Harabasz pseudo F-statistic. In red (circle) the selected two-cluster solution. C) Dendrogram of cluster solution, green dashed line (top) for the selected two-cluster solution and red dashed line (bottom) for a potential three-cluster solution.....103

**Fig. 3.9:** Monothetic clustering on orientation of *Fractofusus misrai*. A) M-fold cross-validation results under 180° made by 10-fold cross-validation (CV). B) Splitting rules tree with *p*-values under 180°. C) M-fold cross-validation results over 180° made by 10-fold CV. D) Splitting rules tree with *p*-values over 180°. A, C) Multi-cluster solutions below the red dashed line.....107

**Fig. 3.10:** Orientation from the specimens excluded from the statistical analysis. A) *Bradgatia* sp. from adjacent slab but part of the Melrose Surface. B) *Bradgatia* sp. from the gridded area. C) Total *Bradgatia* sp.. D) *Pectinifrons abyssalis*. Where not indicated, one specimen is present.....108

**Figure 3.11:** Specimens of *Bradgatia* sp. (*Br* in the image) facing opposite directions from a fossiliferous surface in the town of Melrose. Scale bar, 3 cm.....117

## Chapter 4

**Fig. 4.1:** Location of the Capelin Gulch site, also known as Melrose Surface in the Fermeuse Formation at Melrose, on the southern portion of the Catalina Dome, in the Discovery UNESCO Global Geopark. A) General map of Newfoundland, Atlantic Canada. B) Detail of the Avalon and Bonavista Peninsulas. C) Geologic map of Catalina area and stratigraphic column.....139

**Fig. 4.2:** Taphonomic variability of *Fractofusus misrai* exemplified by specimens from the E Surface at Mistaken Point, NL. A) *F. misrai* partially rotated by the current to produce a kink in the axis. B) Specimen (yellow) with a branch that has been lifted by the current leaving a triangular gap in the row of rangeomorph branches. C) Tightly packed branches in a specimen showing a combination of rangeomorph branches rotated through 90° to show only one row of secondary-order branches (yellow) and unrotated branches with the tips curled away from the bedding plane to produce straight lateral margins (blue). D) Largely undisturbed *F. misrai* with displayed tips to

the primary-order branches. E) Straight margined specimen inferred to have been created by the lifting of the tips of the primary-order branches by a current meaning that they were not in contact with the seafloor at the time of casting. Scale bars 1 cm.....140

**Fig. 4.3:** Digital three-dimensional reconstruction of *Fractofusus misrai* and computational domain. A–D) Different perspectives of the *F. misrai* geometry. A) Top view. B) Bottom view. C) Front view, and D) lateral view. E) *F. misrai* tetrahedral mesh and detail view (zoomed in). F) Flow volume region mesh and boundary conditions: I) slip boundary condition, II) velocity inlet, III) pressure outlet, and IV) no-slip boundary condition. Scale bars 2 cm except C 1 cm, and F 50 cm. See Figures 4.S1 and 4.S2.....143

**Fig. 4.4:** CFD simulations of large *Fractofusus misrai* in different orientations relative to the simulated flow from (left to right). A–R) Two-dimensional horizontal and cross-sectional surface plots of streamlines and different  $U_x$  regimes: first column (A, D, G, J, M, and P) simulated flow of 0.05 m/s; second column (B, E, H, K, N, and Q) flows of 0.1 m/s; and third column (C, F, I, L, O, and R) 0.2 m/s. S and T) Detailed cross-sectional view of flow retention patterns and eddying of current-parallel (SI-SII) and current-perpendicular *Fractofusus misrai* (TI-TIV) in 0.1 m/s flow. Both orientations show the eddying at the frond margin (SI-SII; TI, TIV). Current-perpendicular *F. misrai* also shows weak vortices on the upper surface of the frond both upcurrent of the axis of the frond (TII), and also in the lee of the axis (TIII). Velocity ranges from 0 to 0.05, 0.1, or 0.2 m/s as indicated in this caption. Scale bars top view 5 cm, cross-sectional view 10 cm except S, and T 2 cm. See Figures 4.S3–4.S5, 4.S7, and 4.S8.....145

**Fig. 4.5:** Detailed top view of flow patterns over the same rangeomorph elements of *Fractofusus misrai* (Re 1 and Re 2) in different orientations relative to the current. Streamlines vary in their paths between current-parallel and current-oblique/perpendicular orientations but are routed by the

surface morphology in all cases. Flow velocity is colored along the streamlines according to velocity (red fastest, blue slowest): (A–D) current-parallel (0°), (E–H) current-oblique (52°), and (I–L) current-perpendicular (90°). A, E, and I are all the case of a small *F. misrai* under 0.05 m/s flow in different orientations; B, F, and J are all small *F. misrai* experiencing a 0.1 m/s flow in different orientations. C, G, and K show the case of large *F. misrai* in a 0.05 m/s flow in different orientations; D, H, and L show the effects of a large *F. misrai* experiencing a 0.1 m/s flow in different orientations. Current flow from left to right. Velocity ranges from 0 to 0.05, or 0.1 m/s as indicated in this caption. Scale bars 0.1 cm for small and 1 cm for large *F. misrai*. See Figure 4.S6.....146

**Fig. 4.6:** Drag forces of *Fractofusus misrai* models in CFD simulations. A–D) Spatial visualization of drag force in *Fractofusus*. A) Parallel (0°). B) Oblique (35°). C) Oblique (52°). D) Perpendicular (90°). Arrows indicate the paleocurrent direction. Scale bars 2 cm. Progressively warmer colors represent increasing drag. See to Table 4.S1.....151

# List of tables

## Chapter 3

<b>Table 3.1:</b> Results from uniformity and von Mises distribution tests on orientation of <i>Fractofusus misrai</i> from the Melrose Surface.....	99
<b>Table 3.2:</b> Medoids and corresponding values in the multivariate matrix for <i>Fractofusus misrai</i> from the Melrose Surface under 180°.....	103
<b>Table 3.3:</b> Medoids and corresponding values in the multivariate matrix for <i>Fractofusus misrai</i> from the Melrose Surface over 180°.....	103
<b>Table 3.4:</b> Morphometric traits and orientation from specimens excluded from the statistical analysis.....	109

# List of appendices

## Appendix A – Supplementary material from Chapter 3

**Table 3.S1:** “Melrosefracto.csv” dataset: a general dataset of *Fractofusus* specimens where morphometric traits, orientation under and over 180°, specimen ID number, and quadrat are recorded.....179

**Table 3.S2:** "Correlation.csv" dataset: consists of all the recorded orientations both under and over 180° merged together and the corresponding values of the morphometric traits.....180

**Table 3.S3:** "Correlationunder180.csv" dataset: shows data from the general dataset "Melrosefracto.csv" filtered according to the under 180° group.....184

**Table 3.S4:** "Correlationover180.csv" dataset: shows data from the general dataset "Melrosefracto.csv" filtered according to the over 180° group.....185

**Table 3.S5:** "Orientationtotal.csv" dataset: solely contains all the recorded orientations in one variable.....187

**R script:** Includes: 1) Morphometric quantitative size-frequency distributions analysis, 2) uniformity analysis and visualization of the circular variable, and 3) correlation and cluster analysis of circular and linear variables.....190

## Appendix B – Supplementary material from Chapter 4

**Figure 4.S1:** Discretization and sensitivity tests for different meshing parameters for the computational domain (A-C) and the *Fractofusus misrai* geometry (D-F), related to Figure 3. A) Coarse FVR mesh. B) Medium FVR mesh. C) Fine FVR mesh. D) 100k polygon mesh. E) 300k polygon mesh. F) 500k polygon mesh. I) Slip-boundary condition. II) Velocity inlet. III) Pressure outlet. IV) No-slip boundary condition. Scale bars A-C 50 cm, and D-F 1 cm.....264

**Figure 4.S2:** Computational domain for CFD simulations, related to Figure 3. A) Entire flow volume region. B) General view of *Fractofusus misrai*. C) Cartesian box as region refinement. D) Detail of primary branches of *Fractofusus misrai*. Scale bars A 30 cm, B 2 cm, C 15 cm, and D 1 cm.....265

**Figure 4.S3:** CFD results of large *Fractofusus misrai* under  $U_x = 0.2$  m/s with different mesh discretization and cartesian box refinements, related to Figure 4. A). Coarse FVR mesh with no refinement. B) Coarse FVR mesh with refinement. C) Medium FVR mesh with no refinement. D) Medium FVR mesh with refinement. E) Fine FVR mesh with no refinement. F) Fine FVR mesh with refinement. G-L) Two-dimensional horizontal and cross-sectional surface plots of streamlines and  $U_x$ . G,I,K) Perpendicular 300k polygon geometry, and (H,J,L) perpendicular 500k polygon geometry. Current flow from left to right. Velocity ranges from 0 to 0.2 m/s. Scale bars A-F 30 cm, G-H, K-L 5 cm, I-J 1 cm.....266

**Figure 4.S4:** CFD simulations of small *Fractofusus misrai* in different orientations relative to the simulated flow from (left to right), related to Figure 4. A-R) Two-dimensional horizontal and cross-sectional surface plots of streamlines and different  $U_x$  regimes: first column (A,D,G,J M, and P) simulated flow of 0.05 m/s; second column (B,E,H,K,N, and Q) flows of 0.1 m/s; and third column (C,F,I,L,O, and R) 0.2 m/s. S-T) Detailed cross-sectional view of flow retention patterns and eddying of current-parallel (SI-SII) and current-perpendicular *Fractofusus misrai* (TI-TIV) in 0.1 m/s flow. Both orientations show the eddying at the frond margin (SI-SII; TI, TIV). Current perpendicular *F. misrai* also shows weak vortices on the upper surface of the frond both upcurrent of the axis of the frond (TII), and also in the lee of the axis (TIII). Velocity ranges from 0 to 0.05, 0.1, or 0.2 m/s as indicated in this caption. Scale bars top view 1 cm, side view 10 cm except S 0.5 cm, and T 0.1 cm.....268

**Figure 4.S5:** CFD simulations of medium *Fractofusus misrai* in different orientations relative to the simulated flow from (left to right), related to Figure 4. First column (A,D,G,J M, and P) simulated flow of 0.05 m/s; second column (B,E,H,K,N, and Q) flows of 0.1 m/s; and third column (C,F,I,L,O, and R) 0.2 m/ s. S-T) Detailed cross-sectional view of flow retention patterns and eddying of current-parallel (SI-SII) and current-perpendicular *Fractofusus misrai* (TI-TIV) in 0.1 m/s flow. Both orientations show the eddying at the frond margin (SI-SII; TI, TIV). Current perpendicular *F. misrai* also shows weak vortices on the upper surface of the frond both upcurrent of the axis of the frond (TII), and also in the lee of the axis (TIII). Velocity ranges from 0 to 0.05, 0.1, or 0.2 m/s as indicated in this caption. Scale bars top view 5 cm, cross-sectional view 10 cm except S 2 cm, and T 0.5 cm.....270

**Figure 4.S6:** General view of streamlines coloured according to  $U_x$  around different orientations of *Fractofusus misrai*, related to Figure 5. A) Perpendicular ( $90^\circ$ ), B) oblique ( $52^\circ$ ), and C) parallel ( $0^\circ$ ). Arrows indicate paleocurrent direction. Velocity ranges from 0 to 0.1 m/s. Scale bars 5 cm.....271

**Figure 4.S7:** CFD simulations of null models, related to Figure 4. A-H) Two-dimensional horizontal and cross-sectional surface plots of streamlines and  $U_x$ . G-H) Detailed cross-sectional view of flow patterns of parallel (GI-GII) and perpendicular (HI-HIII) null models under 0.1 m/s flow. Velocity ranges from 0 to 0.1 m/s. Current flow from left to right. Scale bars 5 cm.....272

**Figure 4.S8:** Velocity profile ( $U_x$ ) along vertical axis ( $z$ ) from the bottom boundary of the fluid domain around *Fractofusus misrai*, related to Figure 4.....273

**Table 4.S1:** CFD simulations numeric results, related to Figure 6.....274

# CHAPTER 1 - Introduction

*The periods which to our narrow apprehension, and compared with our ephemeral existence, appear of incalculable duration, are in all probability but trifles in the calendar of nature. It is Geology that, above all other sciences, makes us acquainted with this important, though humiliating fact. Every step we take in its pursuit forces us to make almost unlimited drafts upon antiquity. The leading idea which is present in all our researches, and which accompanies every fresh observation, the sound of which to the student of Nature seems continually echoed from every part of her work, is -*

*Time! - Time! - Time!*

George Poulett Scrope, *Geology of Central France* (1827)

## 1.1 THE EDIACARAN BIOTA

The base of the Cambrian period (ca. 540 Mya) is renowned for the rapid emergence of nearly all animal phyla within a few million years, a phenomenon known as the 'Cambrian explosion' of complex animal life (Knoll and Carroll 1999; Narbonne et al. 2012). This sudden appearance of crown-group metazoans (including the last common ancestor of all extant members of a group and all its descendants) in the fossil record follows the enigmatic Precambrian rocks, once believed to be devoid of life (Walcott 1914; Dunn and Liu 2017). However, evidence now shows that the 'Cambrian explosion' was preceded by an extensive Ediacaran record of macroscopic animal and animal-like life (Brasier 2000). Early attempts to describe members of the Ediacaran Biota beneath Cambrian strata were made by Billings (1872), Gürich (1930, 1933), and Sprigg (1949), although they were initially considered abiogenic or mistakenly attributed to younger Paleozoic rocks. It was not until Ford's (1958, 1962, 1963) description of *Charnia masoni*

and *Charniodiscus concentricus* in the UK that these organisms were formally recognized as Precambrian (Glaessner 1959). The ratification of the Ediacaran System was further established by Knoll et al. (2004, 2006). Since then, numerous fossil-rich successions have been reported globally, significantly advancing Ediacaran biostratigraphy (Narbonne et al. 2012).

The Ediacaran Biota (ca. 580-540 Mya) (Fedonkin et al. 2007; Xiao and Laflamme 2009; Narbonne et al. 2012) records some of the oldest evidence for macroscopic and largely soft-bodied, possibly metazoan life forms on Earth (Liu et al. 2015) (Figure 1.1). These organisms dominate the period from just above the Gaskiers Glaciation (ca. 579 Mya) (Pu et al. 2016) to the base of the Cambrian ( $541 \pm 0.13$  Mya), marked by the first appearance of the trace fossil *Treptichnus pedum* (Landing 1994). The Ediacaran biota showcases unprecedented body plans (e.g., Narbonne 2004; Brasier et al. 2012; Hoyal Cuthill and Conway Morris 2014), critical ecological innovations (e.g., Liu et al. 2010; Evans et al. 2019), diverse feeding strategies (e.g., Laflamme et al. 2009; Rahman et al. 2015; Dufour and McIlroy 2017), enigmatic reproduction modes (e.g., Mitchell et al. 2015; Pasinetti et al. 2023), and complex community structure and dynamics (e.g., Clapham and Narbonne 2002; Clapham et al. 2003; Darroch et al. 2013; Mitchell et al. 2015, 2019; Droser et al. 2017; Boan et al. 2024; Stephenson et al. 2024). Traditionally, Ediacaran organisms have been interpreted as stem or crown group metazoans (Glaessner and Wade 1966; Wade 1972), or even as higher-order non-metazoan groups (Pflug 1972; Seilacher 1989, 1992). Due to their disparate anatomical and developmental plans, modern consensus views the Ediacaran macrobiota as a polyphyletic group (Xiao and Laflamme 2009; Erwin et al. 2011; Dunn and Liu 2019), with some widely accepted metazoan candidates (Clapham et al. 2004; Liu et al. 2014; Wang et al. 2024; McIlroy et al. 2024).

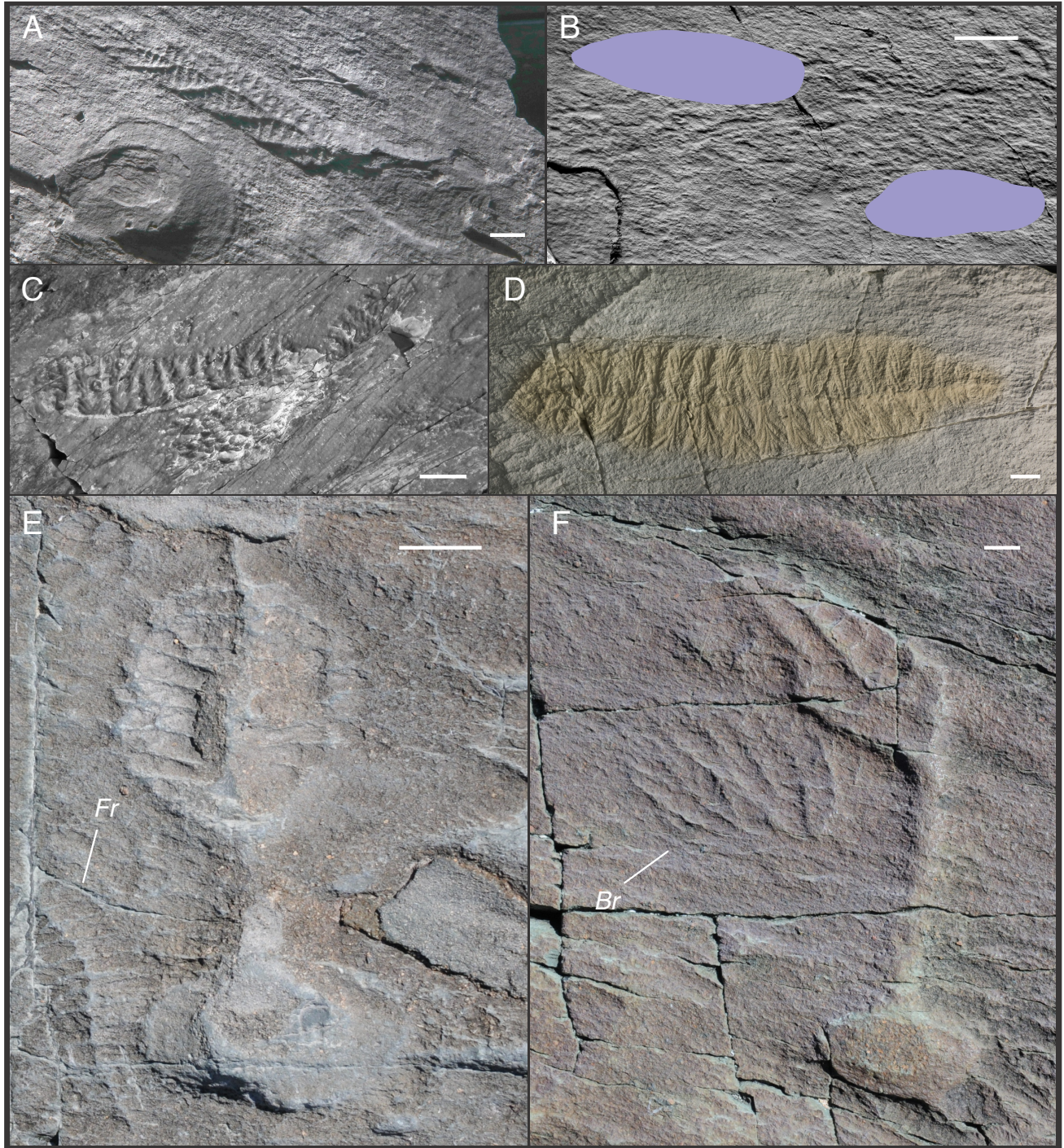


Figure. 1.1: Fossil plate of iconic Ediacaran rangeomorphs and arboreomorphs. A) *Charnia* sp. (MUN Surface, Catalina Dome in the Bonavista Peninsula). B) Opposing *Charnia* sp. (Catalina area, Bonavista Peninsula). C) *Pectinifrons abyssalis* (Mistaken Point Formation at Mistaken Point Ecological Reserve). D) *Fractofusus misrai* (E Surface, Mistaken Point Ecological

Reserve). E) *Charniodiscus spinosus* (E Surface, Mistaken Point Ecological Reserve). D) *Charniodiscus procerus* (E Surface, Mistaken Point Ecological Reserve). Fr: *Fractofusus*. Br: *Bradgatia*. All scale bars 1 cm but C 5cm.

## 1.2 THE AVALON ASSEMBLAGE

Global-scale temporal and environmental studies on the distribution of the Ediacaran macrofossils have revealed three temporally-successive biostratigraphy subdivisions (Waggoner 2003; Boag et al. 2016; Evans et al. 2022): the Avalon Assemblage, which spans at least the interval ca. 574–564 Mya (Matthews et al. 2021), which is succeeded by the White Sea Assemblage (ca. 560–550 Ma) and then the Nama Assemblage (ca. 550–541 Ma) (Xiao and Laflamme 2009; Droser et al. 2017; Mitchell et al. 2020; Eden et al. 2022). Despite preserving limited ecological and morphological diversity, the Avalon Assemblage is crucial in understanding the early evolutionary patterns of complex multicellular life (Liu et al. 2015) such as spatial ecology (e.g., Mitchell et al. 2015), reproduction processes (e.g., Darroch et al. 2013; Pasinetti and McIlroy 2023); and feeding strategies (e.g., Dufour and McIlroy 2017; Darroch et al. 2023).

### 1.2.1 Geological context of the Avalon Assemblage in Newfoundland

The Avalon Assemblage formed as part of the peri-Gondwanan Avalonian volcanic arc system at high southern palaeolatitudes (Murphy et al. 2004; McIlroy and Horák 2006; Pisarevsky et al. 2012; Wen et al. 2020). This assemblage is geographically diverse, encompassing outcrops from the Avalon and Bonavista Peninsulas of Newfoundland (Hofmann et al. 2008; Matthews et al. 2021), the Mackenzie Mountains in northwestern Canada (Narbonne and Aitken 1990), and Charnwood Forest in the UK (Noble et al. 2015).

In Newfoundland, fossiliferous successions belong to the Conception and St. John's groups, which comprise ~3 km predominantly turbiditic basin floor-to-slope facies. These groups are thought to have been deposited within a system of sub-basins (including Upper Island Cove and Bonavista on the west, and Mistaken Point Ecological Reserve on the east), possibly in fore-arc settings, divided by the topographic prominence of the Harbour Main Group isolating the sub-basin from the main fore-arc basin (Wood et al. 2003; Ichaso et al. 2007; Mason et al. 2013). The associated facies changes on a gross scale document a transition from deepwater basinal depositional settings to slope and shallower prodeltaic (Fermeuse Formation) and eventually alluvial/fluvial depositional settings. Fossil-bearing deposits are located more than one kilometer below the presence of wave-generated structures in muddy settings, and thus generally interpreted as sub-photic (O'Brien and King 2004, 2005; Wood et al. 2003; Ichaso et al. 2007; Mason et al. 2013). These fossiliferous successions prominently outcrop in the Mistaken Point Ecological Reserve (MPER) (Anderson and Misra 1968), Conception Bay (Narbonne 2004), and the Bonavista Peninsula (O'Brien and King 2004, 2005; Hofmann et al. 2008). In the latter, the lithostratigraphic composition of the Late Neoproterozoic sequences east of the Spillars Cove–English Harbour Fault Zone correlates to the Conception, St. John's, and Signal Hill groups of the Avalon Peninsula (O'Brien and King 2004, 2005).

Avalonian fossils of Ediacaran age are typically preserved as two-dimensional impressions on fine-grained volcanoclastic substrates beneath ash deposits or sandstones (Narbonne 2005; McKean et al. 2023). In the absence of bioturbation, the low porosity of the sediments, and the sealing of underlying buried sediments by microbial matgrounds, a low redoxcline emerges. Under anoxic conditions, microbial biofilms are thought to have played a crucial role the preservation of soft tissue impressions (e.g., Gehling et al. 1999; Bobrovsky et al. 2018; Pasinetti and McIlroy

2023) through the precipitation of iron sulphides (Laflamme et al. 2011; Wacey et al. 2015; Liu 2016). The actual mode of preservation results from a combination of early lithification and soft-sediment rheology (encompassing strength and viscosity affecting the capacity of the sediments to resist plastic deformation) (Bobrovskiy et al. 2019), histological consistency (MacGabhann et al. 2019), and life-attitude (Seilacher 1999; Gehling and Narbonne 2007). Generally, the external impression of robust tissues, which are cast by early cementation of the overlying (usually ash-rich) sediments, are cast from below by less competent sediments moving upwards and result in features preserved as positive epireliefs. In contrast, the external ventral impressions of labile tissues, especially those of reclining organisms that smother the underlying matground, are cast by the collapsing overlying sediments, resulting in negative epireliefs (e.g., Narbonne 2005; McKean et al. 2023) (Figure 1.2). Additionally, organisms can be preserved on different bedding planes (e.g., Evans et al. 2015; Burzynski et al. 2017) or associated with other organisms (Seilacher 1999; Gehling and Narbonne 2007; Taylor et al. 2023).

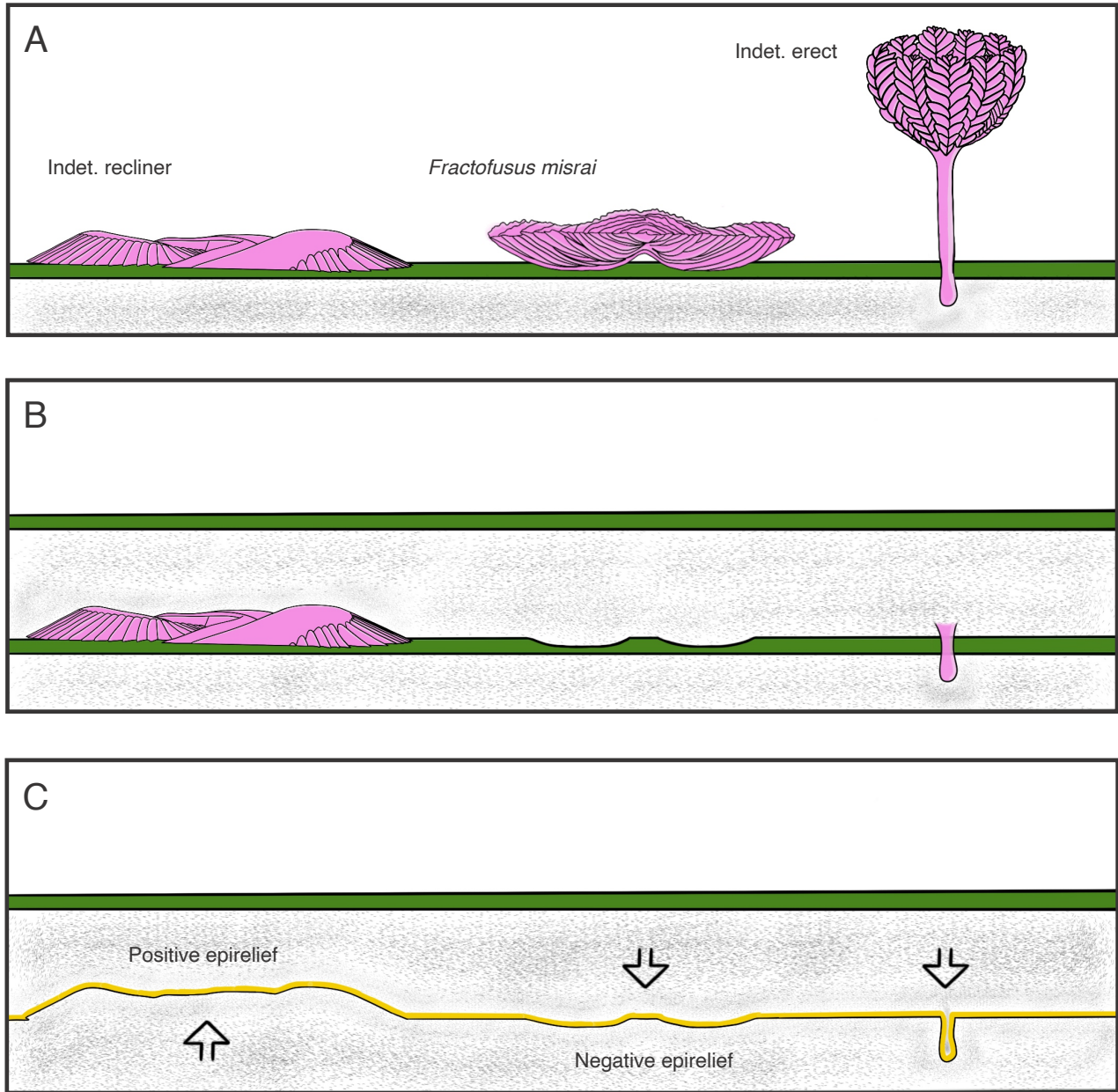


Figure 1.2: General preservation model. A) Living benthic community consisting of an indeterminate reclining frond, *Fractofusus misrai*, and an indeterminate erect frond. B) Burial of community and sealing of the new sediment by new colonization of microbial matground (green). Decay of *F. misrai* and erosion of the frondose section of the indeterminate erect frond. C) Decay of the microbial mat forming a pyritic veneer in the sole of the burying bed (yellow). Resistant tissues from the indeterminate recliner leave a positive relief with underlying sediments

moving up casting the top surface of the organism. Gravitational movement from the overlying sediments to cast the void left by the ventral impressions of *F. misrai* and the holdfast of the indeterminate erect frond producing a negative epirelief of the bottom surface. Movement of sediment indicated by arrows. Figure modified from and inspired by Kenchington (2015), MacGabhann et al. (2019), and @paleobiome.

### 1.2.2 The Rangeomorpha and the Arboreomorpha

The Ediacaran biota of Newfoundland is largely comprised of immotile sessile taxa ranging from centimeter to meter scale impressions of deformable, possibly fluid filled structures as evidenced by wrinkled and collapsed tissues (Narbonne and Gehling 2003; Liu et al. 2010, 2012; Dunn et al. 2019; McIlroy et al. 2021; Delahooke et al. 2024). This biota includes enigmatic species such as *Hadryniscala* and *Hadrynichorde* (Hofmann et al. 2008), diverse discoidal forms (Gehling et al. 2000; Burzynski and Narbonne 2015; Burzynski et al. 2017), the protistan *Palaeopascichnus* (Hawco et al. 2021), taphomorphs of effaced organic remains known as ivesheadiomorphs (Liu et al. 2011, 2015), putative poriferans (i.e., *Thectardis* Clapham et al. 2004; Sperling et al. 2011) and crown group cnidarians (*Haootia* and *Mamsetia* Liu et al. 2014; McIlroy et al. 2024), and the most numerically abundant clades Rangeomorpha and Arboreomorpha (e.g., Laflamme et al. 2004; Narbonne 2004; Narbonne et al. 2009).

The Rangeomorpha is the most numerically and taxonomically dominant clade in the Ediacaran of Newfoundland. It first appears in the Drook Formation (ca. 575 Mya) in the MPER and ranges into to the Fermeuse Formation of the Bonavista Peninsula (Erwin et al. 2011; Hofmann et al. 2008; Dececchi et al. 2018; Matthews et al. 2021). Rangeomorphs are characterized by modular frondose body plans and pseudo-fractal branching architecture, consisting of several

orders of self-repeating branches along a glide plane of symmetry. This branching architecture results in high surface area-to-volume ratios (SA/V) that largely lack modern analogues (Narbonne 2004; Narbonne et al. 2009; Erwin et al. 2011; Hoyal Cuthill and Conway Morris 2014). The basic rangeomorph element is essentially a building block that can grow in different ways and lead to a range of morphologies in the preserved bedding plane expression of the 3D form (Jenkins 1985; Brasier et al. 2012; Hoyal Cuthill and Conway Morris 2014; McIlroy et al. 2021). The clade is divided into the orders Charnida and Rangida (Figure 1.3). The Charnida have single-sided, undisplayed, and furled primary order branches, while the Rangida have double-sided, sometimes multipolar fronds, with displayed, predominantly unfurled, primary order branches (Narbonne et al. 2009; Brasier et al. 2012; Dececchi et al. 2018).

The clade Arboreomorpha shares a similar stratigraphic distribution within the Avalon Assemblage as the Rangeomorpha (Hofmann et al. 2008; Erwin et al. 2011; Dececchi et al. 2018; Matthews et al. 2021). Unlike rangeomorphs, the arboreomorphs exhibit 'Arborea-type branching' as is typified by the genus *Arborea* (Laflamme and Narbonne 2008). This branching architecture consists of non-fractal, predominantly parallel, peapod-shaped first-order branches that stem from a central stalk at acute to right angles. At their distal end, these branches terminate at an outer rim, suggesting the presence of a backing sheet of tissue (Dunn et al. 2019). Primary branches may also be ornamented or subdivided into orthogonally-directed higher-order branches (Laflamme and Narbonne, 2008; Dunn et al. 2019) (Figure 1.3). The generic diagnosis of *Arborea* differs significantly from that of the first described arboreomorph genus *Charniodiscus*, which has been interpreted as a multifoliate frond bearing undisplayed and rotated fractal branching, though without observable rangeomorph elements nor a backing sheet of tissue (cf. Dzik 2002, 2003; Brasier and Antcliffe 2009; Brasier et al. 2012; Dunn et al. 2019).

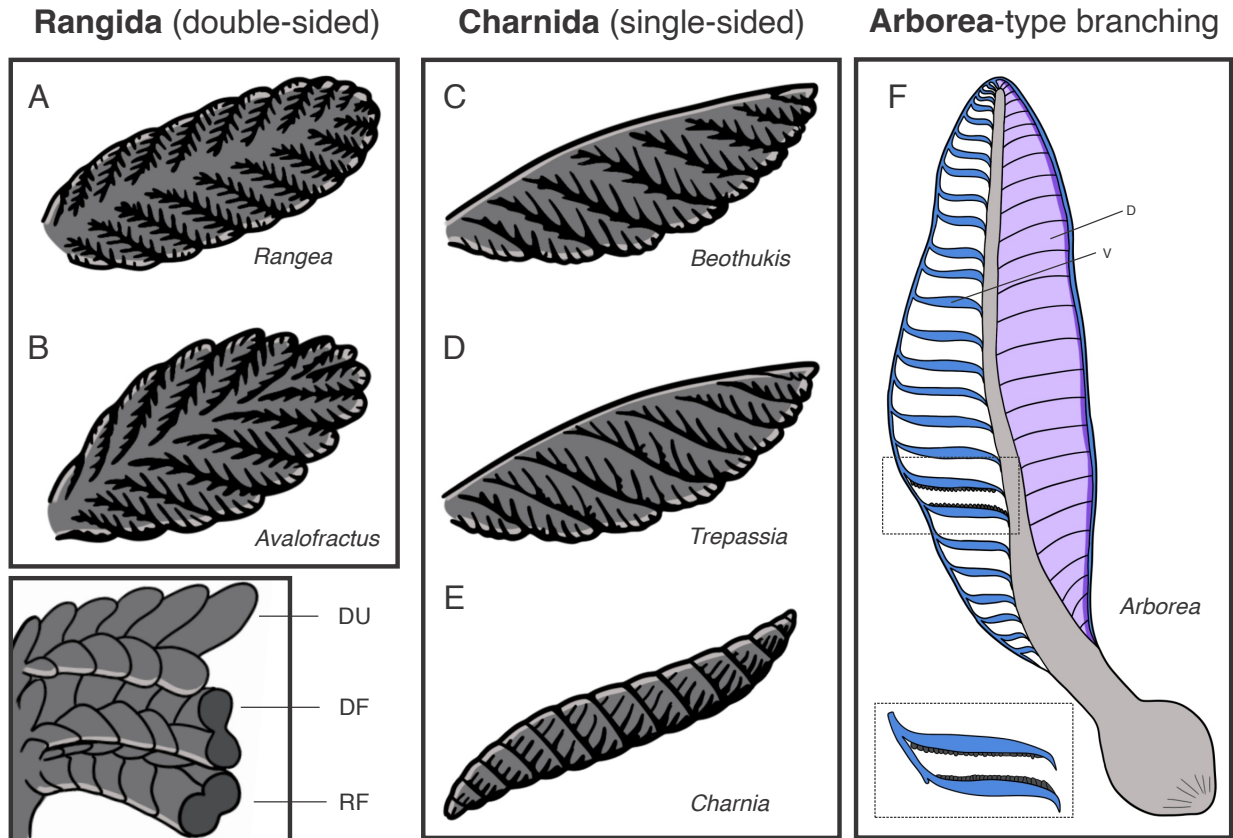


Figure 1.3: Branching architecture of Ediacaran fronds. Rangeomorphs including Rangida (A, B), typified by *Rangia* and *Avalofractus*, and Charnida (C, D, E), illustrated by *Beothukis*, *Trepassia*, and *Charnia*. F) Arboreomorphs exemplified by *Arborea arborea*. DU: Displayed and unfurled. DF: Displayed and furled. RF: Rotated and furled. D: Dorsal. V: Ventral. Figure modified from and inspired by Narbonne et al. (2009); Brasier et al. (2012), and Dunn et al. (2019).

### 1.3 AVALONIAN PALEOECOLOGY

Ediacaran paleocommunities preserved in situ, comprising near-census (living organisms killed and preserved rapidly) sessile communities, offer a remarkable opportunity to elucidate the ecological drivers of early metazoan evolution (Seilacher 1992; Clapham et al. 2003; Liu 2011;

Gehling and Droser 2013; Antcliffe et al. 2015). Interestingly, the rationale that community composition was primarily dictated by epifaunal tiering and suspension feeding strategies has recently been challenged (e.g., Antcliffe et al. 2015; Mitchell and Kenchington 2018; Dufour and McIlroy 2017; McIlroy et al. 2020, 2021, 2022; Pasinetti and McIlroy 2023; McKean et al 2023).

### 1.3.1 Community structure

Avalon Assemblage paleocommunities are found from deep basinal to mid-shelf settings (Wood et al. 2003; O'Brian and King 2004, 2005; Ichaso et al. 2007; Hofmann et al. 2008; Mason et al. 2013) recording relatively limited ecological diversity (e.g., composition and taxa interactions) (Shen et al. 2008; Laflamme et al. 2013; Droser et al. 2017; Mitchell and Butterfield 2018). Early studies proposed meter-scale epifaunal tiering akin to modern suspension-feeding communities (Clapham and Narbonne 2002, Clapham et al. 2003; Laflamme et al. 2012). Such tiering would have allowed organisms to exploit faster flows within the benthic boundary layer, thereby benefiting from resource partitioning and optimized feeding efficiency or oxygen gathering (Ghisalberti et al. 2014). However, this interpretation has been contested by evidence indicating that stemmed taxa reduced distinct vertical stratification (DVS), and therefore tiering, with height instead being an adaptation for enhanced offspring dispersal (Mitchell and Kenchington 2018). Additionally, it has been proposed that community composition was influenced by neutral stochastic demographic processes rather than deterministic niche-driven dynamics (Mitchell et al. 2019; Stephenson et al. 2024), which led to the homogenization of frond-dominated communities independently of succession processes (Stephenson et al. 2024).

Within these erect communities, reclining organisms such as the rangeomorph *Fractofusus* would have occupied the lowest tiers (Seilacher 1999; Gehling and Narbonne 2007; Taylor et al.

2023). This taxon has been suggested to reproduce via continuous, aseasonal reproduction, resulting in a single cohort on the D and E surfaces at MPER (Darroch et al. 2013). This contrasts with the multigenerational, interspaced, waterborne propagules that result in pioneering, randomly oriented individuals surrounded by clusters of smaller specimens, which grew from stolon-like asexual reproduction as proposed by Mitchell et al. (2015). However, the only tentative paleontological evidence for this are filamentous structures on a limited number of surfaces, occasionally connecting different species of rangeomorphs (Liu and Dunn 2020). Alternative evidence regarding reproduction comes from conserved morphologies with respect to ontogeny, and budding structures or fission (“kissing” *Aspidella*) (Tarhan et al. 2015; Pasinetti and McIlroy 2023).

### **1.3.1 Feeding strategies**

Suspension feeding strategies, which rely on collection of particulate organic matter (POM), have traditionally been invoked for Ediacaran organisms based on reconstructed tiered communities and the assumed erect body postures (Jenkins and Gehling 1978; Gehling and Rigby 1996; Clapham and Narbonne 2002; Clapham et al. 2003). However, this feeding mode has been challenged by several lines of evidence: the absence of preserved pores or specialized zooids (Liu et al. 2015; McIlroy et al. 2021; but see Butterfield 2022), flawed anatomical comparisons with the Pennatulacea (Antcliffe and Brasier 2007, 2008), the lack of consistent flow recirculation patterns towards specific areas in computational fluid dynamics (CFD) studies (Darroch et al. 2023), and reconstructions of reclining life habits for many rangeomorphs (Seilacher 1992,1999; Grazhdankin 2004; Grazhdankin and Seilacher 2005; Dufour and McIlroy 2017; McIlroy et al. 2020, 2021, 2022; Pasinetti and McIlroy 2023; McKean et al. 2023).

Alternatively, osmotrophy has been proposed, particularly due to the fractally enhanced SA/V of the Rangeomorpha (Laflamme et al. 2009). This feeding strategy involves the secretion of digestive enzymes to catalyze the breakdown of molecules in the extracellular environment, followed by the passive transport of dissolved organic matter (DOM) into the organism (Richards and Talbot 2018). However, there is only a marginal SA/V overlap with strict osmotrophic megabacteria when mathematical fractality and large internal vacuolization or metabolically inert mesenchyme are assumed (Laflamme et al. 2009). To reduce the adventive loss of exoenzymes, Butterfield (2022) proposed a modified form of osmotrophy for *Charnia*, based on a chamber system similar to the gastrovascular cavities of Cnidaria (Steinmetz 2019). However, the applicability of this model to other taxa remains questionable given processes like furling or branch overlapping (McIlroy et al. 2020, 2021). Even if this strategy was feasible, there are concerns regarding whether the Ediacaran DOC pool was sufficiently large to support macroscopic osmotrophs (McIlroy and Logan 1999; Liu et al. 2015; Droser et al. 2017; Fakhraee et al. 2021).

Given this context, an alternative feeding strategy for the deep marine Ediacaran biotas, based on symbiotic relationships with chemolithoautotrophic bacteria, has been proposed (Seilacher 1992; Dufour and McIlroy 2017; Pasinetti and McIlroy 2023; McKean et al. 2023). In essentially non-bioturbated, low porosity, and microbially sealed sediments, a redoxcline would form close to the sediment-water interface, leading to the toxic buildup of sulphides due to the activity of sulphur-reducing bacteria (McIlroy and Logan 1999). Ediacaran organisms, particularly reclining taxa such as *Fractofusus*, could have benefited from symbiotic relationships with sulphur-oxidizing bacteria. These reclining species could transport oxygen dorsoventrally to enhance bacterial metabolic activity which would oxidize reduced forms of sulfur, thereby detoxifying sulfidic porewaters (Dufour and McIlroy 2017). Reduction of SA/V ratios through

furling or other architectural adaptations could have minimized exposure to reduced forms of sulfur and lowered oxygen costs (McIlroy et al. 2021).

## **1.4 PALAEOCURRENTS AND BODY POSTURE**

Reconstructions of most frondose Rangeomorphs and Arboreomorphs have traditionally followed Glaessner (1984), depicting them as pennatulacean-grade organisms erect into the water column (e.g., Droser et al. 2017; Vixseboxse et al. 2021; Eden et al. 2022). These reconstructions often rely on flawed comparisons to modern cnidarian octocorals (Antcliffe and Brasier 2007), utilizing descriptive anatomy (e.g., holdfast and stem) to imply taxonomic affinities, biomechanical properties, life habits, and ecology (Mitchell et al. 2015; Mitchell et al. 2019; Mitchell and Butterfield 2018; Mitchell and Kenchington 2018; McIlroy et al. 2021). However, notable exceptions to this trope of erect fronds do exist (Seilacher 1992,1999; Grazhdankin 2004; Grazhdankin and Seilacher 2005; Dufour and McIlroy 2017; McIlroy et al. 2020, 2021, 2022; Pasinetti and McIlroy 2023; McKean et al. 2023) and other authors have theorized alternative functions for holdfasts and stems beyond structural integrity, similar to some vascular plants (Bamforth et al. 2008; Hoyal Cuthill and Conway Morris 2014; Burzynski et al. 2017). While the assumed erect body postures may be congruent with the sedimentological evidence for certain species, the applicability of an erect mode of life for many taxa in the Avalon Assemblage remains questionable (McIlroy et al. 2020, 2021).

### **1.4.1 Felling of erect fronds**

Seemingly current-oriented fossils from MPER have supported the notion that these erect fronds were “felled”, becoming sediment parallel while still intact, and preserved in the direction

of downslope ash-laden density currents triggered by volcanic activity (Seilacher 1992, 1999) or ash-reworking tuffaceous turbidity currents (Benus 1988; Seilacher 1999; Matthews et al. 2021). These flows are gravity-driven, sediment-rich, turbulent flows which lead to sedimentary deposits known as turbidites including mostly partial Bouma sequences (Nichols 2009). Alternatively, it has been suggested that fronds were felled by orthogonally-directed inter-turbiditic contour currents and preserved by subsequent obrution deposits such as water-lain ash falls, in the absence of Bouma sequences (Wood et al. 2003; Ichaso et al. 2007; Bamforth et al. 2008; Brasier et al. 2012; McIlroy et al. 2020) (Figure 1.4). Paleocurrent direction can sometimes be inferred from sedimentological proxies on Ediacaran fossil surfaces such as current ripple trends in turbidites (e.g., Wood et al. 2003), stretch or ‘mop’ marks (Tarhan et al. 2010; Paterson et al. 2017), swing marks (i.e., *Kullingia concentrica* in Jensen et al. 2018), and obstacle scours (McKean et al. 2023). However, in some instances and in the absence of sedimentological evidence, paleocurrent direction has solely been inferred from fossil orientation, based on poorly-supported assumptions of erect life habits (McIlroy et al. 2021). Regardless of the hydrodynamic regime invoked, there are several inconsistencies that need further investigation.

Turbidity currents generate up-slope velocity pulses at the interface along the density stratification with ambient fluid in the form of Kelvin-Helmholtz waves under high Froude numbers (i.e., Kneller and McCaffrey 2003). These roll waves emerge after strong upward-directed turbulence at the leading head but are unreported near the bottom boundary, where turbulent velocity variation follows the net downstream fluid motion, rarely approaching zero (Haughton et al. 2009; Baas et al. 2011; Kostaschuk et al. 2018). Consequently, turbulent gravity flows fail to explain the felling direction of fronds preserved orthogonal to, or even against, the prevailing current (McIlroy et al. 2022). Moreover, the conjectural Harbour Main High (Ichaso et

al. 2007) would not have allowed arc-sourced turbidites to be deposited on the eastern sub-basin (Matthews et al. 2021).

Invoking the presence of background (contour) currents in the absence of sedimentological proxies is problematic (Wood et al. 2003; Ichaso et al. 2007; Mason et al. 2013). If erect living fronds were flattened in a direction orthogonal to the downslope direction by a contour current, it is difficult to explain the lack of current-realignment generated by subsequent, much more violent, turbidity currents. Moreover, contour currents fail to account for the complex orientation of fronds at different stratigraphic levels and less parsimonious up- and downslope currents of tidal and (or) wind-forced origin (e.g., Petrie 1975; Allen 1997) are assumed (Wood et al. 2003). These flow regimes would interfere with the pre-existing contour currents which are generally slow and non-episodic (Zhao et al. 2015). It is also important to note that the northeasterly oriented contour currents generally hypothesized at the MPER sub-basin (Wood et al. 2003) are radically opposed to the southwesterly flow inferred in the Conception Bay sub-basin (Ichaso et al. 2007). This inconsistency is contrary to the global deep-water thermohaline system (Rhein et al. 1995).

In the absence of sedimentological evidence, resorting to fossil orientation to infer submarine paleocurrents is questionable due to the unresolved life habits of many Ediacaran taxa. Given the models discussed and assuming erect body postures, it is evident that understanding the hydrodynamics responsible for the varied orientations of fronds across different surfaces and stratigraphic units remains challenging (e.g., Bamforth et al. 2008; Flude and Narbonne 2008).

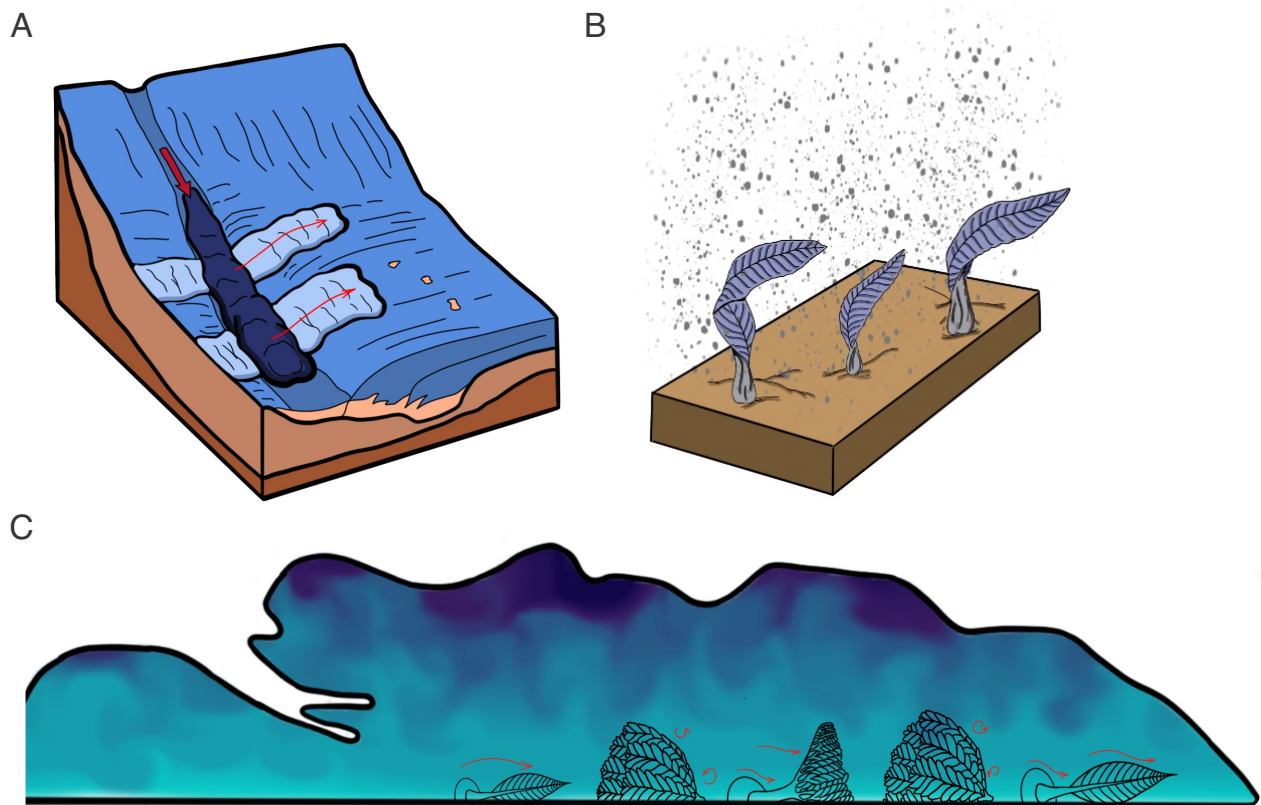


Figure 1.4: Submarine hydrodynamic processes thought to be relevant in the preservation of the Ediacaran organisms of the Avalon Assemblage. A) Conceptual diagram showing a downslope turbidity current (dark blue), and orthogonally-directed contour currents parallel to the slope (light blue). B) Frondose organisms in a recumbent position by the action of contour currents and pelagic deposition of ash. C) Tuffaceous turbidity current felling and preserving Ediacaran fronds. Figure modified from and inspired by Fonesu et al. (2020); Vixseboxse et al. (2021), and A. Reimann.

#### 1.4.2 *Fractofusus* as a randomly oriented recliner

The rangeomorph genus *Fractofusus* is common in the offshore to deep basinal Ediacaran facies of Newfoundland, with a single poorly preserved putative specimen from the McKenzie

Mountains (Narbonne et al. 2014). The genus was first described by Anderson and Misra (1968) from the Mistaken Point Formation in the MPER and was eventually formally named by Gehling and Narbonne (2007). The species *Fractofusus misrai* dominates the D and E surfaces at MPER (Clapham et al. 2003; Mitchell et al. 2015), whereas *F. andersoni* is the most abundant in the Catalina Dome (Hofmann et al. 2008). On the Bonavista Peninsula, *F. misrai* is only known from poorly preserved specimens from the Murphy's Cove Member, which has been lithostratigraphically correlated with the Mistaken Point Formation of the Avalon Peninsula, as well as a possible specimen in the Fermeuse Formation (Hofmann et al. 2008; until Pérez-Pinedo et al. 2023).

*Fractofusus misrai* is a flat, fusiform bipolar rangeomorph with two rows of laterally independent primary branches consisting of principal and subsidiary frondlets meeting at a straight to zigzagged midline (Gehling and Narbonne 2007; Taylor et al. 2023). Some specimens have been described as having the same number of primary branches on both sides of the midline, whereas others are thought to have a glide plane of symmetry (Hofmann et al. 2008; Brasier et al. 2012) with differing number of branches possibly due to ecological factors (Taylor et al. 2023). Initial interpretations of *F. misrai* reconstructed the top and bottom surfaces as being identical based on specimens that were inferred to have been folded (Seilacher 1999; Gehling and Narbonne 2007). Recent models of *Fractofusus* spp. invoked significant biconvexity (Gehling and Narbonne 2007; Liu et al. 2015), and some have suggested pronounced high relief (Mitchell and Kenchington 2018) with no clear supporting evidence (McIlroy et al. 2022; Taylor et al. 2023).

While the debate concerning the erect vs reclining mode of life of many arboreomorphs and rangeomorphs is unresolved, the sessile epibenthic recliner mode of life for *Fractofusus* is widely accepted (e.g., Seilacher 1999; Gehling and Narbonne 2007; Vixseboxse et al. 2021). This

is primarily based on their consistently extraordinarily well-preserved lower surfaces (Dufour and McIlroy 2017; Taylor et al. 2023) and their apparent current-independent random orientations at the E Surface at MPER, and the Johnson/H14 Surface at Discovery Global Geopark (Seilacher 1999; Gehling and Narbonne 2007; Mitchell et al. 2015; Vixseboxse et al. 2021). However, these studies have relied on visual inspection to determine orientation trends (Seilacher 1999; Gehling and Narbonne 2007), fail to consider rheotropic growth, or have inferred questionable turbidity current dynamics (Vixseboxse et al. 2021; see McIlroy et al. 2022).

## **1.5 THESIS OBJECTIVES AND INTEGRATIVE METHODOLOGY**

This PhD thesis focuses on the newly described Melrose Surface at the southern end of the Catalina Dome in the Discovery UNESCO Global Geopark. This fossil assemblage is significant as it records the presence of previously interpreted erect rangeomorph and arboreomorph taxa, while being dominated by the reclining *F. misrai*. Additionally, the sedimentological succession features evidence of paleocurrent activity in the form of current ripple trends and ripple cross-lamination. Consequently, the Melrose Surface offers a unique opportunity to reconstruct the different life attitudes of characteristic Ediacaran taxa along both the vertical axis (erect vs reclining postures) and the horizontal axis (frond orientation), as well as to model the paleocurrents that were active at the time without resorting to inferring current directions from fossil orientation. The work presented herein consists of an integrative approach to life attitude encompassing taphonomic, sedimentological, statistical, and computational evidence:

- 1) Taphonomic analysis: through the reinterpretation of taphonomic clues—such as differential reliefs, preservation planes, and architectural fossil features—the life-position

of some iconic Avalonian arboreomorph taxa was reconstructed, and previously existing taxonomic inconsistencies were resolved.

- 2) Statistical treatment: special statistical treatment based on circular clustering algorithms was applied to describe orientation trends (horizontal axes) within the population of reclining *F. misrai*. This approach avoids reliance on visual inspection, accounts for the mathematical periodicity in orientation, and considers rheotropic responses to paleoflow.
- 3) Computational Fluid Dynamics (CFD): using highly detailed three-dimensional reconstructions of the Rangeomorpha for the first time, the turbulent flows present in the section were modelled over the dominant orientation trends. This allows the study of critical mechanical and physiological aspects of Ediacaran taxa living in dynamic fluid environments.

## 1.6 THESIS STRUCTURE AND SUMMARY

The main body of the text of this PhD thesis is structured in the ‘Manuscript Style’, with Chapters 2, 3, and 4 presented as stand-alone manuscripts published in international peer-reviewed scientific journals. As independent chapters, each features the contribution of different co-authors with Daniel Pérez-Pinedo as the lead author. Detailed information on the authors and academic affiliations can be found in the co-authorship in each chapter. These chapters expand on the taphonomic, statistical, and computational approaches to position in life of Ediacaran taxa mentioned previously. To improve readability of the thesis, the content and main findings of the chapters are briefly outlined below. All papers are already published:

- Chapter 2 — Through the taphonomic reinterpretation of the holotype of *C. concentricus*, this taxon is reconstructed as a bifoliate sub-conical erect/recumbent

frond with no evidence of fractal branching or backing sheets of tissues. In contrast, *C. procerus* is interpreted as having lived reclining onto the sediment due to the extraordinary preservation of the stems. Our emendation of the generic diagnosis of *Charniodiscus* distinguishes the genus from the planar, leaf-like *Arborea* which additionally has a backing sheet absent in *Charniodiscus* spp.

Paper reference: Pérez-Pinedo, D., McKean, C., Taylor, R., Nicholls, R., & McIlroy, D. (2022). *Charniodiscus* and *Arborea* are separate genera within the Arboreomorpha: using the holotype of *C. concentricus* to resolve a taphonomic/taxonomic tangle. *Frontiers in Earth Science*, 9, 785929.

- Chapter 3 — Special statistical treatment based on modified circular clustering algorithms is applied to find orientation trends among the population of *F. misrai* from the newly described Melrose Surface. Contrary to previous inferences of randomly oriented recliners, we find oblique preferential orientation groups with respect to the sedimentologically recorded paleocurrent. We hypothesize that these orientation trends reveal a rheotropic response to the paleocurrent by *F. misrai*. This interpretation is extended to other rangeomorph genera based on qualitative evidence.

Paper Reference: Pérez-Pinedo, D., Neville, J. M., Pasinetti, G., McKean, C., Taylor, R., & McIlroy, D. (2023). Frond orientations with independent current indicators demonstrate the reclining rheotropic mode of life of several Ediacaran rangeomorph taxa. *Paleobiology*, 49(3), 471-492.

- Chapter 4 — We model turbulent flows using k- $\omega$  SST turbulence model over a new highly detailed reinterpretation of *F. misrai* bearing three orders of fractal branching. We reveal hydrodynamic phenomena relevant to interpreting feeding efficiency and explain the recently documented rheotropic oblique orientation trends from the Melrose Surface. These trends result from a trade-off between the maximization of aspect ratio without compromising mechanical stability through reduced drag.

Paper reference: Pérez-Pinedo, D., Nicholls, R., Neville, J. M., & McIlroy, D. (2024). Hydrodynamic insights into the paleobiology of the Ediacaran rangeomorph *Fractofusus misrai*. *iScience*, 27(6).

We advocate for the more parsimonious alternative hypothesis that Ediacaran organisms lived in a reclined position, as preserved in the fossil record (Seilacher 1992; Grazhdankin 2004; Grazhdankin and Seilacher 2005) unless there is evidence to the contrary (Pérez-Pinedo et al. 2022). These flat recliners likely grew in response to water currents, exhibiting rheotropic behavior (Pérez-Pinedo et al. 2023, 2024). They maintained permanent ventral contact with sulphidic, toxic porewaters, possibly benefiting from symbiotic relationships with chemolithoautotrophic bacteria (Dufour and McIlroy 2017; McIlroy et al. 2021; Pasinetti and McIlroy 2023; McKean et al. 2023).

During my PhD thesis, I have also co-authored several published scientific papers that are listed below:

Huang, H., Pérez-Pinedo, D., Morley, R. J., Dupont-Nivet, G., Philip, A., Win, Z., ... & Hoorn, C. (2021). At a crossroads: The late Eocene flora of central Myanmar owes its composition to plate collision and tropical climate. *Review of Palaeobotany and Palynology*, 291, 104441.

McIlroy, D., Pérez-Pinedo, D., Pasinetti, G., McKean, C., Taylor, R. S., & Hiscott, R. N. (2022). Rheotropic epifaunal growth, not felling by density currents, is responsible for many Ediacaran fossil orientations at Mistaken Point. *Frontiers in Earth Science*, 10, 849194.

Huang, H., Morley, R. J., Licht, A., Dupont-Nivet, G., Pérez-Pinedo, D., Westerweel, J., ... & Hoorn, C. (2023). A proto-monsoonal climate in the late Eocene of Southeast Asia: Evidence from a sedimentary record in central Myanmar. *Geoscience Frontiers*, 14(1), 101457.

McIlroy, D., Pasinetti, G., Pérez-Pinedo, D., McKean, C., Dufour, S. C., Matthews, J. J., ... & Taylor, R. S. (2024). The Palaeobiology of Two Crown Group Cnidarians: *Haootia quadriformis* and *Mamsetia manunis* gen. et sp. nov. from the Ediacaran of Newfoundland, Canada. *Life*, 14(9), 1096.

Pasinetti, G., Fitzgerald, H.G., Pérez-Pinedo, D., & McIlroy, D. (2024). A taxonomic and palaeobiologic consideration of *Charnia* spp. from the Bonavista Peninsula of Newfoundland (CA). Submitted to *Journal of Systematic Palaeontology*.

Pasinetti, G., Menon, L.R., Chida, N., McKean, C., Olschewski, P., Pérez-Pinedo, D., Taylor, R.S., & McIlroy, D. (2024). The macrofossil *Lydonia jiggamintia* gen. et sp. nov. from the Ediacaran of Newfoundland: from pseudofossil to metazoan-grade epibiont. Submitted to *Palaeontologia Electronica*.

## 1.7 REFERENCES

Allen, P.A. (1997). *Earth Surface Processes*. Blackwell Science, Oxford, U.K.

Antcliffe, J. B., & Brasier, M. D. (2007). *Charnia* and sea pens are poles apart. *Journal of the Geological Society*, 164(1), 49-51.

Antcliffe, J. B., & Brasier, M. D. (2008). *Charnia* at 50: developmental models for Ediacaran fronds. *Palaeontology*, 51(1), 11-26.

Antcliffe, J. B., Hancy, A. D., & Brasier, M. D. (2015). A new ecological model for the ~565 Ma Ediacaran biota of Mistaken Point, Newfoundland. *Precambrian Research*, 268, 227-242.

Anderson, M. M., & Misra, S. B. (1968). Fossils found in the Pre-Cambrian Conception Group of south-eastern Newfoundland. *Nature*, 220(5168), 680-681.

Bamforth, E. L., Narbonne, G. M., & Anderson, M. M. (2008). Growth and ecology of a multi-branched Ediacaran rangeomorph from the Mistaken Point assemblage, Newfoundland. *Journal of Paleontology*, 82(4), 763-777.

Baas, J. H., Best, J. L., & Peakall, J. (2011). Depositional processes, bedform development and hybrid bed formation in rapidly decelerated cohesive (mud–sand) sediment flows. *Sedimentology*, 58(7), 1953-1987.

Benus, A. P. (1988). Sedimentological context of a deep-water Ediacaran fauna (Mistaken Point Formation, Avalon Zone, eastern Newfoundland): *Bulletin of the New York State Museum*, v. 463.

Billings, E., 1872. On some fossils from the Primordial rocks of Newfoundland. *The Canadian Naturalist*, 6, 465-479.

Boag, T. H., Darroch, S. A., & Laflamme, M. (2016). Ediacaran distributions in space and time: testing assemblage concepts of earliest macroscopic body fossils. *Paleobiology*, 42(4), 574-594.

Boan, P. C., Evans, S. D., & Droser, M. L. (2024). And now for something completely random: spatial distribution of *Dickinsonia* on the Ediacaran seafloor. *Global and Planetary Change*, 238, 104467.

Bobrovskiy, I., Hope, J. M., Krasnova, A., Ivantsov, A., & Brocks, J. J. (2018). Molecular fossils from organically preserved Ediacara biota reveal cyanobacterial origin for *Beltanelliformis*. *Nature Ecology & Evolution*, 2(3), 437-440.

Bobrovskiy, I., Krasnova, A., Ivantsov, A., Luzhnaya, E., & Brocks, J. J. (2019). Simple sediment rheology explains the Ediacara biota preservation. *Nature Ecology & Evolution*, 3(4), 582-589.

Bowring, S. A., Grotzinger, J. P., Condon, D. J., Ramezani, J., Newall, M. J., & Allen, P. A. (2007). Geochronologic constraints on the chronostratigraphic framework of the Neoproterozoic Huqf Supergroup, Sultanate of Oman. *American Journal of Science*, 307(10), 1097-1145.

Brasier, M.D., (2000). The Cambrian explosion and the slow burning fuse. *Sci. Prog.* 83, 77–92.

Brasier, M. D., & Antcliffe, J. B. (2009). Evolutionary relationships within the Avalonian Ediacara biota: new insights from laser analysis. *Journal of the Geological Society*, 166(2), 363-384.

Brasier, M. D., Antcliffe, J. B., & Liu, A. G. (2012). The architecture of Ediacaran fronds. *Palaeontology*, 55(5), 1105-1124.

Burzynski, G., & Narbonne, G. M. (2015). The discs of Avalon: relating discoid fossils to frondose organisms in the Ediacaran of Newfoundland, Canada. *Palaeogeography, Palaeoclimatology, Palaeoecology*, 434, 34-45.

Burzynski, G., Narbonne, G. M., Dececchi, T. A., & Dalrymple, R. W. (2017). The ins and outs of Ediacaran discs. *Precambrian Research*, 300, 246-260.

Butterfield, N. J. (2022). Constructional and functional anatomy of Ediacaran rangeomorphs. *Geological Magazine*, 159(7), 1148-1159.

Clapham, M. E., & Narbonne, G. M. (2002). Ediacaran epifaunal tiering. *Geology*, 30(7), 627-630.

Clapham, M. E., Narbonne, G. M., & Gehling, J. G. (2003). Paleoecology of the oldest known animal communities: Ediacaran assemblages at Mistaken Point, Newfoundland. *Paleobiology*, 29(4), 527-544.

Clapham, M. E., Narbonne, G. M., Gehling, J. G., Greentree, C., & Anderson, M. M. (2004). *Thectardis avalonensis*: a new Ediacaran fossil from the Mistaken Point biota, Newfoundland. *Journal of Paleontology*, 78(6), 1031-1036.

Darroch, S. A., Laflamme, M., & Clapham, M. E. (2013). Population structure of the oldest known macroscopic communities from Mistaken Point, Newfoundland. *Paleobiology*, 39(4), 591-608.

Darroch, S. A., Gutarra, S., Masaki, H., Olaru, A., Gibson, B. M., Dunn, F. S., ... & Rahman, I. A. (2023). The rangeomorph *Pectinifrons abyssalis*: Hydrodynamic function at the dawn of animal life. *iScience*, 26(2).

Dececchi, T. A., Narbonne, G. M., Greentree, C., & Laflamme, M. (2018). Phylogenetic relationships among the Rangeomorpha: the importance of outgroup selection and implications for their diversification. *Canadian Journal of Earth Sciences*, 55(11), 1223-1239.

Delahooke, K. M., Liu, A. G., Stephenson, N. P., & Mitchell, E. G. (2024). 'Conga lines' of Ediacaran fronds: insights into the reproductive biology of early metazoans. *Royal Society Open Science*, 11(5), 231601.

Droser, M. L., Tarhan, L. G., & Gehling, J. G. (2017). The rise of animals in a changing environment: global ecological innovation in the late Ediacaran. *Annual review of earth and planetary sciences*, 45(1), 593-617.

Dufour, S. C., & McIlroy, D. (2017). Ediacaran pre-placozoan diploblasts in the Avalonian biota: the role of chemosynthesis in the evolution of early animal life. *Geological Society of London Special Publication*, 448, 211–219.

Dunn, F. S., & Liu, A. G. (2017). Fossil focus: The Ediacaran biota. *Palaeontology*, 7, 1–15.

Dunn, F. S., & Liu, A. G. (2019). Viewing the Ediacaran biota as a failed experiment is unhelpful. *Nature Ecology & Evolution*, 3(4), 512-514.

Dunn, F. S., Liu, A. G., & Gehling, J. G. (2019). Anatomical and ontogenetic reassessment of the Ediacaran frond *Arborea arborea* and its placement within total group Eumetazoa. *Palaeontology*, 62(5), 851-865.

Dzik, J. (2002). Possible ctenophoran affinities of the Precambrian “sea-pen” *Rangea*. *Journal of morphology*, 252(3), 315-334.

Dzik, J. (2003). Anatomical information content in the Ediacaran fossils and their possible zoological affinities. *Integrative and Comparative Biology*, 43(1), 114-126.

Eden, R., Manica, A., & Mitchell, E. G. (2022). Metacommunity analyses show an increase in ecological specialisation throughout the Ediacaran period. *PLoS Biology*, 20(5), e3001289.

Erwin, D. H., Laflamme, M., Tweedt, S. M., Sperling, E. A., Pisani, D., & Peterson, K. J. (2011). The Cambrian conundrum: early divergence and later ecological success in the early history of animals. *Science*, 334(6059), 1091-1097.

Evans, S. D., Droser, M. L., & Gehling, J. G. (2015). *Dickinsonia* liftoff: evidence of current derived morphologies. *Palaeogeography, Palaeoclimatology, Palaeoecology*, 434, 28-33.

Evans, S. D., Gehling, J. G., & Droser, M. L. (2019). Slime travelers: early evidence of animal mobility and feeding in an organic mat world. *Geobiology*, 17(5), 490-509.

Evans, S. D., Tu, C., Rizzo, A., Surprenant, R. L., Boan, P. C., McCandless, H., ... & Droser, M. L. (2022). Environmental drivers of the first major animal extinction across the Ediacaran White Sea-Nama transition. *Proceedings of the National Academy of Sciences*, 119(46), e2207475119.

Fakhraee, M., Tarhan, L. G., Planavsky, N. J., & Reinhard, C. T. (2021). A largely invariant marine dissolved organic carbon reservoir across Earth's history. *Proceedings of the National Academy of Sciences*, 118(40), e2103511118.

Fedonkin, M. A. (2007). *The rise of animals: evolution and diversification of the kingdom Animalia*. JHU Press.

Flude, L. I., & Narbonne, G. M. (2008). Taphonomy and ontogeny of a multibranching Ediacaran fossil: *Bradgatia* from the Avalon Peninsula of Newfoundland. *Canadian Journal of Earth Sciences*, 45(10), 1095-1109.

Fonnesu, M., Palermo, D., Galbiati, M., Marchesini, M., Bonamini, E., & Bendias, D. (2020). A new world-class deep-water play-type, deposited by the syndepositional interaction of turbidity flows and bottom currents: The giant Eocene Coral Field in northern Mozambique. *Marine and Petroleum Geology*, 111, 179-201

Ford, T. D. (1958). Pre-Cambrian fossils from Charnwood Forest. *Proceedings of the Yorkshire Geological Society*, 31(3), 211-217.

Ford, T. D. (1962) The oldest fossils. *New Scientist*, 15, 191–194.

Ford, T. D. (1963). The Pre-Cambrian fossils of Charnwood Forest. *Leicester Literary and Philosophical Society Transactions*, 57, 57-62.

Gehling, J. G. (1999). Microbial mats in terminal Proterozoic siliciclastics; Ediacaran death masks. *Palaios*, 14(1), 40-57.

Gehling, J. G., Narbonne, G. M., & Anderson, M. M. (2000). The first named Ediacaran body fossil, *Aspidella terranovica*. *Palaeontology*, 43(3), 427-456.

Gehling, JG, & Narbonne, GM (2007). Spindle-shaped Ediacara fossils from the Mistaken Point assemblage, Avalon Zone, Newfoundland. *Canadian Journal of Earth Sciences*, 44 (3), 367-387.

Gehling, J. G., & Droser, M. L. (2013). How well do fossil assemblages of the Ediacara Biota tell time?. *Geology*, 41(4), 447-450.

Gehling, J. G., & Rigby, J. K. (1996). Long expected sponges from the Neoproterozoic Ediacara fauna of South Australia. *Journal of Paleontology*, 70(2), 185-195.

Ghisalberti, M., Gold, D. A., Laflamme, M., Clapham, M. E., Narbonne, G. M., Summons, R. E., ... & Jacobs, D. K. (2014). Canopy flow analysis reveals the advantage of size in the oldest communities of multicellular eukaryotes. *Current Biology*, 24(3), 305-309.

Glaessner, M. F. (1959). Precambrian Coelenterata from Australia, Africa and England. *Nature*, 183(4673), 1472-1473.

Glaessner, M. F. (1984). *The dawn of animal life: a biohistorical study*. CUP Archive.

Glaessner, M.F., Wade, M. (1966). The late Precambrian fossils from Ediacara, South Australia. *Palaeontology*, 9, 599–628.

Grazhdankin, D. (2004). Patterns of distribution in the Ediacaran biotas: facies versus biogeography and evolution. *Paleobiology*, 30(2), 203-221.

Grazhdankin, D., & Seilacher, A. (2005). A re-examination of the Nama-type Vendian organism *Rangea schneiderhoehni*. *Geological Magazine*, 142(5), 571-582.

Gürich, G. (1930). Die bislang ältesten Spuren von Organismen in Südafrika. In *International Geological Congress (XV)*, Pretoria, Union of South Africa, Die ältesten Fossilien Sud-Afrikas (Vol. 2, pp. 670-680).

Gürich, G. V. (1933). Die Kuibis-Fossilien der Nama-Formation von Südwestafrika: Nachtraege und Zusätze. *Paläontologische Zeitschrift*, 15(2), 137-154.

Haughton, P., Davis, C., McCaffrey, W., & Barker, S. (2009). Hybrid sediment gravity flow deposits—classification, origin and significance. *Marine and Petroleum Geology*, 26(10), 1900-1918.

Hawco, J. B., Kenchington, C. G., & McIlroy, D. (2021). A quantitative and statistical discrimination of morphotaxa within the Ediacaran genus *Palaeopascichnus*. *Papers in Palaeontology*, 7(2), 657-673.

Hofmann, H. J., O'Brien, S. J., & King, A. F. (2008). Ediacaran biota on Bonavista Peninsula, Newfoundland, Canada. *Journal of Paleontology*, 82(1), 1-36.

Hoyal Cuthill, J. F., & Conway Morris, S. (2014). Fractal branching organizations of Ediacaran rangeomorph fronds reveal a lost Proterozoic body plan. *Proceedings of the National Academy of Sciences*, 111(36), 13122-13126.

Ichaso, A. A., Dalrymple, R. W., & Narbonne, G. M. (2007). Paleoenvironmental and basin analysis of the late Neoproterozoic (Ediacaran) upper Conception and St. John's groups, west Conception Bay, Newfoundland. *Canadian Journal of Earth Sciences*, 44(1), 25-41.

Jenkins, R. J. (1985). The enigmatic Ediacaran (late Precambrian) genus *Rangea* and related forms. *Paleobiology*, 11(3), 336-355.

Jenkins, R. J. F. and Gehling, J. G. (1978). A review of the frond-like fossils of the Ediacara assemblage. *Records of the South Australian Museum*, 17, 347-359.

Jensen, S., Högström, A. E., Almond, J., Taylor, W. L., Meinhold, G., Høyberget, M. A. G. N. E., ... & Palacios, T. (2018). Scratch circles from the Ediacaran and Cambrian of Arctic Norway and southern Africa, with a review of scratch circle occurrences. *Bulletin of Geosciences*, 93(3), 287-304.

Kenchington, C. G. (2015). *The Palaeobiology of Avalonian (Ediacaran) Rangeomorphs*. PhD thesis. University of Cambridge. Cambridge, UK.

Kneller, B. C., & McCaffrey, W. D. (2003). The interpretation of vertical sequences in turbidite beds: the influence of longitudinal flow structure. *Journal of Sedimentary Research*, 73(5), 706-713.

Knoll, A. H., & Carroll, S. B. (1999). Early animal evolution: emerging views from comparative biology and geology. *Science*, 284(5423), 2129-2137.

Knoll, A. H., Walter, M. R., Narbonne, G. M., & Christie-Blick, N. (2004). A new period for the geologic time scale. *Science*, 305(5684), 621-622.

Knoll, A. H., Javaux, E. J., Hewitt, D., & Cohen, P. (2006). Eukaryotic organisms in Proterozoic oceans. *Philosophical Transactions of the Royal Society B: Biological Sciences*, 361(1470), 1023-1038.

Kostaschuk, R., Nasr-Azadani, M. M., Meiburg, E., Wei, T., Chen, Z., Negretti, M. E., ... & Parsons, D. R. (2018). On the causes of pulsing in continuous turbidity currents. *Journal of Geophysical Research: Earth Surface*, 123(11), 2827-2843.

LaFlamme, M. A. R. C., Narbonne, G. M., & Anderson, M. M. (2004). Morphometric analysis of the Ediacaran frond *Charniodiscus* from the Mistaken Point Formation, Newfoundland. *Journal of Paleontology*, 78(5), 827-837.

Laflamme, M., & Narbonne, G. M. (2008). Ediacaran fronds. *Palaeogeography, Palaeoclimatology, Palaeoecology*, 258(3), 162-179.

Laflamme, M., Xiao, S., & Kowalewski, M. (2009). Osmotrophy in modular Ediacara organisms. *Proceedings of the National Academy of Sciences*, 106(34), 14438-14443.

Laflamme, M., Schiffbauer, J. D., Narbonne, G. M., & Briggs, D. E. (2011). Microbial biofilms and the preservation of the Ediacara biota. *Lethaia*, 44(2), 203-213.

Laflamme, M., Flude, L. I., & Narbonne, G. M. (2012). Ecological tiering and the evolution of a stem: the oldest stemmed frond from the Ediacaran of Newfoundland, Canada. *Journal of Paleontology*, 86(2), 193-200.

Laflamme, M., Darroch, S. A., Tweedt, S. M., Peterson, K. J., & Erwin, D. H. (2013). The end of the Ediacara biota: Extinction, biotic replacement, or Cheshire Cat?. *Gondwana Research*, 23(2), 558-573.

Landing, E. (1994). Precambrian-Cambrian boundary global stratotype ratified and a new perspective of Cambrian time. *Geology*, 22(2), 179-182.

Liu, A. G., McIlroy, D., & Brasier, M. D. (2010). First evidence for locomotion in the Ediacara biota from the 565 Ma Mistaken Point Formation, Newfoundland. *Geology*, 38(2), 123-126.

Liu, A. G. 2011. Understanding the Ediacaran Assemblages of Avalonia: a palaeoenvironmental, taphonomic and ontogenetic study. PhD thesis. University of Oxford. Oxford, U.K.

Liu, A. G., McIlroy, D., Antcliffe, J. B., & Brasier, M. D. (2011). Effaced preservation in the Ediacara biota and its implications for the early microfossil record. *Palaeontology*, 54(3), 607-630.

Liu, A. G., McIlroy, D., Matthews, J. J., & Brasier, M. D. (2012). A new assemblage of juvenile Ediacaran fronds from the Drook Formation, Newfoundland. *Journal of the Geological Society*, 169(4), 395-403.

Liu, A. G., Matthews, J. J., Menon, L. R., McIlroy, D., & Brasier, M. D. (2014). *Haootia quadriformis* n. gen., n. sp., interpreted as a muscular cnidarian impression from the Late Ediacaran period (approx. 560 Ma). *Proceedings of the Royal Society B*, 281, 20141202.

Liu, A. G., Kenchington, C. G., & Mitchell, E. G. (2015). Remarkable insights into the paleoecology of the Avalonian Ediacaran macrobiota. *Gondwana Research*, 27(4), 1355-1380.

Liu, A. G. (2016). Framboidal pyrite shroud confirms the 'death mask' model for moldic preservation of Ediacaran soft-bodied organisms. *Palaios*, 31(5), 259-274.

Liu, A. G., & Dunn, F. S. (2020). Filamentous connections between Ediacaran fronds. *Current Biology*, 30(7), 1322-1328.

MacGabhann, B. A., Schiffbauer, J. D., Hagadorn, J. W., Van Roy, P., Lynch, E. P., Morrison, L., & Murray, J. (2019). Resolution of the earliest metazoan record: Differential taphonomy of Ediacaran and Paleozoic fossil molds and casts. *Palaeogeography, Palaeoclimatology, Palaeoecology*, 513, 146-165.

Matthews, J. J., Liu, A. G., Yang, C., McIlroy, D., Levell, B., & Condon, D. J. (2021). A chronostratigraphic framework for the rise of the Ediacaran macrobiota: new constraints from Mistaken Point Ecological Reserve, Newfoundland. *Geological Society of America Bulletin*, 133(3-4), 612-624.

Mason, S. J., Narbonne, G. M., Dalrymple, R. W., & O'Brien, S. J. (2013). Paleoenvironmental analysis of Ediacaran strata in the Catalina Dome, Bonavista Peninsula, Newfoundland. *Canadian Journal of Earth Sciences*, 50(2), 197-212.

McIlroy, D., & Horák, J. M. (2006). Neoproterozoic: the late Precambrian terranes that formed Eastern Avalonia. in *The Geology of England and Wales*. Editors P. R. Brenchley and P. F. Rawson. Bath, UK. Geological Society 1434 Publishing House, 9–25.

McIlroy, D., & Logan, G. A. (1999). The impact of bioturbation on infaunal ecology and evolution during the Proterozoic-Cambrian transition. *Palaios*, 14(1), 58-72.

McIlroy, D., Hawco, J., McKean, C., Nicholls, R., Pasinetti, G., & Taylor, R. (2020). Palaeobiology of the reclining rangeomorph *Beothukis* from the Ediacaran Mistaken Point Formation of southeastern Newfoundland. *Geological Magazine*, 159(7), 1160-1174.

McIlroy, D., Dufour, S. C., Taylor, R., & Nicholls, R. (2021). The role of symbiosis in the first colonization of the seafloor by macrobiota: insights from the oldest Ediacaran biota (Newfoundland, Canada). *Biosystems*, 205, 104413.

McIlroy, D., Pérez-Pinedo, D., Pasinetti, G., McKean, C., Taylor, R. S., & Hiscott, R. N. (2022). Rheotropic epifaunal growth, not felling by density currents, is responsible for many Ediacaran fossil orientations at Mistaken Point. *Frontiers in Earth Science*, 10, 849194.

McIlroy, D., Pasinetti, G., Pérez-Pinedo, D., McKean, C., Dufour, S. C., Matthews, J. J., ... & Taylor, R. S. (2024). The palaeobiology of two crown group cnidarians: *Haootia quadriformis* and *Mamsetia manunis* gen. et sp. nov. from the Ediacaran of Newfoundland, Canada. *Life*, 14(9), 1096.

McKean, C., Taylor, R. S., & McIlroy, D. (2023). New taphonomic and sedimentological insights into the preservation of high-relief Ediacaran fossils at Upper Island Cove, Newfoundland. *Lethaia*, 56(4), 1-17.

Mitchell, E. G., Kenchington, C. G., Liu, A. G., Matthews, J. J., & Butterfield, N. J. (2015). Reconstructing the reproductive mode of an Ediacaran macro-organism. *Nature*, 524(7565), 343-346.

Mitchell, E. G., Harris, S., Kenchington, C. G., Vixseboxse, P., Roberts, L., Clark, C., ... & Wilby, P. R. (2019). The importance of neutral over niche processes in structuring Ediacaran early animal communities. *Ecology Letters*, 22(12), 2028-2038.

Mitchell, E. G., Bobkov, N., Bykova, N., Dhungana, A., Kolesnikov, A. V., Hogarth, I. R., ... & Grazhdankin, D. V. (2020). The influence of environmental setting on the community ecology of Ediacaran organisms. *Interface Focus*, 10(4), 20190109.

Mitchell, E. G., & Kenchington, C. G. (2018). The utility of height for the Ediacaran organisms of Mistaken Point. *Nature Ecology & Evolution*, 2(8), 1218-1222.

Mitchell, E. G., & Butterfield, N. J. (2018). Spatial analyses of Ediacaran communities at Mistaken Point. *Paleobiology*, 44(1), 40-57.

Murphy, J. B., Pisarevsky, S. A., Nance, R. D., & Keppie, J. D. (2004). Neoproterozoic—Early Paleozoic evolution of peri-Gondwanan terranes: implications for Laurentia-Gondwana connections. *International Journal of Earth Sciences*, 93, 659-682.

Narbonne, G. M. (2004). Modular construction of early Ediacaran complex life forms. *Science*, 305(5687), 1141-1144.

Narbonne, G. M., & Aitken, J. D. (1990). Ediacaran fossils from the Sekwi Brook area, Mackenzie Mountains, northwestern Canada. *Palaeontology*, 33(4), 945-980.

Narbonne, G. M., & Gehling, J. G. (2003). Life after snowball: the oldest complex Ediacaran fossils. *Geology*, 31(1), 27-30.

Narbonne, G. M. (2005). The Ediacara biota: Neoproterozoic origin of animals and their ecosystems. *Annual Review of Earth and Planetary Science*, 33(1), 421-442.

Narbonne, G. M., Laflamme, M., Greentree, C., & Trusler, P. (2009). Reconstructing a lost world: Ediacaran rangeomorphs from Spaniard's Bay, Newfoundland. *Journal of Paleontology*, 83(4), 503-523.

Narbonne, G. M., Xiao, S., Shields, G. A., & Gehling, J. G. (2012). The Ediacaran Period. *The geologic time scale*, 1, 413-435.

Narbonne, G. M., Laflamme, M., Trusler, P. W., Dalrymple, R. W., & Greentree, C. (2014). Deep-water Ediacaran fossils from northwestern Canada: taphonomy, ecology, and evolution. *Journal of Paleontology*, 88(2), 207-223.

Nichols, G. (2009). *Sedimentology and stratigraphy*. Blackwell Science Ltd., London

Noble, S. R., Condon, D. J., Carney, J. N., Wilby, P. R., Pharaoh, T. C., & Ford, T. D. (2015). U-Pb geochronology and global context of the Charnian Supergroup, UK: constraints on the age of key Ediacaran fossil assemblages. *Geological Society of America Bulletin*, 127(1-2), 250-265.

O'Brien, S. J., & King, A. F. (2004). Ediacaran fossils from the Bonavista Peninsula (Avalon Zone), Newfoundland: Preliminary descriptions and implications for regional correlation. *Current Research (2004) Newfoundland Department of Mines and Energy. Geological Survey, Report*, 4(1), 203-212.

O'Brien, S. J., & King, A. F. (2005). Late Neoproterozoic (Ediacaran) stratigraphy of Avalon Zone sedimentary rocks, Bonavista Peninsula, Newfoundland. *Current Research, Newfoundland and Labrador Department of Natural Resources Geological Survey*, 5(1), 101-113.

Paterson, J. R., Gehling, J. G., Droser, M. L., & Bicknell, R. D. (2017). Rheotaxis in the Ediacaran epibenthic organism *Parvancorina* from South Australia. *Scientific Reports*, 7(1), 45539.

Pasinetti, G., & McIlroy, D. (2023). Palaeobiology and taphonomy of the rangeomorph *Culmofrons plumosa*. *Palaeontology*, 66(4), e12671.

Petrie, B. (1975). M2 surface and internal tides on the Scotian Shelf and slope. *Journal of Marine Research*, 33, 303–323.

Pflug, H. D. (1972). Systematik der jung-präkambrischen Petalonamae Pflug 1970. *Paläontologische Zeitschrift*, 46, 56-67.

Pisarevsky, S. A., McCausland, P. J., Hodych, J. P., O'Brien, S. J., Tait, J. A., & Murphy, J. B. (2012). Paleomagnetic study of the late Neoproterozoic Bull Arm and Crown Hill formations (Musgravetown Group) of eastern Newfoundland: implications for Avalonia and West Gondwana paleogeography. *Canadian Journal of Earth Sciences*, 49(1), 308-327.

Pu, J. P., Bowring, S. A., Ramezani, J., Myrow, P., Raub, T. D., Landing, E., ... & Macdonald, F. A. (2016). Dodging snowballs: Geochronology of the Gaskiers glaciation and the first appearance of the Ediacaran biota. *Geology*, 44(11), 955-958.

Rahman, I. A., Darroch, S. A., Racicot, R. A., & Laflamme, M. (2015). Suspension feeding in the enigmatic Ediacaran organism *Tribrachidium* demonstrates complexity of Neoproterozoic ecosystems. *Science Advances*, 1(10), e1500800.

Rhein, M., Stramma, L., & Send, U. (1995). The Atlantic deep western boundary current: Water masses and transports near the equator. *Journal of Geophysical Research: Oceans*, 100(C2), 2441-2457.

Richards, T. A., & Talbot, N. J. (2018). Osmotrophy. *Current Biology*, 28(20), R1179-R1180.

Seilacher, A. (1989). Vendozoa: organismic construction in the Proterozoic biosphere. *Lethaia*, 22(3), 229-239.

Seilacher, A. (1992). Vendobionta and Psammocorallia: lost constructions of Precambrian evolution. *Journal of the Geological Society, London*, 149(4), 607-613.

Seilacher, A. (1999). Biomat-related lifestyles in the Precambrian. *Palaios*, 14(1), 86-93.

Shen, B., Dong, L., Xiao, S., & Kowalewski, M. (2008). The Avalon explosion: evolution of Ediacara morphospace. *Science*, 319(5859), 81-84.

Sperling, E. A., Peterson, K. J., & Laflamme, M. (2011). Rangeomorphs, *Thectardis* (Porifera?) and dissolved organic carbon in the Ediacaran oceans. *Geobiology*, 9(1), 24-33.

Sprigg, R. C. (1949). Early Cambrian 'jellyfishes' of Ediacara, South Australia, and Mount John, Kimberley District, Western Australia. *Transactions of the Royal Society of South Australia*, 73(1), 72-99.

Stephenson, N. P., Delahooke, K. M., Barnes, N., Rideout, B. W., Kenchington, C. G., Manica, A., & Mitchell, E. G. (2024). Morphology shapes community dynamics in early animal ecosystems. *Nature Ecology & Evolution*, 1-10.

Steinmetz, P. R. (2019). A non-bilaterian perspective on the development and evolution of animal digestive systems. *Cell and Tissue Research*, 377(3), 321-339.

Tarhan, L. G., Droser, M. L., & Gehling, J. G. (2010). Taphonomic controls on Ediacaran diversity: uncovering the holdfast origin of morphologically variable enigmatic structures. *Palaios*, 25(12), 823-830.

Tarhan, L. G., Droser, M. L., Gehling, J. G., & Dzaugis, M. P. (2015). Taphonomy and morphology of the Ediacara form genus *Aspidella*. *Precambrian Research*, 257, 124-136.

Taylor, R. S., Nicholls, R., Neville, J. M., & McIlroy, D. (2023). Morphological variation in the rangeomorph organism *Fractofusus misrai* from the Ediacaran of Newfoundland, Canada. *Geological Magazine*, 160(1), 146-166.

Vixseboxse, P. B., Kenchington, C. G., Dunn, F. S., & Mitchell, E. G. (2021). Orientations of Mistaken Point fronds indicate morphology impacted ability to survive turbulence. *Frontiers in Earth Science*, 9, 762824.

Wade, M., 1972. *Dickinsonia*: polychaete worms from the late Precambrian Ediacara fauna, South Australia. *Memoirs of the Queensland Museum*, 16, 171–190.

Waggoner, B. (2003). The Ediacaran biotas in space and time. *Integrative and Comparative Biology*, 43(1), 104-113.

Walcott, C.D., 1914. Cambrian geology and paleontology II. *Smithsonian Miscellaneous Collections* 57, 14.

Wacey, D., Kilburn, M. R., Saunders, M., Cliff, J. B., Kong, C., Liu, A. G., Matthews, J. J., & Brasier, M. D. (2015). Uncovering framboidal pyrite biogenicity using nano-scale CNorg mapping. *Geology*, 43(1), 27-30.

Wang, X., Liu, A. G., Chen, Z., Wu, C., Liu, Y., Wan, B., Pang, K., Zhou, C., Yuan, X., & Xiao, S. (2024). A late-Ediacaran crown-group sponge animal. *Nature*, 630, 905-911.

Wen, B., Evans, D. A., Anderson, R. P., & McCausland, P. J. (2020). Late Ediacaran paleogeography of Avalonia and the Cambrian assembly of West Gondwana. *Earth and Planetary Science Letters*, 552, 116591.

Wood, D. A., Dalrymple, R. W., Narbonne, G. M., Gehling, J. G., & Clapham, M. E. (2003). Paleoenvironmental analysis of the late Neoproterozoic Mistaken Point and Trepassey formations, southeastern Newfoundland. *Canadian Journal of Earth Sciences*, 40(10), 1375-1391.

Xiao, S., & Laflamme, M. (2009). On the eve of animal radiation: phylogeny, ecology and evolution of the Ediacara biota. *Trends in Ecology & Evolution*, 24(1), 31-40.

Zhao, Y., Liu, Z., Zhang, Y., Li, J., Wang, M., Wang, W., & Xu, J. (2015). In situ observation of contour currents in the northern South China Sea: Applications for deepwater sediment transport. *Earth and Planetary Science Letters*, 430, 477-485.

## **CHAPTER 2 - *Charniodiscus* and *Arborea* are separate genera within the Arboreomorpha: using the holotype of *C. concentricus* to resolve a taphonomic/taxonomic tangle**

Daniel Pérez-Pinedo<sup>1\*</sup>, Christopher McKean<sup>1</sup>, Rod Taylor<sup>1</sup>, Robert Nicholls<sup>2</sup> and Duncan McIlroy<sup>1</sup>

<sup>1</sup> Department of Earth Sciences, Memorial University of Newfoundland, St. John's, NL, Canada,

<sup>2</sup> Paleocreations, Bristol, United Kingdom

\* Corresponding author: Daniel Pérez-Pinedo [dperezpinedo@mun.ca](mailto:dperezpinedo@mun.ca) 0000-0001-5607-1164

### **PREFACE:**

This paper has been published in the international scientific peer-reviewed journal *Frontiers in Earth Sciences* ([doi.org/10.3389/feart.2021.785929](https://doi.org/10.3389/feart.2021.785929)) as an original research article as of 19<sup>th</sup> January 2022. The paper is available from the section Paleontology as a part of the research topic Precambrian paleontology. This chapter has been formatted according to the guidelines for thesis submission and is otherwise identical to the original publication. When found, typos and similar non-substantial corrections have been made. Conceptualization, D.P-P., and D.M; methodology, D.P-P., and D.M; investigation, DP.-P., C.M., R.T., R.N., and D.M; figures, D.P-P., and C.M; project administration, D.P-P., and D.M; writing, D.P-P., with editorial input by C.M., R.T., R.N., and D.M; funding acquisition, D.M.

Reference: Pérez-Pinedo, D., McKean, C., Taylor, R., Nicholls, R., & McIlroy, D. (2022). *Charniodiscus* and *Arborea* are separate genera within the Arboreomorpha: using the holotype of *C. concentricus* to resolve a taphonomic/taxonomic tangle. *Frontiers in Earth Science*, 9, 785929.

## ABSTRACT

*Charniodiscus* is one of the most iconic and first described of the Ediacaran frondose taxa. Since the diagnosis of the holotype of *C. concentricus* in 1958, the scarcity and poor preservation of unequivocal specimens has resulted in genus-level taxonomic uncertainty. Since the recent reinterpretation of *C. concentricus* as a multifoliate frond, other *Charniodiscus* species—all of which are bifoliate—have been left in taxonomic limbo, with most authors comparing them to the clade Arboreomorpha and also the Rangeomorpha. Reconsideration of the taphonomy of the holotype of *C. concentricus* has revealed that the frond is bifoliate as first described, and also that the frondose portion was broadly conical rather than planar as previously inferred. The conical frond of *Charniodiscus* is thus morphologically quite different from all other frondose taxa within the Arboreomorpha. Our emendation of the generic diagnosis of *Charniodiscus* to encompass bifoliate arboreomorphs with conical fronds without a backing sheet distinguishes *Charniodiscus concentricus* and *C. procerus* from more planar leaf-like arboreomorphs such as *Arborea arborea*, *A. longa* and *A. spinosa*, all of which have a distinctive backing sheet. Additionally, we find no evidence of rangeomorph-type fractal branching in *Charniodiscus*.

**Key words:** *Charniodiscus*, *Arborea*, holotype, taxonomy, taphonomy, Ediacaran, Avalon

## 2.1 INTRODUCTION

*Charniodiscus* Ford, 1958 was one of the first described fossils from the Ediacaran and is one of the most iconic—and most often illustrated—of the frondose Ediacaran taxa. The type species of the genus, *Charniodiscus concentricus*, was described from Charnwood Forest, UK (Ford 1958) (Figure 2.1). *C. concentricus* was originally described as an organ taxon i.e., the disc part of *Charnia masoni* (Ford 1958), but subsequently as a bifoliate frond with a stem and a basal disc (Ford 1963). However, more recently consensus has shifted towards it being a multifoliate frond (Dzik 2002, 2003; Brasier and Antcliffe 2009; Liu et al. 2017). The genus has been compared to both the Rangeomorpha (Brasier et al. 2012) and the Arboreomorpha (Erwin et al. 2011) with current consensus being that most, if not all, *Charniodiscus* species are arboreomorphs (e.g., Laflamme et al. 2018; Dunn et al. 2019). The commonly accepted species of *Charniodiscus* include *C. concentricus* Ford 1958; *C. longus* Glaessner and Wade 1966; *C. yorgensis* Borchardt and Nesson 1999; *C. procerus* Laflamme et al. 2004; and *C. spinosus* Laflamme et al. 2004 (Figure 2.2).

The taxonomy of *Charniodiscus* remains incompletely resolved in large part due to the complex preservation of the type species of *Charniodiscus* (cf. Brasier and Antcliffe 2009; Brasier et al. 2012; Figure 2.3). While some species previously described as *Charniodiscus* are currently considered to be arboreomorphs (e.g., *Arborea*) (Laflamme et al. 2018; Dunn et al. 2019), those works have not addressed the morphology and taphonomy of the type species of the genus directly. *Charniodiscus* has been reported to have a worldwide distribution from sites in: Charnwood Forest, UK (e.g., Ford 1958, 1962, 1963; Wilby et al. 2011); South Australia (e.g., Glaessner and Daily 1959; Glaessner and Wade 1966; Jenkins and Gehling 1978; Gehling 1991; Jenkins 1992—though most of these occurrences are now considered to be *Arborea*); the White Sea region of

Russia (Fedonkin 1985; Ivantsov 2016); north-western Canada (Narbonne and Hofmann 1987); and Newfoundland, Canada (e.g., Jenkins 1992; Seilacher 1992; Hofmann et al. 2008). *Charniodiscus* is thus a cosmopolitan taxon whose taxonomy and relationship to the somewhat similar *Arborea* is of global relevance. This study aims to improve palaeobiological understanding of the common species within *Charniodiscus* by reconsideration of the taphonomy and morphology of the type material from Charnwood Forest, UK, and the abundant *Charniodiscus* of the Newfoundland Ediacaran biotas of the Avalon and Bonavista peninsulas.

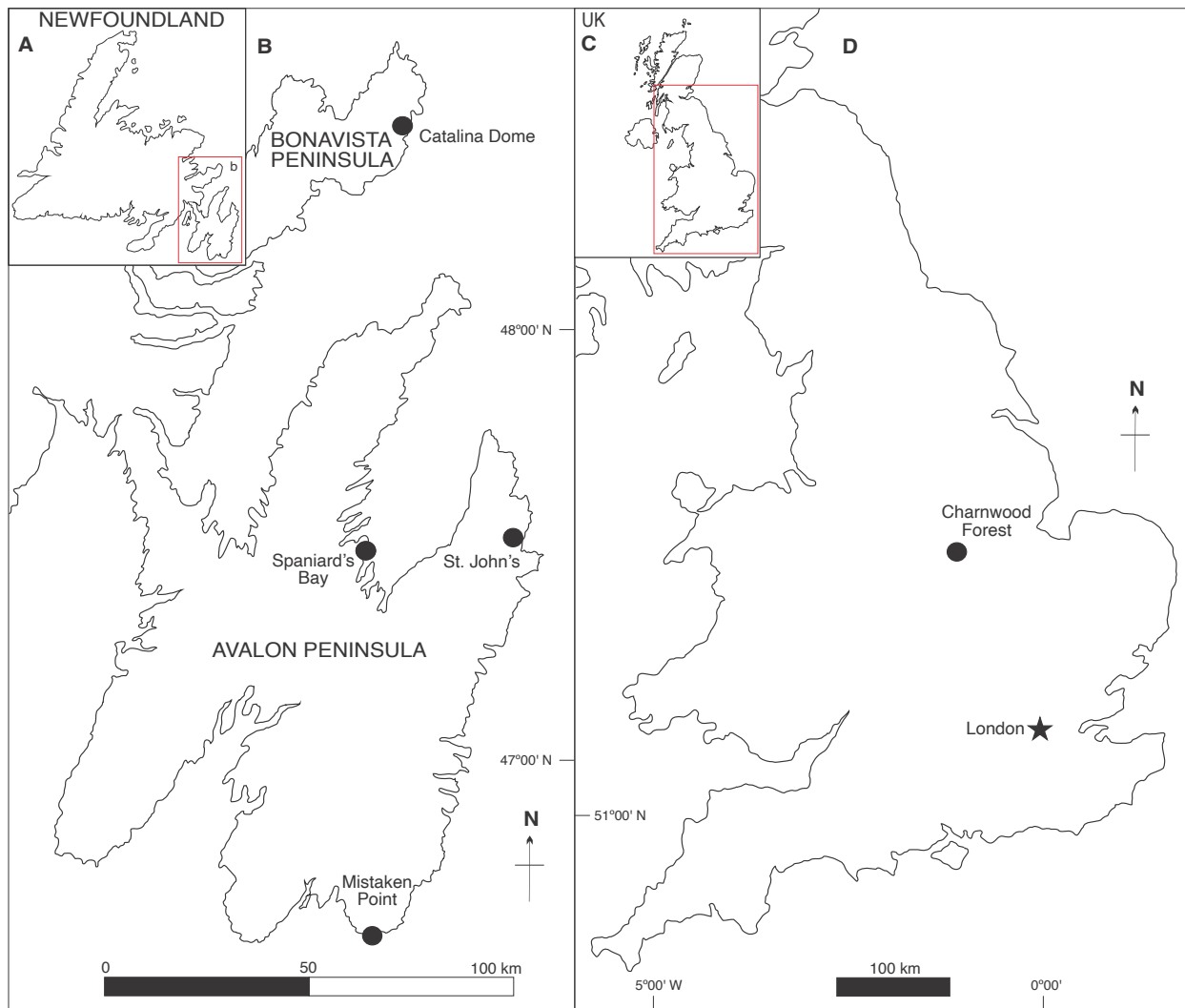


Figure 2.1: Map of some of the most relevant Avalonian fossil assemblages (black circles). A) General map of Newfoundland, Atlantic Canada. B) Detail of the Avalon and Bonavista Peninsulas. C) General map of the United Kingdom. D) Detail of England.

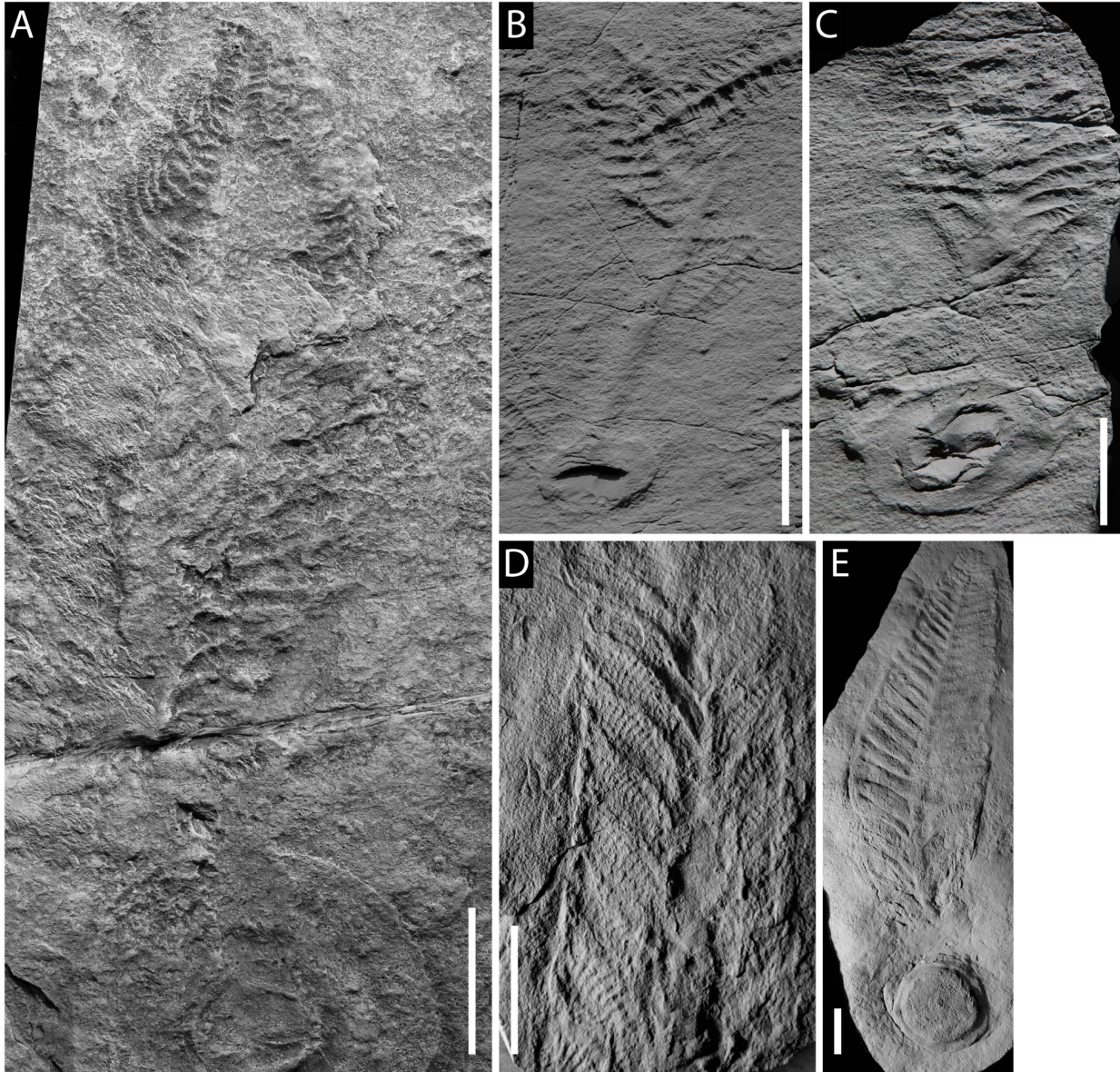


Figure 2.2: Casts of relevant *Charniodiscus* species. A) *C. concentricus* holotype (LEIUG 2383) from Charnwood Forest, UK. B,C) *C. procerus* and *C. spinosus* respectively from the upper part of the Mistaken Point Formation (E Surface) at Mistaken Point, Newfoundland. Jesmonite cast of field specimens. D,E) *C. longus* cast (SAM P13777) and *C. arboreus* (*Arborea*) cast

(OUMNH AW.00043/p) respectively from Ediacara, South Australia. Scale bars 3 cm. Not retrodeformed.

### **2.1.1 Preservation in the Avalon Assemblage**

During periods of low sedimentation rates or hiatus, Ediacaran seafloors were commonly colonized by microbial matgrounds, likely mainly photosynthetic in shallow marine settings and chemosynthetic or chemoheterotrophic in deep marine settings. Matgrounds in waters of all depths in the Ediacaran were exceptionally well developed and well preserved, owing to the rarity of motile macrobionts (e.g., Liu et al. 2010), macrobioturbation (McIlroy and Logan 1999), and ecosystem services like scavenging and grazing (Herringshaw et al. 2017); this would also have led to the persistence of abundant seafloor necromass (Liu et al. 2011; McIlroy et al. 2021). The importance of matgrounds for soft bodied preservation of Ediacaran organisms has been extensively explored based around the death mask model of mouldic preservation proposed by Gehling (1999) and extended to encompass aspects of early diagenetic mineralization (Mapstone and McIlroy 2006; Liu 2016) and preservation as original carbonaceous compressions (e.g., Steiner and Reitner 2001; Xiao et al. 2002). The role of sedimentological parameters as they interface with taphonomic processes in taphonomy is pivotal but remains under-studied (Kenchington and Wilby 2014).

The Avalon Assemblage (Waggoner 2003) is the oldest of the Ediacaran assemblages. The earliest known Ediacaran fossils are from deep marine volcanoclastic settings of the Avalon Terrane in Newfoundland spanning at least the interval ca. 574–564 Ma (Matthews et al. 2021) and Charnwood Forest, UK, (Noble et al. 2015). These successions form part of the peri-Gondwanan Avalonian volcanic arc system (Murphy et al. 2004; McIlroy and Horák 2006; Wen

et al. 2020) and predominantly consist of turbidites and laterally extensive tuffites (McIlroy et al. 1998; Wood et al. 2003; Matthews et al. 2021). The soft bodied Ediacaran fossils are typically preserved as impressions on top of volcanoclastic siltstones, particularly where they are overlain by tuffites (Narbonne 2005; Liu et al. 2015; Matthews et al. 2021). Positive epireliefs are the most common mode of preservation for stems and some basal discs of frondose organisms, which implies that they maintained their integrity long enough for lithification of the overlying tuff. Negative epirelief moulds are typically associated with the less resistant frondose portions of quasi- infaunal reclining organisms (permanently affixed to the seafloor), produced by smothering of matgrounds by dead/ felled erect or recumbent (parallel and elevated above the seafloor in a windsock-like manner) organisms (McIlroy et al. 2009) or by sediment-displacing growth of quasi-infaunal reclining organisms (McIlroy et al. 2020; Taylor et al. 2021; McIlroy et al. 2021) (Figure 2.4). Soft bodied Ediacaran taphonomic style is influenced by a combination of: 1) differential decomposition rates of labile vs relatively refractory body tissues; 2) the influence of currents and related sedimentary processes; 3) body posture in life; and 4) the nature of seafloor microbial matgrounds associated with the organism in life (e.g., Wade 1968; Gehling 1999; Narbonne 2005; McIlroy et al. 2020, McIlroy et al. 2021).

Aside from the holotype of the type species of *Charniodiscus* (Charnwood Forest, UK) most of the specimens of the genus are known from Newfoundland and have been described from either Mistaken Point (Laflamme et al. 2004) or the Catalina Dome (Hofmann et al. 2008). In both locations, the top surfaces of the basal discs and stems—as well as the junction between them—are commonly preserved as positive epireliefs whereas the frondose portions commonly lie beneath the ambient bedding plane. This suggests preservation by matground smothering (McIlroy et al. 2009; Figure 2.4) with sharp ridges occurring due to post-mortem sediment infiltration

between frondose elements. In the younger Charnian assemblage of the UK the Ediacaran biotas are typically preserved as very low negative and positive epirelief impressions on fine-grained surfaces under a thin tuffaceous layer (Brasier and Antcliffe 2009; Wilby et al. 2011), like the Conception-type preservation (Narbonne 2005). This assemblage shares some genera with Newfoundland, but like Newfoundland also includes several endemic taxa.

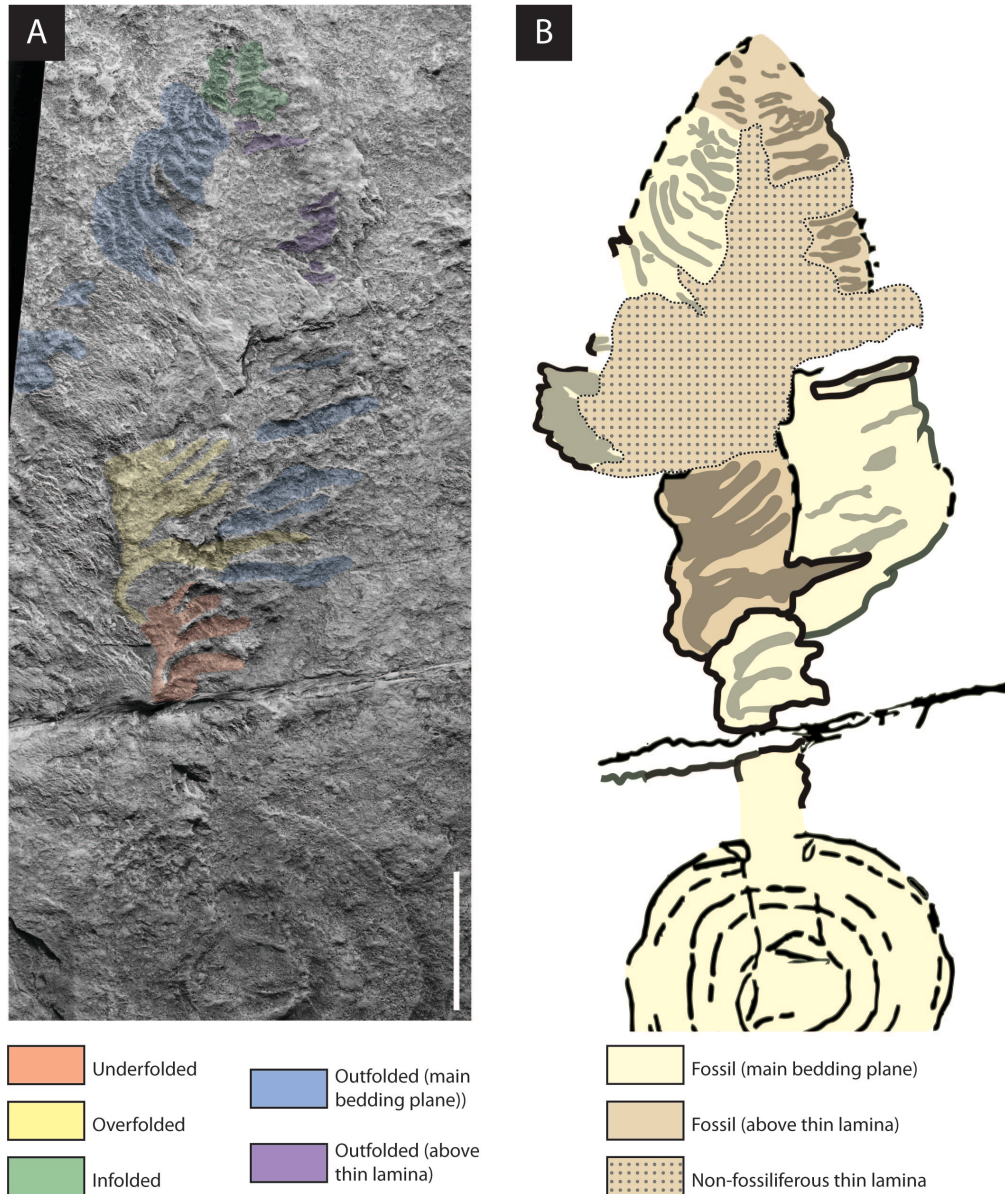


Figure 2.3: Preservation of the holotype of *C. concentricus* (LEIUG 2383) from Charnwood Forest, UK. A) Differential branch folding; underfolded (orange), overfolded (yellow), outfolded (blue and purple) and infolded (green). B) Interpretive drawing of the fossil showing features preserved in different bedding planes; main bedding plane (yellow), above bedding plane (brown), and non-fossiliferous sediment (dotted brown pattern). Scale bar 3 cm. Not retrodeformed.

### **2.1.2 Previous taphonomic/morphological consideration of the *Charniodiscus concentricus* holotype**

Arboreomorpha (Erwin et al. 2011; cf. the Frondomorpha of Grazhdankin 2014) encompasses numerous frondose species that lack the fractal-like branching of the Rangeomorpha (Narbonne 2004; Brasier and Antcliffe 2004, Brasier and Antcliffe 2009). Arboreomorphs are characterized by arboreomorph branching architecture in which rows of primary branches project from the central stalk extending to an outer rim and may have transverse structures called second order branches (Laflamme and Narbonne 2008; Erwin et al. 2011). The clade encompasses two genera, *Charniodiscus* and *Arborea*, whose taxonomic relationship has hitherto been confused. Some authors have considered *Arborea* to be a junior synonym of *Charniodiscus* on the basis of similar gross morphology (Glaessner and Daily 1959; Jenkins and Gehling 1978). The Newfoundland *Charniodiscus* species (*C. spinosus*, *C. procerus* and *C. arboreus*) have been attributed to the Arboreomorpha, but not closely related to the type species of *Charniodiscus* (e.g., Laflamme et al. 2004; Hofmann et al. 2008; Liu et al. 2015), however, there has been no attempt to formally move these taxa out of *Charniodiscus*. These taxonomic interpretations are further confused by differing opinions on the morphology and taphonomy of the holotype of

*Charniodiscus concentricus* (Dzik 2002, 2003; Brasier and Antcliffe 2009). It has been suggested that *C. concentricus* is a multifoliate rangeomorph rather than an arboreomorph, albeit without observable rangeomorph branching (undivided and furled morphology cf. Brasier and Antcliffe 2009; Brasier et al. 2012), which we do not consider to be objectively testable.

*Charniodiscus concentricus* is a soft-bodied unipolar, lanceolate to ovate frondose organism consisting of a segmented frond and a cylindrical stem, which is associated with a basal disc (e.g., Brasier and Antcliffe 2009; Figure 2.2A). The term holdfast is not used herein as it implies a biomechanical function that cannot be unequivocally demonstrated. The frond presents 30 to 50 primary branches attached to both sides of the stem in either alternating or opposing arrangements. The primary branches of *C. concentricus* have secondary order bar-like transverse structures (e.g., Laflamme et al. 2004) (Figure 2.3A). There is also a pronounced curvature to the primary branches, and a notable decrease in branch width and length towards the frond apex (which has been considered a species-level difference between *C. concentricus* and *Arborea* (Jenkins and Gehling 1978; Laflamme et al. 2004). The widely accepted multifoliate nature of *C. concentricus* (Dzik 2002, 2003; Brasier and Antcliffe 2009, figure 12) is currently considered to be one of the fundamental differences between *Charniodiscus* and *Arborea* spp. (Liu et al. 2017; Dunn et al. 2019).

The holotype of *C. concentricus* combines both positive and negative epirelief impressions and includes some preservation on the tuffaceous siltstone that is at a level slightly above the main microbially-dominated bedding plane associated with the basal disc (Figure 2.3B). Both the basal disc and the stem are preserved in low positive epirelief, although the latter may be a partially collapsed remnant of what was originally a cylindrical structure. The central and distal-most sections of the frond are preserved in negative relief but at a level slightly above the main bedding

plane, while the proximal arcuate subparallel primary branches are in negative epirelief on the same surface as the basal disc and stem (Brasier and Antcliffe 2009; Figure 2.3B).

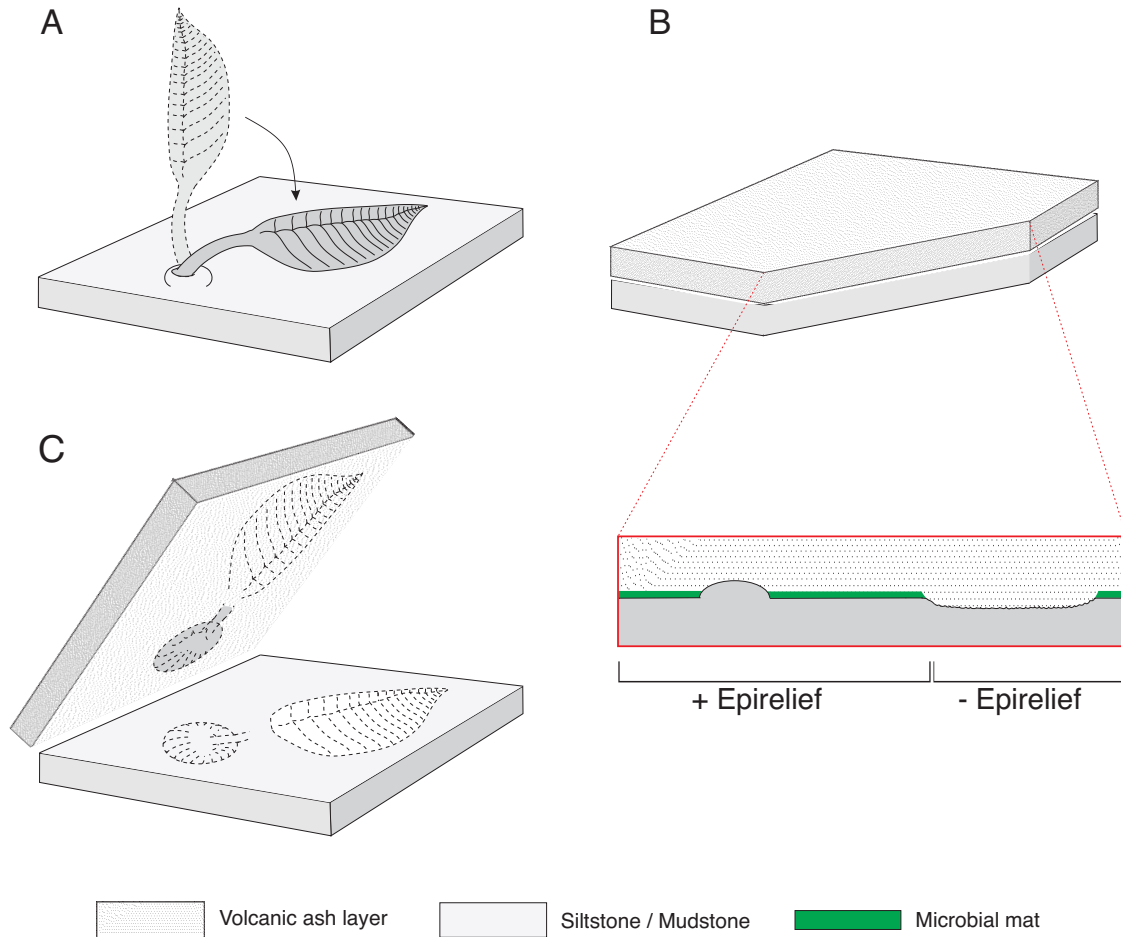


Figure 2.4: Preservation style observed in Ediacaran organisms in Avalonia. A) Felling of an undetermined erect stemmed frond. B) Transversal cut of the felled frond preserved between the underlying volcanoclastic siltstone and the overlying tuffite; close-up shows features preserved in positive and negative reliefs and smothered matground. C) Resulting reliefs in the underlying volcaniclastic siltstone and their counterparts in the tuffaceous layer.

### 2.1.3 Historical reasoning for a multifoliate *Charniodiscus concentricus*

Explanation of the biostratinomy of the *Charniodiscus* type species as a bifoliate frond in which the bottom-left part of the frond was overfolded (Jenkins and Gehling 1978, figures 4X,Y) has more recently been superseded by a multifoliate model (Dzik 2002, 2003; Brasier and Antcliffe 2009, figure 12). The multifoliate model invokes the presence of at least three foliate sheets of primary branches resembling rangeomorph branching (Brasier and Antcliffe 2009; Brasier et al. 2012).

The acceptance of the multifoliate nature of the holotype of the type species of *Charniodiscus* resulted in taxonomic inconsistencies regarding the other bifoliate species of the genus (Laflamme et al. 2018). Moreover, since there is no evidence to support fractal branching architecture, assignment of the genus to the Rangeomorpha (undivided rangeomorph branching of Brasier et al. 2012) is unsupported. The Newfoundland species of *Charniodiscus* have remained within the genus, despite the inferred multifoliate nature of the type species (Laflamme and Narbonne 2008) but have also been considered to be separate from *Arborea* based on branching criteria of Brasier et al. (2012). The need to unravel this taphonomic, and taxonomic, tangle has been mentioned in the literature by numerous authors (e.g., Brasier and Antcliffe 2009; Liu et al. 2015; Laflamme et al. 2018; Wang et al. 2020) but remains unresolved.

## **2.2 A NEW TAPHONOMIC UNDERSTANDING OF THE *CHARNIODISCUS CONCENTRICUS* HOLOTYPE**

The 8 or 9 most apical primary branches of the holotype are negative epireliefs that are short, narrow, and rounded close to the axis and are directed slightly towards the frond base. There is no central stem preserved at the tip owing to the fact that the branches are impressed into sediment lying atop the plane of the inferred axial stem (Figure 2.3A—green). These apical

branches do not have any preserved transverse ornament, which is typical of some branches of the holotype. These transverse branches could have escaped preservation thus their actual existence cannot be ruled out. The arrangement of the branches is consistent with infolding of originally curved branches resulting in the impression of the interior surface of the branch into the sediments overlying the stem. This type of infolding preservation is also common in specimens attributed to *C. arboreus* from the Catalina Dome by Hofmann et al. (2008, figure 16 7–8).

The longer arcuate branches immediately adjacent to the apex of the holotype of *C. concentricus* are strongly curved and slightly imbricated towards the tip; there is no evidence of a clearly preserved axial stem, which may also be buried in this portion of the fossil (Figure 2.3A—blue, purple). We consider that branch curvature is due to the unfolding collapse of a sub-conical frond (Figures 2.5D–I). The strongly curved branches have sharp transverse ridges formed by sediment infilling the gaps between the transverse second order branches. Since these branches are unfolded, it would suggest that in life the external surfaces of the primary order ridge-like branches are what would be impressed into the sediment, and thus that the external surfaces were covered in transverse ridges. The curved portion of the unfolded set of branches on the right is observed in a slightly higher plane than the ambient plane (Figure 2.3—purple).

Our study of the holotype supports the interpretation of the bottom-left proximal region of the frond being folded across the central axis (Jenkins and Gehling, 1978, figures 4X,Y), albeit with some modifications. We interpret the first set of proximal branches (Figures 2.3A—orange) as being underfolded beneath the stem (Figures 2.5A–C). Evidence for this underfolding comes from: 1) the underfolded branches being the topographically lowest structures preserved in the holotype; and 2) the absence of a preserved stem, which would have lain above the underfolded branches and could not therefore have been impressed into the sediment.

The presence of underfolding is important for considering the life attitude of the organism because, in order to be able to underfold the branches, the stem cannot have lain upon the sediment surface in life. This leaves an erect or recumbent lifestyle as the only realistic modes of life. Additionally, underfolding would have necessarily occurred prior to the felling of the frond. Of the branches preserved in the proximal part of the frond, these are the only ones to preserve obliquely orientated secondary units in the inner surface of the branches.

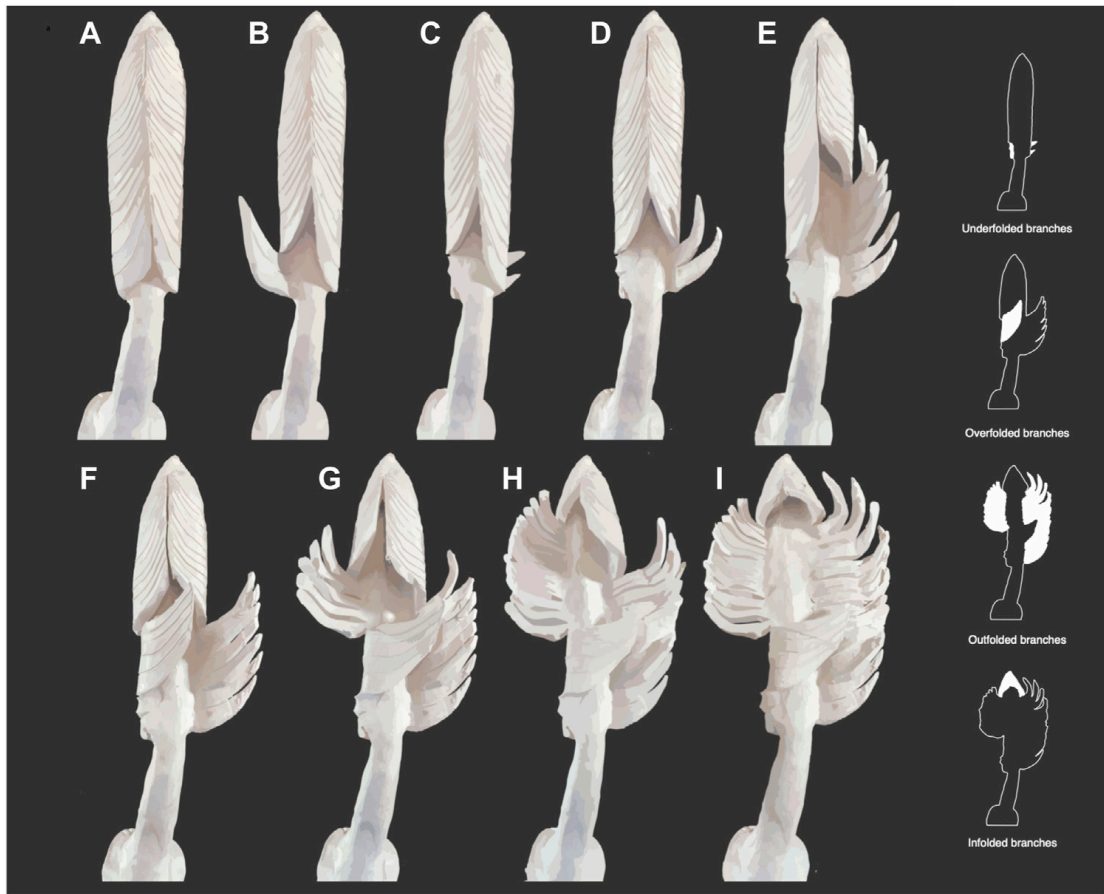


Figure 2.5: Taphonomic stop-motion model of the holotype of *C. concentricus* showing different branch folding. A–C) Underfolding of proximal-most branches. A–I) Infolding of distal-most branches. D–I) Outfolding of bottom-right and central branches. F–I) Overfolding of bottom-left branches.

The second set of proximal branches on the left-hand side of the fossil are preserved as impressions in sediment that lay at a higher level than the stem (Figures 2.3A—yellow) and above the ambient bedding plane (Figure 2.3B). The branches preserved at this higher level are the basis for inferring that *Charniodiscus* was a multifoliate frond (Dzik 2002, 2003; Brasier and Antcliffe 2009). However, we follow Jenkins and Gehling (1978) in considering that these branches were swept across the axis from left to right such that the bases of the branches are approximately aligned with the position of the stem, which we infer lay at a lower level below the sediment that casts the branches (Figures 2.5F–I). The sediment on top of the stem was either present inside the subconical frond during life, or shortly after death/felling, but before collapse and complete burial of the frond. In our model the stem is not preserved due to its position at a level below the rock surface (Figure 2.3B). The apparently smooth surface of the distal branches (Figures 2.3A—green) suggests that the inner surface of the branches may have been unornamented in the arcuate portion of the sub-conical frond.

### **2.3 EVIDENCE FOR *CHARNIODISCUS* BEING A COLLAPSED SUB-CONICAL STRUCTURE**

The marked curvature of the outfolded branches of *C. concentricus*, the straight basally-directed infolded branches of the tip, and the preservation of sediment atop the central axis of much of the frond is most consistent with the frond being a collapsed sub-conical structure with a more flattened side adjacent to the stem (Figure 2.2A). The curvature of the branches suggests that the tips of the branches met in an apically-directed zipper-like fashion on the front side of the sub-conical frond. Actualistic modeling of the frond branches as they are preserved in the holotype is consistent with the tips of the branches meeting in a chevron-like seam when reconstructed (Figure

2.5A). Since the bases of the branches meet the axis at nearly 90° it seems logical that these branches have not been greatly modified by compression; this suggests that the basal portion of the branches were rather flat, producing a flattened base to the sub-conical frond (Figures 2.5–2.7).

The pronounced curvature of the apical branches is a prominent feature of *Charniodiscus concentricus* and a significant difference between it and *Arborea* (Jenkins and Gehling 1978; Laflamme et al. 2004). Other arboreomorphs with strongly curved branches in the Avalon Assemblage include *Charniodiscus procerus* (Laflamme et al. 2004; Figure 2.6) and another unnamed *Charniodiscus* species with broad strongly arcuate branches (Figure 2.7). We consider all of these forms to be species of *Charniodiscus* and each of them probably had a similar conical frond without a “backing sheet” (sensu Dunn et al. 2019).

Arboreomorphs without pronounced branch curvature include: *Charniodiscus arboreus* (sensu Hofmann et al. 2008, figure 16 7–8); *C. longus* (Figure 2.2D); *C. oppositus*; and *C. spinosus* (Figure 2.2C). Most if not all of these taxa also have a prominent backing sheet and are thus likely to be species of *Arborea*.

We thus consider that there are two different unipolar bifoliate frond morphologies within the Arboreomorpha: 1) sub-conical fronds with arboreomorph branching and no backing sheet, typical of *Charniodiscus*; and 2) planar fronds with a prominent backing sheet on one side and arboreomorph branching on the other, which are attributable to *Arborea*.

## 2.4 SYSTEMATIC PALAEOLOGY

Phylum Indet.

Clade Arboreomorpha

Genus *Charniodiscus* Ford 1958

- 1958 *Charniodiscus concentricus* Ford, p. 212 pl. 13, fig. 2-3 (originally as a form taxon, basal disc of *Charnia*)
- 1963 *Charniodiscus concentricus* Ford, pl. 1, fig. 1 a-d
- non 1966 *Charniodiscus arboreus* Glaessner and Wade, pl. 102, fig. 1-2
- non 1966 *Charniodiscus longus* Glaessner and Wade, pl. 100, fig. 4
- non 1978 *Charniodiscus oppositus* Jenkins and Gehling, p. 204 pl. 3, fig. 4
- ? 1999 *Charniodiscus yorgensis* Borchvardt and Nesson, p. 54, text-fig. 2
- 2004 *Charniodiscus procerus* Laflamme et al., p. 830, fig. 3
- non 2004 *Charniodiscus spinosus* Laflamme et al., p. 830-831, fig. 3-4

Type species. — *Charniodiscus concentricus*, described from the Charnian Supergroup of the UK (Ford, 1958).

Emended generic diagnosis. — Unipolar frondose arboreomorphs with basal disc, stem, a bifoliate frond without a backing sheet and loosely constrained branches. The bases of the branches are commonly straight and attached to the stem at nearly right angles but are distally curved forming a sub-conical frond in life. Outer surface of the branches of the sub-conical frond has transverse ridges orthogonal to the long axis of the branches. The internal surface of the branch has similar oblique ridges close to the junction with the stem.

Discussion. — The species of *Charniodiscus* considered valid herein are *C. concentricus* and *C. procerus*. The status of *C. yorgensis* requires restudy of the type material that is beyond the scope of this study. All other taxa hitherto attributed to *Charniodiscus* (*C. arboreus*, *C. longus*, *C. oppositus*, and *C. spinosus*) should likely be considered to be species of *Arborea* but require further study and comparison with the type species (cf. Laflamme et al. 2018; Wang et al. 2020). The

branches of *C. concentricus* are considered to be homologous with the pea-pod-like units of *Arborea* (cf. Dunn et al. 2019).

*Charniodiscus concentricus* Ford 1958

1958 *Charniodiscus concentricus* Ford, p. 212 pl. 13, fig. 2-3 [as a form taxon, basal disc of *Charnia*]

1963 *Charniodiscus concentricus* Ford, pl. 1, fig.1 a-d [description of frond associated with basal disc]

1978 *Charniodiscus concentricus* Jenkins and Gehling, p. 350-352, fig. 2, 4

2002 *Charniodiscus concentricus* Dzik, p. 322 - 323

2009 *Charniodiscus concentricus* Brasier and Antcliffe, p. 375-377, fig. 12-14

2012 *Charniodiscus concentricus* Brasier et al., p. 1109-1114, fig. 3

2017 *Charniodiscus concentricus* Liu et al. fig. 3 a-c

Emended specific diagnosis. — *Charniodiscus* with basal disc, stem, and a bifoliate frond, lacking a supporting backing sheet, composed of approximately 25 independent branches that were strongly curved inward and upward in life to form a sub-conical frond, which becomes lanceolate to ovate upon collapse/compression.

Description. — *Charniodiscus concentricus* has a round basal disc bearing concentric rings without a prominent central boss, from which a broad stem emerges. The stem is short (~4 cm) and relatively poorly preserved in the holotype. The primary arboreomorph branches are attached to the lateral margins of the stem. The impression of the frond is bifoliate and lanceolate to ovate in outline (16.2 cm length: 6.3 cm wide). The external distal portion and the internal proximal section of the primary branches have secondary order transverse bar- like morphology. There is no evidence of fractal branching pattern characteristic of the Rangeomorpha.

Discussion. — The junction between the branches and the stem in the holotype *Charniodiscus concentricus* is not preserved except at the base. The stem of the holotype is poorly preserved, especially in comparison to *C. procerus* from the Newfoundland Ediacaran biota (Figure 2.6). This may relate to a combination of different tissue composition/resilience and different body postures in life. Curvature of the branches in *C. concentricus* and *C. procerus* is considerably more pronounced than in other species of the genus, occasionally leading to compromised preservation of the branches towards distal sections (Figure 2.6).

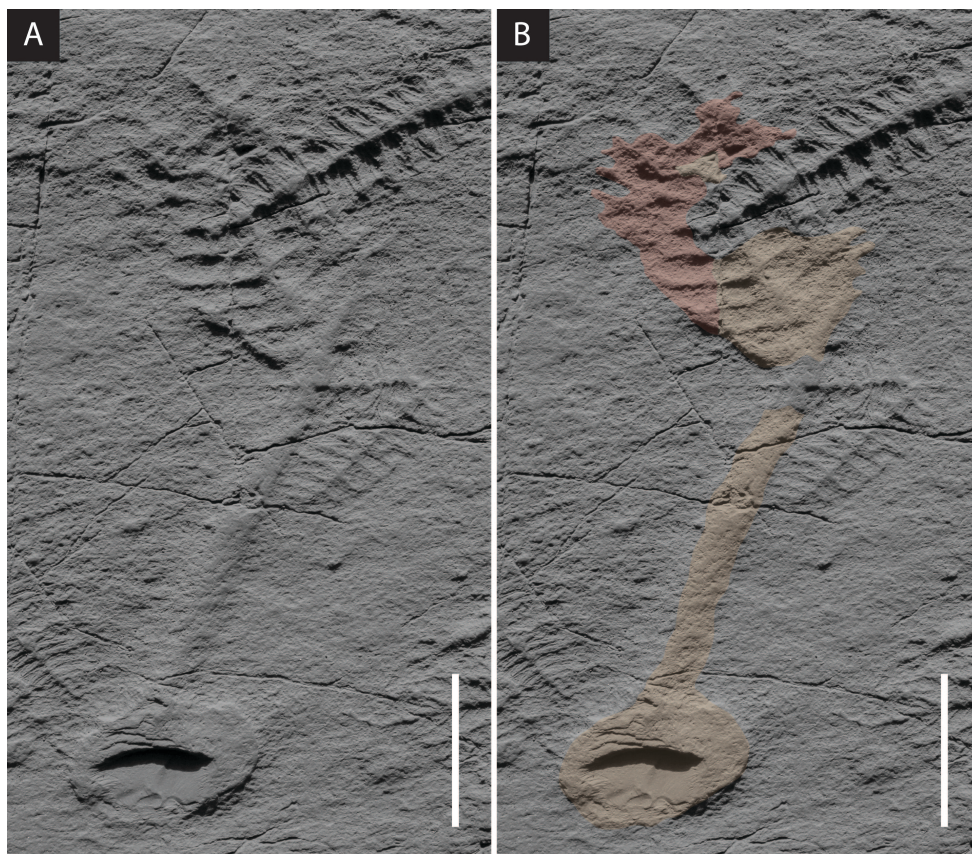


Figure 2.6: *Charniodiscus procerus* from the so-called “Seilacher’s Corner”, upper part of the Mistaken Point Formation (E Surface) at Mistaken Point, Newfoundland. A) Cast. B) Basal disc, stem and flat basal section of the branches meeting the central axis at  $\sim 90^\circ$  in orange; apical

section of the branches showing pronounced curvature in red. Scale bars 3 cm. Jesmonite cast of field specimen. Not retrodeformed.

*Charniodiscus concentricus* has parallel transverse ridges preserved in the external distal-most section of certain apical branches and in the internal side of the proximal-most section of certain proximal branches. However, there is no evidence of the fractal branching pattern which would be required to assign the genus to the Rangeomorpha (Brasier et al. 2012). Additionally, the absence of the prominent backing sheet of *Arborea* further distinguishes *Charniodiscus* from *Arborea*. Our reinterpretation of the holotype is significantly different from previous models (Ford 1958; Jenkins and Gehling 1978; Dzik 2002, 2003; Brasier and Antcliffe 2009; Brasier et al. 2012) in that the holotype is herein demonstrated to be bifoliate, non-fractal, lacking the backing sheets characteristic of *Arborea*, and having a conical shape defined by Arboreomorph-type branches (Laflamme and Narbonne 2008).

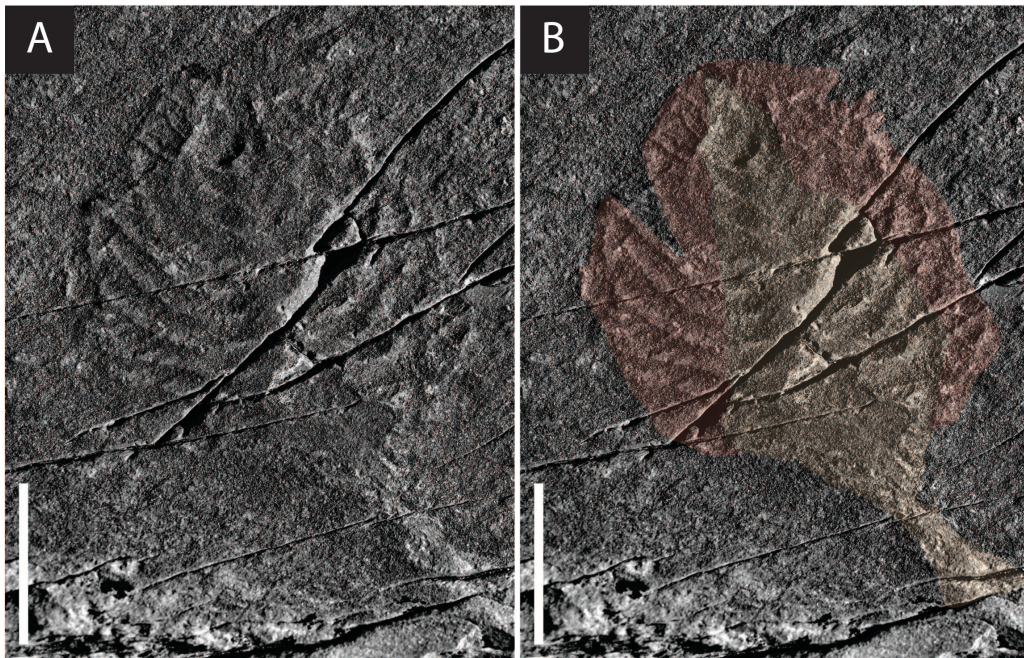


Figure 2.7: *Charniodiscus* sp. from the Mistaken Point Formation (D Surface) at Mistaken Point, Newfoundland. A) Field photograph of the specimen. B) Stem and flat basal section of the branches meeting the central axis at  $\sim 90^\circ$  in orange; apical section of the branches showing pronounced curvature in red. Scale bars 3 cm. Field photography. Not retrodeformed.

## 2.5 MODE OF LIFE OF *CHARNIODISCUS CONCENTRICUS*

Reconstructions of most frondose Ediacaran taxa have followed Glaessner (1984) in depicting them as being erect, pennatulacean-like organisms and the coining of descriptive terms such as stems, basal disc, and frondlets belies attempts to draw analogies to extant taxa (e.g., pennatulaceans, algae). This imparts an implicit bias towards palaeobiological reconstructions presenting many Ediacaran organisms as having an erect mode of life. This standard paradigm has recently been challenged (McIlroy et al. 2020, McIlroy et al. 2021), in an assertion that the null hypothesis for orientation should be the preserved (i.e., reclined on the sediment) position unless there is evidence to the contrary.

Arboreomorphs generally possess well-preserved basal discs, possibly representing anchoring structures that were partially immersed in the sediment (Burzynski and Narbonne 2015; Tarhan et al. 2015). Some discs have folds consistent with originally inflated bodies that eventually experienced collapse (Dunn et al. 2019; McIlroy et al. 2021) which might imply the presence of some form of cnidarian-like hydrostatic skeleton in life. Since some species of *Charniodiscus* and *Arborea* commonly have poor preservation of the stem, this can be taken to suggest that: 1) the stem did not lie upon the seafloor surface during preservation (i.e., stems arched upward due to the displacement of the frond allowing deposition of sediment between the stem and the bedding plane; Figure 2.4); or 2) stems of some taxa decayed more rapidly than the other tissues. The stem

of the *Charniodiscus concentricus* holotype is remarkably flat, and relatively poorly preserved. The stem, as previously interpreted, is apparently offset from the axis of the frond. We consider that this is an artifact of the underfolding of the branches under the stem, which obscures one margin of it (Figure 2.3A). There is no evidence of swing marks associated with the holotype unlike some frondose taxa (Jensen et al. 2018) and only erect (e.g., Glaessner and Daily 1959; Glaessner 1984) or recumbent (Laflamme et al. 2018) modes of life are consistent with underfolding and the commonly poor preservation of the stem. The impression of the upper parts of the branches into sediment that lay above the level of the stem strongly suggests the presence of sediment above the stem before post-mortem collapse of the frond. This taphonomic mode is consistent with a curved front surface to the bifoliate frond.

Additional evidence for sub-conical frondose arboreomorphs comes from the recent discovery of a specimen of *Charniodiscus* sp. preserved in full relief in a thin Tc sand unit immediately above the Spaniard's Bay assemblage in Newfoundland (Narbonne et al. 2009; Brasier et al. 2013). The three-dimensional morphology of the *Charniodiscus* frond can be inferred from the well-preserved collapsed sub-conical frond with indication of the transverse cross section (Figure 2.8). The frond is characterized by basally-directed infolding collapse of the frond with the junctions between the tips of opposing primary branches being well preserved. This mode of infolding collapse is also seen in the very tip of the holotype of *C. concentricus* and the partial fill of the originally sub-conical Spaniard's Bay specimen above the level of the stem is similar to that of parts of the holotype (Figures 2.3A—green). The primary branches of the Spaniard's Bay *Charniodiscus* have no evidence for fractal rangeomorph branching, further supporting the non-rangeomorph nature of *Charniodiscus*.

The most common Avalonian arboreomorph with strongly curved broad branches is *Charniodiscus procerus* (Laflamme et al. 2004, figure 3.1) which has a central triangular section adjacent to the stem that is typically well preserved as deep negative epireliefs (Figures 2.6—orange). In well preserved material, the arcuate portion of branches extends from the triangular portion in a manner similar to the more numerous very narrow branches close to the tip of *C. concentricus*. The distal curved portion of the primary branches of *C. procerus* (Figures 2.6—red) are interpreted—by analogy with *C. concentricus* and *C. sp.* from Spaniards Bay—as casts of the impressions made by the external surfaces of the curved portion of the conical frond that we consider to be typical of *Charniodiscus*.

In contrast to the flattened stem of *C. concentricus* and the poorly preserved stem of other Arboreomorphs and Rangeomorphs in the same Newfoundland assemblages (Laflamme et al. 2004; Laflamme et al. 2012), the stem of *C. procerus* is generally well preserved and covered in matground textures (Figure 2.6) and even other reclining taxa such as *Fractofusus*. As such it would seem that *C. procerus* conforms to the null hypothesis of McIlroy et al. (2020), McIlroy et al. (2021) that unless there is positive evidence to support an erect mode of life, the stem of the frond should be considered to have lain on or in the seafloor during life. However, the presence of a specimen of *Fractofusus* below the frond of one specimen may also suggest that the frondose portion may have been erect arising from the end of the reclined stem, only falling post-mortem onto the seafloor on top of the aforementioned *Fractofusus* (Figure 2.6). A second hitherto undescribed *Charniodiscus* with highly curved broad primary branches with transverse ornament is also present in the Newfoundland assemblage (Figure 2.7).

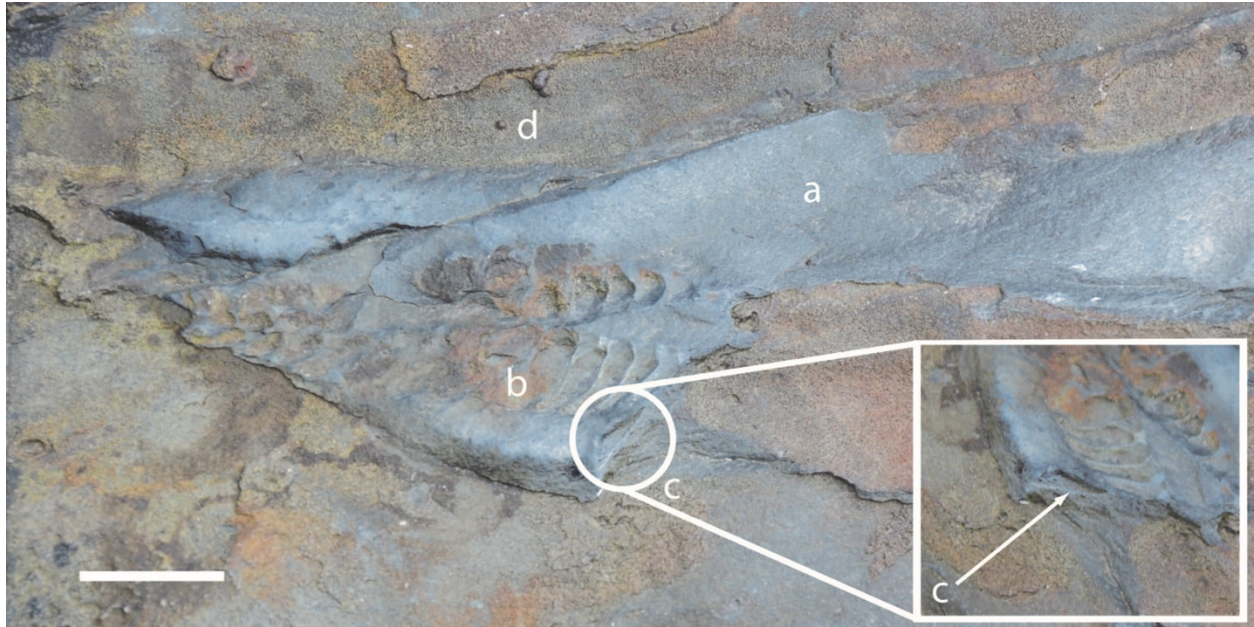


Figure 2.8: *Charniodiscus* sp. from Spaniard's bay, Newfoundland. A) Overlying siltstone. B) collapsed sub-conical frond preserved in sandstone. C) Cross section view. D) Underlying siltstone. Scale bar 1 cm. Field photography. Not retrodeformed.

## 2.6 PALAEOBIOLOGICAL MODEL OF *CHARNIODISCUS*

The original cnidarian affinities of frondose Ediacaran organisms (e.g., *Charnia* and *Bradgatia*) have recently been questioned (e.g., Brasier and Antcliffe 2004; Narbonne 2004, Narbonne 2005; Antcliffe and Brasier 2008), though their utility as functional morphological analogs may still be valid (Dunn et al. 2019). If *Charniodiscus* is accepted as a sub-conical stemmed frondose arboreomorph, then it might function biomechanically erect in the water column like most pennatulaceans (cf. Kushida et al. 2020, figure 2A) in which case it might draw water up through the cone by Bernoulli effect. The same morphotype might also be an adaption to funnel water if held in a recumbent or reclined position parallel to the seafloor, either with the cone directed into or away from the current. If held in a recumbent or reclining position the broad end

of the cone would face into the current in the manner of a windsock. In erect or seafloor-parallel recumbent positions, the frond would be exposed to the water column as a foliate feeding structure. This could result in ecological benefits from resource partitioning and reduced competition in ecosystems with crowded lower tiers (but see Mitchell and Kenchington 2018). Both absorption of dissolved matter and filter feeding strategies are congruent with tiered epifaunal models (Clapham and Narbonne 2002; Ghisalberti et al. 2014).

While presumed erect or recumbent positions are plausible body postures for some taxa, it remains uncertain for some others which pose important challenges to the interpretation of Ediacaran tiering models (McIlroy et al. 2021). The stems that connect holdfasts and fronds in arboreomorphs (e.g. *Arborea*, *C. concentricus*, *C. spinosus*) are poorly preserved (Figure 2.2). This is likely due to the arching of the stem as fronds are felled from their erect or recumbent position onto the seafloor (cf. Glaessner and Daily 1959; Glaessner 1984; McIlroy et al. 2021). In contrast, *C. procerus* generally has a long well-preserved stem with a semicircular cross section and no supporting evidence for erect or recumbent stem positions (Figure 2.6). This suggests that in life the stem of *C. procerus* lay flat on the seafloor implying exposure of the lower surface to sedimentary microbial ecosystems and pore water hypoxia (cf. Dufour and McIlroy 2017). The stem could have therefore had other functions than merely structural support, possibly establishing symbiotic relationships with chemosynthetic, sulphur-oxidising bacteria to mitigate the elevated toxicity (McIlroy et al. 2021). Whether the stem of a *Charniodiscus* was reclined on/in the sediment or held in a recumbent position just above it, there is significant potential for sediment to become trapped inside the sub-conical frondose portion. This is especially true during periods of rapid sediment influx, accumulating at a level above the stem and into which the distal portion of the branches might become impressed (Figures 2.3A—green).

*Charniodiscus procerus* shows flat proximal sections of the primary branches meeting the central axis at nearly right angles providing support for the distally curved section of the same branches in a similar fashion to other *Charniodiscus* specimens (Figures 2.7, 2.8). These branches were curved inward and apically directed, forming a reclined sub-conical or erect frondose portion whose lumen would be exposed to the water column. The sub-conical structure would funnel water in a similar manner as in seafloor-parallel recumbent positions.

It has been considered that Ediacaran fronds with primary branches annexed together or having a “backing sheet” could not have fed like the Pennatulacea, which require water flow between primary branches (Seilacher 1992). Our functional morphological understanding of *Charniodiscus concentricus* as a recumbent (sediment-parallel) or erect frond allows funneled flow between the branches of the frond, which was held slightly above the benthic boundary layer. The branches of *C. concentricus* are interpreted as fascicled, loosely constrained branches not supported by a backing sheet of tissue similar to some Shibatan charnids or *Arborea* spp. (Xiao et al. 2021). However, due to the lack of preserved specialized zooids or feeding structures, the feeding mechanisms of *Charniodiscus* and other arboreomorphs remain uncertain but may have included osmotrophy and/or filter feeding (Laflamme et al. 2018).

### **2.6.1 Taxonomic consideration of other *Charniodiscus* species**

Throughout the ~35 My of evolutionary history of the Ediacaran biota we observe a contrast between highly unique morphological disparity (Shen et al. 2008) and low taxonomic diversity (Waggoner 2003). This has led to the creation of numerous monospecific genera, a lack of unified consensus regarding higher taxonomic ranks (Xiao and Laflamme 2009), and genus and

clade-level taxonomic inconsistencies (Brasier and Antcliffe 2009; Liu et al. 2015; Laflamme et al. 2018; Wang et al. 2020).

Cladistic classification for Ediacaran macrofossils based on branching architecture, body symmetry, and growth parameters (Erwin et al. 2011) recognized the clade Arboreomorpha, which encompasses bifoliate fronds bearing annexed primary branches attached to a dorsal sheet. Those primary branches were considered to have orthogonal teardrop-shaped secondary branches. All species of *Charniodiscus* and *Arborea* were included in this clade except for *C. concentricus*. Dececchi et al. (2017) supported Erwin et al. (2011), using autapomorphically-constructed clades, in the recognition of the clade Arboreomorpha, which was defined as having spherical to hemispherical secondary branches with no further orders of branching and lacking a modular petalodium. We consider these transverse ridges to be semicircular. Arboreomorpha was also reported to show conserved inflating growth patterns and diagnostic numbers of branches (Laflamme et al. 2004).

In the light of our work there are several bifoliate planar arboreomorphs that require further taxonomic revision, including:

- 1) *C. longus* Glaessner and Wade, 1966 (formerly *Rangea longa* and *Glaessnerina longa*; Fedonkin et al. 2007), an elongate and lanceolate frond bearing at least 40 primary branches and uniform secondary subdivisions without a preserved stem or basal disc (Glaessner and Wade 1966; Laflamme et al. 2004; Wang et al. 2020). The branching is clearly *Arborea*-like and there appears to be a prominent backing sheet (Figure 2.2D), indicating that it should likely be considered as *Arborea longa*.
- 2) The endemic Newfoundland species *C. spinosus*, which has a backing sheet, a stem that is typically poorly preserved, and an apical spine. Careful photography of the

branching allows the recognition of *Arborea*-like branches (Figure 2.2C), suggesting that this species should also be included in *Arborea*, as *Arborea spinosa*.

- 3) Material from the Bonavista Peninsula of Newfoundland described as *C. arboreus* and *C. sp.* by Hofmann et al. (2008) bear little resemblance to the type material of *Arborea* (Glaessner and Wade 1966) in being non-tapering without prominent holdfasts or robust stems. Specimens from Bonavista are commonly preserved in a manner akin to the tip of *C. concentricus* (i.e., collapse infolding) and should likely be retained within *Charniodiscus*, probably as a distinct species with fewer branches than the holotype.

## 2.7 CONCLUSION

The inferred multifoliate nature of the holotype of *Charniodiscus concentricus* (Dzik 2002, 2003; Brasier and Antcliffe 2009) made it considerably different from all the other (bifoliate) species of the genus. Newfoundland species of *Charniodiscus* have hitherto been retained in the genus but separated from *Arborea* based on the inferred rangeomorph-like branching architecture of *Charniodiscus* (Brasier and Antcliffe 2009). Our taphonomic and morphological reinterpretation of *Charniodiscus concentricus* allows the resolution of existing taxonomic inconsistencies. The pronounced curvature of the outfolded branches, taken alongside the straight basally-directed infolded collapsed branches of the tip, the observed differential branch folding, and the preservation of sediment atop the central axis of much of the frond suggests that the frond was a bifoliate collapsed sub-conical structure with apically directed branches meeting in an echelon fashion characterized by *Arborea*-type branching lacking a continuous sheet of tissue.

Based on the poorly preserved stem in *Charniodiscus concentricus*—likely due to the arching that would occur during the felling of the frond to the seafloor from its erect or recumbent

life position—and the underfolding of the branches under the stem we infer an erect or recumbent lifestyle as the only plausible options for life attitude. *C. concentricus* as reconstructed herein (Figure 2.5) could have functioned biomechanically either erect in the water column like a cone on a stick, similar to the mode of life of many pennatulacean cnidarians, or if held in a recumbent position parallel to the seafloor the cone might have functioned to funnel water over and possibly between the branches.

*Charniodiscus procerus* generally has high relief well-preserved stems with no additional evidence for erect or recumbent body postures in life. This is likely due to a dominantly reclining position of the organism, which would have had the stem laid upon or even partly embedded within the matground. This challenges the paradigm that all Ediacaran stemmed taxa were erect fronds in the water column (e.g. Vixseboxse et al. 2021). Similarly, the distal curved portions of the primary branches of *C. procerus* are interpreted—by analogy with *C. concentricus* and *C. sp.* from Spaniards Bay—as casts of the impressions made by the external surfaces of the curved portion of the conical frond smothering the surrounding matground due to post-mortem unfolding.

We propose emendation of the generic diagnosis of *Charniodiscus* to encompass bifoliate arboreomorphs with sub-conical petalodiums, while retaining *Arborea* for the bifoliate planar arboreomorphs with a backing sheet. As such we infer two distinct frond morphologies: 1) sub-conical fronds with arboreomorph branching which we consider to be typical of *Charniodiscus*; versus 2) planar foliate sheets of the genus *Arborea* in which the arboreomorph branching is considered to be on the front surface. Our model supports the retention of both *Charniodiscus* and *Arborea*, solving the existing taxonomic inconsistencies. Additionally, we find no evidence of rangeomorph-type fractal branching in *Charniodiscus* and thus reject its inclusion in the Rangeomorpha.

The non-vertical (recumbent or reclining) life attitude invoked for *Charniodiscus* spp. herein is based on our improved taphonomic understanding of the genus and is consistent with other proposals for Ediacaran fronds (Laflamme and Narbonne 2008; Laflamme et al. 2018). We also note here that the presence of a backing sheet in *Arborea* spp. would be a significant impediment to flow increasing the aspect ratio of the frond. This suggests that it might also be an adaptation to modify the life attitude of *Arborea* spp. to become recumbent in a current, allowing for current orientation of the frond and increased turbulent flow over the frond surface.

## **2.8 DATA AVAILABILITY STATEMENT**

The original contributions presented in the study are included in the article/supplementary material, further inquiries can be directed to the corresponding author.

## **2.9 AUTHOR CONTRIBUTIONS**

D.P.-P. and D.M. conceived the project. D.P.-P. and C.M. constructed figures. D.P.-P., C.M., R.T., R.N., and D.M. analyzed the data and prepared the manuscript.

## **2.10 FUNDING**

Funding was provided to D. Mc. by Discovery Grant and Discovery Accelerator Supplement awards from the Natural Sciences and Engineering Research Council, which are acknowledged with thanks.

## **2.11 ACKNOWLEDGMENTS**

Jenna Neville and Giovanni Pasinetti are thanked for their assistance through both discussions related to this topic and their support in the field. We acknowledge with thanks the Oxford University Museum of Natural History for access to the Brasier collections. Fieldwork and fossil casting in Newfoundland was conducted under permit from the Parks and Natural Areas Division of the Government of Newfoundland and Labrador. This project was supported by an NSERC Discovery Grant and Discovery Accelerator Supplement to DMc.

## 2.12 REFERENCES

Antcliffe, J. B., & Brasier, M. D. (2008). *Charnia* at 50: developmental models for Ediacaran fronds. *Palaeontology*, 51(1), 11-26.

Borchardt, D. V., & Nessonov, L. A. (1999). New records of metaphytes from the Vendian (Precambrian) of Zimnii Bereg of the White Sea. *Trudy Zoologicheskogo Instituta, Akademiya Nauk*, 277, 50-57.

Brasier, M., & Antcliffe, J. (2004). Decoding the Ediacaran enigma. *Science*, 305(5687), 1115-1117.

Brasier, M. D., & Antcliffe, J. B. (2009). Evolutionary relationships within the Avalonian Ediacara biota: new insights from laser analysis. *Journal of the Geological Society*, 166(2), 363-384.

Brasier, M. D., Antcliffe, J. B., & Liu, A. G. (2012). The architecture of Ediacaran fronds. *Palaeontology*, 55(5), 1105-1124.

Brasier, M. D., Liu, A. G., Menon, L., Matthews, J. J., McIlroy, D., & Wacey, D. (2013). Explaining the exceptional preservation of Ediacaran rangeomorphs from Spaniard's Bay, Newfoundland: a hydraulic model. *Precambrian Research*, 231, 122-135.

Burzynski, G., & Narbonne, G. M. (2015). The discs of Avalon: relating discoid fossils to frondose organisms in the Ediacaran of Newfoundland, Canada. *Palaeogeography, Palaeoclimatology, Palaeoecology*, 434, 34-45.

Clapham, M. E., & Narbonne, G. M. (2002). Ediacaran epifaunal tiering. *Geology*, 30(7), 627-630.

Decechi, T. A., Narbonne, G. M., Greentree, C., & Laflamme, M. (2017). Relating Ediacaran fronds. *Paleobiology*, 43(2), 171-180.

Dufour, S. C., & McIlroy, D. (2017). Ediacaran pre-placozoan diploblasts in the Avalonian biota: the role of chemosynthesis in the evolution of early animal life. *Geological Society of London Special Publication*, 448, 211–219.

Dunn, F. S., Liu, A. G., & Gehling, J. G. (2019). Anatomical and ontogenetic reassessment of the Ediacaran frond *Arborea arborea* and its placement within total group Eumetazoa. *Palaeontology*, 62(5), 851-865.

Dzik, J. (2002). Possible ctenophoran affinities of the Precambrian “sea-pen” *Rangea*. *Journal of morphology*, 252(3), 315-334.

Erwin, D. H., Laflamme, M., Tweedt, S. M., Sperling, E. A., Pisani, D., & Peterson, K. J. (2011). The Cambrian conundrum: early divergence and later ecological success in the early history of animals. *Science*, 334(6059), 1091-1097.

Fedonkin, M. A. (1985). “Systematic Description of Vendian Metazoa,” in *The Vendian System: Historic-Geological and Palaeontological Basis*. Editor B. S. Sokolov and A. B. Ivanovskiy (PaleontologyMoscow: Nauka), 1, 70–107.

Ford, T. D. (1958). Pre-Cambrian fossils from Charnwood Forest. *Proceedings of the Yorkshire Geological Society*, 31(3), 211-217.

- Ford, T. D. (1962). The oldest fossils. *New Scientist*, 15, 191–194.
- Ford, T. D. (1963). The Pre-Cambrian fossils of Charnwood Forest. *Leicester Literary and Philosophical Society Transactions*, 57, 57-62.
- Gehling, J. G. (1999). Microbial mats in terminal Proterozoic siliciclastics; Ediacaran death masks. *Palaios*, 14(1), 40-57.
- Gehling, J. G. (1991). The case for Ediacaran fossil roots to the metazoan tree. *Geological Society of India Memoir*, 20, 181-224.
- Ghisalberti, M., Gold, D. A., Laflamme, M., Clapham, M. E., Narbonne, G. M., Summons, R. E., ... & Jacobs, D. K. (2014). Canopy flow analysis reveals the advantage of size in the oldest communities of multicellular eukaryotes. *Current Biology*, 24(3), 305-309.
- Glaessner, M. F., & Daily, B. (1959). The geology and Late Precambrian fauna of the Ediacara fossil reserve. *Records of the South Australian Museum*, 13(3), 369-401.
- Glaessner, M. F. (1984). *The dawn of animal life: a biohistorical study*. Cambridge, United Kingdom: Cambridge University Press Archive.
- Glaessner, M. F. (1966). The late Precambrian fossils from Ediacara, South Australia. *Palaeontology*, 9, 599-628.
- Grazhdankin, D. (2014). Patterns of evolution of the Ediacaran soft-bodied biota. *Journal of Paleontology*, 88(2), 269-283.
- Herringshaw, L. G., Callow, R. H., & McIlroy, D. (2017). Engineering the Cambrian explosion: the earliest bioturbators as ecosystem engineers. *Geological Society, London, Special Publications*, 448, 369–382.
- Hofmann, H. J., O'Brien, S. J., & King, A. F. (2008). Ediacaran biota on Bonavista peninsula, Newfoundland, Canada. *Journal of Paleontology*, 82(1), 1-36.

Ivantsov, A. Y. (2016). Reconstruction of *Charniodiscus yorgensis* (macrobiota from the Vendian of the White Sea). *Paleontological Journal*, 50, 1-12.

Jenkins, R. J. (1992). Functional and ecological aspects of Ediacaran assemblages. In *Origin and early evolution of the Metazoa* (pp. 131-176). Boston, MA: Springer US.

Jenkins, R. J. F., and Gehling, J. G. (1978). A Review of the Frond-like Fossils of the Ediacara Assemblage. *Records of the Australian Museum*, 17, 347–359.

Jensen, S., Högstöm, A. E., Almond, J., Taylor, W. L., Meinhold, G., Høyberget, M. A. G. N. E., ... & Palacios, T. (2018). Scratch circles from the Ediacaran and Cambrian of Arctic Norway and southern Africa, with a review of scratch circle occurrences. *Bulletin of Geosciences*, 93(3), 287-304.

Kenchington, C., & Wilby, P. R. (2014). *Of Time and Taphonomy: Preservation in the Ediacaran*. London, United Kingdom: Cambridge University Press.

Kushida, Y., Higashiji, T., & Reimer, J. D. (2020). First observation of mole-like burrowing behavior observed in a sea pen. *Marine Biodiversity*, 50, 1-9.

Laflamme, M., Flude, L. I., & Narbonne, G. M. (2012). Ecological tiering and the evolution of a stem: the oldest stemmed frond from the Ediacaran of Newfoundland, Canada. *Journal of Paleontology*, 86(2), 193-200.

Laflamme, M., Gehling, J. G., & Droser, M. L. (2018). Deconstructing an Ediacaran frond: three-dimensional preservation of *Arborea* from Ediacara, South Australia. *Journal of Paleontology*, 92(3), 323-335.

Laflamme, M., Narbonne, G. M., & Anderson, M. M. (2004). Morphometric analysis of the Ediacaran frond *Charniodiscus* from the Mistaken Point Formation, Newfoundland. *Journal of Paleontology*, 78(5), 827-837.

Laflamme, M., & Narbonne, G. M. (2008). Ediacaran fronds. *Palaeogeography, Palaeoclimatology, Palaeoecology*, 258(3), 162-179.

Liu, A. G. (2016). Framboidal pyrite shroud confirms the 'death mask' model for moldic preservation of Ediacaran soft-bodied organisms. *Palaaios*, 31(5), 259-274.

Liu, A. G., Kenchington, C. G., & Mitchell, E. G. (2015). Remarkable insights into the paleoecology of the Avalonian Ediacaran macrobiota. *Gondwana Research*, 27(4), 1355-1380.

Liu, A. G., McIlroy, D., Antcliffe, J. B., & Brasier, M. D. (2011). Effaced preservation in the Ediacara biota and its implications for the early macrofossil record. *Palaeontology*, 54(3), 607-630.

Liu, A. G., McIlroy, D., & Brasier, M. D. (2010). First evidence for locomotion in the Ediacara biota from the 565 Ma Mistaken Point Formation, Newfoundland. *Geology*, 38(2), 123-126.

Liu, A. G., Menon, L. R., Shields, G. A., Callow, R. H., & McIlroy, D. (2017). Martin Brasier's contribution to the palaeobiology of the Ediacaran–Cambrian transition. *Geological Society, London, Special Publications*, 448(1), 179-193.

Mapstone, N. B., & McIlroy, D. (2006). Ediacaran fossil preservation: taphonomy and diagenesis of a discoid biota from the Amadeus Basin, central Australia. *Precambrian Research*, 149(3-4), 126-148.

Matthews, J. J., Liu, A. G., Yang, C., McIlroy, D., Levell, B., & Condon, D. J. (2021). A chronostratigraphic framework for the rise of the Ediacaran macrobiota: new constraints from Mistaken Point Ecological Reserve, Newfoundland. *Geological Society of America Bulletin*, 133(3-4), 612-624.

McIlroy, D., Brasier, M. D., & Lang, A. S. (2009). Smothering of microbial mats by macrobiota: implications for the Ediacara biota. *Journal of the Geological Society*, 166(6), 1117-1121.

McIlroy, D., Brasier, M. D., & Moseley, J. B. (1998). The Proterozoic–Cambrian transition within the ‘Charnian Supergroup’ of central England and the antiquity of the Ediacara fauna. *Journal of the Geological Society*, 155(2), 401-411.

McIlroy, D., Dufour, S. C., Taylor, R., & Nicholls, R. (2021). The role of symbiosis in the first colonization of the seafloor by macrobiota: insights from the oldest Ediacaran biota (Newfoundland, Canada). *Biosystems*, 205, 104413.

McIlroy, D., Hawco, J., McKean, C., Nicholls, R., Pasinetti, G., & Taylor, R. (2022). Palaeobiology of the reclining rangeomorph *Beothukis* from the Ediacaran Mistaken Point Formation of southeastern Newfoundland. *Geological Magazine*, 159(7), 1160-1174.

McIlroy, D., and Horák, J. M. (2006). “Neoproterozoic: the Late Precambrian Terranes that Formed Eastern Avalonia,” in *The Geology of England and Wales*. Editors P. R. Brenchley and P. F. Rawson (Bath, UK: Geological Society Publishing House), 9–25.

McIlroy, D., & Logan, G. A. (1999). The impact of bioturbation on infaunal ecology and evolution during the Proterozoic-Cambrian transition. *Palaios*, 14(1), 58-72.

Murphy, J. B., Pisarevsky, S. A., Nance, R. D., & Keppie, J. D. (2004). Neoproterozoic—Early Paleozoic evolution of peri-Gondwanan terranes: implications for Laurentia-Gondwana connections. *International Journal of Earth Sciences*, 93, 659-682.

Narbonne, G. M. (1987). Ediacaran biota of the Wernecke Mountains, Yukon, Canada. *Palaeontology*, 30, 647-676.

Narbonne, G. M., Laflamme, M., Greentree, C., & Trusler, P. (2009). Reconstructing a lost world: Ediacaran rangeomorphs from Spaniard's Bay, Newfoundland. *Journal of Paleontology*, 83(4), 503-523

Narbonne, G. M. (2004). Modular construction of early Ediacaran complex life forms. *Science*, 305(5687), 1141-1144.

Narbonne, G. M. (2005). The Ediacara biota: Neoproterozoic origin of animals and their ecosystems. *Annual Review of Earth and Planetary Sciences*, 33(1), 421-442.

Noble, S. R., Condon, D. J., Carney, J. N., Wilby, P. R., Pharaoh, T. C., & Ford, T. D. (2015). U-Pb geochronology and global context of the Charnian Supergroup, UK: constraints on the age of key Ediacaran fossil assemblages. *Geological Society of America Bulletin*, 127(1-2), 250-265.

Seilacher, A. (1992). Vendobionta and Psammocorallia: lost constructions of Precambrian evolution. *Journal of the Geological Society, London*, 149(4), 607-613.

Shen, B., Dong, L., Xiao, S., & Kowalewski, M. (2008). The Avalon explosion: evolution of Ediacara morphospace. *Science*, 319(5859), 81-84.

Steiner, M., & Reitner, J. (2001). Evidence of organic structures in Ediacara-type fossils and associated microbial mats. *Geology*, 29(12), 1119-1122.

Tarhan, L. G., Droser, M. L., Gehling, J. G., & Dzaugis, M. P. (2015). Taphonomy and morphology of the Ediacara form genus *Aspidella*. *Precambrian Research*, 257, 124-136.

Taylor, R. S., Matthews, J. J., Nicholls, R., & McIlroy, D. (2021). A re-assessment of the taxonomy, palaeobiology and taphonomy of the rangeomorph organism *Hapsidophyllas flexibilis* from the Ediacaran of Newfoundland, Canada. *PalZ*, 95(2), 187-207.

Vixseboxse, P. B., Kenchington, C. G., Dunn, F. S., & Mitchell, E. G. (2021). Orientations of Mistaken Point fronds indicate morphology impacted ability to survive turbulence. *Frontiers in Earth Science*, 9, 762824.

Wade, M. (1968). Preservation of soft-bodied animals in Precambrian sandstones at Ediacara, South Australia. *Lethaia*, 1(3), 238-267.

Waggoner, B. (2003). The Ediacaran biotas in space and time. *Integrative and Comparative Biology*, 43(1), 104-113.

Wang, X., Pang, K., Chen, Z., Wan, B., Xiao, S., Zhou, C., & Yuan, X. (2020). The Ediacaran frondose fossil *Arborea* from the Shibantan limestone of South China. *Journal of Paleontology*, 94(6), 1034-1050.

Wen, B., Evans, D. A., Anderson, R. P., & McCausland, P. J. (2020). Late Ediacaran paleogeography of Avalonia and the Cambrian assembly of West Gondwana. *Earth and Planetary Science Letters*, 552, 116591.

Wilby, P. R., Carney, J. N., & Howe, M. P. (2011). A rich Ediacaran assemblage from eastern Avalonia: evidence of early widespread diversity in the deep ocean. *Geology*, 39(7), 655-658.

Wood, D. A., Dalrymple, R. W., Narbonne, G. M., Gehling, J. G., and Clapham, M. E. (2003). Paleoenvironmental Analysis of the Late Neoproterozoic Mistaken Point and Trepassey Formations, southeastern Newfoundland. *Canadian Journal of Earth Sciences*, 40, 1375–1391.

Xiao, S., Chen, Z., Pang, K., Zhou, C., & Yuan, X. (2021). The Shibantan Lagerstätte: Insights into the Proterozoic–Phanerozoic transition. *Journal of the Geological Society*, 178(1), 2020-135.

Xiao, S., & Laflamme, M. (2009). On the eve of animal radiation: phylogeny, ecology and evolution of the Ediacara biota. *Trends in Ecology & Evolution*, 24(1), 31-40.

Xiao, S., Yuan, X., Steiner, M., & Knoll, A. H. (2002). Macroscopic carbonaceous compressions in a terminal Proterozoic shale: a systematic reassessment of the Miaohu biota, South China. *Journal of Paleontology*, 76(2), 347-376.

# **CHAPTER 3 - Frond orientations with independent current indicators demonstrate the reclining rheotropic mode of life of several Ediacaran rangeomorph taxa**

Daniel Pérez-Pinedo<sup>1\*</sup>, Jenna M. Neville<sup>1</sup>, Giovanni Pasinetti<sup>1</sup>, Christopher McKean<sup>1</sup>, Rod Taylor<sup>1</sup>, and Duncan McIlroy<sup>1</sup>

<sup>1</sup> Department of Earth Sciences, Memorial University of Newfoundland, St. John's, NL, Canada,

\* Corresponding author: Daniel Pérez-Pinedo [dperezpinedo@mun.ca](mailto:dperezpinedo@mun.ca) 0000-0001-5607-1164

## **PREFACE:**

This paper has been published in the international scientific peer-reviewed journal *Paleobiology* ([doi.org/10.1017/pab.2023.2](https://doi.org/10.1017/pab.2023.2)) as an original research article as of 23<sup>rd</sup> February 2023. The paper is available from the volume 49, issue 3. This chapter has been formatted according to the guidelines for thesis submission and is otherwise identical to the original publication. When found, typos and non-substantial corrections have been made. Conceptualization, D.P-P., J.N., and D.M; methodology, D.P-P; formal analysis, D.P-P; software, D.P-P; investigation, DP.-P., and D.M; figures: D.P.-P., G.P., C.M; validation, D.P-P; data curation, D.P-P., G.P., and J.M; project administration, D.P-P., and D.M; writing, D.P-P. with editorial input by J.N., G.P., C.M., R.T., and D.M; funding acquisition, D.M.

Reference: Pérez-Pinedo, D., Neville, J. M., Pasinetti, G., McKean, C., Taylor, R., & McIlroy, D. (2023). Frond orientations with independent current indicators demonstrate the reclining rheotropic mode of life of several Ediacaran rangeomorph taxa. *Paleobiology*, 49(3), 471-492.

## ABSTRACT

Fossils from the deep-sea Ediacaran biotas of Newfoundland are among the oldest architecturally complex soft-bodied macroorganisms on Earth. Most organisms in the Mistaken Point-type biotas of Avalonia—particularly the fractal-branching frondose Rangeomorpha— have been traditionally interpreted as living erect within the water column during life. However, due to the scarcity of documented physical sedimentological proxies associated with fossiliferous beds, Ediacaran paleocurrents have been inferred in some instances from the preferential orientation of fronds. This calls into question the relationship between frond orientation and paleocurrents. In this study, we present an integrated approach from a newly described fossiliferous surface (the Melrose Surface in the Fermeuse Formation at Melrose, on the southern portion of the Catalina Dome in the Discovery UNESCO Global Geopark) combining: (1) physical sedimentological evidence for paleocurrent direction in the form of climbing ripple cross-lamination and (2) a series of statistical analyses based on modified polythetic and monothetic clustering techniques reflecting the circular nature of the recorded orientation of *Fractofusus misrai* specimens. This study demonstrates the reclining rheotropic mode of life of the Ediacaran rangeomorph taxon *Fractofusus misrai* and presents preliminary inferences suggesting a similar mode of life for *Bradgatia* sp. and *Pectinifrons abyssalis* based on qualitative evidence. These results advocate for the consideration of an alternative conceptual hypothesis for position of life of Ediacaran organisms in which they are interpreted as having lived reclined on the seafloor, in the position that they are preserved.

**Keywords:** *Fractofusus*, *Bradgatia*, *Pectinifrons*, paleocurrents, clusters, orientation, rheotropism

### 3.1 INTRODUCTION

The Ediacaran biotas of Newfoundland have some of the oldest known well-dated complex soft-bodied macroorganisms (Narbonne 2005; Xiao and Laflamme 2009; Liu et al. 2015; Matthews et al. 2021) and are essential in furthering our understanding of the evolution of complex macroorganisms. The earliest macrofossils of the Ediacaran biota are widely considered to be stem eumetazoans (Dunn et al. 2021), and many had unusual fractal-like growth patterns that have no good modern analogues (Narbonne 2005; Brasier et al. 2012; Hoyal Cuthill and Conway Morris 2014). Understanding these enigmatic organisms has been a challenge since their initial discovery (Gürich 1930; Ford 1958). The Ediacaran biota has been much explored in recent years, with research debating aspects of their phylogenetic affinity (Seilacher 1989, 1992; Budd and Jensen 2017; Dunn and Donoghue 2018), ecology (Clapham et al. 2003; Darroch et al. 2018; Mitchell et al. 2020), mode of life (Glaessner 1985; Laflamme et al. 2009; Dufour and McIlroy 2017; McIlroy et al. 2021), and taphonomy (Gehling 1999; Narbonne 2005; Liu et al. 2011; Bobrovskiy et al. 2019). Inferences that most of the Ediacaran biota—particularly the fractal-branching frondose Rangeomorpha—lived erect within the water column during life (i.e., Glaessner 1985; Laflamme et al. 2007) have recently been contested (McIlroy et al. 2020, 2021, 2022; Pérez-Pinedo et al. 2022). The high fidelity of preservation of originally soft tissues such as fractal-like fronds (Figure 3.1) and the lack of taphonomic evidence for an erect mode of life (e.g., swing marks imparted by a current, see Jensen et al. [2018]) challenge a priori assumptions about erect body postures. There is therefore a need to consider the alternative hypothesis that these organisms were reclined on the sea floor, as they are preserved on bedding planes (McIlroy et al. 2020, 2021, 2022; Pérez-Pinedo et al. 2022).

Sedimentological evidence for paleocurrent directions in the Ediacaran of Newfoundland is mainly in the form of current ripple trends in turbidites (i.e., Wood et al. 2003; Ichaso et al. 2007; Mason et al. 2013). At some localities, geostrophic paleocurrent directions are also inferred but are solely based on frond orientation. Preferential orientation of Ediacaran fronds has been thought to be due to current “felling” in the Mistaken Point–type biotas of Avalonia, particularly at Mistaken Point (following Seilacher 1992, 1999). The poorly supported felling model has been used to propose an erect mode of life for all the fossil organisms in the Mistaken Point assemblages, except *Fractofusus* spp. (e.g., Wood et al. 2003; Vixseboxse et al. 2021). An alternative model invoking rheotropic epifaunal growth of reclining taxa has been proposed (McIlroy et al. 2022), which calls into question the causal relationship between frond orientation and paleocurrents. There is therefore a clear need to assess the orientation of Ediacaran fronds from surfaces with physical sedimentary structures as independent proxies for paleocurrent direction. The clearest documented relationships between frond orientation and current structures are the fronds of the “Spaniard’s Bay” assemblage (King 1982, 1988, 1990; Narbonne 2004; Narbonne et al. 2009) that are oriented subparallel to flute marks (cf. Brasier et al. 2013), but such clear relationships are uncommon in the rest of the Ediacaran assemblages of Avalonia. This paper details the orientation of Ediacaran taxa from a newly discovered fossil surface in the Fermeuse Formation at Melrose, on the southern portion of the Catalina Dome in the Discovery UNESCO Global Geopark (Figure 3.2). The importance of this surface derives from its well-constrained paleocurrent indicators in the form of wavy bedding and climbing current ripples (Figure 3.3).

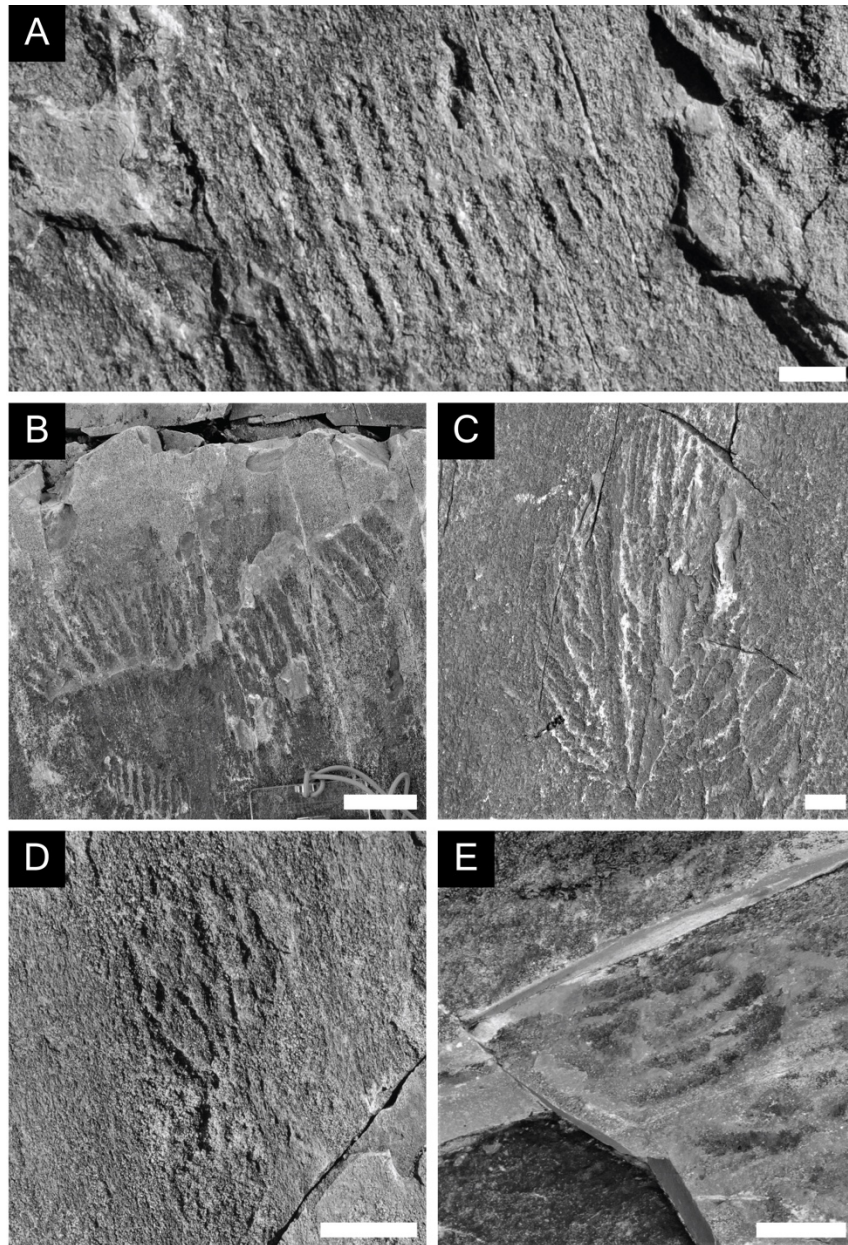


Figure 3.1: Ediacaran fossils from the Melrose Surface. A) *Fractofusus misrai*. B) *Pectinifrons abyssalis*. C) *Bradgatia* sp.. D) *Primocandelabrum* sp.. E) *Charniodiscus* sp. Scale bars, A, C–E 1 cm, B 3 cm.

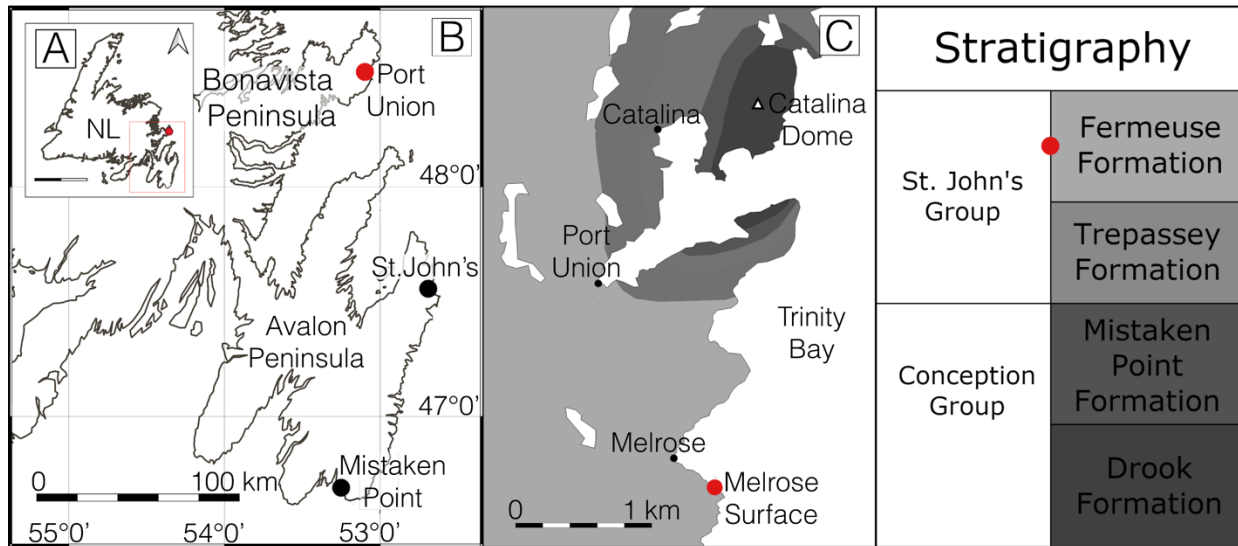


Figure 3.2: Location of the Melrose Surface in the Fermeuse Formation at Melrose, on the southern portion of the Catalina Dome, in the Discovery UNESCO Global Geopark. A) General map of Newfoundland, Atlantic Canada. Scale bar, 200 km. B) Detail of the Avalon and Bonavista Peninsulas. C) Geologic map of Catalina area and stratigraphic column.

### 3.1.1 Geologic setting

The fossil assemblage at Melrose bears some resemblance in terms of taxonomy and community composition to that of the famous D and E Surface assemblages of the Mistaken Point Ecological Reserve (MPER) (see Clapham et al. 2003). The assemblage was discovered in 2018 by a team from Cambridge University (Emily Mitchell, Alexander Liu, and William McMahon), U.K., and is here named the Melrose Surface, given its location in the town of Melrose. Tectonostratigraphic reconstructions of the Conception Group suggest that deposition occurred in a continental slope environment adjacent to an island-arc setting on the northwest margin of Gondwana (Murphy et al. 2004; Pollock et al. 2009; Pisarevsky et al. 2012). The Conception Group is dominated by fine-grained turbidites (Williams and King 1979; Wood et al. 2003; Ichaso

et al. 2007). The tuffite overlying the E Surface at MPER is dated at  $565 \pm 0.64$  Ma (Matthews et al. 2021), slightly older than the undated Fermeuse Formation at Melrose (Figure 3.2).

Ecological reconstructions of Mistaken Point–type biotas have hitherto depicted these Ediacaran organisms as living erect within the water column, influenced by and felled in the direction of paleocurrents. However, due to the lack of sedimentological proxies on such fossiliferous beds, paleocurrent direction has been inferred in some cases from frond orientation. Paleocurrent analysis of the Mistaken Point Formation has shown a predominantly southeasterly flow direction, as evinced from both the abundant fronds and the uncommon physical sedimentary structures in turbidite beds (Wood et al. 2003; Ichaso et al. 2007). It has, however, also been noted that there is a second preferential frond orientation direction that is roughly orthogonal to the downslope current, previously attributed to contour currents that felled the fronds before rapid ash burial; this aided in the high fidelity of preservation seen on these fossiliferous surfaces (Seilacher 1992, 1999; Wood et al. 2003; Narbonne 2005). There is a range of frond orientations on the MPER surfaces, and some taxa are commonly orthogonal to slope (*Beothukis mistakensis*; Hawco et al. 2020; McIlroy et al. 2020, 2022); some even have fronds oriented against the inferred paleocurrent direction (e.g., *Bradgatia* sp., orientations in Flude and Narbonne [2008]). This is more likely to be a rheotropic growth response, as it is incompatible with flow hydrodynamics (McIlroy et al. 2022; contra Vixseboxse et al. 2021).

The Melrose Surface assemblage, while similar in taxonomic character to the older Mistaken Point assemblages, is part of the later Fermeuse Formation of the St. John's Group (Hofmann et al. 2008; Figure 3.2). The lithofacies of the Fermeuse Formation suggest deposition in an upper slope to distal prodelta setting (King et al. 1988; Mason et al. 2013), and thus in shallower waters than the ecologically similar Mistaken Point biota, which is from a deep basinal

setting. The presence of what is normally considered a deep basinal biota in the shallower Fermeuse Formation requires detailed sedimentological consideration beyond the scope of this work, but it may be possible to invoke a regional increase in relative sea level. The fossiliferous surfaces of the Fermeuse Formation are typically dominated by matgrounds with *Ediacaria* and *Cyclomedusa* morphs of *Aspidella* sensu lato (Gehling et al. 2000; Brasier et al. 2010) and the protist-like *Palaeopascichnus delicatus* (Hawco et al. 2021). Beds deposited in similar paleoenvironments with discoidal features comparable to *Aspidella* have been used to suggest that these discoidal features may be pseudofossils, possibly formed by fluid escape or matground-associated sediment injection rather than by organisms (Menon et al. 2016). The Melrose Surface assemblage considerably extends the upper stratigraphic ranges of several taxa (*Fractofusus misrai*, *Pectinifrons abyssalis*, *Primocandelabrum* sp., *Bradgatia* sp., and *Charniodiscus* sp.).

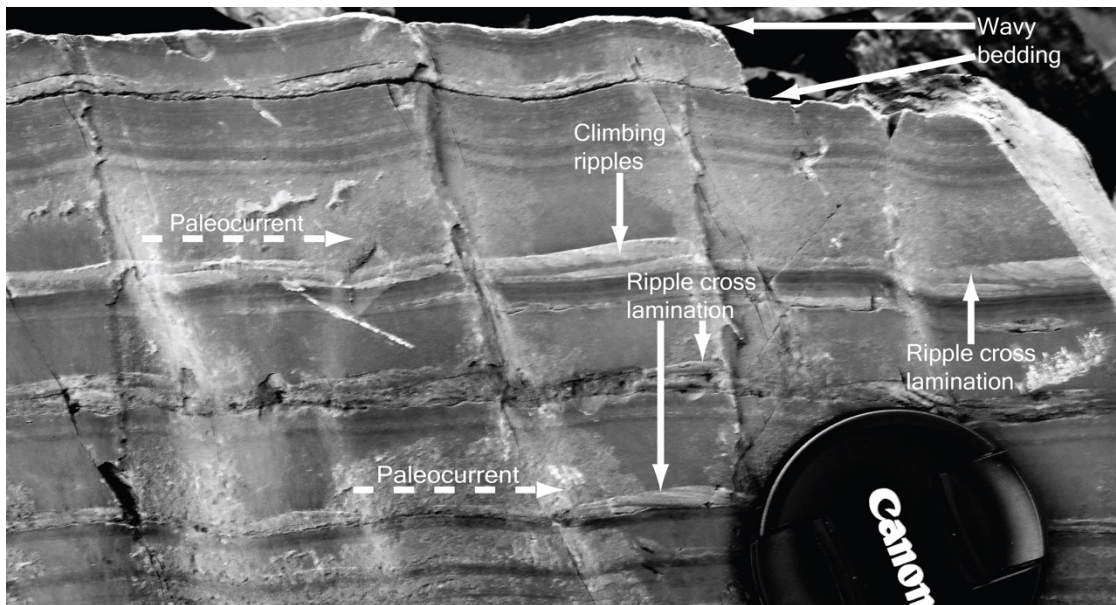


Figure 3.3: Climbing current ripples and corresponding cross-lamination used as physical sedimentological evidence to infer paleocurrent direction at the Melrose Surface. Paleocurrent direction: 102° SE. Note wavy bedding partly coincident with the cleavage

### 3.1.2 Historical paleobiological interpretation

Traditional paleobiological reconstructions of stemmed frondose Ediacaran fossils have followed Glaessner (1985), interpreting these fossils as pennatulacean-like organisms that lived erect in the water column. The descriptive terminology used (i.e., holdfast, stem, frondlet) is unfortunate, in that it evokes affinities to extant taxa and infers biomechanical properties and life habit. The most significant divergence from this paradigm of ubiquitously erect Ediacaran macroorganisms was the work of Seilacher (1992, 1999), which suggested a more protistan-like mode of life for some taxa and inferred a reclining mode of life for others, such as *Beothukis*. This alternative hypothesis—in which life position should be the same as that in which fronds are preserved (McIlroy et al. 2020, 2021) unless there is evidence to the contrary—has been successfully applied to demonstrate that *Charniodiscus concentricus* (and possibly the frondose portion of *Charniodiscus procerus*), *Arborea arborea*, *Arborea spinosa*, and *Arborea longa* were likely held erect or recumbent in the water column (Laflamme et al. 2004, 2018; Pérez-Pinedo et al. 2022).

### 3.1.3 Surface Assemblage

The Melrose Surface assemblage is taxonomically similar to the D and E Surface assemblages at Mistaken Point (shared occurrence of all taxa in the Melrose Surface) and has a comparable community composition but shows a much lower generic diversity (5 vs. 8 [D] and 12 [E]), a lower Shannon diversity (0.375 vs. 0.7 [D] and 1.52 [E]), and a lower Shannon evenness (0.23 vs. 0.33 [D] and 0.61 [E]) (cf. Clapham et al. 2003).

*Fractofusus misrai*, the most abundant species in the Mistaken Point Ecological Reserve (i.e., Mitchell et al. 2015; Mitchell and Butterfield 2018), dominates the Melrose Surface

assemblage (91% of all specimens) but is otherwise very rare in the Catalina Dome (cf. Hofmann et al. 2008). The second most abundant species on the surface is *P. abyssalis* (6% of the total specimens), which is occasionally found on surfaces with *F. misrai* (i.e., MPER D Surface [Clapham and Narbonne 2002; Clapham et al. 2003; Bamforth et al. 2008], although we note the lack of statistically significant co-occurrence indices in Eden et al. [2022]) and is otherwise unreported from the Catalina Dome. *Pectinifrons abyssalis* has been interpreted as having frondlets elevated into the water column (Bamforth et al. 2008). Similarly, “multifoliate” rangeomorphs such as *Bradgatia* sp. and *Primocandelabrum* sp. are poorly represented in the assemblage (2% and 0.5%, respectively). These have typically been interpreted as living erect in the water column (e.g., Flude and Narbonne 2008; Hofmann et al. 2008) and preserved by felling by tuff-laden turbidity currents (though this is at odds with the hydrodynamics of the inferred turbidity currents, as noted by McIlroy et al. [2022]). A single *Charniodiscus* sp. is the only arboreomorph fossil on the Melrose Surface. *Charniodiscus* has also been occasionally found in association with *F. misrai*, *P. abyssalis*, and *Bradgatia* (cf. D and E surfaces at MPER; Clapham and Narbonne 2002; Pérez-Pinedo et al. 2022; but see Eden et al. 2022).

*Fractofusus misrai*.—*Fractofusus misrai* was discovered by Anderson and Misra (1968) in the Mistaken Point Ecological Reserve, where it is restricted to the Mistaken Point Formation and was named by Gehling and Narbonne (2007) along with *Fractofusus andersoni*. In the Catalina Dome, *F. misrai* is otherwise only known from three ambiguous specimens from the Murphy’s Cove Member, which has been correlated with the Mistaken Point Formation of the Avalon Peninsula as well as a possible specimen in the Fermeuse Formation (Hofmann et al. 2008).

Orientation data of *F. misrai* from the E Surface at Mistaken Point (Seilacher 1992; Gehling and Narbonne 2007) suggest no preferential orientation of the population. The

appropriateness of log transformations to study population structure is much debated, and two approaches have been conducted on morphometric traits. Clustering algorithms and Bayesian information criterion (BIC) analysis of *F. misrai* on transformed data from both the D and E surfaces suggest that both assemblages were composed of specimens of different ages and with a large size range, suggesting a slow-growth model with aseasonal (continuous) reproduction (Darroch et al. 2013). Similarly, alternative studies on non-transformed data suggest that the *F. andersoni* assemblage from the H14 Surface (Bonavista Peninsula) represents a multigenerational population, possibly the result of continuous asexual reproduction via stolons or propagules (Mitchell et al. 2015).

*Pectinifrons abyssalis*.—*Pectinifrons abyssalis* was described from the Mistaken Point Ecological Reserve (MPD, MPN, SH, and Watern Cove surfaces) and Green Head (Bamforth et al. 2008) and is considered to be a rangeomorph with a curved pedicle rod and two series of parallel first-order rangeomorph branches that are typically found on the concave side of the rod. The only known exceptions to this branch positioning are two specimens from the Mistaken Point North Surface that may have been twisted or folded before burial (Bamforth et al. 2008). The first-order rangeomorph branches of *Pectinifrons* are interpreted as being held above the seafloor, emerging from the upper surface of the pedicle rod. No preferential orientation was found at the Mistaken Point Ecological Reserve, whereas an apparent bimodal orientation was reported from Green Head (Bamforth et al. 2008).

*Bradgatia* sp.—*Bradgatia* was originally described by Boynton and Ford (1995) based on material from the Charnwood Forest (U.K.), while the Newfoundland material was later reviewed by Flude and Narbonne (2008). *Bradgatia linfordensis* is a multifoliate rangeomorph, showing several first-order branches stemming from a central region. The fronds have typically been

interpreted as being held in clusters subvertically in the water column and felled by depositional events. Taphomorphs of *Bradgatia* include elongate specimens (“I-shaped”) to specimens showing first-order branches oriented in all directions (“O-shaped”), while in others the fronds are all on one side of the point of origin (Flude and Narbonne 2008).

It has been previously noted that *Bradgatia* sp. are commonly bimodally oriented in both the inferred up-current and down-current directions on the G Surface at MPER (Flude and Narbonne 2008), while at other localities (E and D surfaces at MPER) there are also abundant specimens oriented perpendicular to the paleocurrent (Flude and Narbonne 2008; Vixseboxse et al. 2021; McIlroy et al. 2022). Orientation data from Bishop’s Cove potentially show unimodal orientation, with several specimens oriented orthogonally and against the paleocurrent direction (Flude and Narbonne 2008). These orientation data have not, however, been incorporated into paleobiological models of the genus.

### **3.2 MATERIALS AND METHODS**

The data presented in this study were collected from a single fossiliferous surface of the Fermeuse Formation that crops out on the southeastern margin of the Catalina Dome, Bonavista Peninsula (see O’Brien and King 2005) (Figure 3.2). The surface is part of a succession of thin-to medium-bedded gray and green fine sandstones and siltstones, with some coarse-grained sandstones (Figure 3.4). The Melrose Surface fossils are preserved on a 2-cm-thick gray to dark gray wavy bedded siltstone, which is overlain by a 5 to 10-cm-thick sandstone with soft-sediment deformation. Under the siltstone bed is a 0.1- to 0.6-mm-thick ripple cross-laminated sandstone bed that indicates a paleocurrent orientation of 102° SE (78° NE with respect to magnetic north);

this feature is consistent with the cleavage-enhanced wavy bedding. The fossiliferous horizon is ferruginous, probably reflecting the weathering/oxidation of pyrite.

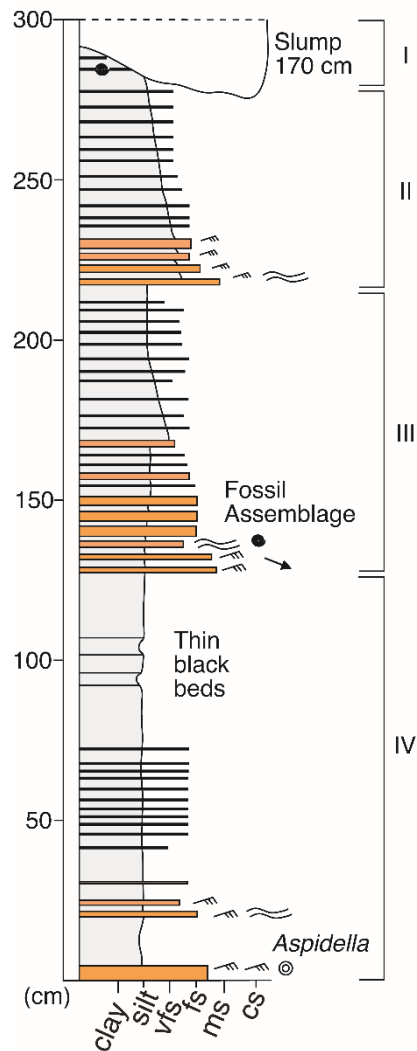


Figure 3.4: Sedimentary log through interbedded siltstones and thin ripple cross-laminated sandstones, including the fossiliferous Melrose Surface, on the southern portion of the Catalina Dome in the Discovery UNESCO Global Geopark. I) Slumped silty sandstones with weakly erosive base. II) Upward-thinning and upward-fining succession with ripple cross-laminated sandstones. III) Thinning and fining. Upward-fining siltstone and thin sandstone beds with wavy bedding. IV) Siltstone with thin sandstones and two black siltstones; some ripple cross-lamination. Vfs, very fine sand; fs, fine sand; ms, medium sand; cs, coarse sand.

Data collection was grid based, with 41 squares of approximately  $1.5 \times 1.5$  m completely documented with respect to their paleontology. Grids were photographed and orientation data collected ( $n_t = 208$  specimens of five different taxa measured: *Fractofusus*  $n_f = 190$ ; *Pectinifrons*  $n_p = 12$ ; *Bradgatia*  $n_b = 4$ ; *Primocandelabrum*  $n_{pr} = 1$ ; and *Charniodiscus*  $n_c = 1$ ). Orientation was recorded for four additional *Bradgatia* specimens from an adjacent slab where access is more difficult, which belongs to the same surface.

Fragmental specimens of all studied taxa were excluded from the analysis due to analytical difficulties and potential to introduce sampling bias. Only *Fractofusus* was included in the statistical analysis due to the low numbers of well-preserved specimens of all other taxa. Given the low numbers of kinked *Fractofusus* specimens (seven specimens) and given the bidirectional straight nature of the remaining specimens, orientation was projected under and over  $180^\circ$  separately, opposed to projections on  $360^\circ$  (following Gehling and Narbonne 2007; Mitchell et al. 2015; Vixseboxse et al. 2021). In this way, we avoided, plotting two images of virtually identical vectors, which could have resulted in misleading interpretation of the data. Climbing ripple cross-lamination was used to infer a southeasterly paleocurrent orientation of  $102^\circ$  ( $78^\circ$  to magnetic north) (cf. Mason et al. 2013; Figure 3.3), providing an independent and unequivocal current direction against which to compare frond orientations.

### 3.2.1 Quantitative Variables

In this study, two quantitative morphometric traits (length and width) of the taxa were recorded and corresponding size-frequency distributions were analyzed (i.e., Darroch et al. 2013). Morphometric traits were retrieved from field photography and analyzed with the software ImageJ (Schneider et al. 2012). Study of size-frequency distributions is a commonly used method in

biology to explore population structure (Darroch et al. 2013). It can provide insights regarding the coefficient of variation across different morphometric variables, the skewness or relative contribution of different age/size classes, and the mode as a proxy for mortality rate and reproductive behavior (e.g., Bak and Meesters 1999; Meesters et al. 2001; Darroch et al. 2013). First, normality of the data was assessed by Shapiro-Wilk test, and logarithmic transformation of the data was conducted as required, as it normally generates a more precise representation of population structure (following Darroch et al. 2013; Figure 3.5). However, alternative approaches with non-transformed data have also been conducted, revealing multigenerational populations (e.g., Mitchell et al. 2015). The data were analyzed by the Gaussian finite mixture model-based clustering algorithms of the package mclust (Scrucca et al. 2016). This method resolves the most likely number of modes of the morphometric traits that represent different age/size classes within the population. The best model was chosen by a criterion for likelihood-based model selection (BIC) (see Darroch et al. [2013] for full methodology). Because univariate size-frequency distribution analyses could result in misleading conclusions, bivariate analyses were also conducted (Figure 3.5).

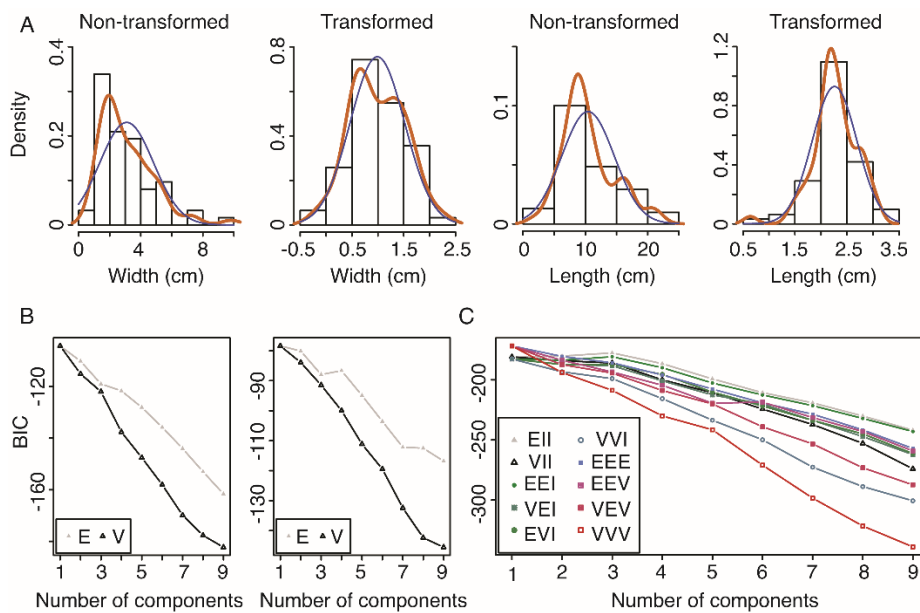


Figure 3.5: Composite figure showing: A) logarithmic transformation of size-frequency distributions of *Fractofusus misrai* with Gaussian curve overlapping for illustrative purposes; B) Bayesian information criterion (BIC) results for univariate data (width and length measured in centimeters) (E and V for equal and unequal variance, respectively); C), BIC results for bivariate data. Model parameterizations: EII, spherical, equal volume; VII, spherical, unequal volume; EEI, diagonal, equal volume, and shape; VEI, diagonal, varying volume, equal shape; EVI, diagonal, equal volume, varying shape; VVI, diagonal, varying volume and shape; EEE, ellipsoidal, equal volume, shape, and orientation; EEV, ellipsoidal, equal volume and shape; VEV, ellipsoidal, equal shape; VVV, ellipsoidal, varying volume, shape, and orientation. Biologically realistic models assume ellipsoidal distributions (see Fraley and Raftery [2007] and Darroch et al. [2013] for more information).

### 3.2.2 Circular Variables

Variables that are measured in scales that are circular or cyclical rather than linear or continuous commonly arise when recording orientation or time, both of which can be accurately represented as a circumference. Using linearized scales for circular variables can lead to misinterpretation of the natural behavior of the circular variables and therefore alternative statistical treatment is required (Landler et al. 2020). Herein we apply an integrated approach to analyze multivariate datasets including quantitative and circular variables together, without treating orientation as a continuous variable. This approach allows us to interpret information derived from all the recorded variables integrated.

The circular variable of species-specific orientation was initially visualized by plotting nonparametric density curves with angular histograms, where bandwidths were chosen by visual

examination (Will 2016; Figure 3.6). To test potential departures from uniformity in the distribution of the circular variable, several statistical tests were considered (see Vixseboxse et al. 2021). A Rayleigh test, designed to detect unimodal von Mises (the circular analogue of the normal distribution) departure from uniformity, was conducted (Batschelet 1981); however, the Rayleigh test has very low potential to detect multimodal distributions. Rao's spacing test was conducted to test for deviations from uniformity without the assumption of a von Mises distribution. Both visualization of angular histograms and Rayleigh and Rao's spacing circular uniformity tests were performed using the package circular in R (Agostinelli and Lund 2017; Vixseboxse et al. 2021). However, the relative performance of these tests against multimodal departures from uniformity bears uncertainty (Landler et al. 2018). As multimodal deviations from uniformity are suspected based on the summary plots (Figure 3.6, see Supplementary R script), and following Landler et al. (2018, 2019, 2020), the Hermans-Rasson test was chosen as the most suitable test to explore multimodal departures from normality. The test was performed using the package CircMLE (Fitak and Johnsen 2017; Landler et al. 2019; Vixseboxse et al. 2021), reducing type I error (Landler et al. 2020). The hypothesis of a von Mises distribution was also tested using Watson's goodness of fit (Agostinelli and Agostinelli 2018; Vixseboxse et al. 2021) (see all results in Table 1). As a preliminary exploration of orientation, Gaussian finite mixture model-based clustering algorithms were employed to identify the most likely number of modes in orientations from under and over 180° (Fig. 6). This analysis was deemed appropriate, as the maximum degree of dissimilarity of the data was 180° (in the case of *Fractofusus* specimens due to their bipolar growth).

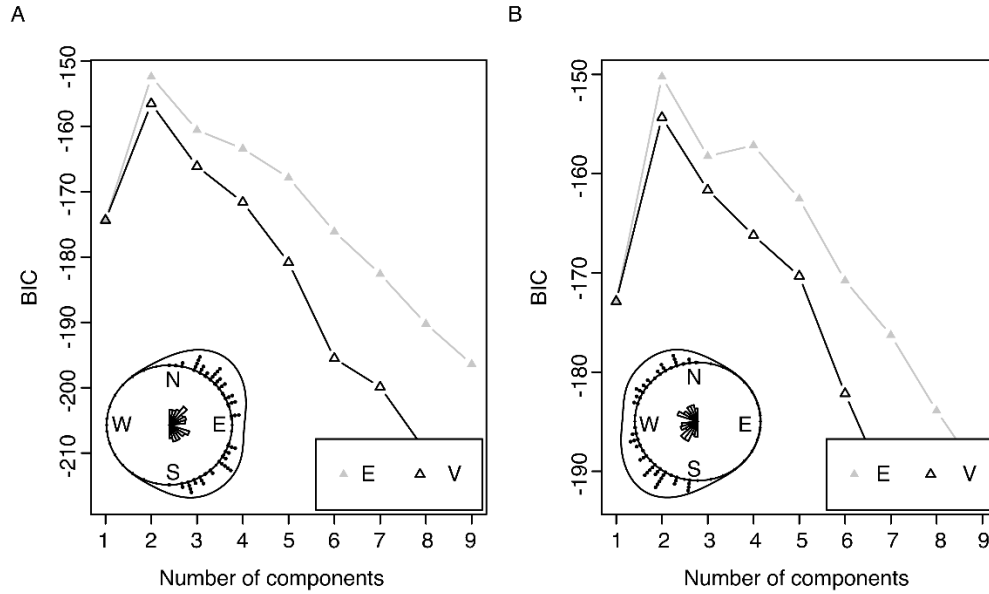


Figure 3.6: Preliminary exploration of *Fractofusus misrai* orientation. A) Bayesian information criterion (BIC) results for orientation under  $180^\circ$  and corresponding rose plot with angular histogram. B) BIC results for orientation over  $180^\circ$  and corresponding rose plot with angular histogram. E and V for equal and unequal variance, respectively.

Dataset	Rayleigh test	Rao spacing test	Hermann-Rasson test	Watson's test
Under $180^\circ$	4.65E-11	< 0.01	1.00E-03	< 0.01
Over $180^\circ$	1.51E-11	< 0.01	1.00E-03	< 0.01

Table 3.1: Results from uniformity and von Mises distribution tests on orientation of *Fractofusus misrai* from the Melrose Surface.

Traditional parallel coordinate plots (PCPs) are sometimes employed to explore the relationships between quantitative variables, treating circular variables as regular continuous variables. These variables can be scaled, with corresponding values in each variable correlated by connecting lines. Although this approach allows the observation of the relationships in multivariate datasets (Hardle and Simar 2019), it is unsuitable for circular variables, because extreme values

( $0^\circ$  and  $360^\circ$ ) would bear the greatest degree of dissimilarity, when in fact they are essentially equal. Therefore, modified PCPs were used to visualize multivariate data with a circular variable. A circle of radius 0.5 was chosen to represent orientation drawn as an ellipse (*sensu* Will 2016). An aspect ratio of 1:1 would generate a circle but would affect the readability of the figure; the mechanics of the PCP do, however, remain unaltered. This approach allows the visualization of relationships across circular and continuous variables. Because the projection of an ellipse could visually alter the spatial interpretation of the figure, density curves used in univariate summary plots were also projected (Figures 3.7, 3.8, Supplementary R script).

To further explore these patterns in the dataset, we conducted cluster analysis on a dissimilarity matrix. Gower's distance was used to account for dissimilarity that introduced a circular variable (Will 2016). In the case of circular variables, distance is measured in either direction around the circumference, with  $180^\circ$  being the largest possible difference. The function for implementing a dissimilarity matrix with a circular variable was retrieved from Will (2016). Gower's general coefficient has applications in the package *ade4* (Dray et al. 2007).

After generating a distance matrix including the circular variable, we performed cluster analysis. Ward's hierarchical bottom-up agglomerative polythetic clustering method was conducted using the *hclust* function in R (Will 2016). All groups of clusters were processed, and the cluster that resulted in the smallest increase in error sums of squares was selected (Everitt and Hothorn 2011). We employed circular variables and a Gower's dissimilarity matrix; therefore, the distance is non-Euclidean. It accounts for a pseudo-error sum of squares (Will 2016). Clusters were visualized in a dendrogram in which height is a nondimensional indication of the dissimilarity between clusters (Figures 3.7, 3.8). Potential solutions were indicated by crosscutting horizontal

lines. When the vertical dissimilarity between splitting clusters is of a small magnitude, the real existence of subsequent clusters is ambiguous.

To resolve the most parsimonious solution, the Caliński-Harabasz pseudo F-statistic (Caliński and Harabasz 1974; Will 2016) was employed (Figures 3.7, 3.8), available in the clusterSim package (Walesiak and Dudek 2020). This test explores the relationship of between-clusters sums of squares compared with within-cluster sums of squares across several cluster solutions ( $k$ ). However, pseudo sums of squares are considered in this case (Will 2016). The largest value of  $G1$  (ratio of between-cluster variability over within-cluster variability) indicates the best solution for the number of clusters. The potential one-cluster solution has no mathematical value, because the calculation is not allowed (Will 2016). The cluster solution was visualized by modified PCPs wherein individual observations belonging to clusters were colored differently. To further facilitate the readability of the figure, medoids of the clusters were projected. A medoid of a cluster is “an observation that has the smallest average dissimilarity with all the other observations in the cluster” (Will 2016: p. 19) (Figures 3.7, 3.8) following Kaufman and Rousseeuw (2009) (see Will [2016] and Tran [2019] for full methodology of circular statistics). The viability of the one-cluster solution was inspected by uniformity and von Mises distribution tests (Vixseboxse et al. 2021) conducted before the cluster analysis described earlier and resolved by modified monothetic clustering analysis (Tran 2019).

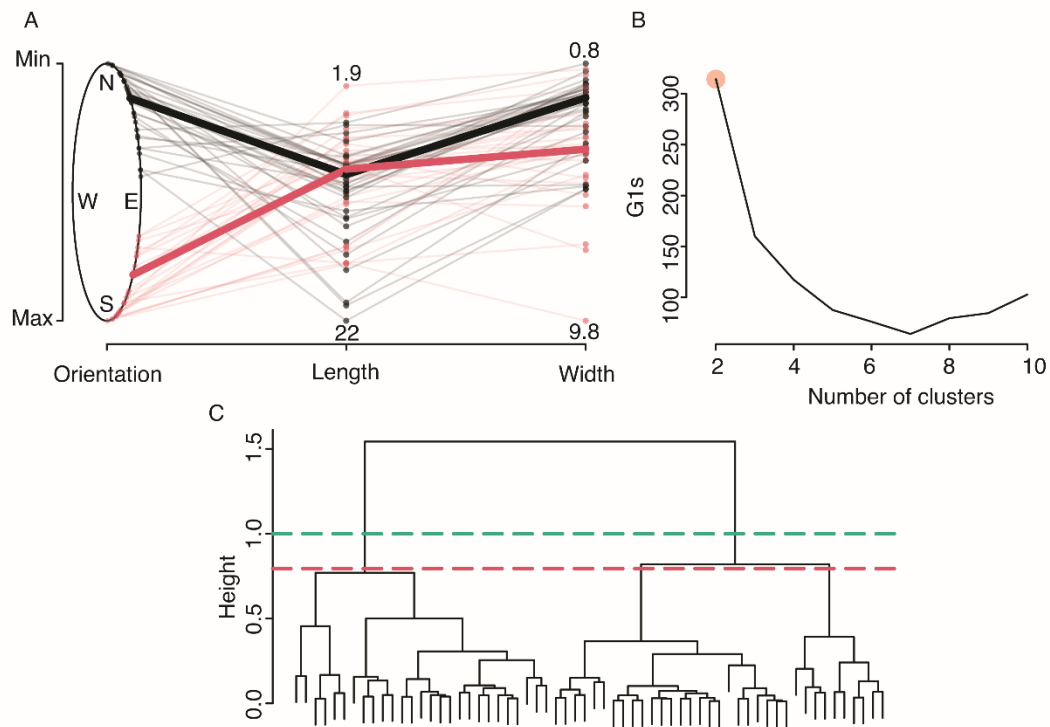


Figure 3.7: Circular statistical analysis of *Fractofusus misrai* under 180°. A) Modified parallel coordinate plot (PCP) with corresponding medoids reflecting the two-cluster solution with proposed Gower's distance and Ward's method. B) G1 values of Caliński-Harabasz pseudo F-statistic. In red (circle) the selected two-cluster solution. C) Dendrogram of cluster solution, green dashed line (top) for the selected two-cluster solution and red dashed line (bottom) for a potential three-cluster solution.

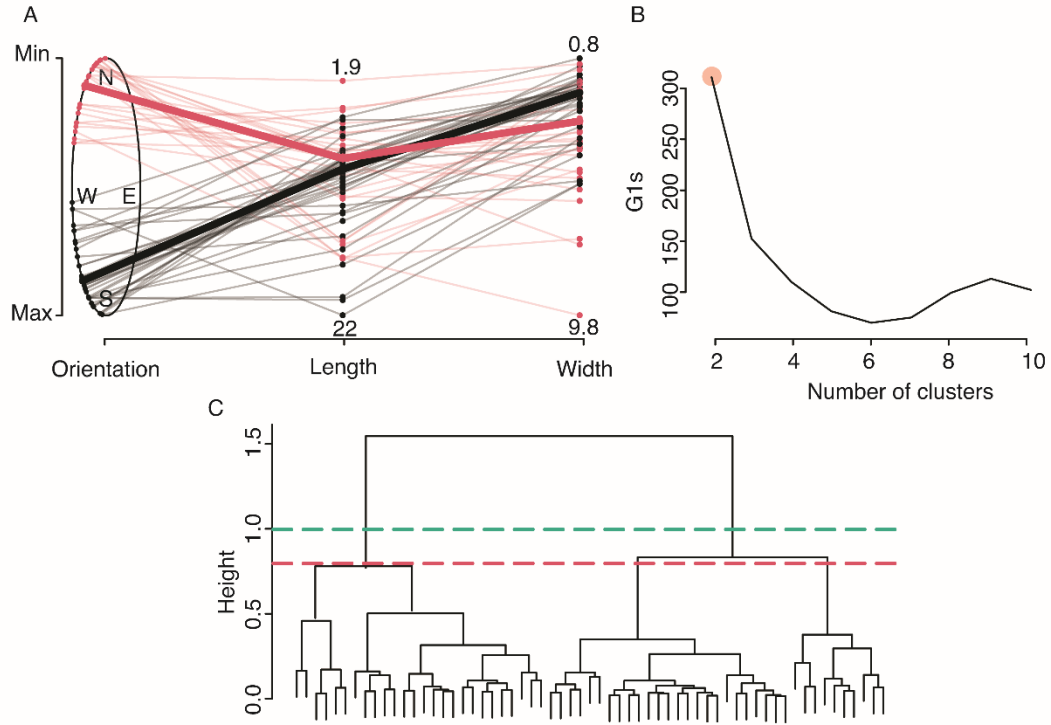


Figure 3.8: Circular statistical analysis of *Fractofusus misrai* over 180°. A) Modified parallel coordinate plot (PCP) with corresponding medoids reflecting the two-cluster solution with proposed Gower’s distance and Ward’s method. B) G1 values of Caliński-Harabasz pseudo F-statistic. In red (circle) the selected two-cluster solution. C) Dendrogram of cluster solution, green dashed line (top) for the selected two-cluster solution and red dashed line (bottom) for a potential three-cluster solution.

Medoids	Observation ID	Orientation	Length	Width
1st medoid	29	43	9.4	2
2nd medoid	44	130	8.95	3.8

Table 3.2: Medoids and corresponding values in the multivariate matrix for *Fractofusus misrai* from the Melrose Surface under 180°.

Medoids	Observation ID	Orientation	Length	Width
1st medoid	29	223	9.4	2
2nd medoid	57	322	8.5	3

Table 3.3: Medoids and corresponding values in the multivariate matrix for *Fractofusus misrai* from the Melrose Surface over 180°.

Monothetic cluster analysis was additionally conducted to support the chosen solution for number of clusters on the variables suspected to drive clustering patterns and test the viability of the one-cluster solution (see Tran 2019). This test is “a divisive clustering method that uses a hierarchical, recursive partitioning of multivariate responses based on binary decision rules that are built from individual response variables” (Tran 2019: p. xiv). Estimation of the optimal number of clusters solution was based on a combination of M-fold cross-validation (Hastie et al. 2016) and permutation-based hypothesis test at each split (Hothorn et al. 2006) adapted to work with monothetic cluster analysis and circular variables with non-Euclidean distances (see Tran 2019).

Because MSE can be calculated for the one-cluster solution, the cross-validation method can compare the one-cluster solution with multi-cluster solutions (Sneath and Sokal 1973; Chavent 1998; Piccarreta and Billari 2007). This test was combined with permutation-based hypotheses, which involved testing the null hypothesis of independence ( $H_0$  = splitting two clusters are identical) at each node of the tree retaining statistically significant  $p$ -values (Hothorn et al. 2006; Tran 2019). This method was conducted using the monoClust package in R (Tran et al. 2021).

### 3.3 RESULTS

#### *Fractofusus misrai*

Untransformed length- and width-frequency distributions were right-skewed (Figure 3.5) and moderately depart from normality (Shapiro- Wilk test,  $\alpha = 0.01$ ,  $p$ -value [length] = 0.0066,  $p$ -

value [width]  $\ll 10^{-4}$ ). Log-transformed quantitative variables (following Darroch et al. 2013) were normally distributed (Shapiro- Wilk test,  $\alpha = 0.01$ ,  $p$ -value [length] = 0.0170,  $p$ -value [width] = 0.6448). Univariate analysis conducted using Gaussian finite mixture model-based clustering algorithms resulted in a single mode or age/size group as the most likely cluster solution assuming both equal and unequal variances (Figure 3.5). Subsequent bivariate analysis generated best-fitting models assuming ellipsoidal, diagonal, and spherical distributions. Only the models assuming ellipsoidal distributions allowing for unequal variances along both axes are biologically realistic (Fraley and Raftery 2007; Darroch et al. 2013). BIC results from the bivariate models derived from the clustering algorithms are congruent with the univariate models in selecting one cohort as the optimal solution. The parametrization of models allude to shape, volume, and orientation of the clusters. (Figure 3.5; see Supplementary R script for BIC values,).

Regarding circular variables, the angular histogram with density curves suggested multimodal (likely bimodal) distributions of essentially identical recorded orientations both under and over  $180^\circ$ . These distributions were supported by the results from the Gaussian finite mixture model-based clustering algorithms, which resolved two modes as the most likely number of clusters in the orientation-frequency distribution (under  $180^\circ$ :  $43^\circ$  [NE] and  $140^\circ$  [SE]; over  $180^\circ$ :  $222^\circ$  [SW] and  $321^\circ$  [NW]) (Figure 3.6). All the tests employed (Rayleigh, Rao's spacing, and Hermans-Rasson) rejected the null hypothesis of uniformity ( $p$ -value  $< 0.05$ ) as well as the existence of von Mises distributions (Watson's test), indicating nonnormal and nonrandom species-specific orientations (see all results in Table 3.1).

Modified PCPs were congruent with angular histograms and the results from the Gaussian finite mixture model-based clustering algorithms (Figure 3.6) in suggesting observable sub-groups in recorded orientation: NE,SE and SW,NW under and over  $180^\circ$  respectively (Figures 3.7, 3.8).

On the other hand, quantitative variables showed a more unified trend with not easily recognizable subgroups (Figure 3.5). The dendrogram cluster obtained by Ward's hierarchical bottom-up agglomerative clustering method on the dissimilarity matrix resulted in two groups, with a three-cluster solution bearing little magnitude between splitting clusters as indicated by cross-cutting horizontal green and red lines (Figures 3.7, 3.8). Caliński-Harabasz pseudo F-statistic resolved the two-cluster solution as the most likely scenario, with the largest value of G1 for both orientations under and over 180° (Figures 3.7, 3.8). Finally, the medoids of the clusters were projected (under 180°: 43° [NE] and 130° [SE]; over 180°: 223° [SW] and 322° [NW]) giving essentially identical orientation results to those obtained from the orientation-frequency distribution analysis (Tables 3.2, 3.3).

Monothetic clustering can operate on non-Euclidean distances, and it was employed to compare the selected two-cluster solution to a potential one-cluster solution. M-fold cross-validation (CV) showed a great difference between the one-cluster and the multi-cluster solutions. The solution made by 10-fold CV shows multi-cluster outcomes showing a great decrease in  $CV_k$  ( $CV_k$ ; mean squared error [MSE]) and reduced error bars ( $MSE \pm 1 SE$ ) for both under and over 180° (Figure 3.9). The cluster solution derived from the permutation-based hypothesis test confirmed two clusters for under and over 180° driven by orientation (Figure 3.9). The two confirmed clusters driven by orientation, and illustrated by the medoids, reveal two groups of *Fractofusus*, with one group being oriented NE-SW and the other oriented SE-NW.

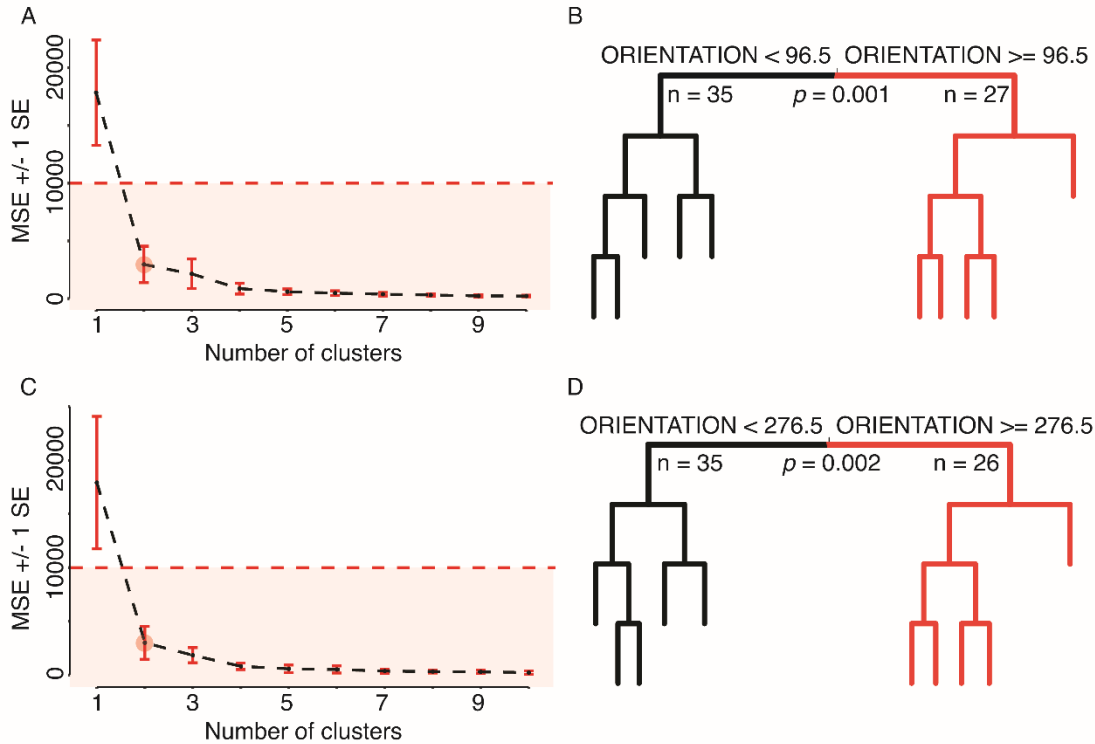


Figure 3.9: Monothetic clustering on orientation of *Fractofusus misrai*. A) M-fold cross-validation results under 180° made by 10-fold cross-validation (CV). B) Splitting rules tree with  $p$ -values under 180°. C) M-fold cross-validation results over 180° made by 10-fold CV. D) Splitting rules tree with  $p$ -values over 180°. A, C) Multi-cluster solutions below the red dashed line.

### *Pectinifrons abyssalis*

Only 11 specimens of *P. abyssalis* are reported from the Melrose Surface and were therefore excluded from the clustering analyses. The specimens do not show a clear orientation pattern, ranging from being almost parallel ( $n_p = 2$ ) to the inferred paleocurrent direction to being almost perpendicular ( $n_p = 7$ ), and even oriented against it ( $n_p = 2$ ) (Table 3.4; Figure 3.10).

One specimen appears to be twisted (Fig. 3.1B), showing first-order branches on the right-hand side of the pedicle rod in the south half of the fossil and on the left-hand side on the north

half. Preservation of the first-order branches appears to be similar between the two halves, but no higher-order branches can be observed.

*Bradgatia* sp.

Only four specimens of *Bradgatia* are reported from the gridded section of the Melrose Surface and four additional specimens are located on an adjacent slab. Due to the low number of specimens, they were therefore excluded from the clustering analyses. The four specimens from the gridded section have the “U-shaped” morphology (sensu Flude and Narbonne 2008) and are characterized by first-order branches arising from a central position, and therefore determine an apical–basal polarity. Three specimens are oriented in a close to orthogonal position to the paleocurrent direction, and another specimen is oriented with the frond tips in the up-current direction. The remaining four specimens show parallel and oblique orientations to the inferred paleocurrent (Table 3.4; Figure 3.10).

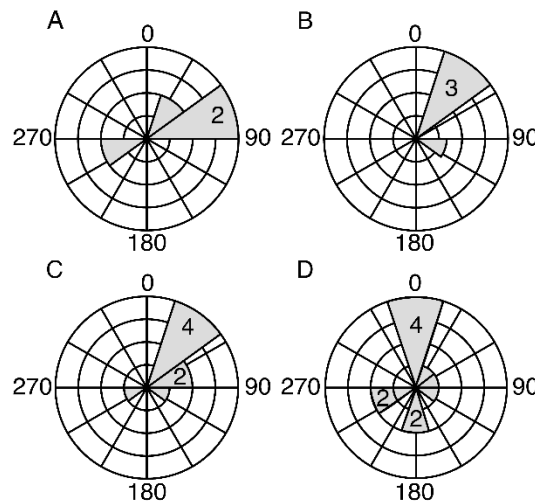


Figure 3.10: Orientation of the specimens excluded from the statistical analysis. A) *Bradgatia* sp. from adjacent slab but part of the Melrose Surface. B) *Bradgatia* sp. from the gridded area. C) Total *Bradgatia* sp.. D) *Pectinifrons abyssalis*. Where not indicated, one specimen is present.

Quadrat	Specimen ID	Genera	Length	Width	Orientation
6A	17	Bradgatia	5.4	2.03	28
7A	23	Bradgatia	8.73	5.05	40
7B	50	Bradgatia	5.23	4.79	51
6C-	202	Bradgatia	NA	NA	118
NA	NA	Bradgatia	NA	NA	50
NA	NA	Bradgatia	NA	NA	56
NA	NA	Bradgatia	NA	NA	84
NA	NA	Bradgatia	NA	NA	247
-2B	1	Pectinifrons	25.3	2.9	355
-2B	2	Pectinifrons	19.4	3.8	180
-2B	3	Pectinifrons	25.2	3.3	245
-2C	4	Pectinifrons	36.5	4	5
-2C	5	Pectinifrons	11.1	1.1	20
-2C	6	Pectinifrons	22.7	3.8	120
-2D	7	Pectinifrons	75.5	1.6	345
-4A	8	Pectinifrons	NA	NA	255
-4A	9	Pectinifrons	15.2	2.6	55
-4A	10	Pectinifrons	24.2	2	10
-4A	11	Pectinifrons	NA	NA	180
5B	14	Primocandelabrum	7.54	3.7	9

Table 3.4: Morphometric traits and orientation from specimens excluded from the statistical analysis.

### 3.4 DISCUSSION

The Ediacaran-aged Avalon Assemblage (Waggoner 2003) is characterized by immotile epibenthic communities of macroorganisms that are preserved in situ. In the absence of evidence for motile scavengers and given the rarity of motile macroorganisms in general (Brasier et al. 2010; Liu et al. 2010; although see horizontal burrows and surface trace fossils in Liu et al. [2014] and Liu and McIlroy [2015]), ecological mechanisms such as competition and dispersal are thought to have led to gradational epifaunal tiering (vertical subdivisions of the water column) and evolutionary innovations in Ediacaran communities (Clapham and Narbonne 2002 but see Mitchell and Kenchington 2018; Mitchell et al. 2019). A tiered epifaunal structure is congruent with suspension feeding or organic matter absorption as a means of resource partitioning (Bottjer and

Ausich 1986), whereby nutrients are provided by bottom currents. The evolution of stems in demonstrably erect taxa increased height and allowed for exploitation of higher tiers, resulting in a competitive advantage and increased feeding capacity (Clapham and Narbonne 2002; but see Mitchell and Kenchington 2018). Reclining organisms such as the spindle-shaped *Fractofusus* and *Beothukis*, which lay flat on or partly within matgrounds, occupied the basal tiers.

Previous inferences on Ediacaran feeding strategies such as suspension feeding or osmotrophy in the Rangeomorpha are based upon analogies with extant Pennatulacea and are inferred based on comparable epifaunal tiering (Laflamme et al. 2009). However, the morphological analogy has been demonstrated to be imperfect (Antcliffe and Brasier 2007), particularly given the absence of preserved pores for fluid flow/organic matter uptake (Liu et al. 2015; but see Butterfield 2022). The organic matter reservoirs of dissolved organic matter (DOM) (Johnston et al. 2012; Liu et al. 2015) are unlikely to have been sufficiently concentrated to support osmotrophy (Fakraee et al. 2021; McIlroy et al. 2021). In the absence of good evidence for either suspension feeding or osmotrophy, it has been proposed that some Ediacaran organisms could have relied on chemosymbiotic strategies (i.e., Seilacher 1984; McMenamin 1998; Dufour and McIlroy 2017; McIlroy et al. 2021, 2022; Taylor et al. 2021; Pérez-Pinedo et al. 2022).

As Ediacaran seafloors lacked significant amounts of macrobioturbation before ~550 Ma (Jensen 2003), the abundant matground-associated seafloors are likely to have experienced buildup of toxic sulfides due to the metabolism of sulphur reducing bacteria in their porewaters (Dufour and McIlroy 2017). This toxicity would have posed a threat to sessile epifaunal sediment-reclining organisms like *Fractofusus* and *Beothukis*, which maintained constant association with the Ediacaran sulfide-rich seafloor. The basal surface of *Fractofusus* is characterized by a large surface area, which has been considered an adaptation for maximizing a chemosymbiotic epithelium, and

to allow transport of oxygen into porewaters to mitigate the impact of reduced forms of sulfur on the lower surface. These organisms are thought to have increased oxygen content at their lower surfaces by diffusion through the body and/or ciliary irrigation. Increasing oxygen supply to sulfidic porewaters increases productivity of chemolithoautotrophic sulfur-oxidizing bacteria and effectively detoxifies porewaters. *Fractofusus* could thus have obtained nutrients from chemolithoautotrophic microbes/symbionts via phagocytotic processes across their fractal-like lower epithelia (Dufour and McIlroy 2017).

*Fractofusus misrai*

*Fractofusus* is the numerically dominant species in the lower tiers at Mistaken Point and the Melrose Surface assemblage ( $n_f = 190$ ; 91%). The Gaussian finite mixture model-based clustering algorithms resolved one mode, interpreted as one age/size class, as the most likely number of modes both for the univariate and bivariate size-frequency distributions. Different population dynamics can generate unimodal distributions such as pioneer colonizing populations, populations with slow growth rates but high recruitment and reproduction rates, and populations showing aseasonal or continuous reproduction (Darroch et al. 2013).

As shown by the medoids projected in the PCPs illustrating the results of the polythetic cluster analysis and the optimal cluster solution (Figures 3.7, 3.8, Tables 3.2, 3.3), there are two orientation groups. Groups under and over  $180^\circ$  are essentially symmetrical, as they differ by  $\sim 180^\circ$  from each other. This pattern validates our initial assessment of the almost null effect of the low number of kinked specimens in the analysis on both sides of the circumference both under and over  $180^\circ$ . These two orientation groups show different positions with respect to the single southeasterly paleocurrent: the first orientation group is closer to a paleocurrent-orthogonal orientation (diverging at a  $>50^\circ$  angle), whereas the second orientation group is oblique to the

paleocurrent, diverging at only an  $\sim 35^\circ$  angle. A near-orthogonal orientation would have maximized the aspect ratio of the organism and caused the flow of relatively unexploited water over all rangeomorph elements, leading to an increased capacity to absorb DOM from the water column. However, the feasibility of the sole reliance on osmotrophy is questionable for such large organisms (Dufour and McIlroy 2017). The high aspect ratio of current perpendicular *Fractofusus* would also increase the capacity for oxygen uptake from the upper surface, thereby potentially increasing diffusion through the organism into the sediment and concomitantly increasing productivity of sulfur-oxidizing bacteria below the organism. On the other hand, this orientation would have led to increased potential for current-related damage due to shear stress. Fluid separation caused by the interaction between bottom currents and *Fractofusus* would have led to reversed velocity profiles and eddying along the entire length of the organisms, increasing the eventual possibility of being detached and washed away by the paleocurrent (Southard 2019). This same trade-off applies to an oblique orientation relative to the paleocurrent, which would minimize aspect ratio and absorption, as distal downcurrent rangeomorph elements would be exposed to more exploited water. However, this position would also reduce current-related damage by confining current eddying to the distal end of the organisms. These trade-offs and orientations are suggestive of a reclining position in life (Seilacher 1992; Gehling and Narbonne 2007; Taylor et al. 2023). The two orientation groups show very small differences in morphometric traits, as shown in Tables 3.2 and 3.3 and the PCPs (Figures 3.7, 3.8), agreeing with the Gaussian finite mixture model-based clustering algorithms that resolved one age/size class (Figure 3.5).

Making a well-grounded decision on the number of clusters resulting from clustering algorithms is critical. Even though the Caliński and Harabasz pseudo F-statistic (Caliński and Harabasz 1974) traditionally shows good performance, it bears limitations, as it cannot select the

one-cluster solution (Will 2016). This obstacle was solved in this approach by monothetic clustering (see Tran 2019). M-fold cross-validation showed that the one-cluster solution is statistically unlikely, as it shows a very high mean squared error ( $CV_k$ ). Higher numbers of cluster solutions showed more viable  $CV_k$  and MSE values and reduced error bars compared with the one-cluster solution. However, picking the smallest  $CV_k$  (minCV rule) is an ingenuous approach, as it can result in an unrealistically high number of clusters if the error rates constantly decrease (Tran 2019; Figure 9). The two-cluster solution driven by orientation selected by permutation-based hypothesis test corroborated previous polythetic clustering results both under and over  $180^\circ$ , illustrated in the PCPs (Figures 3.7–3.9). A three-cluster solution was also highlighted in polythetic clustering as the second most likely solution, as illustrated by the Caliński and Harabasz pseudo F-statistic, Ward’s hierarchical bottom-up agglomerative clustering dendrogram (Figures 3.7, 3.8), and the clustering algorithms on size-frequency distributions (Figure 3.6). Both cross-validation and the permutation-based hypothesis test bear certain stochasticity in their algorithms. However, the variability in the outcomes of cross-validation is more relevant and may have a greater effect on its performance (Tran 2019).

Given the absence of appropriate extant analogues for comparison, clustering analyses may offer very ambiguous solutions where no correct answer can be guaranteed. The outcomes derived from clustering analysis require a certain degree of interpretation to identify structural patterns in the dataset (Tran 2019). Overall, the selected two-cluster solution regarding orientation maintains both an optimal cohesion within clusters and external isolation between clusters and is congruent with all polythetic and monothetic clustering analyses. It is also consistent with the trade-off between the nutrient/oxygen gathering strategies and the current shear stress experienced by a

linear benthic organism living fixed to the seafloor while exposed to a current. Both orientation clusters offer adaptative advantages to a reclining lifestyle.

*Pectinifrons abyssalis*

*Pectinifrons abyssalis* has been reported from the Avalon Peninsula (Bamforth et al. 2008), but its presence in the Catalina Dome assemblages has not been documented hitherto (Figure 3.1). The species is found in association with *F. misrai*, although the relative abundance of both species is highly variable between fossil assemblages, and the co-occurrence is not statistically significant (Eden et al. 2022). The species has been reconstructed by Bamforth et al. (2008) as being tethered to the seafloor by a curved “pedicle rod,” with two rows of first-order branches held erect in the water column. Several specimens up to 74 cm in length have been reported. The first-order branches are typically visible on the concave side of the pedicle rod; the specimens that are subject to a change in the curvature of the rod also show a change on the side on which the first-order branches are visible (Bamforth et al. 2008).

The *Pectinifrons abyssalis* specimens at Green Head have bimodal orientations that are incompatible with felling by a paleocurrent (see McIlroy et al. 2022). There are several specimens that have their frondlets oriented perpendicular and against both the turbidity flow and contour current direction. Moreover, there are no specimens oriented in the direction of the inferred contour current at Green Head (Bamforth et al. 2008). Near-substrate upstream-directed velocity pulses have never been reported in turbidity flows (McIlroy et al. 2022), as such felling cannot happen in the up-current direction. Variations in down-current velocity within the net downstream motion of the fluids have been described (e.g., Baas et al. 2011; Kostaschuk et al. 2018). Kelvin-Helmholtz waves at the interface with the ambient fluid at high Froude numbers include up-current directions of particle movement but not net near-bed upstream velocity pulses within the rapidly moving

density current (McIlroy et al. 2022). Therefore, vortices within turbidity currents cannot be used to explain bimodal felling directions; instead, the orientation of the organisms must reflect the presence of positive and negative rheotropic growth controlled by a clear-water background current, not a density flow event (see McIlroy et al. 2022).

This rationale is further supported by *P. abyssalis* specimens on both the Mistaken Point Ecological Reserve (Bamforth et al. 2008) and the Melrose Surface that do not show any preferential orientation, suggesting that the mode of life of the organism was not significantly impacted by paleocurrent. Only one row of first-order branches is discernible in all observed specimens. As the species had been described as a filter feeder erected in the water column, capable of reaching considerable sizes, it seems unlikely that it would not have been affected by currents. Therefore, we suggest the possibility that *Pectinifrons* might have lain its first-order branches on the substrate to feed via a chemosymbiotic relationship with sulfur-oxidizing bacteria, as suggested for *F. misrai* and other Rangeomorpha (Dufour and McIlroy 2017; McIlroy et al. 2020, 2021), or perhaps even like the modern *Zoothamnium* (Moriyama et al. 1999; McIlroy et al. 2009).

One specimen from the Melrose Surface shows a change in the pedicle curvature approximately coincident with a change in the side of the pedicle with first-order branches (twisted specimen in Figure 3.1B). In this specimen, first-order branches are in opposite and almost parallel orientations (N-S) on the concave sides of the pedicle rod, and the whole organism has a rough W-E orientation. It is possible that the west side had been flipped via mechanical damage and folded onto the opposite side but could equally be due to growth. This “twisting” differs from non-idiomorphic “kinked” *Fractofusus* specimens that were bent and repositioned with the original side still facing down (Taylor et al. 2023).

*Bradgatia* sp.

*Bradgatia* is a highly variable taxon, interpreted to have been tethered to the seafloor with first-order branches erected in the water column. In the Newfoundland successions, it is considered to have been susceptible to “felling” by inferred paleocurrents (Flude and Narbonne 2008). The specimens described here do not show evidence of felling, as several are instead oriented in a close to orthogonal position and against the only measurable paleocurrent, as is the case for several specimens in all the surfaces sampled by Flude and Narbonne (2008) for both turbidity flows and contour currents. Even in surfaces where *Bradgatia* specimens show relatively unimodal distributions (e.g., Bishop’s Cove and arguably the E Surface) and potential alignment to a paleocurrent (contour and turbidity currents respectively), several specimens are oriented perpendicularly and against these currents despite the high aspect ratio that they would have had should they have lived with an erect mode of life. This trend becomes more evident in the G and D surfaces (Flude and Narbonne 2008). Moreover, there are specimens oriented close to perpendicular to the paleocurrent that are close to being oriented 180° from each other at the Melrose Surface. These orientations make the felling precept unlikely, even if an orthogonal bottom current to the one observed was inferred, as they would have been felled into and against the current (Figure 3.11) (see McIlroy et al. 2022).

The specimens show a tightly constricted arrangement of first- and higher-order branches, typical of U-shaped *Bradgatia*. The most basal first-order branches on the downcurrent side of some specimens appear to be inflated relative to those on the upcurrent side. The lack of current reorientation suggests that *Bradgatia* was most likely growing along the seafloor, rather than living erect in the water column as typically reconstructed (cf. McIlroy et al. 2021, 2022). The tightly organized branching hierarchy coupled with the basal down-current inflation suggests a functional morphology that simultaneously maximizes the surface area in contact with the seafloor and

exchange with the water column. Similar lifestyles have been suggested for the rangeomorphs *Beothukis mistakensis* (McIlroy et al. 2020) and *Fractofusus misrai* (Dufour and McIlroy 2017).

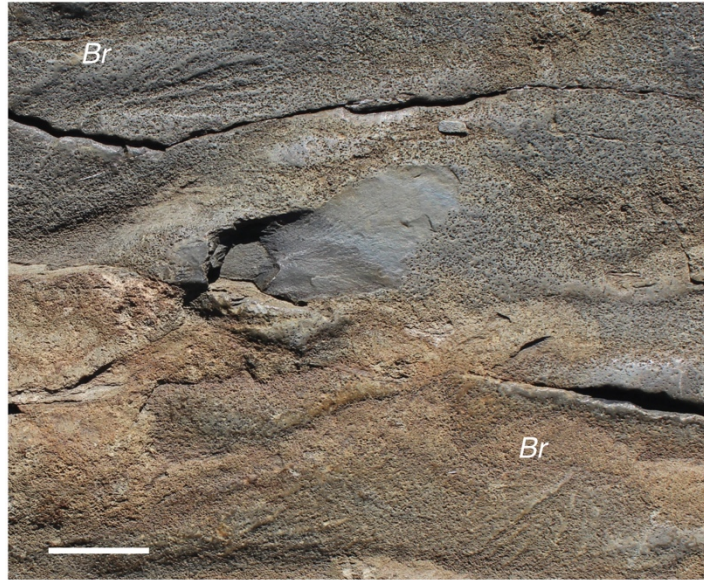


Figure 3.11: Specimens of *Bradgatia* sp. (*Br* in the image) facing opposite directions from a fossiliferous surface in the town of Melrose. Scale bar, 3 cm.

### 3.5 CONCLUSION

Paleocurrent direction in Ediacaran assemblages of Avalonia has occasionally been inferred from the preferential orientation of purportedly felled fronds. There is thus an assumption of erect modes of life that calls into question the causal relationship between inferred paleocurrent direction and the preserved orientation of fronds. In this study, we present an integrated approach conducted on a newly described fossiliferous surface combining: 1) unequivocal physical sedimentological evidence for paleocurrent direction in the form of climbing ripple cross-lamination; 2) a novel approach based on polythetic and monothetic clustering analyses reflecting the circular nature of the recorded orientation of fronds; and 3) an intuitive representation of the data based on modified PCPs including the projection of a circular variable.

1. The *Fractofusus* population presents two orientation groups with respect to the southeasterly paleocurrent (102° SE). The first group is oriented >50° to the paleocurrent, whereas the second orientation group diverges only at an ~35° angle from the paleocurrent. An almost current-transverse orientation could have increased the aspect ratio of the specimen, maximizing the ability to absorb DOM as well as the capacity to diffuse oxygen from the dorsal to the ventral surface. This dorsoventrally transported oxygen could have increased productivity of chemolithoautotrophic bacteria and reduced buildup of sulfides. On the other hand, a more oblique orientation would have reduced specimen aspect ratio as well as reducing the effect of lee-side current eddying and erosion, and therefore the eventual possibility of being washed away by the paleocurrent.
2. *Pectinifrons* specimens do not show any preferential orientation, suggestive of a mode of life not heavily influenced by paleocurrent direction. This notion challenges the previous reconstruction of *Pectinifrons* as a filter feeder but is compatible with a reclining mode of life with first-order branches in permanent contact with the seafloor. Alternative feeding strategies via a chemosymbiotic relationship with sulfur-oxidizing bacteria should be explored.
3. *Bradgatia* specimens show oblique to current-transverse and upstream orientations to the only measurable paleocurrent. The most basal first-order branches on the down-current side appear to be inflated compared with the respective first-order branches on the up-current side. These lines of evidence suggest that *Bradgatia* grew along the seafloor, responding to the current in a rheotropic manner, rather than being erect in the water column. The suggested reclining mode of life is indicative of a functional

morphology that simultaneously maximizes surface area in contact with the seafloor and exchange with the water column suggestive of chemosymbiosis.

The analytical method herein presented offers great potential to explore datasets consisting of fronds with unidirectional directions with respect to the inferred paleocurrents, particularly at sites with independent current indicators. The findings of this work support recent interpretations of some rangeomorphs as being reclining (McIlroy et al. 2021, 2022) showing a rheotropic response to the paleocurrent (cf. rheotropic bryozoan growth in Ryland et al. [1977]), which will require a closer look at paleoecological datasets that have generally assumed an erect mode of life for all the Rangeomorpha excluding *Fractofusus* (i.e., Clapham and Narbonne 2002; Clapham et al. 2003; Liu 2011; Hoyal Cuthill and Conway Morris 2014; Antcliffe et al. 2015; Mitchell and Kenchington 2018; Vixseboxse et al. 2021).

### **3.6 ACKNOWLEDGMENTS**

We acknowledge the constructive criticism by Emily Mitchell and an anonymous reviewer and associate editor A. Tomasovych, as well as the support from E. Samson and Discovery UNESCO Global Geopark. Fieldwork and fossil casting in Newfoundland were conducted under permit from the Parks and Natural Areas Division of the Government of Newfoundland and Labrador. This project was supported by a Discovery Grant and Discovery Accelerator Supplement from the Natural Sciences and Engineering Research Council to D.M.

### **3.7 DECLARATION OF COMPETING INTERESTS**

The authors declare no competing interests.

### 3.8 DATA AVAILABILITY STATEMENT

Data available from the Dryad Digital Repository:

<https://doi.org/10.5061/dryad.dbrv15f4x>.

### 3.9 REFERENCES

Agostinelli, C., & Agostinelli, M.C. (2018). CircStats package. In S. R. Jammalamadaka and A. Sengupta, eds. Topics in circular statistics. World Scientific, Singapore.

Agostinelli, C., & Lund, U. (2017). Circular: circular statistics. In S. R. Jammalamadaka and A. Sengupta, eds.. Topics in circular statistics. World Scientific, Singapore.

Anderson, M. M., & Misra, S. B. (1968). Fossils found in the Pre-Cambrian Conception Group of south-eastern Newfoundland. *Nature*, 220(5168), 680-681.

Antcliffe, J. B., & Brasier, M. D. (2007). *Charnia* and sea pens are poles apart. *Journal of the Geological Society*, 164(1), 49-51.

Antcliffe, J. B., Hancy, A. D., & Brasier, M. D. (2015). A new ecological model for the ~565 Ma Ediacaran biota of Mistaken Point, Newfoundland. *Precambrian Research*, 268, 227-242.

Baas, J. H., Best, J. L., & Peakall, J. (2011). Depositional processes, bedform development and hybrid bed formation in rapidly decelerated cohesive (mud–sand) sediment flows. *Sedimentology*, 58(7), 1953-1987.

Bak, R. P., & Meesters, E. H. (1999). Population structure as a response of coral communities to global change. *American Zoologist*, 39(1), 56-65.

Bamforth, E. L., Narbonne, G. M., & Anderson, M. M. (2008). Growth and ecology of a multi-branched Ediacaran rangeomorph from the Mistaken Point assemblage, Newfoundland. *Journal of Paleontology*, 82(4), 763-777.

- Batschelet, E. 1981. *Circular statistics in biology*. Academic Press, New York.
- Bobrovskiy, I., Krasnova, A., Ivantsov, A., Luzhnaya, E., & Brocks, J. J. (2019). Simple sediment rheology explains the Ediacara biota preservation. *Nature Ecology & Evolution*, 3(4), 582-589.
- Bottjer, D. J., & Ausich, W. I. (1986). Phanerozoic development of tiering in soft substrata suspension-feeding communities. *Paleobiology*, 12(4), 400-420.
- Boynton, H. E., & Ford, T. D. (1995). Ediacaran fossils from the Precambrian (Charnian Supergroup) of Charnwood Forest, Leicestershire, England. *Mercian Geologist*, 13(4), 165-182.
- Brasier, M. D., Callow, R.H., Menon, L.R., & Liu, A.G. (2010). Osmotrophic biofilms: from modern to ancient. Pp. 131–148 in J. Seckbach and A. Oren, eds. *Microbial mats: modern and ancient microorganisms in stratified systems, cellular origin, life in extreme habitats and astrobiology*. Springer, London.
- Brasier, M. D., Antcliffe, J. B., & Liu, A. G. (2012). The architecture of Ediacaran fronds. *Palaeontology*, 55(5), 1105-1124.
- Brasier, M. D., Liu, A. G., Menon, L., Matthews, J. J., McIlroy, D., & Wacey, D. (2013). Explaining the exceptional preservation of Ediacaran rangeomorphs from Spaniard's Bay, Newfoundland: a hydraulic model. *Precambrian Research*, 231, 122-135.
- Budd, G. E., & Jensen, S. (2017). The origin of the animals and a 'Savannah' hypothesis for early bilaterian evolution. *Biological Reviews*, 92(1), 446-473.
- Butterfield, N. J. (2022). Constructional and functional anatomy of Ediacaran rangeomorphs. *Geological Magazine*, 159(7), 1148-1159.
- Caliński, T., & Harabasz, J. (1974). A dendrite method for cluster analysis. *Communications in Statistics-theory and Methods*, 3(1), 1-27.

Chavent, M. (1998). A monothetic clustering method. *Pattern Recognition Letters*, 19(11), 989-996.

Clapham, M. E., & Narbonne, G. M. (2002). Ediacaran epifaunal tiering. *Geology*, 30(7), 627-630.

Clapham, M. E., Narbonne, G. M., & Gehling, J. G. (2003). Paleoecology of the oldest known animal communities: Ediacaran assemblages at Mistaken Point, Newfoundland. *Paleobiology*, 29(4), 527-544.

Darroch, S. A., Laflamme, M., & Clapham, M. E. (2013). Population structure of the oldest known macroscopic communities from Mistaken Point, Newfoundland. *Paleobiology*, 39(4), 591-608.

Darroch, S. A., Laflamme, M., & Wagner, P. J. (2018). High ecological complexity in benthic Ediacaran communities. *Nature Ecology & Evolution*, 2(10), 1541-1547.

Dray, S., Dufour, A. B., & Chessel, D. (2007). The ade4 package-II: Two-table and K-table methods. *R news*, 7(2), 47-52.

Dufour, S. C., & D. McIlroy. (2017). Ediacaran pre-placozoan diploblasts in the Avalonian biota: the role of chemosynthesis in the evolution of early animal life. *Geological Society of London Special Publication*, 448, 211–219.

Dunn, F. S., Liu, A. G., & Donoghue, P. C. (2018). Ediacaran developmental biology. *Biological Reviews*, 93(2), 914-932.

Dunn, F. S., Liu, A. G., Grazhdankin, D. V., Vixseboxse, P., Flannery-Sutherland, J., Green, E., ... & Donoghue, P. C. (2021). The developmental biology of *Charnia* and the eumetazoan affinity of the Ediacaran rangeomorphs. *Science Advances*, 7(30), eabe0291.

Eden, R., Manica, A., & Mitchell, E. G. (2022). Metacommunity analyses show an increase in ecological specialisation throughout the Ediacaran period. *PLoS Biology*, 20(5), e3001289.

Everitt, B., and T. Hothorn. 2011. *An introduction to applied multivariate analysis with R*. Springer, New York.

Fakraee, M., Tarhan, L. G., Planavsky, N. J., & Reinhard, C. T. (2021). A largely invariant marine dissolved organic carbon reservoir across Earth's history. *Proceedings of the National Academy of Sciences*, 118(40), e2103511118.

Fitak, R. R., & Johnsen, S. (2017). Bringing the analysis of animal orientation data full circle: model-based approaches with maximum likelihood. *Journal of Experimental Biology*, 220(21), 3878-3882.

Flude, L. I., & Narbonne, G. M. (2008). Taphonomy and ontogeny of a multibranching Ediacaran fossil: *Bradgatia* from the Avalon Peninsula of Newfoundland. *Canadian Journal of Earth Sciences*, 45(10), 1095-1109.

Ford, T. D. (1958). Pre-cambrian fossils from Charnwood Forest. *Proceedings of the Yorkshire Geological Society*, 31(3), 211-217.

Fraley, C., & Raftery, A. E. (2007). Bayesian regularization for normal mixture estimation and model-based clustering. *Journal of Classification*, 24(2), 155-181.

Gehling, J. G. (1999). Microbial mats in terminal Proterozoic siliciclastics; Ediacaran death masks. *Palaios*, 14(1), 40-57.

Gehling, J. G., & Narbonne, G. M. (2007). Spindle-shaped Ediacara fossils from the Mistaken Point assemblage, Avalon Zone, Newfoundland. *Canadian Journal of Earth Sciences*, 44(3), 367-387.

Gehling, J. G., Narbonne, G. M., & Anderson, M. M. (2000). The first named Ediacaran body fossil, *Aspidella terranovica*. *Palaeontology*, 43(3), 427-456.

Glaessner, M. F. 1985. The dawn of animal life: a biohistorical study. Cambridge University Press, Cambridge.

Gürich, G. 1930. Die bislang ältesten Spuren von Organismen in Südafrika. Pp. 670–680 in International Geological Congress (XV), Pretoria, Union of South Africa, Die ältesten Fossilien Sud-Afrikas.

Hardle, W. K., and L. Simar. 2019. Applied multivariate statistical analysis. Springer, Berlin.

Hastie, T., Tibshirani, R., Friedman, J. H., & Friedman, J. H. (2009). The elements of statistical learning: data mining, inference, and prediction (Vol. 2, pp. 1-758). New York: Springer.

Hawco, J. B., Kenchington, C. G., Taylor, R. S., & McIlroy, D. (2020). A multivariate statistical analysis of the Ediacaran rangeomorph taxa *Beothukis* and *Culmofrons*. *Palaios*, 35(12), 495-511.

Hawco, J. B., Kenchington, C. G., & McIlroy, D. (2021). A quantitative and statistical discrimination of morphotaxa within the Ediacaran genus *Palaeopascichnus*. *Papers in Palaeontology*, 7(2), 657-673.

Hofmann, H. J., O'Brien, S. J., & King, A. F. (2008). Ediacaran biota on Bonavista peninsula, Newfoundland, Canada. *Journal of Paleontology*, 82(1), 1-36.

Hothorn, T., Hornik, K., & Zeileis, A. (2006). Unbiased recursive partitioning: A conditional inference framework. *Journal of Computational and Graphical statistics*, 15(3), 651-674.

Hoyal Cuthill, J. F., & Conway Morris, S. (2014). Fractal branching organizations of Ediacaran rangeomorph fronds reveal a lost Proterozoic body plan. *Proceedings of the National Academy of Sciences*, 111(36), 13122-13126.

Ichaso, A. A., Dalrymple, R. W., & Narbonne, G. M. (2007). Paleoenvironmental and basin analysis of the late Neoproterozoic (Ediacaran) upper Conception and St. John's groups, west Conception Bay, Newfoundland. *Canadian Journal of Earth Sciences*, 44(1), 25-41.

Jensen, S. (2003). The Proterozoic and earliest Cambrian trace fossil record; patterns, problems and perspectives. *Integrative and Comparative Biology*, 43(1), 219-228.

Jensen, S., Högström, A. E., Almond, J., Taylor, W. L., Meinhold, G., Høyberget, M. A. G. N. E., ... & Palacios, T. (2018). Scratch circles from the Ediacaran and Cambrian of Arctic Norway and southern Africa, with a review of scratch circle occurrences. *Bulletin of Geosciences*, 93(3), 287-304.

Johnston, D. T., Poulton, S. W., Goldberg, T., Sergeev, V. N., Podkovyrov, V., Vorob'Eva, N. G., ... & Knoll, A. H. (2012). Late Ediacaran redox stability and metazoan evolution. *Earth and Planetary Science Letters*, 335, 25-35.

Kaufman, L., & P. J. Rousseeuw. (2009). *Finding groups in data: an introduction to cluster analysis*. Wiley, Hoboken, N.J.

King, A. F. (1982). *Guidebook for Avalon and Maguma Zones of Atlantic Canada. The Caledonide Orogen, International Geological Correlation Project 27. Report 9*. Department of Earth Sciences, Memorial University of Newfoundland, Canada.

King, A. F. (1988). *Geology of the Avalon Peninsula, Newfoundland (parts of 1 K, 1L, 1 M, 1 N and 2C), Map 88-01*. Government of Newfoundland and Labrador, Geological Survey, Department of Mines and Energy, St. John's.

King, A. F. (1990). Geology of the St. John's area. Report 90-2. Government of Newfoundland and Labrador, Geological Survey, Department of Mines and Energy, St. John's, Canada.

Kostaschuk, R., Nasr-Azadani, M. M., Meiburg, E., Wei, T., Chen, Z., Negretti, M. E., ... & Parsons, D. R. (2018). On the causes of pulsing in continuous turbidity currents. *Journal of Geophysical Research: Earth Surface*, 123(11), 2827-2843.

Laflamme, M., Narbonne, G. M., & Anderson, M. M. (2004). Morphometric analysis of the Ediacaran frond *Charniodiscus* from the Mistaken Point Formation, Newfoundland. *Journal of Paleontology*, 78(5), 827-837.

Laflamme, M., Narbonne, G. M., Greentree, C., & Anderson, M. M. (2007). Morphology and taphonomy of an Ediacaran frond: *Charnia* from the Avalon Peninsula of Newfoundland. *Geological Society, London, Special Publications*, 286(1), 237-257.

Laflamme, M., Xiao, S., & Kowalewski, M. (2009). Osmotrophy in modular Ediacara organisms. *Proceedings of the National Academy of Sciences*, 106(34), 14438-14443.

Laflamme, M., Gehling, J. G., & Droser, M. L. (2018). Deconstructing an Ediacaran frond: three-dimensional preservation of *Arborea* from Ediacara, South Australia. *Journal of Paleontology*, 92(3), 323-335.

Landler, L., Ruxton, G. D., & Malkemper, E. P. (2018). Circular data in biology: advice for effectively implementing statistical procedures. *Behavioral Ecology and Sociobiology*, 72, 1-10.

Landler, L., Ruxton, G. D., & Malkemper, E. P. (2019). The Hermans–Rasson test as a powerful alternative to the Rayleigh test for circular statistics in biology. *BMC Ecology*, 19, 1-8.

Landler, L., Ruxton, G. D., & Malkemper, E. P. (2018). Circular data in biology: advice for effectively implementing statistical procedures. *Behavioral Ecology and Sociobiology*, 72, 1-10.

Liu, A. G. 2011. Understanding the Ediacaran Assemblages of Avalonia: a palaeoenvironmental, taphonomic and ontogenetic study. PhD Thesis. University of Oxford. Oxford, U.K.

Liu, A. G., & D. McIlroy. (2015). Horizontal surface traces from the Fermeuse Formation, Ferryland (Newfoundland, Canada), and their place within the late Ediacaran ichnological revolution. *Ichnology: publications arising from ICHNIA III*, Geological Association of Canada, Miscellaneous Publication 9:141–156.

Liu, A. G., McIlroy, D., & Brasier, M. D. (2010). First evidence for locomotion in the Ediacara biota from the 565 Ma Mistaken Point Formation, Newfoundland. *Geology*, 38(10), e224-e224.

Liu, A. G., McIlroy, D., Antcliffe, J. B., & Brasier, M. D. (2011). Effaced preservation in the Ediacara biota and its implications for the early macrofossil record. *Palaeontology*, 54(3), 607-630.

Liu, A. G., McIlroy, D., Matthews, J. J., & Brasier, M. D. (2014). Confirming the metazoan character of a 565 Ma trace-fossil assemblage from Mistaken Point, Newfoundland. *Palaios*, 29(8), 420-430.

Liu, A. G., Kenchington, C. G., & Mitchell, E. G. (2015). Remarkable insights into the paleoecology of the Avalonian Ediacaran macrobiota. *Gondwana Research*, 27(4), 1355-1380.

Mason, S. J., Narbonne, G. M., Dalrymple, R. W., & O'Brien, S. J. (2013). Paleoenvironmental analysis of Ediacaran strata in the Catalina Dome, Bonavista Peninsula, Newfoundland. *Canadian Journal of Earth Sciences*, 50(2), 197-212.

Matthews, J. J., Liu, A. G., Yang, C., McIlroy, D., Levell, B., & Condon, D. J. (2021). A chronostratigraphic framework for the rise of the Ediacaran macrobiota: new constraints from Mistaken Point Ecological Reserve, Newfoundland. *Geological Society of America Bulletin*, 133(3-4), 612-624.

McIlroy, D., Brasier, M. D., & Lang, A. S. (2009). Smothering of microbial mats by macrobiota: implications for the Ediacara biota. *Journal of the Geological Society*, 166(6), 1117-1121.

McIlroy, D., Hawco, J., McKean, C., Nicholls, R., Pasinetti, G., & Taylor, R. (2022). Palaeobiology of the reclining rangeomorph *Beothukis* from the Ediacaran Mistaken Point Formation of southeastern Newfoundland. *Geological Magazine*, 159(7), 1160-1174.

McIlroy, D., Dufour, S. C., Taylor, R., & Nicholls, R. (2021). The role of symbiosis in the first colonization of the seafloor by macrobiota: insights from the oldest Ediacaran biota (Newfoundland, Canada). *Biosystems*, 205, 104413.

McIlroy, D., Pérez-Pinedo, D., Pasinetti, G., McKean, C., Taylor, R. S., & Hiscott, R. N. (2022). Rheotropic epifaunal growth, not felling by density currents, is responsible for many Ediacaran fossil orientations at Mistaken Point. *Frontiers in Earth Science*, 10, 849194.

McMenamin, M. A. (1998). *The Garden of Ediacara*. Columbia University Press, New York.

Meesters, E. H., Hilterman, M., Kardinaal, E., Keetman, M., DeVries, M., & Bak, R. P. M. (2001). Colony size-frequency distributions of scleractinian coral populations: spatial and interspecific variation. *Marine Ecology Progress Series*, 209, 43-54.

Menon, L. R., McIlroy, D., Liu, A. G., & Brasier, M. D. (2016). The dynamic influence of microbial mats on sediments: fluid escape and pseudofossil formation in the Ediacaran Longmyndian Supergroup, UK. *Journal of the Geological Society, London*, 173(1), 177-185.

Mitchell, E. G., & Butterfield, N. J. (2018). Spatial analyses of Ediacaran communities at Mistaken Point. *Paleobiology*, 44(1), 40-57.

Mitchell, E. G., & Kenchington, C. G. (2018). The utility of height for the Ediacaran organisms of Mistaken Point. *Nature Ecology & Evolution*, 2(8), 1218-1222.

Mitchell, E. G., Kenchington, C. G., Liu, A. G., Matthews, J. J., & Butterfield, N. J. (2015). Reconstructing the reproductive mode of an Ediacaran macroorganism. *Nature*, 524 (7565), 343-346.

Mitchell, E. G., Harris, S., Kenchington, C. G., Vixseboxse, P., Roberts, L., Clark, C., ... & Wilby, P. R. (2019). The importance of neutral over niche processes in structuring Ediacaran early animal communities. *Ecology letters*, 22(12), 2028-2038.

Mitchell, E. G., Bobkov, N., Bykova, N., Dhungana, A., Kolesnikov, A. V., Hogarth, I. R., ... & Grazhdankin, D. V. (2020). The influence of environmental setting on the community ecology of Ediacaran organisms. *Interface Focus*, 10(4), 20190109.

Moriyama, Y., Okamoto, H., & Asai, H. (1999). Rubber-like elasticity and volume changes in the isolated spasmoneme of giant *Zoothamnium* sp. under Ca<sup>2+</sup>-induced contraction. *Biophysical Journal*, 76(2), 993-1000.

Murphy, J. B., Pisarevsky, S. A., Nance, R. D., & Keppie, J. D. (2004). Neoproterozoic—Early Paleozoic evolution of peri-Gondwanan terranes: implications for Laurentia-Gondwana connections. *International Journal of Earth Sciences*, 93, 659-682.

Narbonne, G. M. (2004). Modular construction of early Ediacaran complex life forms. *Science*, 305(5687), 1141-1144.

Narbonne, G. M. (2005). The Ediacara biota: Neoproterozoic origin of animals and their ecosystems. *Annual Review of Earth and Planetary Sciences*, 33(1), 421-442.

Narbonne, G. M., Laflamme, M., Greentree, C., & Trusler, P. (2009). Reconstructing a lost world: Ediacaran rangeomorphs from Spaniard's Bay, Newfoundland. *Journal of Paleontology*, 83(4), 503-523.

O'Brien, S. J., & King, A. F. (2005). Late Neoproterozoic (Ediacaran) stratigraphy of Avalon Zone sedimentary rocks, Bonavista Peninsula, Newfoundland. *Current Research, Newfoundland and Labrador Department of Natural Resources Geological Survey*, 5(1), 101-113.

Pérez-Pinedo, D., McKean, C., Taylor, R., Nicholls, R., & McIlroy, D. (2022). *Charniodiscus* and *Arborea* are separate genera within the Arboreomorpha: using the holotype of *C. concentricus* to resolve a taphonomic/taxonomic tangle. *Frontiers in Earth Science*, 9, 785929.

Piccarreta, R., & Billari, F. C. (2007). Clustering work and family trajectories by using a divisive algorithm. *Journal of the Royal Statistical Society Series A: Statistics in Society*, 170(4), 1061-1078.

Pisarevsky, S. A., McCausland, P. J., Hodych, J. P., O'Brien, S. J., Tait, J. A., & Murphy, J. B. (2012). Paleomagnetic study of the late Neoproterozoic Bull Arm and Crown Hill formations (Musgravetown Group) of eastern Newfoundland: implications for Avalonia and West Gondwana paleogeography. *Canadian Journal of Earth Sciences*, 49(1), 308-327.

Pollock, J. C., Hibbard, J. P., & Sylvester, P. J. (2009). Early Ordovician rifting of Avalonia and birth of the Rheic Ocean: U–Pb detrital zircon constraints from Newfoundland. *Journal of the Geological Society*, 166(3), 501-515.

Ryland, J., R. Woollacott, & R. Zimmer. (1977). Taxes and tropisms of bryozoans. Pp. 411–436 in W. Robert and Z. Russel, eds. *Biology of Bryozoans*. Academic, New York.

Schneider, C. A., Rasband, W. S., & Eliceiri, K. W. (2012). NIH Image to ImageJ: 25 years of image analysis. *Nature Methods*, 9(7), 671-675.

Scrucca, L., Fop, M., Murphy, T. B., & Raftery, A. E. (2016). Mclust 5: clustering, classification and density estimation using Gaussian finite mixture models. *The R Journal*, 8(1), 289.

Seilacher, A. (1984). Late Precambrian and Early Cambrian Metazoa: preservational or real extinctions?. In *Patterns of Change in Earth Evolution: Report of the Dahlem Workshop Patterns of Change in Earth Evolution Berlin 1983, May 1–6*(pp. 159-168). Berlin, Heidelberg: Springer Berlin Heidelberg.

Seilacher, A. (1989). Vendozoa: organismic construction in the Proterozoic biosphere. *Lethaia*, 22(3), 229-239.

Seilacher, A. (1992). Vendobionta and Psammocorallia: lost constructions of Precambrian evolution. *Journal of the Geological Society, London*, 149(4), 607-613.

Seilacher, A. (1999). Biomat-related lifestyles in the Precambrian. *Palaios*, 14(1), 86-93.

Sneath, P. H., & R. R. Sokal. (1973). *Numerical Taxonomy. The principles and practice of numerical classification*. Freeman, San Francisco.

Southard, J. (2019). *Introduction to fluid motions and sediment transport*. Massachusetts Institute of Technology, Cambridge, Mass.

Taylor, R. S., Matthews, J. J., Nicholls, R., & McIlroy, D. (2021). A re-assessment of the taxonomy, palaeobiology and taphonomy of the rangeomorph organism *Hapsidophyllas flexibilis* from the Ediacaran of Newfoundland, Canada. *PalZ*, 95(2), 187-207.

Taylor, R. S., Nicholls, R., Neville, J. M., & McIlroy, D. (2023). Morphological variation in the rangeomorph organism *Fractofusus misrai* from the Ediacaran of Newfoundland, Canada. *Geological Magazine*, 160(1), 146-166.

Tran, T., B. McGuire, & M. Greenwood. (2021). MonoClust: perform monothetic clustering with extensions to circular data, R package version 1.2.1. <https://CRAN.R-project.org/package=monoClust>

Tran, T., (2019). Monothetic cluster analysis with extensions to circular and functional data. PhD thesis. Montana State University, Bozeman, Mont.

Vixseboxse, P. B., Kenchington, C. G., Dunn, F. S., & Mitchell, E. G. (2021). Orientations of Mistaken Point fronds indicate morphology impacted ability to survive turbulence. *Frontiers in Earth Science*, 9, 762824.

Waggoner, B. (2003). The Ediacaran biotas in space and time. *Integrative and Comparative Biology*, 43(1), 104-113.

Walesiak, M., & Dudek, A. (2020). The choice of variable normalization method in cluster analysis. Pp. 325–340 in K. S. Soliman, eds. *Education excellence and innovation management: a 2025 vision to sustain economic development during global challenges*, Proceedings of the 35th International Business Information Management Association Conference (IBIMA), Seville, Spain, April 1–2, 2020.

Will, G. (2016). Visualizing and clustering data that includes circular variables. Technical report. Master's thesis. Montana State University, Bozeman, Mont.

Williams, H., & A. F. King.(1979). Trepassey map area, Newfoundland. Geological Survey of Canada Memoir, 389.

Wood, D. A., Dalrymple, R. W., Narbonne, G. M., Gehling, J. G., & Clapham, M. E. (2003). Paleoenvironmental analysis of the late Neoproterozoic Mistaken Point and Trepassey formations, southeastern Newfoundland. *Canadian Journal of Earth Sciences*, 40(10), 1375-1391.

Xiao, S., & M. Laflamme. (2009). On the eve of animal radiation: phylogeny, ecology and evolution of the Ediacara biota. *Trends in Ecology and Evolution*, 24(1), 31–40.

# **CHAPTER 4 - Hydrodynamic insights into the paleobiology of the Ediacaran rangeomorph *Fractofusus misrai***

Daniel Pérez-Pinedo<sup>1\*</sup>, Robert Nicholls<sup>2</sup>, Jenna M. Neville<sup>1</sup>, and Duncan McIlroy<sup>1</sup>

<sup>1</sup> Department of Earth Sciences, Memorial University of Newfoundland, St. John's, NL, Canada,

<sup>2</sup> Paleocreations, Bristol, United Kingdom

\* Corresponding author: Daniel Pérez-Pinedo [dperezpinedo@mun.ca](mailto:dperezpinedo@mun.ca) 0000-0001-5607-1164

## **PREFACE:**

This paper has been published in the international scientific peer-reviewed journal iScience ([doi.org/10.1016/j.isci.2024.110107](https://doi.org/10.1016/j.isci.2024.110107)) as an original research article as of 24<sup>th</sup> May 2024. The paper is available from the volume 27, issue 6. This chapter has been formatted according to the guidelines for thesis submission and is otherwise identical to the original publication. When found, typos and non-substantial corrections have been made. Conceptualization, D.P-P., R.N., J.N., and D.M; methodology, D.P-P and R.N; formal analysis, D.P-P; software D.P-P., investigation, D.P-P., J.N., and D.M; figures: D.P-P., and R.N; software, D.P.-P; validation, D.P-P; project administration, D.P.-P., and D.M., writing, D.P.-P. with editorial input by J.N., and D.M; funding acquisition, D.M.

Reference: Pérez-Pinedo, D., Nicholls, R., Neville, J. M., & McIlroy, D. (2024). Hydrodynamic insights into the paleobiology of the Ediacaran rangeomorph *Fractofusus misrai*. iScience, 27(6).

## ABSTRACT

The Ediacaran of Newfoundland preserves some of the oldest complex macroscopic communities, several of which are dominated by the fractal-like rangeomorph genus *Fractofusus*. Here we use computational fluid dynamics and a detailed reconstruction of *Fractofusus misrai* to document for the first time hydrodynamic phenomena associated with this sediment-reclining organism and its rangeomorph elements that are relevant to interpreting feeding strategies, explain the recently documented rheotropic growth oblique to currents, and provide insights into their impact on the Ediacaran seafloor. Obliquely oriented *Fractofusus* are common, likely representing a compromise between maximized aspect ratio and minimization of drag. Flow patterns on the upper surface of *Fractofusus* are consistent with the collection of dissolved and finely particulate nutrients, as well as gas exchange. *Fractofusus* produce a wake downstream, demonstrating that reclining rangeomorphs had potential to modify sedimentation patterns on the ancient seafloor by potentially allowing deposition of fine-grained sediment.

**Keywords:** *Fractofusus*, computational flow dynamics, turbulence, suspension feeding, osmotrophy, drag

## 4.1 INTRODUCTION

Fossil assemblages that preserve the soft-bodied Ediacaran biota include the oldest remains of architecturally complex macroscopic life on Earth and therefore are essential in furthering our understanding of the evolution of complex macroorganisms (Waggoner 2003; Narbonne 2005; Hofmann et al. 2008; Liu et al. 2015; Matthews et al. 2021; McIlroy et al. 2021). The Avalon Assemblage is the oldest of the Ediacaran assemblages and includes the deep marine volcanoclastic settings of the Avalon Terrane in Newfoundland spanning at least the interval ca. 574–564 Ma (Matthews et al. 2021) and Charnwood Forest, UK (Noble et al. 2015). The Ediacaran of Newfoundland is largely dominated by the clade Rangeomorpha (Brasier et al. 2012) which is considered to include the oldest examples of stem eumetazoans (Xiao and Laflamme 2009; Budd and Jensen 2017; Dunn et al. 2018; Dunn et al. 2021). These organisms are characterized by frondose body plans, pseudo-fractal branching architecture consisting of similar orders of self-repeating branches, and high surface area/volume ratios that are not seen in modern organisms (Laflamme et al. 2009; Brasier et al. 2012). The basic rangeomorph unit can grow in a number of different orientations to create a range of morphologies in the preserved bedding plane expression of the 3D form (Jenkins 1985; Brasier et al. 2012; Hoyal Cuthill and Conway Morris 2014; McIlroy et al. 2021).

Species of the rangeomorph genus *Fractofusus* (*F. misrai* and *F. andersoni*) are endemic to the offshore to deep basinal Ediacaran facies of the island of Newfoundland (and putative examples from McKenzie Mountains Canada) (Anderson and Misra 1968; Gehling and Narbonne 2007; Hofmann et al. 2008; Narbonne et al. 2014; Taylor et al. 2023) where they are found on minor hiatal surfaces in turbiditic successions associated with well-developed matgrounds (Gehling and Narbonne 2007). *Fractofusus misrai* dominates the D and E surfaces at Mistaken

Point (Clapham et al. 2003; Mitchell et al. 2015) and the Melrose Surface at Capelin Gulch in the Discovery UNESCO Global Geopark (Pérez-Pinedo et al. 2023). These organisms inhabited deep marine paleoenvironments and are preserved by obrution and smothering beneath volcanic ashes or tuffites (Seilacher 1992; Wood et al. 2003; O'Brien and King 2005; Hofmann et al. 2008; Matthews et al. 2021).

Early considerations of the mode of feeding in the Rangeomorpha focused on filter feeding by comparison with morphological analogues in the Cnidaria (Glaessner 1984) and also through inferences based on the tiered community structure (Clapham and Narbonne 2002; Clapham et al. 2003). Earlier inferences of suspension feeding (relying on particulate organic matter [POM]; Glaessner 1984; Clapham and Narbonne 2002) and absorption of dissolved organic matter (DOM; Laflamme et al. 2009) as the primary mode of feeding in the Rangeomorpha have been contested (Antcliffe and Brasier 2007; Brasier et al. 2012; Fakhraee et al. 2021; McIlroy et al. 2021; McIlroy et al. 2022; Pérez-Pinedo et al. 2023) and phagocytotic/chemosymbiotic feeding at the organism-substrate interface has been proposed for feeding in reclining organisms (Dufour and McIlroy 2017; Matthews et al. 2021; Taylor et al. 2021; McIlroy et al. 2022; Pérez-Pinedo et al. 2022). Determining the feeding strategies for rangeomorphs like *Fractofusus* is problematic due to the lack of direct modern analogues (Seilacher 1992), their unique body plan (Jenkins 1985; Brasier et al. 2012), and incomplete (mostly 2D) preservation (but see Narbonne 2004; Brasier et al. 2013; Vickers-Rich et al. 2013; Sharp et al. 2017; McKean et al. 2023).

While the debate over the mode of life of the Rangeomorpha is ongoing, the mode of life of *Fractofusus* as a sessile epibenthic recliner is widely accepted. Preferential orientation of Ediacaran fronds in the Avalon Assemblage has been interpreted as a result of current alignment due to felling of erect fronds (Seilacher 1992, 1999). Taphonomic evidence to support erect modes

of life in some taxa comes from poorly preserved distal features obscured by the deposition of sediment/tuff in between these features and the preservation plane (Pérez-Pinedo et al. 2022). However, *Fractofusus* has always been interpreted as a reclining organism lying flat on the seafloor (Wood et al. 2003; Vixseboxse et al. 2021) supported by their apparently random orientation at Bristy Cove, the E Surface at Mistaken Point Ecological Reserve (MPER), and the Johnson/H14 Surface at Discovery Global Geopark (Seilacher 1999; Darroch et al. 2013; Mitchell et al. 2015; Vixseboxse et al. 2021; McIlroy et al. 2022) and also the ubiquitously well-preserved nature of their lower surface impressions (Dufour and McIlroy 2017; Taylor et al. 2023). Preferential orientations of *Fractofusus misrai*, oblique to a paleocurrent, have however been reported at Capelin Gulch near Melrose in the Catalina Dome (Pérez-Pinedo et al. 2023; Figure 4.1). This fossiliferous surface is significant because paleocurrents at the site can be determined from current ripples associated with the fossiliferous bedding plane (Pérez-Pinedo et al. 2023). Using Ediacaran fossil orientations to infer paleocurrents is problematic owing to debate concerning the mode of life of many frondose taxa, particularly the Rangeomorpha (McIlroy et al. 2022). The determination of non-random *Fractofusus* orientation trends oblique to a paleocurrent at Capelin Gulch poses new questions regarding the paleobiology and paleoecology of *F. misrai* that we address herein (Figure 4.2).

Computational fluid dynamics (CFD) has been used to understand the feeding strategies of some Ediacaran organisms and to determine their roles in Ediacaran ecosystems. It has been proposed that passive suspension feeders generate patterns of flow recirculation toward feeding structures (e.g., pores) or specific parts of the anatomy creating areas of low velocity facilitating the gravitational deposition of particles. On the other hand, the passive absorption of DOM is related to high surface area (SA)/volume (V) ratios (i.e., fractal branching) and an even, relatively

undisturbed, distribution of flow over the entire organism surface (Rahman et al. 2015; Darroch et al. 2017; Gibson et al. 2019; Cracknell et al. 2021; Gibson et al. 2021; Darroch et al. 2022; Liu et al. 2022; Darroch et al. 2023). However, previous hydrodynamic studies of the Rangeomorpha have not addressed the complex surface morphology of rangeomorphs and have instead focused on gross morphology rather than detailed paleobiological reconstructions (Darroch et al. 2023). In this study, we present a novel hydrodynamic approach to studying *F. misrai*, integrating the detailed three-dimensional geometry published by Taylor et al. (2023) (Figure 4.3) and the statistically significant orientation groups found by Pérez-Pinedo et al. (2023). We aim to document the fluid flow near the reconstructed *F. misrai* relevant to feeding strategies and metabolite collection (cf. Dufour and McIlroy 2017; Darroch et al. 2023), analyze the hydrodynamic behavior of preferential orientation clusters (cf. Taylor et al. 2023; Pérez-Pinedo et al. 2023), and gain insights into the paleoecology of *F. misrai*.

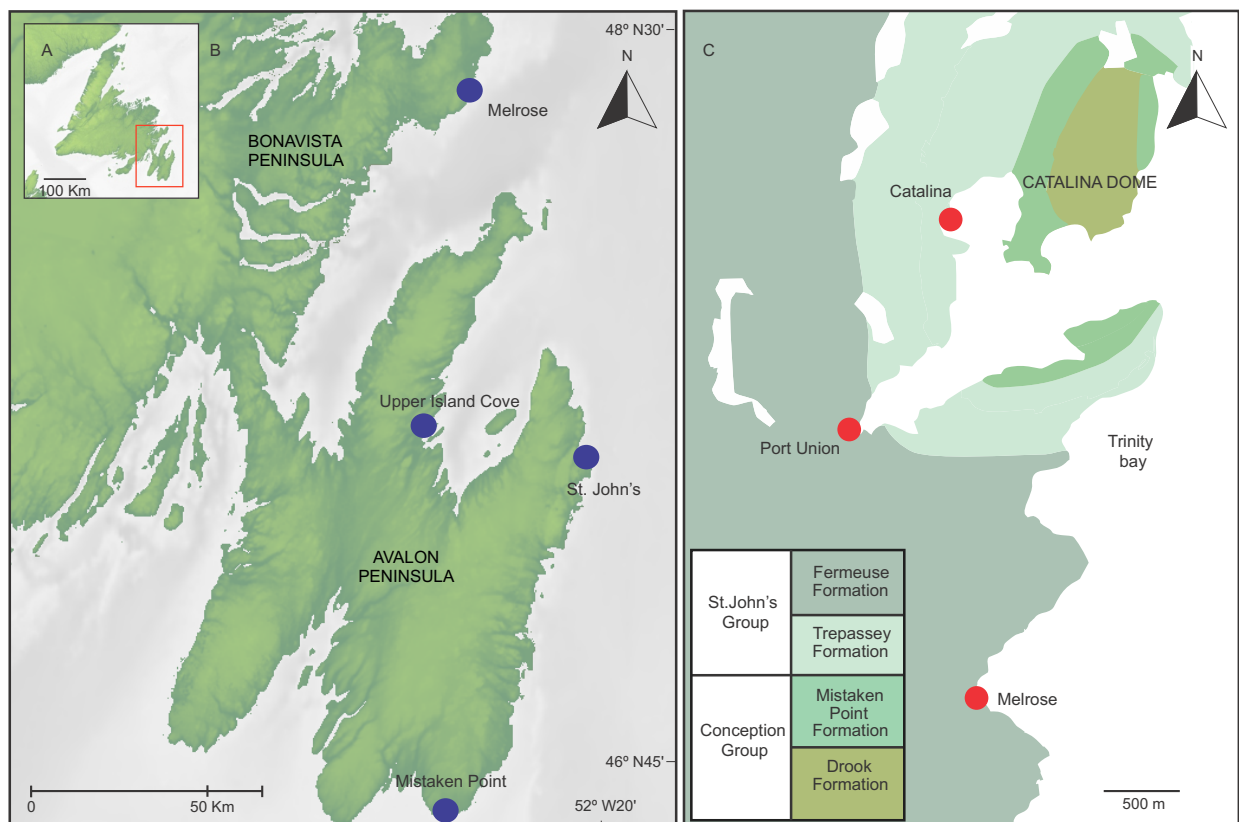


Figure 4.1: Location of the Capelin Gulch site, also known as Melrose Surface in the Fermeuse Formation at Melrose, on the southern portion of the Catalina Dome, in the Discovery UNESCO Global Geopark. A) General map of Newfoundland, Atlantic Canada. B) Detail of the Avalon and Bonavista Peninsulas. C) Geologic map of Catalina area and stratigraphic column.

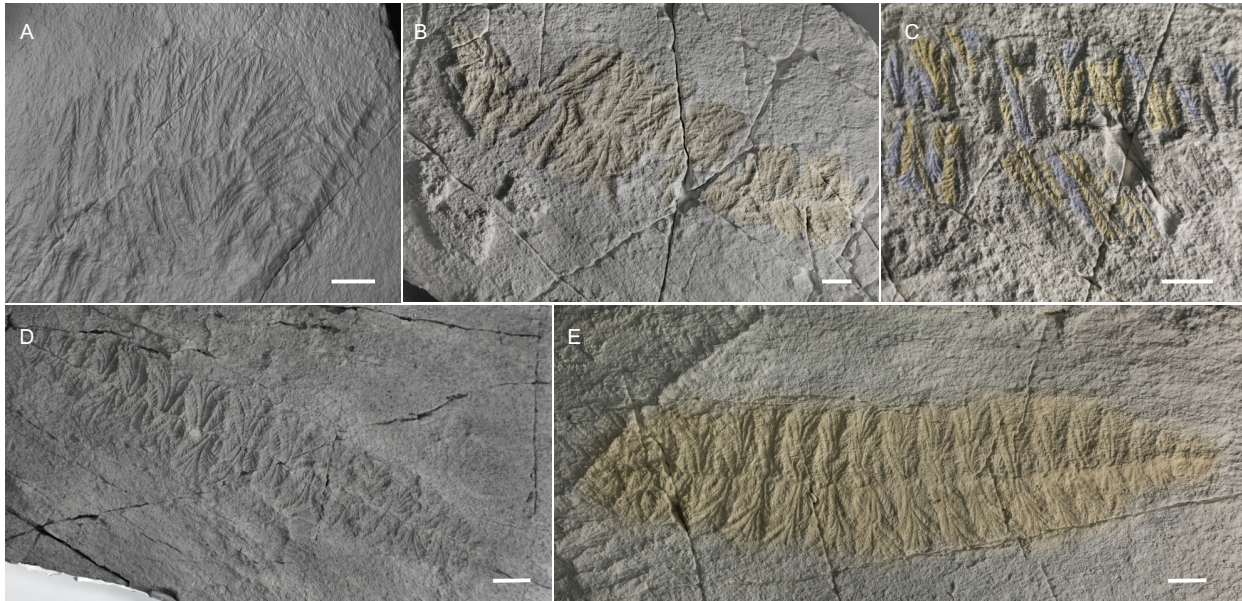


Figure. 2: Taphonomic variability of *Fractofusus misrai* exemplified by specimens from the E surface at Mistaken Point, NL. A) *F. misrai* partially rotated by the current to produce a kink in the axis. B) Specimen (yellow) with a branch that has been lifted by the current leaving a triangular gap in the row of rangeomorph branches. C) Tightly packed branches in a specimen showing a combination of rangeomorph branches rotated through 90° to show only one row of secondary-order branches (yellow) and unrotated branches with the tips curled away from the bedding plane to produce straight lateral margins (blue). D) Largely undisturbed *F. misrai* with displayed tips to the primary-order branches. E) Straight margined specimen inferred to have been created by the lifting of the tips of the primary-order branches by a current meaning that they were not in contact with the seafloor at the time of casting. Scale bars 1 cm.

## 4.2 RESULTS

### 4.2.1 Meshing parameters of the computational domain and the *F. misrai* geometry

The resulting meshes consisted of approximately 2–4 million cells and 500,000–1 million nodes (Figure 4.3). The final mesh was created using medium global mesh fineness, with 3 prismatic boundary layers, of 0.4 thickness of the local mesh size at a growth rate of 1.5. Physics-based meshing was employed to consider the physics in the simulation setup including refinements at the inlet and outlet of the flow volume region (FVR). Hexahedral element core was used to fill the inner mesh with hexahedral elements. The conversion from hexahedral to triangulated elements was done using pyramidal and tetrahedral elements. The small feature suppression was set at 0.015 mm, the gap refinement factor at 0.05, and the global gradation rate at 1.22 to guarantee a good resolution. The overall mesh quality (based on the 99.99 percentile) was between 0.035 and 1.0 as indicated by the CFD software, and minimum edge length was ~0.015 mm. This captures anatomical details of even third-order branches (0.3 mm) in the smallest *Fractofusus*. Cartesian boxes of 1 x 0.5 x 0.2 m and 0.01 m maximum edge length were employed to assess the impact of mesh region refinements around the *F. misrai* geometry; however, their use was deemed unnecessary as standard-finite-volume meshing algorithms automatically generated finer meshes in the desired areas based on geometric estimations. Additionally, higher-resolution meshes, or region refinements, led to increased computational demands without relevant changes in terms of flow patterns and the quantification of forces (Figures 4.S1– 4.S3; Table 4.S1; see *F. misrai* geometry in supplemental information).

### 4.2.2 Velocity field and flow recirculation patterns

In all CFD simulations,  $U_x$  decreased on the downstream side of the obstacle, after the fluid encountered the *F. misrai* geometry (Figures 4.4 and 4.S4–4.S6). This resulted in the development of a pronounced velocity gradient from the bottom boundary of the flow domain. The thickness of this boundary layer decreased as the inlet velocity increased (cf. Cracknell et al. 2021). Slow-flow regions (wakes) extending approximately 2.5 m in length formed downstream of *F. misrai*. This zone of reduced flow velocity was weaker in the null model simulations (Figure 4.S7). The wake was found to be wider and higher in experiments with 1) slower current velocities and 2) increasing size of *Fractofusus* (Figures 4.4, 4.S4, and 4.S5). Velocity profiles ( $U_z$ ) were visualized and affirmed the logarithmic law of the wall ensuring fully developed flows by the time the flows encounter the fossil geometry (cf. Gibson et al. 2021; Figure 4.S8).

At a small scale, current-parallel *Fractofusus* show flow retention in the form of funneled flow vortices that are routed toward the axis along the length of the concave grooves of the secondary-order branches. The flow that is entrained into these depressions shows marked reduction in  $U_x$ , starting at the distal end of the branches and progressing toward the midline (Figures 4.5A–D and 4.S6). Additionally, weak eddying was found on the lee side of the geometry, which creates potential for lifting of the distal margin of the secondary-order branches (Figure 4.4SII). Increasingly perpendicular frond orientations show a relatively undisturbed, even distribution of flow at the secondary-order branch-water interface (Figures 4.5E–L). This uniform flow is accelerated at the distal end of the upstream branches as it is channeled by the grooves formed by the secondary-order branches. The flow decelerates toward the axis where secondary-order branches are more concave (Figures 4.5E–L) and accelerates again on the lee side of the midline (Figure 4.S6). The progressively perpendicular orientations also show minor flow retention manifesting as small and highly constrained vortices parallel to the secondary-order

branches on the distal end of the upstream branches and downstream of the midline (Figure 4.4TII-TIII). In addition, enhanced eddying where flow recirculation resulted in velocity pulses against the organism (Figure 4.4TI, TIV) formed on both the stoss and lee sides of increasingly current-perpendicular fronds compared to parallel orientations. These flow patterns were observed in all simulations in turbulent flows regardless of flow velocities and organism size (Figures 4.4, 4.S4, and 4.S5). No flow retention was observed on top of the smooth null models (Figure 4.S7).

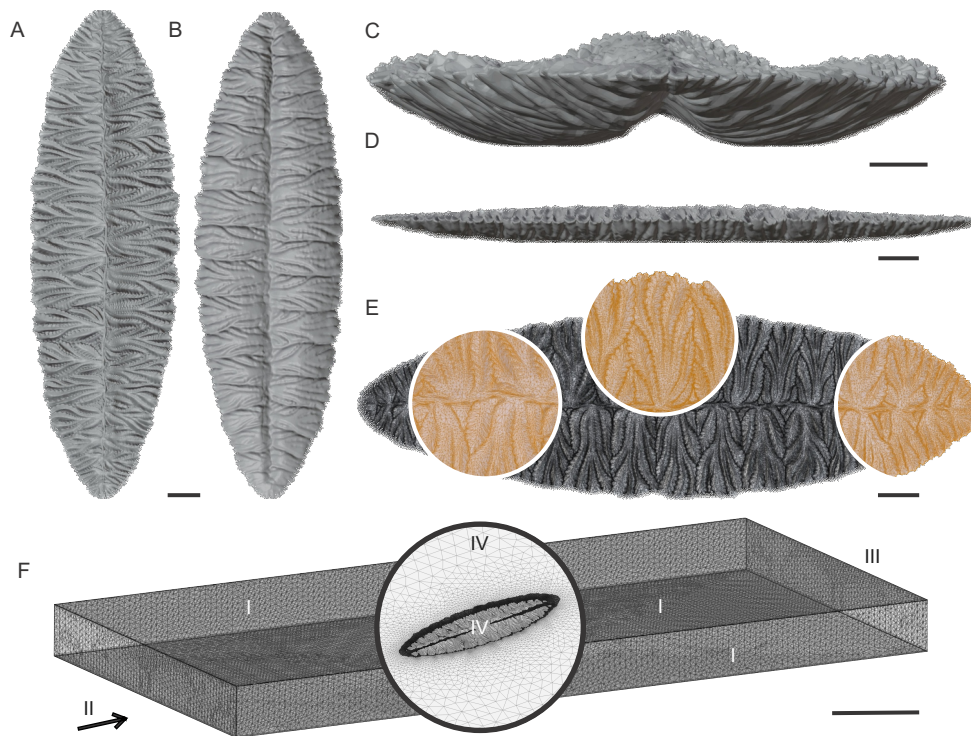


Figure 4.3: Digital three-dimensional reconstruction of *Fractofusus misrai* and computational domain. A–D) Different perspectives of the *F. misrai* geometry. A) Top view. B) Bottom view. C) Front view, and D) lateral view. E) *F. misrai* tetrahedral mesh and detail view (zoomed in). F) Flow volume region mesh and boundary conditions: I) slip boundary condition, II) velocity inlet, III) pressure outlet, and IV) no-slip boundary condition. Scale bars 2 cm except C 1 cm, and F 50 cm. See Figures 4.S1 and 4.S2.

### 4.2.3 Drag force

Drag force ( $F_D$ ) was found to increase with 1) increasing flow velocity, 2) larger *F. misrai* geometries, and 3) increasingly current-perpendicular *Fractofusus* orientations (cf. Darroch et al. 2017; Figure 4.6; Table 4.S1). In current-parallel orientations, drag-induced high-stress areas were found to be concentrated on both sides of the laterally directed secondary-order branches of *Fractofusus* (Figure 4.6A). In progressively current-perpendicular orientations, high-stress areas exhibited a more widespread distribution: 1) concentrated along both sides of the midline, 2) following the ridges formed by the secondary-order branches, and 3) associated with the distal portion of both rows of first-order branches (Figures 4.6B–D). Final result convergence in all CFD simulations was confirmed by the examination of the residuals, the solution imbalances (close or below  $1e^{-3}$ ), and boundary conditions convergence plots grouped as domain, inlets, outlets, and walls. These show the average values of the studied parameters for every iteration and present them normalized and scaled. This revealed the absence of relevant global or local imbalances (see CFD files in supplemental information; additional results are available upon request).

## 4.3 DISCUSSION

*Fractofusus misrai* is one of the best known, most abundant, and least contentious elements of the Ediacaran biotas of Newfoundland. Improved understanding of how *Fractofusus* might have interacted with its environment is key to better understanding the paleobiology of the Rangeomorpha as a whole. Our approach of integrating, taphonomy, morphological reconstruction, sedimentological context, and CFD highlights a number of phenomena of note.

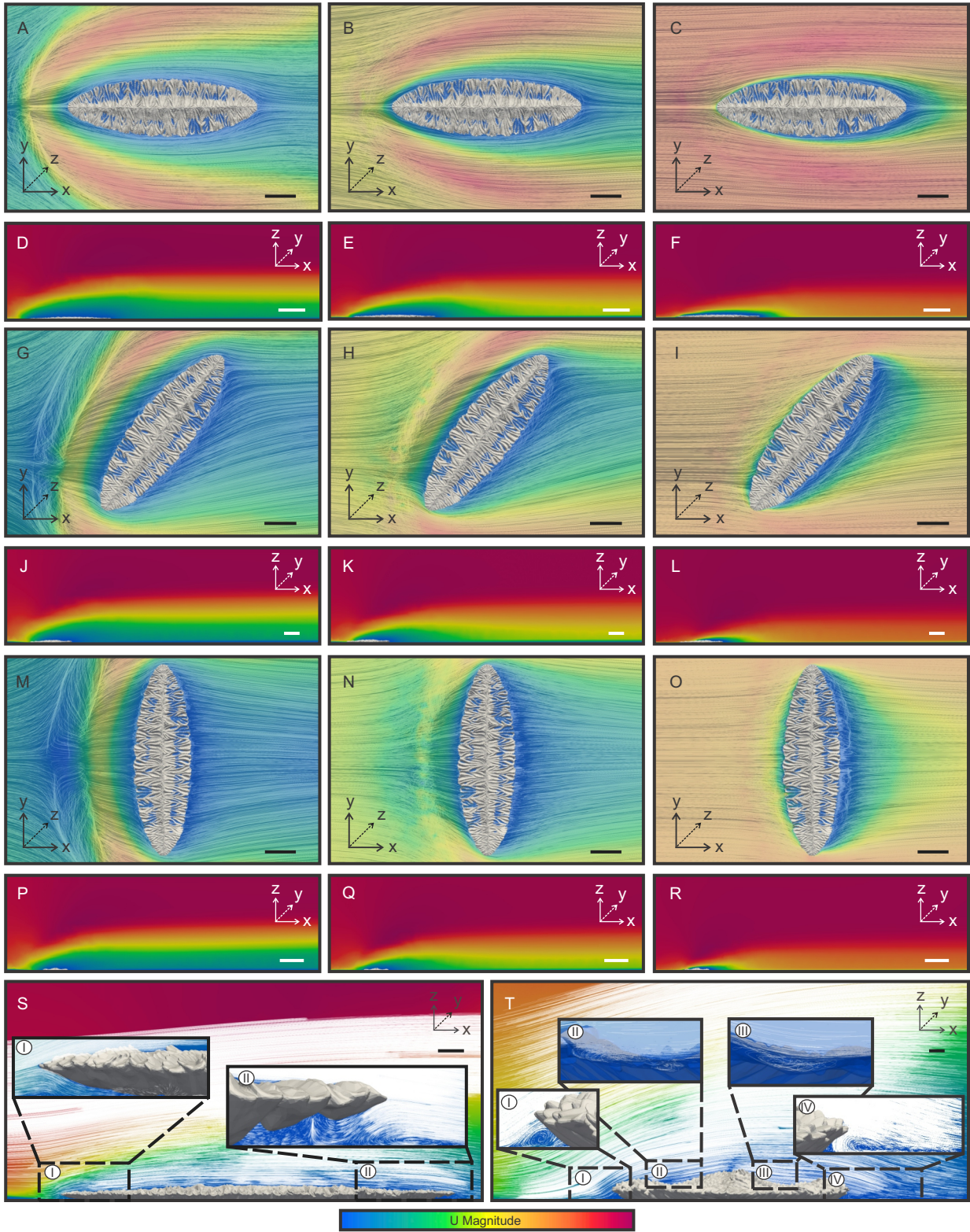


Figure 4.4: CFD simulations of large *Fractofusus misrai* in different orientations relative to the

simulated flow from (left to right). A–R) Two-dimensional horizontal and cross-sectional surface plots of streamlines and different  $U_x$  regimes: first column (A, D, G, J, M, and P) simulated flow of 0.05 m/s; second column (B, E, H, K, N, and Q) flows of 0.1 m/s; and third column (C, F, I, L, O, and R) 0.2 m/s. S and T) Detailed cross-sectional view of flow retention patterns and eddying of current-parallel (SI-SII) and current-perpendicular *Fractofusus misrai* (TI-TIV) in 0.1 m/s flow. Both orientations show the eddying at the frond margin (SI-SII; TI, TIV). Current-perpendicular *F. misrai* also shows weak vortices on the upper surface of the frond both upcurrent of the axis of the frond (TII), and also in the lee of the axis (TIII). Velocity ranges from 0 to 0.05, 0.1, or 0.2 m/s as indicated in this caption. Scale bars top view 5 cm, cross-sectional view 10 cm except S, and T 2 cm. See Figures 4.S3–4.S5, 4.S7, and 4.S8.

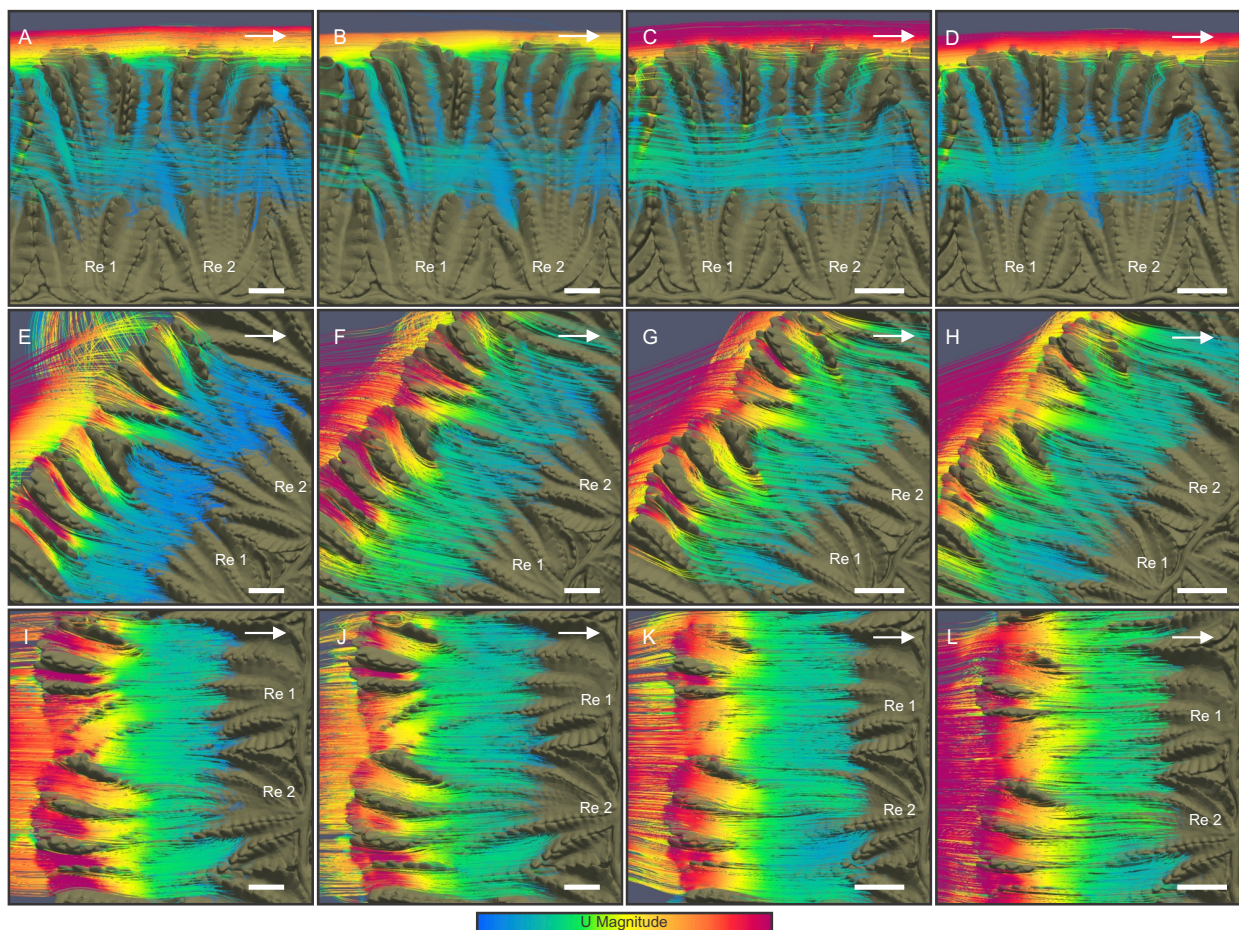


Figure 4.5: Detailed top view of flow patterns over the same rangeomorph elements of *Fractofusus misrai* (Re 1 and Re 2) in different orientations relative to the current. Streamlines vary in their paths between current-parallel and current-oblique/perpendicular orientations but are routed by the surface morphology in all cases. Flow velocity is colored along the streamlines according to velocity (red fastest, blue slowest): (A–D) current-parallel ( $0^\circ$ ), (E–H) current-oblique ( $52^\circ$ ), and (I–L) current-perpendicular ( $90^\circ$ ). A, E, and I are all the case of a small *F. misrai* under 0.05 m/s flow in different orientations; B, F, and J are all small *F. misrai* experiencing a 0.1 m/s flow in different orientations. C, G, and K show the case of large *F. misrai* in a 0.05 m/s flow in different orientations; D, H, and L show the effects of a large *F. misrai* experiencing a 0.1 m/s flow in different orientations. Current flow from left to right. Velocity ranges from 0 to 0.05, or 0.1 m/s as indicated in this caption. Scale bars 0.1 cm for small and 1 cm for large *F. misrai*. See Figure 4.S6.

#### 4.3.1 Feeding strategies

The funneled vortices in the grooves of secondary-order branches in current-parallel *F. misrai* are of benefit to a range of feeding strategies (e.g., suspension feeding and DOM absorption) due to entrainment of flow and irrigation of the upper surface of the organism. The retention of flow within these depressions arises from flow separation over the secondary branches and lateral flow being drawn into the perpendicularly directed grooves (Figures 4.5A–D). The slowed flow forms pronounced vortices progressing from the distal end of the branches toward the axis of the organism where it is flushed by the faster overlying ambient current. *Fractofusus* lived in association with very slow currents; further slowing of currents in the grooves may have enhanced active capture of low-density food particles (e.g., very fine POM) on the upper surface of

*Fractofusus*. Sediment supply in these low velocity background currents was likely very low and fine grained with no associated erosional or depositional sedimentary structures. The flow velocity over the rangeomorph elements across all modeled scenarios is in the range  $\sim 0.005\text{--}0.08$  m/s. Moreover, it has previously been hypothesized that *Fractofusus* could have also relied on ciliated cells to remove small amounts of sediment and to enhance feeding efficiency on the upper surface of the organism (Dufour and McIlroy 2017). However, caution is required for the interpretation of this phenomenon as it is governed by Archimedes and Froude numbers (Mrokowska 2020), and the behavior of very small particles in the flow has not been simulated in this work and the exact means of organic matter collection by ciliated or choanocyte-like cells is not tested either. The potential for using the entire upper surface of *Fractofusus* for capture of organic matter and subsequent phagocytotic ingestion has been previously predicted (Dufour and McIlroy 2017) and invited comparison of the Rangeomorpha with organisms of a pre-sponge grade of organization (Cavalier 2017; Dufour and McIlroy 2017; Dufour and McIlroy 2018). Some previous studies of flow in association with non-rangeomorph Ediacaran organisms have demonstrated the routing of funneled vortices toward particular portions of the organism, which have been inferred to have had unpreserved specialized suspension-feeding organs (Rahman et al. 2015; Darroch et al. 2017; Cracknell et al. 2021). However, invoking suspension-feeding strategies in the Rangeomorpha falls short due to: 1) the absence of paleontological evidence for pores or zooids (Liu et al. 2015; McIlroy et al. 2021; but see Butterfield 2022), 2) flawed anatomical comparisons to the Pennatulacea (Antcliffe and Brasier 2007), 3) the lack of consistent flow recirculation patterns toward specific areas (Darroch et al. 2023), and 4) disagreements concerning the mode of life of many rangeomorphs, which underpin ecological tiering models that have been used to infer that

the Rangeomorpha formed suspension-feeding communities (Clapham and Narbonne 2002; Ghisalberti et al. 2014; McIlroy et al. 2022; Darroch et al. 2023; Pérez-Pinedo et al. 2023).

Oblique orientations of *Fractofusus* relative to a current demonstrate flow retention on the surface of the fronds in the form of minor vortices due to flow separation on the lee side of the distal end of the upstream primary branches and downstream of the midline (Figure 4.4TII-TIII). The flow vortices are weak and tightly constrained to the middle section of the organisms therefore showing very limited potential to aid the vertical mixing of the water column or play a relevant role in feeding efficiency. Flow on the upper surface of *Fractofusus* on both sides of the axis is highly constrained within the concave morphology of the secondary-order branches, resembling a creeping flow, which is channeled by the branches (Figures 4.5E–L). On the upcurrent side of the fossil, flow is directed toward the axis showing a progressive reduction in velocity, but on the downcurrent side flow is drawn away from the axis featuring a reverse velocity trend (Figure 4.S6). This disparity in flow direction relative to the axis argues against the presence of food-capturing loci along the midline and instead supports the inference that the whole upper surface of the organism was used to exploit nutrients from the slowed current (Dufour and McIlroy 2017). The even distribution of relatively undisturbed flow is compatible with the collection of metabolites such as DOM (Singer et al. 2012; Rahman et al. 2015; Darroch et al. 2017; Cracknell et al. 2021) and aligns with the inference of Dufour and McIlroy (2017) that, while the lower surface likely harbored chemosymbionts, the upper surface of *Fractofusus* could be used for DOM and/or oxygen uptake. Previous studies hypothesized that (non-rangeomorph) fronds could have been suited for oxygen uptake benefiting from oscillatory behavior of the frond in a current (Singer et al. 2012) and by reaching faster fluids occurring at greater heights (Ghisalberti et al. 2014). Following Darroch et al. (2023) the high SA/V of *Fractofusus* and the faster flowing fluid over

the primary branches might have reduced the thickness of the diffusive boundary layer, thereby improving gas exchange. Eddying observed on the stoss and lee sides of the distal margin of primary branches, which project above the sediment-water interface, is likely to have caused some oscillatory movement of the distal portions of rangeomorph elements resulting in similar dynamics as those observed in arboreomorphs (Singer et al. 2012) and the erect rangeomorph *Pectinifrons* (Darroch et al. 2023).

Inferences that rangeomorphs like *Fractofusus* were giant obligate osmotrophs (Laflamme et al. 2009) have been challenged on grounds of palaeobiology/morphology (McIlroy et al. 2021; Butterfield 2022; McIlroy et al. 2022), and also in terms of the concentration of the DOM reservoir of Ediacaran oceans, which is now considered to be too low to have supported obligate osmotrophic macroorganisms (Johnston et al. 2012; Fakhraee et al. 2021). Moreover, the SA/V ratios calculated for our geometry (0.31–2.06 mm<sup>1</sup>; Table 4.S1) are significantly lower than those estimated by Laflamme et al. (2009). The pseudo-fractal lower surface of sessile recliners like *F. misrai* (Seilacher 1992; Gehling and Narbonne 2007) is considered to be an adaptation to maximize SA in contact with the sediment (Dufour and McIlroy 2017; Figures 4.2, 4.3B). In the absence of surficial bioturbation (Jensen 2003) a redoxcline would have developed at or close to the sediment-water interface (McIlroy and Logan 1999), so the lower surface would have been exposed to the, potentially toxic, buildup of reduced sulfur produced in the underlyingly anoxic pore waters (Dufour and McIlroy 2017; McIlroy et al. 2021). This has led to the suggestion that epibenthic recliners like *F. misrai* may have benefited from symbiotic interactions with, for example, sulfur-oxidizing chemolithoautotrophic bacteria (Dufour and McIlroy 2017; McIlroy et al. 2021). In this scenario, the even oxygen flow along the secondary branches might have been dorsoventrally transported by diffusion through the thin organism, or by ciliary action around the

frondlet, to increase the productivity of chemolithoautotrophs both in the underlying porewater system and on the lower surface of the reclining organism. The mode of feeding probably involved a combination of ectosymbiosis and phagocytosis (McIlroy and Dufour 2017). Given the results shown by the CFD simulations of *F. misrai*, in the context of the orientation trends determined by Pérez-Pinedo et al. (2023), we support the hypothesis that *F. misrai* could have fed on both particulate and truly dissolved DOM via its upper surface if covered by cilia/choanocytes (Cavalier-Smith 2017; Dufour and McIlroy 2018) and employed chemosymbiotic strategies on its lower surface, perhaps facultatively changing feeding mode as demonstrated for some chemosymbiotic clams (Zanzerl et al. 2019).

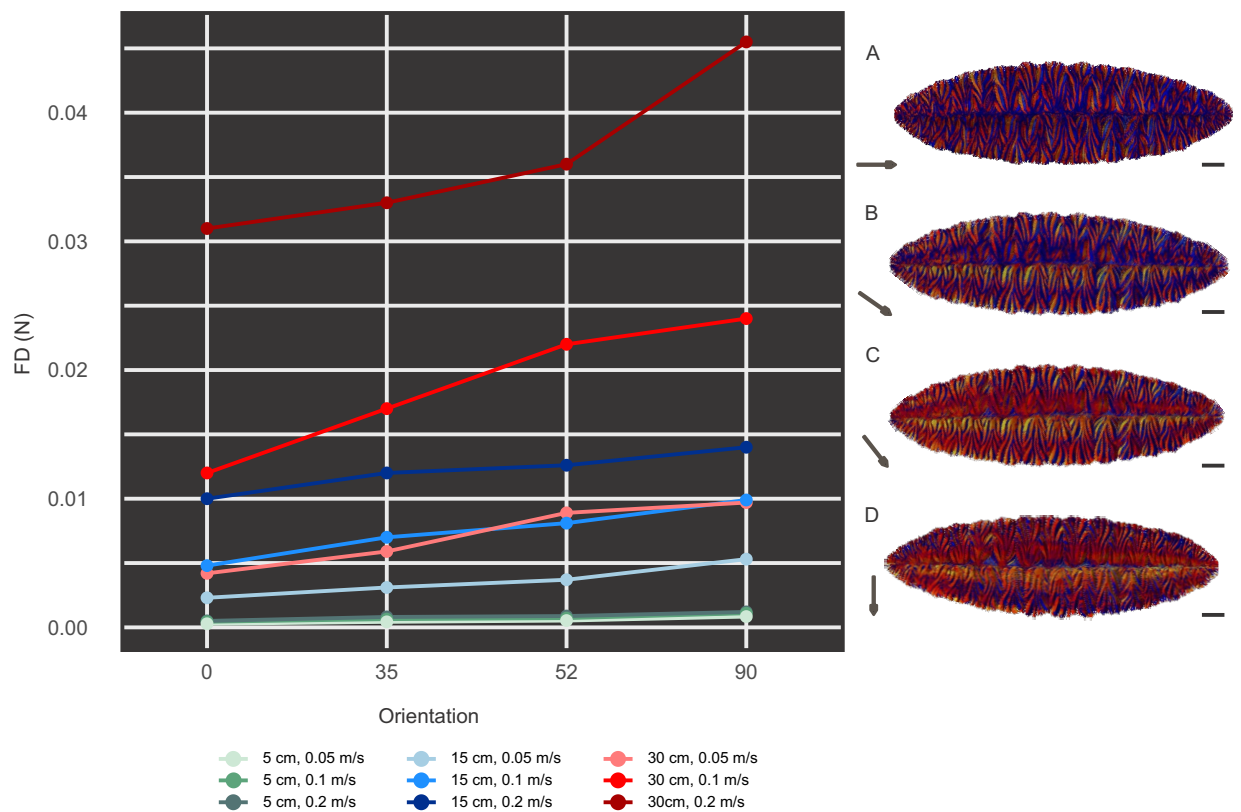


Figure 4.6: Drag forces of *Fractofusus misrai* models in CFD simulations. A–D) Spatial visualization of drag force in *Fractofusus*. A) Parallel (0°). B) Oblique (35°). C) Oblique (52°).

D) Perpendicular (90°). Arrows indicate the paleocurrent direction. Scale bars 2 cm.

Progressively warmer colors represent increasing drag. See to Table 4.S1.

#### 4.3.2 Orientation and drag

The erect mode of life invoked for frondose Ediacaran taxa (Glaessner 1984; Laflamme et al. 2007) has recently been challenged (Seilacher 1992; McIlroy et al. 2020; McIlroy et al. 2021; McIlroy et al. 2022; Pérez-Pinedo et al. 2023) on the basis of high-fidelity preservation and the absence of expected taphonomic evidence like swing marks (cf. Jensen et al. 2018; McKean et al. 2023). The orientation of rangeomorph and arboreomorph fronds orthogonal to the inferred paleoslope (Hawco et al. 2020; McIlroy et al. 2020; McIlroy et al. 2022) or even against the inferred paleocurrent direction (e.g., *Bradgatia* sp.; Flude et al. 2008), is incompatible with the dynamics of density flow events (McIlroy et al. 2022) but is consistent with the epifaunal growth of reclining taxa on hiatal surfaces beneath a turbulent clear-water current prior to the more violent ash-rich turbidity current events that smothered and preserved the fronds (McIlroy et al. 2022; Pérez-Pinedo et al. 2023).

Previous literature has documented random orientations of *Fractofusus* in populations from Bristy Cove, the E Surface at Mistaken Point, and the Johnson/H14 Surface at Discovery Global Geopark (Seilacher 1999; Gehling and Narbonne 2007; Mitchell et al. 2015; Vixseboxse et al. 2021). However, these studies have failed to consider rheotropic growth or have inferred unrealistic turbidity current dynamics (discussed in Pérez-Pinedo et al. 2023). Our previous work from the Capelin Gulch site (Pérez-Pinedo et al. 2023) has used an integrated approach, combining physical sedimentological evidence for paleocurrent direction in the form of current ripple trends and a novel statistical approach based on modified polythetic and monothetic clustering techniques

including circular and quantitative variables. Pérez-Pinedo et al. (2023) have interpreted the multimodal orientation trends oblique to the observed southeasterly paleocurrent as the result of rheotropic growth. The distinctive morphology and preferential orientation of *F. misrai* (Pérez-Pinedo et al. 2023) suggest a trade-off between mechanical stability and feeding efficiency (cf. Darroch et al. 2017). Multimodal orientation trends do not necessarily suggest stochastic orientation trends but can be the result of rheotropic growth. It is critical to interpret orientation trends, together with taphonomic clues regarding life attitude, and the most parsimonious hydrodynamic interpretation (Pérez-Pinedo et al. 2023).

*Fractofusus misrai* has a low-relief fusiform body plan (Seilacher 1999; Taylor et al. 2023; Figures 4.2, 4.3) and is exclusively found in the low-energy deep marine settings of Avalonia. This contrasts with later Ediacaran taxa with broadly hemispherical morphologies, which thrived in shallow-water environments characterized by shifting currents (Rahman et al. 2015; Darroch et al. 2017; Cracknell et al. 2021). Several of the deep-marine Ediacaran organisms of Avalonia are considered to have been rheotropic epibenthic organisms (McIlroy et al. 2022) growing in response to clear-water paleocurrents and oriented to maximize the efficiency of their reclining lifestyle (Pérez-Pinedo et al. 2023). Such organisms commonly dominate the intervals between the frequent density current and ashfall events that both smothered and preserved them (Wood et al. 2003; Ichaso et al. 2007).

Current-parallel orientations of *Fractofusus* generate minor downstream eddies and consistently exhibit lower  $F_D$  across all flow velocities and size classes (Figures 4.4SII, 4.6). High-stress areas are locally constrained, posing only a slight structural threat of current-related damage (Figure 4.6A). Despite current-parallel growth being the most hydrodynamic orientation, it also minimizes aspect ratio, which affects the flow experienced by the upper surface of the fossil. When

*Fractofusus* is modeled in current-parallel orientations, all primary-order fronds are exposed to the same section of the water column thereby facing progressively decreasing food/oxygen concentrations and increasing concentrations of waste metabolites in the downcurrent direction (Pérez-Pinedo et al. 2023; Figure 4.S6). However, case-dependent consideration is required since some food particles can show different inertia and the behaviors of very small particles and/or gas bubbles in the flow have not been simulated as part of this work. This is determined by the Stokes number and Archimedes number (Garg et al. 2012). In contrast, non-parallel orientations would experience better flushing and increased exposure to food and oxygen, but the higher aspect ratio generates more pronounced eddying on both the lee and stoss sides, generating recirculating pulses of current against the lateral margins of the organism (Pérez-Pinedo et al. 2023; Figures 4.4TI, TIV, 4.S4, and 4.S5). This is demonstrated by the consistent higher  $F_D$  values simulated across all flow velocities and size classes of *Fractofusus*, and the more evenly distributed high-stress areas (Figure 4.6). The increased mechanical threat to non-current-parallel *Fractofusus* could have led to increased stress, lifting entire primary branches or the upstream margin of the frond. Detachment from the seafloor is possible but not demonstrated; transportation might have been terminal for *F. misrai*, but there are no transported individuals known in the Mistaken Point biotas, just partially reoriented individuals (Taylor et al. 2023). The *F. misrai* at the Capelin Gulch site are preferentially obliquely oriented, which likely reflects a trade-off between enhancing metabolism without compromising mechanical stability. However, it is also possible that populations that show preferential orientation trends resulted from regional paleoenvironmental controls encompassing faster flows or low nutrient availability and therefore a need to maximize feeding efficiency or reduce mechanical stress.

### 4.3.3 Ecological role and paleobiology

*Fractofusus* is considered to have grown by both insertion of new elements and inflation of existing elements (Brasier et al. 2012). The large size range of individuals on some surfaces suggests that differential growth could allow *Fractofusus* to slowly respond rheotropically to assume preferential orientations (Taylor et al. 2023). They are not considered to have been motile and as such could not respond to changes in current orientation in any way except by growth (Taylor et al. 2023). Since early ontogenetic stages are not preserved at the Capelin Gulch site (Pérez-Pinedo et al. 2023), it is not possible to address such issues quantitatively. Juveniles with less than eight pairs of first-order branches are rare, suggesting that they had a lifestyle that in some way hindered their preservation (Taylor et al. 2023).

*Fractofusus* is commonly the most abundant fossil organism on fossiliferous surfaces in the Ediacaran of Newfoundland, which may partially be due to its capacity for continuous asexual reproduction (Darroch et al. 2013; Mitchell et al. 2015; Pérez-Pinedo et al. 2023). This sets it apart from other less abundant rangeomorphs, which may have had other modes of reproduction (Pasinetti and McIlroy 2023; Delahooke et al. 2024). Even our low-relief three-dimensional reconstruction of *F. misrai* (Taylor et al. 2023; Figure 4.3) which is flatter than previous interpretations (Gehling and Narbonne 2007; Mitchell and Kenchington 2018) creates a wake of decreased current velocity that extended over two meters downstream of the organism (Figure 4.4). This zone of decreased flow likely altered conditions in the benthic boundary layer, potentially impacting all species living in its wake, particularly small or juvenile organisms. We have suggested that the background clear-water current at Capelin Gulch was similar to that at Mistaken Point (Wood et al. 2003; McIlroy et al. 2022), estimated at approximately 0.05–0.1 m/s, based on comparisons with measurements from modern offshore shelf to slope settings (Fowler

2014). Any further reduction in the flow velocity below 0.05 m/s is likely to have led to sedimentation of fine-grained material (including POM), potentially making the seafloor more habitable. Consequently, the presence of current-slowing organisms on the seafloor leads to the baffling of bypassing sediment, where alterations in sediment rates contribute to making the seafloor more hospitable for subsequent generations (cf. Miatta et al. 2022).

#### 4.4 CONCLUSION

CFD is a powerful tool that has been effectively used to address aspects of the paleobiology of several Ediacaran organisms (Rahman et al. 2015; Darroch et al. 2017; Cracknell et al. 2021; Darroch et al. 2022; Liu et al. 2022; Darroch et al. 2023). However, previous studies have not attempted to study the complex rangeomorph anatomies beyond the first order of branching (Darroch et al. 2023). In this work, we present the first approach to the hydrodynamics of *F. misrai* using a highly detailed morphological reconstruction with respect to three orders of rangeomorph branching on the upper surface and geometries supported by taphonomic evidence (Taylor et al. 2023) and consistent with statistical orientation clusters determined from the field (Pérez-Pinedo et al. 2023). This has revealed some new insights into the paleobiology of *F. misrai*.

1. Rangeomorph branching at the secondary and tertiary order both funnels and slows currents on the surface of *F. misrai* (Figure 4.5). The oblique frond orientations determined from the Melrose Surface at Capelin Gulch (Pérez-Pinedo et al. 2023) show an even distribution of slowed flow over the upper surface of the organism. The upper surface could thus be an adaptation to increase the efficiency of 1) collecting fine POM, 2) direct absorption of DOM, 3) direct absorption of oxygen from the entire upper surface, and 4) flushing of waste metabolites (Dufour and McIlroy 2017).

2. Organism orientation and rheotropism relative the paleocurrent direction control the amount of drag experienced by *Fractofusus*. Given the degree of scatter, and the lack of a basal attachment, sessile reclining *Fractofusus* were likely to have been able to orientate themselves by progressively growing into the rheotropically desirable orientation. The preferred oblique bimodal orientation trends and the lack of evidence for passive or active mobility suggest that *F. misrai* at the Capelin Gulch site responded to changes in current orientation by growth rather than being passively aligned by the current (cf. Ivantsov 2013; Paterson et al. 2017). Progressively perpendicular orientations show increasing  $F_D$  values and eddying on the lee side of the organism which could have led to structural damage, mechanical tension, and eventual lifting of individual branches as evidenced by taphonomic clues, or even terminal detachment from the seafloor (Figures 4.4, 4.6). The preferential orientation of *F. misrai* previously documented at the Capelin Gulch site (Pérez-Pinedo et al. 2023) can be explained as a compromise between maximizing exposure to the current without experiencing excessive drag. *Fractofusus* had the potential to grow in a manner that maximized aspect ratio, accessing an increased volume of unexploited water, while maintaining mechanical integrity through reduced drag. If drag was too great, then the organism would have been removed by the current; if the aspect ratio is too low, then the feeding/flushing efficiency of the organism would be compromised (Figure 4.S6). Additionally, the wake generated downstream of the *F. misrai* hints at its potential to entrap bypassing sediment, altering the conditions in the benthic boundary layer, and sedimentation rates in its lee, especially organic particle deposition which may have benefitted organisms downstream of it (Figure 4.4). The assemblages of *Fractofusus*,

and other reclining taxa, on other fossil-rich Ediacaran surfaces should be studied to assess the utility of our findings in better understanding the ecology and paleobiology of Ediacaran epibenthic taxa.

## **4.5 LIMITATIONS OF THE STUDY**

This study presents certain simplifications toward natural conditions such as smooth bottom boundaries, as opposed to real textured surfaces; rigid non-mobile geometries; and individual specimen simulations. The hydrodynamics of entire *Fractofusus* communities, which would be expected from real fossiliferous surfaces, has not yet been tested due to the high computational demands. Fluid-structure interactions (FSIs) would allow mechanical deformation of organism reconstructions. It is possible that these organisms were deformed by the paleocurrents. These simplifications were implemented to reduce the computational cost of the simulations. Future research should incorporate dynamic mechanical deformation of fossil geometries and CFD-discrete element method (DEM) coupling. The behaviors of very small particles have not been simulated as part of this work because of the active nature of particle collection by organisms with—for example—choanocytes being more complex than simple consideration of flow strengths and settling.

## **4.6 STAR METHODS**

### **4.6.1 Key resources table**

See published paper.

### **4.6.2 Resource availability**

Lead contact: Further information and requests for resources should be directed to and will be fulfilled by the lead contact, Daniel Pérez-Pinedo (dperezpinedo@mun.ca).

Materials availability: This study did not generate new materials.

Data and code availability : Digital models and CFD simulation files have been deposited at Dryad (<https://doi.org/10.5061/dryad.fxpnvx103>) and are publicly available as of the date of publication. DOIs are listed in the key resources table.

This paper does not report original code.

Any additional information required to reanalyze the data reported in this paper is available from the lead contact upon request.

#### 4.6.3 Method details

##### Material and digital geometry

The upper and lower surfaces of *F. misrai* have been considered to be identical (Seilacher 1999; Gehling and Narbonne 2007), based on specimens that were inferred to have been folded, though the same specimens have more recently been considered to be rotated (Taylor et al. 2023; Figure 4.2A). Some recent published reconstructions of *Fractofusus* spp. invoked significant biconvexity (Gehling and Narbonne 2007; Liu et al. 2015) and some have suggested pronounced high relief (Mitchell and Kenchington 2018), though without any clear supporting evidence (McIlroy et al. 2022; Taylor et al. 2023). In this study we use the geometry of *F. misrai* generated from the taphonomic studies of Taylor et al. (2023) based on specimens from the E Surface fossil assemblage in the Mistaken Point Ecological Reserve ( $565.00 \pm 0.64$  Ma) (Matthews et al. 2021). The reconstructed height is compatible with the organisms pivoting around a point, which is inconsistent with a more voluminous biconvex model of *Fractofusus* (Taylor et al. 2023; Figure

4.3). The primary order branches of *F. misrai* have high morphological variability and lateral independence as shown by some specimens evidencing the lifting of individual branches from the sediment surface (Figure 4.2B). Where primary branches are densely packed, secondary order branch tips are not preserved on the lateral margins, which suggests curvature of the primary order branch away from the organism-sediment interface (Figure 4.2C). This rule of logic was used to reconstruct a complete *F. misrai* (Figure 4.3) that is significantly thinner than previous models, with the upper surfaces of branches being concave, and with the laterally-directed secondary order branches being rather curved and abutting against each other (Figure 4.3). In less densely packed regions of the frond (e.g., at the tips of the primary order branches), branches may be flared and have round ended secondary order branches (Taylor et al. 2023; Figure 4.2D), except where the frond margin has been lifted by a contemporaneous current, which results in a rather straight margin to the entire frond, with truncated branch tips (Figure 4.2E). The lower surface of *Fractofusus* is commonly preserved in extraordinary detail (sub-mm) in the form of negative relief impressions, partly below the ambient bedding plane (Dufour and McIlroy 2017), with positive ridges separating the rangeomorph elements (Narbonne 2005; Liu et al. 2011). Preservation relies on the overlying unlithified tuff collapsing and casting the underlying mudstone following decomposition of the organism (Narbonne 2005; Gehling and Narbonne 2007; Liu et al. 2011). In most specimens, the proximal portion of the primary order branches close to the longitudinal axis is preserved as a deeper negative epirelief, whereas the distal margins and the longest first-order rangeomorph units show low-relief preservation (Taylor et al. 2023; Figures 4.2C, 4.3A,C). The distal margin of first order branches are more loosely packed and range from straight to scalloped outlines suggesting they could not have displaced underlying sediment as much as the axial region.

This suggests that the organisms smothered the adjacent matground and grew at a slightly lower topographic level (cf. McIlroy et al. 2009; Taylor et al. 2023).

The three-dimensional models of *F. misrai* were created using ZBrush Pixologic, Inc. (<https://www.maxon.net/en/zbrush>; by R. Nicholls), then post-processed using Rhinoceros 3D v.7 (<https://www.rhino3d.com>) and Blender v.3.4.1 (<https://www.blender.org>). The geometry was built as a smoothed three million polygon mesh, capturing three orders of rangeomorph branching (Figure 4.3). Scaling followed published fossil dimensions (Taylor et al. 2023), and geometries were oriented according to the statistical clusters in Pérez-Pinedo et al. (2023). Finally, results were analyzed with the post-processing visualization engine Paraview (e.g., Figures 4.4-4.6) (<https://www.paraview.org>). Simplified digital geometry is available from Dryad (<https://doi.org/10.5061/dryad.fxpnvx103>).

#### Computational fluid dynamics (CFD)

Discretization and sensitivity tests were conducted to determine optimal mesh sizes, balancing anatomical resolution with computational efficiency (computing cores, CPU usage, Figures 4.S1–4.S3) at which results are independent of the mesh size. *Fractofusus misrai* geometries, consisting of approximately 300,000 to 500,000 polygons, and the corresponding flow volume region (FVRs) were meshed using SimScale standard-finite-volume meshing algorithms with automatic sizing and a medium factor fineness. The resulting mesh consists of tetrahedral and hexahedral elements. Various mesh fineness factors and region refinements were applied around the fossil geometry to explore the ideal computational parameters (Figures 4.3 and 4.S1–4.S3). Simulations of incompressible water flow [density ( $\rho$ ) x 1,000 kg/m<sup>3</sup>; dynamic viscosity ( $\mu$ ) x 0.001 kg/(m·s)] around the reconstructed *F. misrai* geometry were performed using CFD SimScale software (<https://www.simscale.com>). Reynold numbers (Re) were calculated based on the

characteristic length of *Fractofusus* ( $L_{0.05, 0.15, 0.30}$ ) ranging from 2683 ~ 64411 (Table 4.S1). Our flow regimes are around the turbulent transition for flows around an obstacle  $Re$  20000 (Menon 2015; Gibson et al. 2021; Ansys 2023). However, it is important to note that our reconstructed fossil geometry shows a complex/rough surface which results in ‘tripped’ boundary layers leading to critical implications in Reynolds number thresholds (Bearman and Harvey 1976; Choi et al. 2006; Smith et al. 2010), meaning it is possible to have turbulent flows at lower Reynolds numbers. Nevertheless, the aim of this study is to simulate the turbulent hydrodynamic conditions experienced by *Fractofusus* on the seafloor during the interval prior to the sediment-laden obrution events that smothered and killed them. The clear-water inter-turbiditic background currents travelled at low velocities over vast distances interacting with the roughness of the seafloor. In doing so they could be expected to have encountered innumerable obstacles of variable shapes and sizes, including seafloor topography (pits, mounds, ripples, scours, clasts, the bodies of living and dead erect and reclining organisms, channelization, etc). That is to say that the fronds we see on the Ediacaran bedding planes were not the first obstacles that the passing current was exposed to. Even if a such a current passed over a smooth seabed for such long distances, the skin friction alone would ensure turbulence at the velocities typical of modern deep ocean settings. Direct measurements of flow at the seafloor demonstrates persistent (turbulent) currents even from the deep featureless ocean abyssal plain (e.g., D’Asaro 1982; McLean and Yean 1987; Cushman-Roisin and Beckers 2011). Additionally, oceanographic measurements (e.g., D’Asaro 1982; McLean and Yean 1987; Cushman-Roisin and Beckers 2011) provide estimates of the viscous sublayer beneath abyssal currents, based on seafloor current data, to be ~5 mm. *Fractofusus* and most other sources of seafloor roughness would have projected through the viscous sublayer serving to maintain turbulent conditions at the Ediacaran seafloor. Reynolds numbers associated

with modern boundary layers are of order  $10^6$  to  $10^7$ . In order to simulate currents of comparable strength ( $U \sim 10$  cm/s;  $U/u^* \sim 30\text{--}35$ ) K-Omega Shear Stress Transport SST model (Menter 1994) was used to solve the Reynolds-averaged Navier–Stokes (RANS) equations, with a stationary solver used to compute the steady-state solution across all simulations. This model is known to better predict flow separation patterns than most RANS models (Menter 1994). Additionally, theoretical laminar model simulations covering the entire spectrum of modelled sizes, velocities, and orientations were tested for comparison, though laminar flows are not expected in natural deep marine settings (Table 4.S1). The computational domain consisted of a three-dimensional rectangular FVR, measuring 400 cm x 200 cm x 40 cm allowing fully developed flows (i.e., Darroch et al. 2023). A velocity inlet condition was fixed at the -X end (Figure 4.3II) of the FVR with three different flow velocities ( $U_x = 0.05$  m/s, 0.1 m/s, 0.2 m/s) while a zero-pressure outlet boundary condition was applied on the opposite +X end (Figure 4.3 III). The boundaries on the sides and top featured wall slip-boundary conditions (Figure 4.4I), whereas the lower boundary and the *F. misrai* geometry were assigned no-slip boundary conditions (Figure 4.3IV). Lastly, our palaeobiological reconstruction of *F. misrai* was affixed to the computational domain on the bottom boundary. The organism reconstructions were modelled in three different sizes: small (5 cm x 1.5 cm), medium (16cm x 5cm), and large (30cm x 10cm) (based on Taylor et al. 2023; Figures 4.4 and 4.S4–4.S6). These were positioned in different orientations with respect to the flow: parallel ( $0^\circ$ ), and perpendicular ( $90^\circ$ ) as well as oblique ( $35^\circ - 52^\circ$ ) based on the clusters determined by Pérez- Pinedo et al. (2023). Flow dynamics from the somewhat analogous modern cold-water coral-rich areas in southwest Grand Banks were used to characterize the background clear water, turbulent, flow regimes from the Capelin Gulch site (Fowler 2014). The results were

compared to a null model in the form of an ellipse lacking rangeomorph elements and fully merged into the bottom boundary without projecting primary branches (Figure 4.S7).

#### **4.6.4 Quantification and statistical analysis**

Using SimScale and Paraview, the Velocity magnitude ( $U_x$ ) and streamlines were visualized and drag forces ( $F_D$ ) were computed for each simulation by integrating pressure and skin-friction over the boundary (Figures 4.4-4.6). The distribution of the pressures and viscous (shear) forces along the elements were integrated, all the overall forces and moments calculated. To compute  $F_D$ , the projected (frontal) area of the fossil geometries was calculated (Table 4.S1). Due to meshing difficulties,  $F_D$  values were calculated using a small millimetre-scale base for *F. misrai* that was bound to the bottom boundary. Finally,  $F_D$  was explored by decomposing the normal force of pressure for each element of the surface mesh (Figure 4.6). CFD simulations results are available from Dryad (<https://doi.org/10.5061/dryad.fxpnvx103>).

#### **4.7 SUPPLEMENTAL INFORMATION**

Supplemental information can be found online at  
<https://doi.org/10.1016/j.isci.2024.110107>.

#### **4.8 ACKNOWLEDGMENTS**

We acknowledge the support from J. Peláez García, B. Colbourne, R. Hiscott, A. Hay, R. Taylor, E and N. Samson, and the Discovery UNESCO Global Geopark. We also acknowledge the constructive criticism by the six reviewers. Fieldwork and fossil casting in Newfoundland were conducted under permit from the Parks and Natural Areas Division of the Government of

Newfoundland and Labrador. This project was supported by a Discovery Grant #RGPIN-2018-04880 from the Natural Sciences and Engineering Research Council of Canada to D.M.

#### **4.9 AUTHOR CONTRIBUTIONS**

Conceptualization, D.P.-P., R.N., J.M.N., and D.M.; Methodology, D.P.-P. and R.N.; Formal analysis, D.P.-P.; Investigation, D.P.-P., J.M.N., and D.M.; Writing, D.P.-P. and D.M.; Review and editing, D.P.-P., J.M.N., and D.M.; Funding acquisition, D.M.

#### **4.10 DECLARATION OF INTERESTS**

The authors declare no competing interests.

#### **4.11 REFERENCES**

Anderson, M. M., & Misra, S. B. (1968). Fossils found in the Pre-Cambrian Conception Group of south-eastern Newfoundland. *Nature*, 220(5168), 680-681.

Ansys. What is Reynolds number? [https:// www.ansys.com/blog/what-is-reynoldsnumber](https://www.ansys.com/blog/what-is-reynoldsnumber).

Antcliffe, J. B., & Brasier, M. D. (2007). *Charnia* and sea pens are poles apart. *Journal of the Geological Society, London*, 164(1), 49-51.

Bearman, P. W., & Harvey, J. K. (1976). Golf ball aerodynamics. *Aeronautical Quarterly*, 27(2), 112-122.

Brasier, M. D., Antcliffe, J. B., & Liu, A. G. (2012). The architecture of Ediacaran fronds. *Palaeontology*, 55(5), 1105-1124.

Brasier, M. D., Liu, A. G., Menon, L., Matthews, J. J., McIlroy, D., & Wacey, D. (2013). Explaining the exceptional preservation of Ediacaran rangeomorphs from Spaniard's Bay, Newfoundland: a hydraulic model. *Precambrian Research*, 231, 122-135.

Budd, G. E., & Jensen, S. (2017). The origin of the animals and a 'Savannah' hypothesis for early bilaterian evolution. *Biological Reviews*, 92(1), 446-473.

Butterfield, N. J. (2022). Constructional and functional anatomy of Ediacaran rangeomorphs. *Geological Magazine*, 159(7), 1148-1159.

Cavalier-Smith, T. (2017). Origin of animal multicellularity: precursors, causes, consequences—the choanoflagellate/sponge transition, neurogenesis and the Cambrian explosion. *Philosophical Transactions of the Royal Society B: Biological Sciences*, 372(1713), 20150476.

Choi, J., Jeon, W. P., & Choi, H. (2006). Mechanism of drag reduction by dimples on a sphere. *Physics of Fluids*, 18(4).

Clapham, M. E., & Narbonne, G. M. (2002). Ediacaran epifaunal tiering. *Geology*, 30(7), 627-630.

Clapham, M. E., Narbonne, G. M., & Gehling, J. G. (2003). Paleoecology of the oldest known animal communities: Ediacaran assemblages at Mistaken Point, Newfoundland. *Paleobiology*, 29(4), 527-544.

Cracknell, K., García-Bellido, D. C., Gehling, J. G., Ankor, M. J., Darroch, S. A., & Rahman, I. A. (2021). Pentaradial eukaryote suggests expansion of suspension feeding in White Sea-aged Ediacaran communities. *Scientific Reports*, 11(1), 4121.

Cushman-Roisin, B., & Beckers, J. M. (2011). *Introduction to geophysical fluid dynamics: physical and numerical aspects*. Academic Press.

Darroch, S. A., Gibson, B. M., Syversen, M., Rahman, I. A., Racicot, R. A., Dunn, F. S., ... & Laflamme, M. (2022). The life and times of *Pteridinium simplex*. *Paleobiology*, 48(4), 527-556.

Darroch, S. A., Gutarra, S., Masaki, H., Olaru, A., Gibson, B. M., Dunn, F. S., ... & Rahman, I. A. (2023). The rangeomorph *Pectinifrons abyssalis*: Hydrodynamic function at the dawn of animal life. *iScience*, 26(2).

Darroch, S. A., Laflamme, M., & Clapham, M. E. (2013). Population structure of the oldest known macroscopic communities from Mistaken Point, Newfoundland. *Paleobiology*, 39(4), 591-608.

Darroch, S. A., Rahman, I. A., Gibson, B., Racicot, R. A., & Laflamme, M. (2017). Inference of facultative mobility in the enigmatic Ediacaran organism *Parvancorina*. *Biology Letters*, 13(5), 20170033.

D'Asaro, E. (1982). Absorption of internal waves by the benthic boundary layer. *Journal of Physical Oceanography*, 12(4), 323-336.

Delahooke, K. M., Liu, A. G., Stephenson, N. P., & Mitchell, E. G. (2024). 'Conga lines' of Ediacaran fronds: insights into the reproductive biology of early metazoans. *Royal Society Open Science*, 11(5), 231601.

Dufour, S.C., and McIlroy, D. (2017). Ediacaran pre-placozoan diploblasts in the Avalonian biota: the role of chemosynthesis in the evolution of early animal life. *Geological Society of London Special Publication*, 448, 211–219.

Dufour, S. C., & McIlroy, D. (2018). An Ediacaran pre-placozoan alternative to the pre-sponge route towards the Cambrian explosion of animal life: a comment on Cavalier-Smith

2017. *Philosophical Transactions of the Royal Society B: Biological Sciences*, 373(1738), 20170148.

Dunn, F. S., Liu, A. G., & Donoghue, P. C. (2018). Ediacaran developmental biology. *Biological Reviews*, 93(2), 914-932.

Dunn, F. S., Liu, A. G., Grazhdankin, D. V., Vixseboxse, P., Flannery-Sutherland, J., Green, E., ... & Donoghue, P. C. (2021). The developmental biology of *Charnia* and the eumetazoan affinity of the Ediacaran rangeomorphs. *Science Advances*, 7(30), eabe0291.

Fakhraee, M., Tarhan, L. G., Planavsky, N. J., & Reinhard, C. T. (2021). A largely invariant marine dissolved organic carbon reservoir across Earth's history. *Proceedings of the National Academy of Sciences*, 118(40), e2103511118.

Flude, L. I., & Narbonne, G. M. (2008). Taphonomy and ontogeny of a multibranching Ediacaran fossil: *Bradgatia* from the Avalon Peninsula of Newfoundland. *Canadian Journal of Earth Sciences*, 45(10), 1095-1109.

Fowler, W.A. (2014). Boundary Layer Velocity Structure in a Coldwater Coral Area of Haddock Channel, Southwest Grand Banks. Doctoral dissertation (Memorial University of Newfoundland).

Garg, R., Galvin, J., Li, T., & Pannala, S. (2012). Documentation of open-source MFIX–DEM software for gas-solids flows. From URL [https://mfix.netl.doe.gov/download/mfix/mfix\\_current\\_documentation/dem\\_doc\\_2012-1.pdf](https://mfix.netl.doe.gov/download/mfix/mfix_current_documentation/dem_doc_2012-1.pdf).

Gehling, JG, & Narbonne, GM (2007). Spindle-shaped Ediacara fossils from the Mistaken Point assemblage, Avalon Zone, Newfoundland. *Canadian Journal of Earth Sciences*, 44 (3), 367-387.

Ghisalberti, M., Gold, D. A., Laflamme, M., Clapham, M. E., Narbonne, G. M., Summons, R. E., ... & Jacobs, D. K. (2014). Canopy flow analysis reveals the advantage of size in the oldest communities of multicellular eukaryotes. *Current Biology*, 24(3), 305-309.

Gibson, B. M., Darroch, S. A., Maloney, K. M., & Laflamme, M. (2021). The importance of size and location within gregarious populations of *Ernietta plateauensis*. *Frontiers in Earth Science*, 9, 749150.

Gibson, B. M., Furbish, D. J., Rahman, I. A., Schmeekle, M. W., Laflamme, M., & Darroch, S. A. (2021). Ancient life and moving fluids. *Biological Reviews*, 96(1), 129-152.

Gibson, B. M., Rahman, I. A., Maloney, K. M., Racicot, R. A., Mocke, H., Laflamme, M., & Darroch, S. A. (2019). Gregarious suspension feeding in a modular Ediacaran organism. *Science Advances*, 5(6), eaaw0260.

Glaessner, M. F. (1984). *The dawn of animal life: a biohistorical study*. CUP Archive.

Hawco, J. B., Kenchington, C. G., Taylor, R. S., & McIlroy, D. (2020). A multivariate statistical analysis of the Ediacaran rangeomorph taxa *Beothukis* and *Culmofrons*. *Palaios*, 35(12), 495-511.

Hofmann, H. J., O'Brien, S. J., & King, A. F. (2008). Ediacaran biota on Bonavista peninsula, Newfoundland, Canada. *Journal of Paleontology*, 82(1), 1-36.

Hoyal Cuthill, J. F., & Conway Morris, S. (2014). Fractal branching organizations of Ediacaran rangeomorph fronds reveal a lost Proterozoic body plan. *Proceedings of the National Academy of Sciences*, 111(36), 13122-13126.

Ichaso, A. A., Dalrymple, R. W., & Narbonne, G. M. (2007). Paleoenvironmental and basin analysis of the late Neoproterozoic (Ediacaran) upper Conception and St. John's groups, west Conception Bay, Newfoundland. *Canadian Journal of Earth Sciences*, 44(1), 25-41.

Ivantsov, A. Y. (2013). Trace fossils of Precambrian metazoans “Vendobionta” and “Mollusks”. *Stratigraphy and Geological Correlation*, 21, 252-264.

Jenkins, R. J. (1985). The enigmatic Ediacaran (late Precambrian) genus *Rangea* and related forms. *Paleobiology*, 11(3), 336-355.

Jensen, S. (2003). The Proterozoic and earliest Cambrian trace fossil record; patterns, problems and perspectives. *Integrative and Comparative Biology*, 43(1), 219-228.

Jensen, S., Höglström, A. E., Almond, J., Taylor, W. L., Meinhold, G., Høyberget, M. A. G. N. E., ... & Palacios, T. (2018). Scratch circles from the Ediacaran and Cambrian of Arctic Norway and southern Africa, with a review of scratch circle occurrences. *Bulletin of Geosciences*, 93(3), 287-304.

Johnston, D. T., Poulton, S. W., Goldberg, T., Sergeev, V. N., Podkovyrov, V., Vorob'Eva, N. G., ... & Knoll, A. H. (2012). Late Ediacaran redox stability and metazoan evolution. *Earth and Planetary Science Letters*, 335, 25-35.

Laflamme, M., Narbonne, G. M., Greentree, C., & Anderson, M. M. (2007). Morphology and taphonomy of an Ediacaran frond: *Charnia* from the Avalon Peninsula of Newfoundland. *Geological Society, London, Special Publications*, 286(1), 237-257.

Laflamme, M., Xiao, S., & Kowalewski, M. (2009). Osmotrophy in modular Ediacara organisms. *Proceedings of the National Academy of Sciences*, 106(34), 14438-14443.

Liu, A. G., Kenchington, C. G., & Mitchell, E. G. (2015). Remarkable insights into the paleoecology of the Avalonian Ediacaran macrobiota. *Gondwana Research*, 27(4), 1355-1380.

Liu, A. G., McIlroy, D., Antcliffe, J. B., & Brasier, M. D. (2011). Effaced preservation in the Ediacara biota and its implications for the early macrofossil record. *Palaeontology*, 54(3), 607-630.

Liu, P., Zhang, Y., Yang, X., Wang, B., Zhang, T., Sun, J., ... & Han, J. (2022). Hydrodynamic Simulations of Millimeter-Scale Cambrian Sedentary Medusozoans. *Journal of Geophysical Research: Biogeosciences*, 127(10), e2022JG006854.

Matthews, J. J., Liu, A. G., Yang, C., McIlroy, D., Levell, B., & Condon, D. J. (2021). A chronostratigraphic framework for the rise of the Ediacaran macrobiota: new constraints from Mistaken Point Ecological Reserve, Newfoundland. *Geological Society of America Bulletin*, 133(3-4), 612-624.

McIlroy, D., Brasier, M.D., and Lang, A.S. (2009). Smothering of microbial mats by macrobiota: implications for the Ediacara biota. *Journal of the Geological Society, London*, 166(6), 1117-1121.

McIlroy, D., Dufour, S. C., Taylor, R., & Nicholls, R. (2021). The role of symbiosis in the first colonization of the seafloor by macrobiota: insights from the oldest Ediacaran biota (Newfoundland, Canada). *Biosystems*, 205, 104413.

McIlroy, D., Hawco, J., McKean, C., Nicholls, R., Pasinetti, G., & Taylor, R. (2020). Palaeobiology of the reclining rangeomorph *Beothukis* from the Ediacaran Mistaken Point Formation of southeastern Newfoundland. *Geological Magazine*, 159(7), 1160-1174.

McIlroy, D., & Logan, G. A. (1999). The impact of bioturbation on infaunal ecology and evolution during the Proterozoic-Cambrian transition. *Palaios*, 14(1), 58-72.

McIlroy, D., Pérez-Pinedo, D., Pasinetti, G., McKean, C., Taylor, R. S., & Hiscott, R. N. (2022). Rheotropic epifaunal growth, not felling by density currents, is responsible for many Ediacaran fossil orientations at Mistaken Point. *Frontiers in Earth Science*, 10, 849194.

McKean, C., Taylor, R. S., & McIlroy, D. (2023). New taphonomic and sedimentological insights into the preservation of high-relief Ediacaran fossils at Upper Island Cove, Newfoundland. *Lethaia*, 56(4), 1-17.

McLean, S. R., & Yean, J. (1987). Velocity and stress in the deep-ocean boundary layer. *Journal of Physical Oceanography*, 17(9), 1356-1365.

Menter, F. R. (1994). Two-equation eddy-viscosity turbulence models for engineering applications. *AIAA Journal*, 32(8), 1598-1605.

Miatta, M., & Snelgrove, P. V. (2022). Sea pens as indicators of macrofaunal communities in deep-sea sediments: Evidence from the Laurentian Channel Marine Protected Area. *Deep Sea Research Part I: Oceanographic Research Papers*, 182, 103702.

Mitchell, E. G., & Kenchington, C. G. (2018). The utility of height for the Ediacaran organisms of Mistaken Point. *Nature Ecology & Evolution*, 2(8), 1218-1222.

Mitchell, E. G., Kenchington, C. G., Liu, A. G., Matthews, J. J., & Butterfield, N. J. (2015). Reconstructing the reproductive mode of an Ediacaran macro-organism. *Nature*, 524(7565), 343-346.

Mrokowska, M. M. (2020). Influence of pycnocline on settling behaviour of non-spherical particle and wake evolution. *Scientific Reports*, 10(1), 20595.

Narbonne, G. M. (2004). Modular construction of early Ediacaran complex life forms. *Science*, 305(5687), 1141-1144.

Narbonne, G. M. (2005). The Ediacara biota: Neoproterozoic origin of animals and their ecosystems. *Annual Review of Earth and Planetary Sciences*, 33(1), 421-442.

Narbonne, G. M., Laflamme, M., Trusler, P. W., Dalrymple, R. W., & Greentree, C. (2014). Deep-water Ediacaran fossils from northwestern Canada: taphonomy, ecology, and evolution. *Journal of Paleontology*, 88(2), 207-223.

Noble, S. R., Condon, D. J., Carney, J. N., Wilby, P. R., Pharaoh, T. C., & Ford, T. D. (2015). U-Pb geochronology and global context of the Charnian Supergroup, UK: constraints on the age of key Ediacaran fossil assemblages. *Geological Society of America Bulletin*, 127(1-2), 250-265.

O'Brien, S. J., & King, A. F. (2005). Late Neoproterozoic (Ediacaran) stratigraphy of Avalon Zone sedimentary rocks, Bonavista Peninsula, Newfoundland. *Current Research, Newfoundland and Labrador Department of Natural Resources Geological Survey*, 5(1), 101-113.

Pasinetti, G., & McIlroy, D. (2023). Palaeobiology and taphonomy of the rangeomorph *Culmofrons plumosa*. *Palaeontology*, 66(4), e12671.

Paterson, J. R., Gehling, J. G., Droser, M. L., & Bicknell, R. D. (2017). Rheotaxis in the Ediacaran epibenthic organism *Parvancorina* from South Australia. *Scientific Reports*, 7(1), 45539.

Pérez-Pinedo, D., McKean, C., Taylor, R., Nicholls, R., & McIlroy, D. (2022). *Charniodiscus* and *Arborea* are separate genera within the Arboreomorpha: using the holotype of *C. concentricus* to resolve a taphonomic/taxonomic tangle. *Frontiers in Earth Science*, 9, 785929.

Pérez-Pinedo, D., Neville, J. M., Pasinetti, G., McKean, C., Taylor, R., & McIlroy, D. (2023). Frond orientations with independent current indicators demonstrate the reclining rheotropic mode of life of several Ediacaran rangeomorph taxa. *Paleobiology*, 49(3), 471-492.

Rahman, I. A., Darroch, S. A., Racicot, R. A., & Laflamme, M. (2015). Suspension feeding in the enigmatic Ediacaran organism *Tribrachidium* demonstrates complexity of Neoproterozoic ecosystems. *Science Advances*, 1(10), e1500800.

Seilacher, A. (1992). Vendobionta and Psammocorallia: lost constructions of Precambrian evolution. *Journal of the Geological Society, London*, 149(4), 607-613.

Seilacher, A. (1999). Biomat-related lifestyles in the Precambrian. *Palaios*, 14(1), 86-93.

Sharp, A. C., Evans, A. R., Wilson, S., & Vickers-Rich, P. (2017). First non-destructive internal imaging of *Rangea*, an icon of complex Ediacaran life. *Precambrian Research*, 299, 303-308.

Shashi Menon, E. (2015). Fluid flow in pipes. In *Transmission Pipeline Calculations and Simulations Manual* (Gulf Professional Publishing), pp. 149–234.

Singer, A., Plotnick, R., and Laflamme, M. (2012). Experimental fluid mechanics of an Ediacaran frond. *Palaeontologia Electronica*, 15, 1–14.

Smith, C. E., Beratlis, N., Balaras, E., Squires, K., & Tsunoda, M. (2010). Numerical investigation of the flow over a golf ball in the subcritical and supercritical regimes. *International Journal of Heat and Fluid Flow*, 31(3), 262-273.

Taylor, R. S., Matthews, J. J., Nicholls, R., & McIlroy, D. (2021). A re-assessment of the taxonomy, palaeobiology and taphonomy of the rangeomorph organism *Hapsidophyllas flexibilis* from the Ediacaran of Newfoundland, Canada. *PalZ*, 95(2), 187-207.

Taylor, R. S., Nicholls, R., Neville, J. M., & McIlroy, D. (2023). Morphological variation in the rangeomorph organism *Fractofusus misrai* from the Ediacaran of Newfoundland, Canada. *Geological Magazine*, 160(1), 146-166.

Vickers-Rich, P., Ivantsov, A. Y., Trusler, P. W., Narbonne, G. M., Hall, M., Wilson, S. A., ... & Schneider, G. I. (2013). Reconstructing *Rangaea*: new discoveries from the Ediacaran of southern Namibia. *Journal of Paleontology*, 87(1), 1-15.

Vixseboxse, P. B., Kenchington, C. G., Dunn, F. S., & Mitchell, E. G. (2021). Orientations of Mistaken Point fronds indicate morphology impacted ability to survive turbulence. *Frontiers in Earth Science*, 9, 762824.

Waggoner, B. (2003). The Ediacaran biotas in space and time. *Integrative and Comparative Biology*, 43(1), 104-113.

Wood, D. A., Dalrymple, R. W., Narbonne, G. M., Gehling, J. G., & Clapham, M. E. (2003). Paleoenvironmental analysis of the late Neoproterozoic Mistaken Point and Trepassey formations, southeastern Newfoundland. *Canadian Journal of Earth Sciences*, 40(10), 1375-1391.

Xiao, S., & Laflamme, M. (2009). On the eve of animal radiation: phylogeny, ecology and evolution of the Ediacara biota. *Trends in Ecology & Evolution*, 24(1), 31-40.

Zanzerl, H., Salvo, F., Jones, S. W., & Dufour, S. C. (2019). Feeding strategies in symbiotic and asymbiotic thyasirid bivalves. *Journal of Sea Research*, 145, 16-23.

## CHAPTER 5 - Conclusion

The thesis presented herein aims to reconstruct the life posture and orientation of key representatives of the clades Rangeomorpha and Arboreomorpha from the Ediacaran Avalon Assemblage. This work focuses on the newly described Melrose Surface at the southern end of the Catalina Dome in the Discovery UNESCO Global Geopark, which shows sedimentological evidence for paleocurrent direction in the form of current ripples and cross-lamination. This site offers a unique opportunity to reconstruct the life attitude of Ediacaran organisms with respect to sedimentologically recorded flows. By integrating taphonomic evaluation, statistical data analysis, and computational fluid dynamics, this work reconstructs both the modes of life of these organisms and the turbulent flow regimes they inhabited.

Chapter 2 – This chapter presents a taphonomic reinterpretation of the holotype of *Charniodiscus concentricus*, reconstructing it as a sub-conical bifoliate frond. Taphonomic clues, such as the poor preservation of stems and proximal branches folded beneath the stem, suggest that *C. concentricus* likely adopted an erect or recumbent life posture. This stands in contrast to the reclining reconstruction of *C. procerus*, which exhibits exceptional preservation of the stem across all stratigraphic units. Additionally, this chapter proposes an emended generic diagnosis of *Charniodiscus*, distinguishing it from the planar, non-conical fronds supported by a backing sheet and an outer rim ascribed to the genus *Arborea*. This chapter underscores the importance of taphonomic evidence in paleobiological interpretations and introduces the null hypothesis that Ediacaran organisms should be presumed to have lived reclined on the seafloor unless evidence suggests otherwise.

Chapter 3- This chapter applies a novel statistical approach adapted to circular variables to identify the optimal cluster solution in the orientation data from the population of *Fractofusus*

*misrai* from the Melrose Surface. The statistical analyses reveal one age/size cohort and preferential orientations oblique to paleocurrents. This suggests continuous aseasonal reproduction and a trade-off in orientation patterns resulting from enhancing feeding efficiency by maximizing aspect ratio and reducing drag to improve mechanical stability. Additional orientation data suggest reclining modes of life for the rangeomorphs *Pectinifrons* and *Bradgatia*, further supporting the null hypothesis proposed in Chapter 2. This chapter emphasizes the role of rheotropic responses in reclining organisms to paleocurrents and presents evidence of non-random, multimodal orientation patterns in *Fractofusus misrai*.

Chapter 4- This chapter presents, for the first time, hydrodynamic phenomena associated with a highly detailed three-dimensional reconstruction of *Fractofusus misrai* incorporating up to three orders of rangeomorph branching. Slowed down flow funneled into second-order branches could have supported a variety of feeding strategies (e.g., suspension feeding and DOM absorption) by entraining flow and irrigating the upper surface of the organism. Alternatively, it is possible that *F. misrai* used their entire surface for uptake and subsequent dorsoventral transport of oxygen. This would enhance the metabolism of sulphur-oxidizing bacteria that could have detoxified sulphidic porewaters. Additionally, the quantification of drag corroborates the hypothesis presented in chapter 3, demonstrating that orientations increasingly perpendicular to the current resulted in higher mechanical stress.

In summary, this thesis significantly advances our understanding of life postures and hydrodynamics of Ediacaran frondose taxa. By integrating taphonomic evidence, ecological data analysis, and computational fluid dynamics, this work challenges prior interpretations that Mistaken Point-type biotas lived predominantly erect in the water column. Instead, it proposes that taxa such as *Fractofusus misrai* grew flat and reclining on the seafloor, exhibiting rheotropic

behavior in response to paleocurrents. These organisms detoxify the sulphidic porewaters in which they live and modify the downstream conditions of the benthic boundary layer potentially making it more hospitable for other organisms. These trends suggest that these organisms are one of the earliest examples of ecosystem engineers and that chemosymbiosis could have been critical in the emergence and colonization of the deep waters by early metazoans.

Future research should prioritize the creation of robust Ediacaran taxonomic databases to interpret ecosystem dynamics and spatial distribution patterns. Additionally, there is a strong need to consider the alternative hypothesis that some organisms grew flat on the seafloor, responding rheotropically to paleocurrents. This hypothesis offers a more parsimonious explanation than attributing fossil preservation to highly complex and variable hydrodynamic regimes across different localities and stratigraphic units.

## Appendix A – Supplementary material from Chapter 3

Table 3.S1: “Melrosefracto.csv” dataset: a general dataset of *Fractofusus* specimens where morphometric traits, orientation under and over 180°, specimen ID number, and quadrat are recorded.

Quadrant	Specimen		Length	Width	Orientation	Or b
	nº	Species				
3A	1	Fractofusus	13.15	3.95	72.5	252.5
3B	4	Fractofusus	11.3	3.35	158	340
3B	5	Fractofusus	8.57	1.92	22	202
4A	12	Fractofusus	8.6	7.33	128	308
4B	13	Fractofusus	11.7	5.8	145	325
7A	18	Fractofusus	11.35	1.54	46	226
7A	19	Fractofusus	10.21	1.07	38	218
7A	20	Fractofusus	8.6	1.37	37	217
7A	25	Fractofusus	16.9	9.81	149	329
7A	26	Fractofusus	6.27	3.11	160	340
7A	28	Fractofusus	11.9	3.75	150	330
7A	37	Fractofusus	7.38	3.7	130	310
7B	40	Fractofusus	7.9	3.4	120	300
7B	42	Fractofusus	8.6	2.38	23.5	201
7B	43	Fractofusus	6.42	2.16	140	320
7B	45	Fractofusus	10.8	1.99	52	232
7B	46	Fractofusus	10.5	1.63	52	232
7B	49	Fractofusus	16.9	7.13	115.5	295.5
-7C-2	59	Fractofusus	15.1	2.2	57	237
-7C-3	60	Fractofusus	7.7	4.2	110	290
-7C-8	65	Fractofusus	8	5.4	160	340
-7C-9	66	Fractofusus	7.9	1.7	65	245
-7C-10	67	Fractofusus	20.5	5.2	30	210
-7D-1	73	Fractofusus	5.9	1.9	70	250
-7D-2	74	Fractofusus	21.8	5.2	80	260
-8C-1	75	Fractofusus	9.5	1.8	40	220
-8C-4	78	Fractofusus	8.5	1.7	45	225
-8C-5	79	Fractofusus	8.6	1.8	31	211
-8C-9	83	Fractofusus	9.4	2	43	223
0A-1	93	Fractofusus	9.4	5	125	305

0A-6	98	Fractofusus	7.8	1.7	10	190
0A-7	99	Fractofusus	5.5	2.6	130	310
0A-9	101	Fractofusus	9.9	4	112	292
0A-10	102	Fractofusus	8.4	2.9	163	343
0B-2	106	Fractofusus	9.8	1.5	35	215
1A-1	111	Fractofusus	13.8	3.2	25	205
1C-2	118	Fractofusus	4.4	1.2	110	290
1C-3	119	Fractofusus	4.2	1.7	120	300
1C-4	120	Fractofusus	1.9	1	150	330
2A-4	125	Fractofusus	17	3.9	171	351
2A-7	128	Fractofusus	15.8	4.7	165	345
2B-1	129	Fractofusus	5.2	3	83	263
2B-2	130	Fractofusus	6.8	4.8	118	298
1a-	131	Fractofusus	8.95	3.8	130	210
1a-	132	Fractofusus	8.8	2.2	22	202
2bx-	149	Fractofusus	13.05	2.65	44	210
2bx-	150	Fractofusus	17.5	4.2	24	186
2d-	156	Fractofusus	8.32	3.6	156	336
2d-	158	Fractofusus	10.45	5.05	2	112
2d-	161	Fractofusus	20.25	3.6	30	210
2d-	164	Fractofusus	16.2	2.5	54	210
3c-	170	Fractofusus	11.02	1.55	40	220
[-4c]	180	Fractofusus	9.15	2.02	64	244
[-4c]	182	Fractofusus	8.6	2.45	8	188
[-4c]	185	Fractofusus	10.12	2.18	70	250
[-2b]	203	Fractofusus	5	0.8	61	241
[-2b]	204	Fractofusus	10.8	2	40	220
[-2b]	205	Fractofusus	8.5	3	142	322
[-2b]	206	Fractofusus	12.5	5.1	80	260
[-2b]	211	Fractofusus	6.6	1.9	10	190
[-2b]	212	Fractofusus	15.5	1.6	179	359
[-2b]	213	Fractofusus	15.5	1.9	170	350

Table 3.S2: "Correlation.csv" dataset: consists of all the recorded orientations both under and over 180° merged together and the corresponding values of the morphometric traits.

<b>Length</b>	<b>Width</b>	<b>Orientation</b>
13.15	3.95	72.5
11.3	3.35	158

8.57	1.92	22
8.6	7.33	128
11.7	5.8	145
11.35	1.54	46
10.21	1.07	38
8.6	1.37	37
16.9	9.81	149
6.27	3.11	160
11.9	3.75	150
7.38	3.7	130
7.9	3.4	120
8.6	2.38	23.5
6.42	2.16	140
10.8	1.99	52
10.5	1.63	52
16.9	7.13	115.5
15.1	2.2	57
7.7	4.2	110
8	5.4	160
7.9	1.7	65
20.5	5.2	30
5.9	1.9	70
21.8	5.2	80
9.5	1.8	40
8.5	1.7	45
8.6	1.8	31
9.4	2	43
9.4	5	125
7.8	1.7	10
5.5	2.6	130
9.9	4	112
8.4	2.9	163
9.8	1.5	35
13.8	3.2	25
4.4	1.2	110
4.2	1.7	120
1.9	1	150
17	3.9	171
15.8	4.7	165
5.2	3	83

6.8	4.8	118
8.95	3.8	130
8.8	2.2	22
13.05	2.65	44
17.5	4.2	24
8.32	3.6	156
10.45	5.05	2
20.25	3.6	30
16.2	2.5	54
11.02	1.55	40
9.15	2.02	64
8.6	2.45	8
10.12	2.18	70
5	0.8	61
10.8	2	40
8.5	3	142
12.5	5.1	80
6.6	1.9	10
15.5	1.6	179
15.5	1.9	170
13.15	3.95	252.5
11.3	3.35	340
8.57	1.92	202
8.6	7.33	308
11.7	5.8	325
11.35	1.54	226
10.21	1.07	218
8.6	1.37	217
16.9	9.81	329
6.27	3.11	340
11.9	3.75	330
7.38	3.7	310
7.9	3.4	300
8.6	2.38	201
6.42	2.16	320
10.8	1.99	232
10.5	1.63	232
16.9	7.13	295.5
15.1	2.2	237
7.7	4.2	290

8	5.4	340
7.9	1.7	245
20.5	5.2	210
5.9	1.9	250
21.8	5.2	260
9.5	1.8	220
8.5	1.7	225
8.6	1.8	211
9.4	2	223
9.4	5	305
7.8	1.7	190
5.5	2.6	310
9.9	4	292
8.4	2.9	343
9.8	1.5	215
13.8	3.2	205
4.4	1.2	290
4.2	1.7	300
1.9	1	330
17	3.9	351
15.8	4.7	345
5.2	3	263
6.8	4.8	298
8.95	3.8	210
8.8	2.2	202
13.05	2.65	210
17.5	4.2	186
8.32	3.6	336
10.45	5.05	112
20.25	3.6	210
16.2	2.5	210
11.02	1.55	220
9.15	2.02	244
8.6	2.45	188
10.12	2.18	250
5	0.8	241
10.8	2	220
8.5	3	322
12.5	5.1	260
6.6	1.9	190

15.5	1.6	359
15.5	1.9	350

Table 3.S3: "Correlationunder180.csv" dataset: shows data from the general dataset "Melrosefracto.csv" filtered according to the under 180° group.

<b>Length</b>	<b>Width</b>	<b>Orientation</b>
13.15	3.95	72.5
11.3	3.35	158
8.57	1.92	22
8.6	7.33	128
11.7	5.8	145
11.35	1.54	46
10.21	1.07	38
8.6	1.37	37
16.9	9.81	149
6.27	3.11	160
11.9	3.75	150
7.38	3.7	130
7.9	3.4	120
8.6	2.38	23.5
6.42	2.16	140
10.8	1.99	52
10.5	1.63	52
16.9	7.13	115.5
15.1	2.2	57
7.7	4.2	110
8	5.4	160
7.9	1.7	65
20.5	5.2	30
5.9	1.9	70
21.8	5.2	80
9.5	1.8	40
8.5	1.7	45
8.6	1.8	31
9.4	2	43
9.4	5	125
7.8	1.7	10
5.5	2.6	130

9.9	4	112
8.4	2.9	163
9.8	1.5	35
13.8	3.2	25
4.4	1.2	110
4.2	1.7	120
1.9	1	150
17	3.9	171
15.8	4.7	165
5.2	3	83
6.8	4.8	118
8.95	3.8	130
8.8	2.2	22
13.05	2.65	44
17.5	4.2	24
8.32	3.6	156
10.45	5.05	2
20.25	3.6	30
16.2	2.5	54
11.02	1.55	40
9.15	2.02	64
8.6	2.45	8
10.12	2.18	70
5	0.8	61
10.8	2	40
8.5	3	142
12.5	5.1	80
6.6	1.9	10
15.5	1.6	179
15.5	1.9	170

Table 3.S4: "Correlationover180.csv" dataset: shows data from the general dataset "Melrosefracto.csv" filtered according to the over 180° group.

<b>Length</b>	<b>Width</b>	<b>Orientation</b>
13.15	3.95	252.5
11.3	3.35	340
8.57	1.92	202
8.6	7.33	308

11.7	5.8	325
11.35	1.54	226
10.21	1.07	218
8.6	1.37	217
16.9	9.81	329
6.27	3.11	340
11.9	3.75	330
7.38	3.7	310
7.9	3.4	300
8.6	2.38	201
6.42	2.16	320
10.8	1.99	232
10.5	1.63	232
16.9	7.13	295.5
15.1	2.2	237
7.7	4.2	290
8	5.4	340
7.9	1.7	245
20.5	5.2	210
5.9	1.9	250
21.8	5.2	260
9.5	1.8	220
8.5	1.7	225
8.6	1.8	211
9.4	2	223
9.4	5	305
7.8	1.7	190
5.5	2.6	310
9.9	4	292
8.4	2.9	343
9.8	1.5	215
13.8	3.2	205
4.4	1.2	290
4.2	1.7	300
1.9	1	330
17	3.9	351
15.8	4.7	345
5.2	3	263
6.8	4.8	298
8.95	3.8	210

8.8	2.2	202
13.05	2.65	210
17.5	4.2	186
8.32	3.6	336
20.25	3.6	210
16.2	2.5	210
11.02	1.55	220
9.15	2.02	244
8.6	2.45	188
10.12	2.18	250
5	0.8	241
10.8	2	220
8.5	3	322
12.5	5.1	260
6.6	1.9	190
15.5	1.6	359
15.5	1.9	350

Table 3.S5: "Orientationtotal.csv" dataset: solely contains all the recorded orientations in one variable.

**Orientation**

72.5  
158  
22  
128  
145  
46  
38  
37  
149  
160  
150  
130  
120  
23.5  
140  
52  
52

115.5  
57  
110  
160  
65  
30  
70  
80  
40  
45  
31  
43  
125  
10  
130  
112  
163  
35  
25  
110  
120  
150  
171  
165  
83  
118  
130  
22  
44  
24  
156  
2  
30  
54  
40  
64  
8  
70  
61  
40

142  
80  
10  
179  
170  
252.5  
340  
202  
308  
325  
226  
218  
217  
329  
340  
330  
310  
300  
201  
320  
232  
232  
295.5  
237  
290  
340  
245  
210  
250  
260  
220  
225  
211  
223  
305  
190  
310  
292  
343  
215

205  
290  
300  
330  
351  
345  
263  
298  
210  
202  
210  
186  
336  
112  
210  
210  
220  
244  
188  
250  
241  
220  
322  
260  
190  
359  
350

R script: Includes: 1) Morphometric quantitative size-frequency distributions analysis, 2) uniformity analysis and visualization of the circular variable, and 3) correlation and cluster analysis of circular and linear variables.

#Frond orientations with independent current indicators demonstrate the reclining rheotropic mode of life of several Ediacaran rangeomorph taxa

#Daniel Pérez-Pinedo1\*, Jenna M. Neville1, Giovanni Pasinetti1, Christopher McKean1, Rod Taylor1, Duncan McIlroy1

#1Department of Earth Sciences, Memorial University of Newfoundland, St. John's, NL, Canada

#\*Correspondence: dperezpinedo@mun.ca (D. Pérez-Pinedo)

## #INDEX

#1. Morphometric quantitative size-frequency distributions analysis

#1.1 Normality analysis

#1.2 Size-frequency distributions on mclust

#2. Uniformity analysis and visualization of the circular variable

#2.1 Angular histograms, roseplots and density lines

#2.2 Uniformity analysis of the circular variable

#2.3 Clustering algorithms of mclust on orientation

#3. Correlation and cluster analysis of circular and linear variables

#3.1 Summary plots

#3.2 Circular parallel coordinate plots (PCPs)

#3.3 Inclusion of distance around a circle (in degrees) in Gowers

#3.4 Monothetic cluster analysis: M-cross-validation and permutation-based hypothesis test

#Load and explore datasets (make sure variables are read as numeric, factors etc.)

```

setwd("~/Desktop/MUN PHD/Our papers/Melrose paper/SUBMISSION FINAL/Datasets Pérez-
Pinedo et al., 2022/Fracto population")

dir()

Melrosefracto <- read.csv("Melrosefracto.csv")

setwd("~/Desktop/MUN PHD/Our papers/Melrose paper/SUBMISSION FINAL/Datasets Pérez-
Pinedo et al., 2022/Orientation")

dir()

Orientationtotal <- read.csv("Orientationtotal.csv")

Correlation <- read.csv("Correlation.csv")

Correlationunder180 <- read.csv("Correlationunder180.csv")

Correlationover180 <- read.csv("Correlationover180.csv")

#Example to explore the dataset with Melrosefracto

dim(Melrosefracto)

colnames(Melrosefracto) # or names()

head(Melrosefracto)

summary(Melrosefracto)

#Download and load packages. Alternative packages might be required. Download as indicated by
R.

#install.packages("MASS")

library(MASS)

library(mclust, quietly=TRUE)

library(circular)

```

```
library(knitr)
```

```
library(CircMLE)
```

```
library(pracma)
```

```
library(dplyr)
```

```
library(ggplot2)
```

```
library(monoClust)
```

```
library(cluster)
```

```
library(ade4)
```

```
#1. Morphometric quantitative size-frequency distributions analysis
```

```
#1.1 Normality analysis
```

```
#Shapiro Wilks test. H0 = Normally distributed.If p-value < alpha (0.01). H0 rejected. Not normally distributed.
```

```
#Logarithmic transformation of the data when required.
```

```
#Width
```

```
shapiro.test(Melrosefracto$WIDTH) #Not normal
```

```
shapiro.test(log(Melrosefracto$WIDTH)) #Normal after transformation
```

```
LOGWIDTH <- log(Melrosefracto$WIDTH)
```

```
Melrosefracto$LOGWIDTH <- LOGWIDTH
```

```
#Length
```

```

shapiro.test(Melrosefracto$LENGTH) #Not normal

shapiro.test(log(Melrosefracto$LENGTH)) #Normal after transformation

LOGLENGTH <- log(Melrosefracto$LENGTH)

Melrosefracto$LOGLENGTH <- LOGLENGTH

#Inspection of histograms before and after transformation

#For width:

par(mfrow=c(1,2))

hist(Melrosefracto$WIDTH, # histogram

     col="white", # column color

     border="black",

     prob = TRUE, # show densities instead of frequencies

     xlab = "Width",

     ylim=c(0,0.4),

     main = "Non-transformed")

lines(density(Melrosefracto$WIDTH), # density plot

      lwd = 2, # thickness of line

      col = "chocolate3")

curve(dnorm(x,      mean=mean(Melrosefracto$WIDTH),      sd=sd(Melrosefracto$WIDTH)),

      add=TRUE, col="blue")

hist(Melrosefracto$LOGWIDTH, # histogram

     col="white", # column color

     border="black",

     prob = TRUE, # show densities instead of frequencies

```

```

xlab = "Width",
ylim=c(0,0.8),
main = "Transformed")
lines(density(Melrosefracto$LOGWIDTH), # density plot
      lwd = 2, # thickness of line
      col = "chocolate3")
curve(dnorm(x,
            mean=mean(Melrosefracto$LOGWIDTH),
            sd=sd(Melrosefracto$LOGWIDTH)), add=TRUE, col="blue")
dev.off()

#For length:
par(mfrow=c(1,2))
hist(Melrosefracto$LENGTH, # histogram
     col="white", # column color
     border="black",
     prob = TRUE, # show densities instead of frequencies
     xlab = "Length",
     ylim=c(0,0.15),
     main = "Non-transformed")
lines(density(Melrosefracto$LENGTH), # density plot
      lwd = 2, # thickness of line
      col = "chocolate3")

```

```

curve(dnorm(x, mean=mean(Melrosefracto$LENGTH), sd=sd(Melrosefracto$LENGTH)),
add=TRUE, col="blue")

hist(Melrosefracto$LOGLENGTH, # histogram
     col="white", # column color
     border="black",
     prob = TRUE, # show densities instead of frequencies
     xlab = "Length",
     ylim=c(0,1.2),
     main = "Transformed")

lines(density(Melrosefracto$LOGLENGTH), # density plot
      lwd = 2, # thickness of line
      col = "chocolate3")

curve(dnorm(x, mean=mean(Melrosefracto$LOGLENGTH),
sd=sd(Melrosefracto$LOGLENGTH)), add=TRUE, col="blue")

dev.off()

```

#1.2 Size-frequency distributions on mclust

```
par(mfrow=c(1,2))
```

#Univariate size-frequency distribution: Width

```
gaus1 = Mclust(Melrosefracto$LOGWIDTH, G=1)
```

```
summary(gaus1)
```

```
gaus2 = Mclust(Melrosefracto$LOGWIDTH, G=2)
```

```

summary(gaus2)

gaus3 = Mclust(Melrosefracto$LOGWIDTH, G=3)

summary(gaus3)

BIC(gaus1,gaus2,gaus3)

mb1 = Mclust(Melrosefracto$LOGWIDTH)

mb1$modelName

mb1$G

head(mb1$z)

mb1$bic

summary(mb1, parameters = TRUE)

BIC <- mclustBIC(Melrosefracto$LOGWIDTH, prior = priorControl())

plot(BIC) #BIC solution for 1 age/size group

#Univariate size-frenquency distribution: Length

gaus1 = Mclust(Melrosefracto$LOGLENGTH, G=1)

summary(gaus1)

gaus2 = Mclust(Melrosefracto$LOGLENGTH, G=2)

summary(gaus2)

gaus3 = Mclust(Melrosefracto$LOGLENGTH, G=3)

summary(gaus3)

BIC(gaus1,gaus2,gaus3)

mb = Mclust(Melrosefracto$LOGLENGTH)

mb$modelName

```

```

mb$G
head(mb$z)
mb$bic
summary(mb, parameters = TRUE)
BIC <- mclustBIC(Melrosefracto$LOGLENGTH, prior = priorControl())
plot(BIC) #BIC solution for 1 age/size group
dev.off ()

#Multivariate size-frequency distribution: Length and Width
par(mfrow=c(1,1))

Melrosefracto <- Melrosefracto[,-c(1:7)]
gaus1 = Mclust(Melrosefracto, G=1)
summary(gaus1)
gaus2 = Mclust(Melrosefracto, G=2)
summary(gaus2)
gaus3 = Mclust(Melrosefracto, G=3)
summary(gaus3)
BIC(gaus1,gaus2,gaus3)
mb = Mclust(Melrosefracto)
mb$modelName
mb$G
head(mb$z)

```

```

mb$bic

summary(mb, parameters = TRUE)

BIC <- mclustBIC(Melrosefracto, prior = priorControl())

plot(BIC) #BIC solution for 1 age/size group

dev.off()

#Alternative visualization of mclust: plot(mb) and commands 1,2,3 or 4

#2. Uniformity analysis and visualization of the circular variable

setwd("~/Desktop/MUN PHD/Our papers/Melrose paper/SUBMISSION FINAL/Datasets Pérez-
Pinedo et al., 2022/Fracto population")

Melrosefracto <- read.csv("Melrosefracto.csv")

par(mfrow=c(1,2))

#2.1 Angular histograms, roseplots and density lines

#Over 180°:

control.circ <- circular(Correlationover180$ORIENTATION, units = "degrees", template =
"geographics")

plot.circular(control.circ, stack = TRUE, pch = 20, sep = 0.06, shrink = 1.2) #plots experimental
data

lines(density.circular(control.circ, bw=10, fill=red))

rose.diag(control.circ, bins=30, add=TRUE)

#Under 180°:

```

```

control.circ <- circular(Correlationunder180$ORIENTATION, units = "degrees", template =
"geographics")
plot.circular(control.circ,stack = TRUE, pch = 20, sep = 0.06, shrink = 1.2) #plots experimental
data
lines(density.circular(control.circ, bw=10, fill=red))
rose.diag(control.circ,bins=30, add=TRUE)
#On 360°:
par(mfrow=c(1,1))
control.circ <- circular(Correlation$ORIENTATION, units = "degrees", template =
"geographics")
plot.circular(control.circ,stack = TRUE, pch = 20, sep = 0.06, shrink = 1.2) #plots experimental
data
lines(density.circular(control.circ, bw=10, fill=red))
rose.diag(control.circ,bins=30, add=TRUE)

#Plot the paleocurrent direction
paleocurrent <- c(282, 102) #assign control data
paleocurrent.mean <- mean(paleocurrent) #calculate and assign control mean
print(paleocurrent.mean)
paleocurrent.circ <- circular(paleocurrent, units = "degrees", template = "geographics")
plot.circular(paleocurrent.circ, shrink = 1.6) #plots experimental data

#2.2 Uniformity analysis of the circular variable

```

```

radiantscorrelationover180 <- deg2rad(Correlationover180$ORIENTATION)
radiantscorrelationunder180 <- deg2rad(Correlationunder180$ORIENTATION)
radiantscorrelation360 <- deg2rad(Correlation$ORIENTATION)

#Rayleigh test
help("rayleigh.test")
rayleigh.test(radiantscorrelationover180) #Reject H0 of uniformity
rayleigh.test(radiantscorrelationunder180) #Reject H0 of uniformity
rayleigh.test(radiantscorrelation360) #Accept H0 of uniformity

#Rao spacing test
help("rao.spacing.test")
rao.spacing.test(radiantscorrelationover180, alpha=.05) #Reject H0 of uniformity
rao.spacing.test(radiantscorrelationunder180, alpha=.05) #Reject H0 of uniformity
rao.spacing.test(radiantscorrelation360, alpha=.05) #Reject H0 of uniformity

#Hermann-Rasson test
help ("HR_test")
HR_test(radiantscorrelationover180, original =F,iter=999) #Reject H0 of uniformity
HR_test(radiantscorrelationunder180,original =F, iter=999) #Reject H0 of uniformity
HR_test(radiantscorrelation360,original =F, iter=999) #Accept H0 of uniformity

#Watson's test

```

```

help("watson.test")

watson.test(radiantscorrelationover180, alpha=0.05, dist= "vonmises") #Reject H0
watson.test(radiantscorrelationunder180, alpha=0.05, dist= "vonmises") #Reject H0
watson.test(radiantscorrelation360, alpha=0.05, dist="vonmises") #Reject H0

# Generate data from a von Mises distribution to test the H0 of Watson's test
x <- rvonmises(n=50, mu=circular(0), kappa=4)

plot (x)

rayleigh.test(x)

rao.spacing.test(x)

HR_test (x)

watson.test(x, alpha=0.05, dist="vonmises")

#2.3 Clustering algorithms of mclust on orientation

par(mfrow=c(1,2))

#under 180°

gaus1 = Mclust(radiantscorrelationunder180, G=1)

summary(gaus1)

gaus2 = Mclust(radiantscorrelationunder180, G=2)

summary(gaus2)

gaus3 = Mclust(radiantscorrelationunder180, G=3)

summary(gaus3)

```

```

BIC(kaus1,kaus2,kaus3)

mb1 = Mclust(radiantscorrelationunder180)

mb1$modelName

mb1$G

head(mb1$z)

mb1$bic

summary(mb1, parameters = TRUE)

BIC <- mclustBIC(radiantscorrelationunder180)

plot(BIC) #Two groups selected according to BIC

#Over 180°:

kaus1 = Mclust(radiantscorrelationover180, G=1)

summary(kaus1)

kaus2 = Mclust(radiantscorrelationover180, G=2)

summary(kaus2)

kaus3 = Mclust(radiantscorrelationover180, G=3)

summary(kaus3)

BIC(kaus1,kaus2,kaus3)

mb1 = Mclust(radiantscorrelationover180)

mb1$modelName

mb1$G

head(mb1$z)

mb1$bic

summary(mb1, parameters = TRUE)

```

```

BIC <- mclustBIC(radiantscorrelationover180)
plot(BIC) #Two groups selected according to BIC
dev.off()

#On 360°:
gaus1 = Mclust(radiantscorrelation360, G=1)
summary(gaus1)

gaus2 = Mclust(radiantscorrelation360, G=2)
summary(gaus2)

gaus3 = Mclust(radiantscorrelation360, G=3)
summary(gaus3)

BIC(gaus1,gaus2,gaus3)

mb1 = Mclust(radiantscorrelation360)
mb1$modelName
mb1$G
head(mb1$z)
mb1$bic
summary(mb1, parameters = TRUE)

BIC <- mclustBIC(radiantscorrelation360)
plot(BIC) #4(3) groups selected according to BIC

#In this case, unlike previous under and over 180° the max degree of difference is not 180°.Does
not make sense as a continuous variable.

dev.off()

```

### #3. Correlation and cluster analysis of circular and linear variables

#Functions from "Visualizing and Clustering Data that Includes Circular Variables" by Garland

Will: [https://math.montana.edu/grad\\_students/writing-projects/2016/16will.pdf](https://math.montana.edu/grad_students/writing-projects/2016/16will.pdf) and expanded by

Tran, 2019

#### #3.1 Summary plots

```
#Summary plots 360°
```

```
Length1 <- summary(Correlation$LENGTH)
```

```
Width1 <- summary(Correlation$WIDTH)
```

```
sum1 <- cbind(Length1, Width1)
```

```
colnames(sum1) <- c("Length (cm)", "Width (cm)")
```

```
direc_sum <- summary(circular(Correlation$ORIENTATION, type = "angles", units = "degrees"))
```

```
mean1 <- direc_sum[5]
```

```
var1 <- var.circular(circular(Correlation$ORIENTATION, type = "angles", units = "degrees"))
```

```
rho1 <- rho.circular(circular(Correlation$ORIENTATION, type = "angles", units = "degrees"))
```

```
dat1 <- t(data.frame(mean1, rho1, var1))
```

```
rownames(dat1) <- c("Orientation", "Mean Resultant Length", "Circular Variance")
```

```
colnames(dat1) <- "Orientation Direction (Deg)"
```

```
par(mfrow = c(1,2))
```

```
hist(Correlation$LENGTH, breaks = 40, main = "Length", xlab = "Length (cm)", freq = F)
```

```
hist(Correlation$WIDTH, breaks = 40, main = "Width", xlab = "Width (cm)", freq = F)
```

```

library(circular, quietly = T)

par(mfrow = c(1,2))

direc3 <- circular(Correlation$ORIENTATION, units = "degrees", type = "angles", template =
'geographics')

plot(direc3, stack = T, sep = 0.08, shrink = 1.2, main = "Orientation")

dens_circ <- density.circular(direc3, bw = 20)

p2 <- plot(density(direc3, bw = 20), rotation = 'counter', shrink = 1.2)

#Summary plots under 180

Length1 <- summary(Correlationunder180$LENGTH)

Width1 <- summary(Correlationunder180$WIDTH)

sum1 <- cbind(Length1, Width1)

colnames(sum1) <- c("Length (cm)", "Width (cm)")

direc_sum <- summary(circular(Correlationunder180$ORIENTATION, type = "angles",units =
"degrees"))

mean1 <- direc_sum[5]

var1 <- var.circular(circular(Correlationunder180$ORIENTATION, type = "angles",units =
"degrees"))

rho1 <- rho.circular(circular(Correlationunder180$ORIENTATION, type = "angles",units =
"degrees"))

dat1 <- t(data.frame(mean1, rho1, var1))

rownames(dat1) <- c("Orientation", "Mean Resultant Length", "Circular Variance")

colnames(dat1) <- "Orientation Direction (Deg)"

```

```

par(mfrow = c(1,2))
hist(Correlationunder180$LENGTH, breaks = 40, main = "Length", xlab = "Length (cm)", freq =
F)
hist(Correlationunder180$WIDTH, breaks = 40, main = "Width", xlab = "Width (cm)",freq = F)
library(circular, quietly = T)
par(mfrow = c(1,2))
direc3 <- circular(Correlationunder180$ORIENTATION, units = "degrees", type = "angles",
template='geographics')
plot(direc3, stack = T, sep = 0.08, shrink = 1.2, main = "Orientation")
dens_circ <- density.circular(direc3, bw = 20)
p2 <- plot(density(direc3, bw = 20), rotation = 'counter', shrink = 1.2)

#Summary plots over 180
Length1 <- summary(Correlationover180$LENGTH)
Width1 <- summary(Correlationover180$WIDTH)
sum1 <- cbind(Length1, Width1)
colnames(sum1) <- c("Length (cm)", "Width (cm)")
direc_sum <- summary(circular(Correlationover180$ORIENTATION, type = "angles",units =
"degrees"))
mean1 <- direc_sum[5]
var1 <- var.circular(circular(Correlationover180$ORIENTATION, type = "angles",units =
"degrees"))

```

```

rho1 <- rho.circular(circular(Correlationover180$ORIENTATION, type = "angles",units =
"degrees"))
dat1 <- t(data.frame(mean1, rho1, var1))
rownames(dat1) <- c("Orientation", "Mean Resultant Length", "Circular Variance")
colnames(dat1) <- "Orientation Direction (Deg)"
par(mfrow = c(1,2))
hist(Correlationover180$LENGTH, breaks = 40, main = "Length", xlab = "Length (cm)", freq =
F)
hist(Correlationover180$WIDTH, breaks = 40, main = "Width", xlab = "Width (cm)",freq = F)
library(circular, quietly = T)
par(mfrow = c(1,2))
direc3 <- circular(Correlationover180$ORIENTATION, units = "degrees", type = "angles",
template='geographics')
plot(direc3, stack = T, sep = 0.08, shrink = 1.2, main = "Orientation")
dens_circ <- density.circular(direc3, bw = 20)
p2 <- plot(density(direc3, bw = 20), rotation = 'counter', shrink = 1.2)
dev.off()

```

### #3.2 Circular parallel coordinate plots (PCPs)

```

#PCPs under 180°
theta <- seq(0, 360, .01)
x1 <- cos(pi*theta/180)

```

```

y1 <- sin(pi*theta/180)
y1_stand <- y1/2 + .5
x1_stand <- x1/2

#dont make data into circular object

Orientation2 <- Correlationunder180$ORIENTATION
ori_rad <- pi*(Orientation2)/180 + (3*pi/2) #Or pi/2

Orientation2
ori_rad

Length2 <- Correlationunder180$LENGTH
length_stand <- Length2 / max(Length2)
length_vec <- rep(3.5, length(length_stand))
barom_vec <- rep(5, length(length_stand))
Width_vec <- rep(7, length(length_stand))
Width_stand <- (Correlationunder180$WIDTH - min(Correlationunder180$WIDTH)) /
  (max(Correlationunder180$WIDTH) - min(Correlationunder180$WIDTH))
seg_dat <- data.frame(cbind((cos(ori_rad)/2), (sin(ori_rad)/2 + .5),
  length_vec, length_stand))
seg_dat1 <- data.frame(cbind(length_vec, length_stand, Width_vec,
  Width_stand))
plot(y1_stand ~ x1_stand, type = "l", xlim = c(-.5, 7), ylim = c(0, 1),
  xaxt = "none", xlab = "", yaxt = 'none', ylab = "", main = "PCP under 180° plot - circular")
labs <- c("Orientation", "Length", "Width")
axis(1, at = c(0, 3.5, 7), labels = labs, las = 1)

```

```

axis(2, at = c(0, 1), labels = c("Min", "Max"), las = 1) #to angle labels
#text(c(0, 4, 7), par("usr")[3] - 0.15, labels = labs, srt = 45, pos = 1, xpd = TRUE)
points(cos(ori_rad)/2, sin(ori_rad)/2 + .5, cex = .75, col = 1)
points(length_stand ~ length_vec, col = 1)
points(Width_stand ~ Width_vec, col = 1)
segments(seg_dat[,1], seg_dat[,2], seg_dat[,3], seg_dat[,4],
         col = adjustcolor(col = 1, alpha.f = .1))
segments(seg_dat1[,1], seg_dat1[,2], seg_dat1[,3], seg_dat1[,4],
         col = adjustcolor(col = 1, alpha.f = .1))
#text(.65, .55, "E")
#text(-.65, .55, "W")
#The graph is rotated. If needs to be corrected it is advised to use graphic softwares or adapt lables.

library(circular, quietly = T)
direc3 <- circular(Correlationunder180$ORIENTATION, units = "degrees", type = "angles",
template='geographics')
plot(density(direc3, bw=20),shrink = 1.2)
dens_circ <- density.circular(direc3, kernel = "vonmises", bw = 20)
p2 <- plot(density(direc3, kernel = "vonmises", bw = 20), zero = pi/2,
         rotation = 'counter', shrink = 1.2)
plot(y1_stand ~ x1_stand, type = "l", xlim = c(-.5, 7), ylim = c(-.5, 1.5),
     xaxt = "none", xlab = "", ylab = "", yaxt = 'none', main = "PCP under 180° plot - circular")
lines(I(p2$y/2 + .5) ~ I(p2$x/2))

```

```

axis(1, at = c(0, 3.5, 7), labels = labs, las = 1)
axis(2, at = c(0, 1), labels = c("Min", "Max"), las = 1)
points(cos(ori_rad)/2, sin(ori_rad)/2 + .5, cex = .5)
points(length_stand*2 -.5 ~ length_vec)
points(Width_stand*2 -.5 ~ Width_vec)
segments(seg_dat[,1], seg_dat[,2], seg_dat[,3], seg_dat[,4]*2 -.5,
         col = rgb(.1, .1, .1, .1))
segments(seg_dat1[,1], seg_dat1[,2]*2 -.5, seg_dat1[,3], seg_dat1[,4]*2 -.5,
         col = rgb(.1, .1, .1, .1))
#text(.65, .55, "E")
#text(-.65, .55, "W")
#The graph is rotated. If needed to be corrected it is advised to use graphic softwares or adapt
lables

#PCPs over 180°

Orientation2 <- Correlationover180$ORIENTATION
ori_rad <- pi*(Orientation2)/180 + (3*pi)/2 #Or pi/2
Orientation2
ori_rad
Length2 <- Correlationover180$LENGTH
length_stand <- Length2 / max(Length2)
length_vec <- rep(3.5, length(length_stand))

```

```

barom_vec <- rep(5, length(length_stand))
Width_vec <- rep(7, length(length_stand))
Width_stand <- (Correlationover180$WIDTH - min(Correlationover180$WIDTH)) /
  (max(Correlationover180$WIDTH) - min(Correlationover180$WIDTH))
seg_dat <- data.frame(cbind((cos(ori_rad)/2), (sin(ori_rad)/2 + .5),
  length_vec, length_stand))
seg_dat1 <- data.frame(cbind(length_vec, length_stand, Width_vec,
  Width_stand))
plot(y1_stand ~ x1_stand, type = "l", xlim = c(-.5, 7), ylim = c(0, 1),
  xaxt = "none", xlab = "", yaxt = 'none', ylab = "", main = "PCP over 180° plot - circular")
labs <- c("Orientation", "Length", "Width")
axis(1, at = c(0, 3.5, 7), labels = labs, las = 1)
axis(2, at = c(0, 1), labels = c("Min", "Max"), las = 1) #to angle labels
#text(c(0, 4, 7), par("usr")[3] - 0.15, labels = labs, srt = 45, pos = 1, xpd = TRUE)
points(cos(ori_rad)/2, sin(ori_rad)/2 + .5, cex = .75, col = 1)
points(length_stand ~ length_vec, col = 1)
points(Width_stand ~ Width_vec, col = 1)
segments(seg_dat[,1], seg_dat[,2], seg_dat[,3], seg_dat[,4],
  col = adjustcolor(col = 1, alpha.f = .1))
segments(seg_dat1[,1], seg_dat1[,2], seg_dat1[,3], seg_dat1[,4],
  col = adjustcolor(col = 1, alpha.f = .1))
#text(.65, .55, "E")
#text(-.65, .55, "W")

```

#The graph is rotated. If needed to be corrected it is advised to use graphic softwares or adapt labels

```
library(circular, quietly = T)

direc3 <- circular(Correlationover180$ORIENTATION, units = "degrees", type = "angles",
template='geographics')

plot(density(direc3, kernel = "vonmises", bw = 20), shrink = 1.2)

dens_circ <- density.circular(direc3, kernel = "vonmises", bw = 20)

p2 <- plot(density(direc3, kernel = "vonmises", bw = 20), zero = pi/2,
rotation = 'counter', shrink = 1.2)

plot(y1_stand ~ x1_stand, type = "l", xlim = c(-.5, 7), ylim = c(-.5, 1.5),
xaxt = "none", xlab = "", ylab = "", yaxt = 'none', main = "PCP over 180° plot - circular")

lines(I(p2$y/2 + .5) ~ I(p2$x/2))

axis(1, at = c(0, 3.5, 7), labels = labs, las = 1)

axis(2, at = c(0, 1), labels = c("Min", "Max"), las = 1)

points(cos(ori_rad)/2, sin(ori_rad)/2 + .5, cex = .5)

points(length_stand*2 -.5 ~ length_vec)

points(Width_stand*2 -.5 ~ Width_vec)

segments(seg_dat[,1], seg_dat[,2], seg_dat[,3], seg_dat[,4]*2 -.5,
col = rgb(.1, .1, .1, .1))

segments(seg_dat1[,1], seg_dat1[,2]*2 -.5, seg_dat1[,3], seg_dat1[,4]*2 -.5,
col = rgb(.1, .1, .1, .1))

#text(.65, .55, "E")
```

```

#text(-.65, .55, "W")

#The graph is rotated. If needed to be corrected it is advised to use graphic softwares or adapt
lables

#PCP 360°

Orientation2 <- Correlation$ORIENTATION

ori_rad <- pi*(Orientation2)/180 + (3*pi/2) #Or pi/2

Orientation2

ori_rad

Length2 <- Correlation$LENGTH

length_stand <- Length2 / max(Length2)

length_vec <- rep(3.5, length(length_stand))

barom_vec <- rep(5, length(length_stand))

Width_vec <- rep(7, length(length_stand))

Width_stand <- (Correlation$WIDTH - min(Correlation$WIDTH)) /
  (max(Correlation$WIDTH) - min(Correlation$WIDTH))

seg_dat <- data.frame(cbind((cos(ori_rad)/2), (sin(ori_rad)/2 + .5),
  length_vec, length_stand))

seg_dat1 <- data.frame(cbind(length_vec, length_stand, Width_vec,
  Width_stand))

#Modified PCP total

plot(y1_stand ~ x1_stand, type = "l", xlim = c(-.5, 7), ylim = c(0, 1),

```

```

xaxt = "none", xlab = "", yaxt = 'none', ylab = "", main = "PCP 360° plot - circular")
labs <- c("Orientation", "Length", "Width")
axis(1, at = c(0, 3.5, 7), labels = labs, las = 1)
axis(2, at = c(0, 1), labels = c("Min", "Max"), las = 1) #to angle labels
#text(c(0, 4, 7), par("usr")[3] - 0.15, labels = labs, srt = 45, pos = 1, xpd = TRUE)
points(cos(ori_rad)/2, sin(ori_rad)/2 + .5, cex = .75, col = 1)
points(length_stand ~ length_vec, col = 1)
points(Width_stand ~ Width_vec, col = 1)
segments(seg_dat[,1], seg_dat[,2], seg_dat[,3], seg_dat[,4],
         col = adjustcolor(col = 1, alpha.f = .1))
segments(seg_dat1[,1], seg_dat1[,2], seg_dat1[,3], seg_dat1[,4],
         col = adjustcolor(col = 1, alpha.f = .1))
#text(.65, .55, "E")
#text(-.65, .55, "W")
#The graph is rotated. If needed to be corrected it is advised to use graphic softwares or adapt
lables

library(circular, quietly = T)
direc3 <- circular(Correlation$ORIENTATION, units = "degrees", type = "angles")
plot(density(direc3, kernel = "vonmises", bw = 20))
dens_circ <- density.circular(direc3, kernel = "vonmises", bw = 20)

p2 <- plot(density(direc3, kernel = "vonmises", bw = 20), zero = pi/2,

```

```

rotation = 'counter', shrink = 1.2)
plot(y1_stand ~ x1_stand, type = "l", xlim = c(-.5, 7), ylim = c(-.5, 1.5),
      xaxt = "none", xlab = "", ylab = "", yaxt = 'none', main = "PCP 360° plot - circular")
lines(I(p2$y/2 + .5) ~ I(p2$x/2))
axis(1, at = c(0, 3.5, 7), labels = labs, las = 1)
axis(2, at = c(0, 1), labels = c("Min", "Max"), las = 1)
points(cos(ori_rad)/2, sin(ori_rad)/2 + .5, cex = .5)
points(length_stand*2 -.5 ~ length_vec)
points(Width_stand*2 -.5 ~ Width_vec)
segments(seg_dat[,1], seg_dat[,2], seg_dat[,3], seg_dat[,4]*2 -.5,
         col = rgb(.1, .1, .1, .1))
segments(seg_dat1[,1], seg_dat1[,2]*2 -.5, seg_dat1[,3], seg_dat1[,4]*2 -.5,
         col = rgb(.1, .1, .1, .1))
#text(.65, .55, "E")
#text(-.65, .55, "W")
#The graph is rotated. If needed to be corrected it is advised to use graphic softwares or adapt
lables

#3.3 Inclusion of distance around a circle (in degrees) in Gowers

#----- ON 360° -----

xc <- Correlation$ORIENTATION

```

```

xr <- data.frame(scale(Correlation$WIDTH), scale(Correlation$LENGTH))

xr <- data.frame(Correlation$WIDTH, Correlation$LENGTH)

#Calculate Gower's first and multiply by number of variables considered, excluding the #circular
variable.

library(cluster)

#Put variables that aren't circular one into xr

d1<-as.dist(as.matrix(daisy(xr,"gower")))*dim(xr)[2]

d1<-as.dist(as.matrix(daisy(xr,"gower")))*dim(xr)[2]

circd <- function(x){

  #Assumes x is just a single variable

  dist1<-matrix(0,nrow=length(x),ncol=length(x))

  for (i in (1:(length(x)-1))) {

    for (j in i:length(x)) {

      dist1[j,i]=min(abs(x[i]-x[j]), (360 - abs(x[i]-x[j])))/180

    }

  }

  return(as.dist(dist1))

}

dc<-(d1+circd(xc))/(dim(xr)[2]+1)

#Divide by total number of variables (assumes no missing values)

#greenwood - circle only

```

```

circ_dist <- cired(Correlation$ORIENTATION)
clust_circle <- hclust(circ_dist, method = 'ward.D2')
clust_circle
summary(clust_circle)
plot(clust_circle)
cuts_circle <- factor(cutree(clust_circle, k = 2))
summary(cuts_circle)
cuts_circle
plot(cuts_circle)

library(ade4)
length <- data.frame(scale(Correlation$LENGTH))
width <- data.frame(scale(Correlation$WIDTH))
direc <- data.frame(Correlation$ORIENTATION)*(pi/180)
direc5 <- prep.circular(direc)
ktab1 <- ktab.list.df(list(length, width, direc5))
dist5 <- dist.ktab(ktab1, type = c("Q", "Q", "C"))
clust5 <- hclust(dist5, method = 'ward.D2') #plot(clust5)
cuts5 <- cutree(clust5, k = 2)

#orientation only
ktab2 <- ktab.list.df(list(direc5))
dist2 <- dist.ktab(ktab2, type = 'C')
clus2 <- hclust(dist2, method = 'ward.D2')

```

```

cut2 <- cutree(clus2, k= 2)

clust_one <- hclust(dc, method = 'ward.D2')

plot(clust_one)

cuts_2 <- factor(cutree(clust_one, k = 2))

cuts_4 <- factor(cutree(clust_one, k = 4))

cuts_3 <- factor(cutree(clust_one, k = 3))

cuts_5 <- factor(cutree(clust_one, k = 5))

med <- function(members,Dist){
  if(length(members)==1){return(members)}
  else{
    if(length(members)==0){return(0)}
    dists<-apply(Dist[members,members],1,sum)
    medoid<-members[which(dists==min(dists))]
    return(medoid[1])
  }
}

ids <- 1:nrow(Correlation)

#medoids 2 cluster solution

k_2_1 <- med(members = ids[cuts_2 == 1], Dist = as.matrix(dc)) #14
k_2_2 <-med(members = ids[cuts_2 == 2], Dist = as.matrix(dc)) #76

meds_2 <- c(k_2_1, k_2_2)

```

```

#medoids 3 cluster solution

k_3_1 <- med(members = ids[cuts_3 == 1], Dist = as.matrix(dc)) #47
k_3_2 <- med(members = ids[cuts_3 == 2], Dist = as.matrix(dc)) #76
k_3_3 <- med(members = ids[cuts_3 == 3], Dist = as.matrix(dc)) #54
meds_3 <- c(k_3_1, k_3_2, k_3_3)

#medoids 4 cluster solution

k_4_1 <- med(members = ids[cuts_4 == 1], Dist = as.matrix(dc)) #47
k_4_2 <- med(members = ids[cuts_4 == 2], Dist = as.matrix(dc)) #12
k_4_3 <- med(members = ids[cuts_4 == 3], Dist = as.matrix(dc)) #54
k_4_4 <- med(members = ids[cuts_4 == 4], Dist = as.matrix(dc)) #119
meds_4 <- c(k_4_1, k_4_2, k_4_3, k_4_4)

#medoids 5 cluster solution

k_5_1 <- med(members = ids[cuts_5 == 1], Dist = as.matrix(dc)) #47
k_5_2 <- med(members = ids[cuts_5 == 2], Dist = as.matrix(dc)) #12
k_5_3 <- med(members = ids[cuts_5 == 3], Dist = as.matrix(dc)) #26
k_5_4 <- med(members = ids[cuts_5 == 4], Dist = as.matrix(dc)) #119
k_5_5 <- med(members = ids[cuts_5 == 5], Dist = as.matrix(dc)) #74
meds_5 <- c(k_5_1, k_5_2, k_5_3, k_5_4, k_5_5)

par(mfrow = c(1,1))

old_par <- par(mar = c(5.1, 4.1, 4.1, 2.1))

par(mar= c(2, 4.1, 4.1, 2.1))

```

```
plot(clust_one, labels = F, xlab = "", sub = "", main= "Cluster Dendrogram on 360°")
```

```
#abline(h = 0.85, lwd = 2, col = 2)
```

```
#abline(h = 1.05, lwd = 2, col = 3)
```

```
par(mar = old_par)
```

```
scale_cape<- data.frame(apply(Correlation[, c(1, 3)], 2, scale), Orientation2)
```

```
noscale_cape <- data.frame(Correlation[,c(1,3) ], Orientation2)
```

```
#package (clusterSim)
```

```
G1s <- numeric(0)
```

```
#Load the function from package clusterSim. I found it on CRAN
```

```
for(j in 1:6){
```

```
  G1s[j] <- index.G1(x = noscale_cape, cl = cutree(clust_one, k = j))
```

```
}
```

```
#If functions gives an error run:
```

```
.medoid<-function(x,d)
```

```
{
```

```
  minj<-0
```

```
  minsumdist<-sum(d)
```

```

if(is.null(dim(x)) && is.null(dim(d))){
  dim(x)<-c(1,length(x))
  x
}
else{
  if(is.null(dim(d))){
    dim(d)<-c(1,1)
  }
  if(is.null(dim(x))){
    dim(x)<-c(length(x),1)
  }
  for(j in 1:nrow(d)){
    if (sum(d[j,])<=minsumdist){
      #minj<-row.names(d)[j]
      minj<-j
      minsumdist<-sum(d[j,])
    }
  }
  resul<-as.matrix(x[minj,])
  resul
}
}

```

```

index.G1<-function(x,cl,d=NULL,centrotypes="centroids")
{
  if(sum(c("centroids","medoids")==centrotypes)==0)
    stop("Wrong centrotypes argument")
  if("medoids"==centrotypes && is.null(d))
    stop("For argument centrotypes = 'medoids' d cannot be null")
  if(!is.null(d)){
    if(!is.matrix(d)){
      d<-as.matrix(d)
    }
    row.names(d)<-row.names(x)
  }

  n <- length(cl)
  k <- max(cl)
  if(is.null(dim(x))){
    dim(x)<-c(length(x),1)
  }
  centers<-matrix(nrow=k,ncol=ncol(x))
  for(i in 1:k)
  {
    x.k = x[cl==i,]
  }
}

```

```

if(centrotypes=="centroids"){
  if(ncol(x)==1){
    centers[i,]<-mean(x.k)
  }
  else{
    if (is.vector(x.k)){
      centers[i,]<-x.k
    }
    else{
      centers[i,]<-apply(x.k,2,mean)
    }
  }
}
else{
  centers[i,]<-medoid(x[cl==i,],d[cl==i,cl==i])
  #print(apply(x[cl==i,],2,mean))
  #print(centers[i,])
}
}
if (centrotypes=="centroids"){
  allmean <- apply(x,2,mean)
}
else{

```

```

# print(apply(x,2,mean))

allmean<-medoid(x,d)

#print(allmean)

}

dmean <- sweep(x,2,allmean,"-")

allmeandist <- sum(dmean^2)

withins <- rep(0, k)

x <- (x - centers[cl,])^2

for(i in 1:k){

  withins[i] <- sum(x[cl==i,])

}

wgss <- sum(withins)

bgss <- allmeandist - wgss

(bgss/(k-1))/(wgss/(n-k))

}

for(j in 1:10){

  G1s[j] <- index.G1(x = noscale_ cape, cl = cutree(clust_one, k = j))

}

plot(1:10, G1s, type = 'l', xlab = "Number of clusters",

```

```
main = "Calinski - Harabasz Pseudo F stat on 360°") #Gives k=5 as the most parsimonius cluster
solution. k=6 second most likely.
```

```
plot(clust_one, labels = F, xlab = "", sub = "", main= "Cluster Dendrogram on 360°; k=5")
```

```
abline(h = 1, lwd = 2, col = 2) #Indicate second most likely solution: k=5
```

```
abline(h = 0.87, lwd = 2, col = 3) #Indicate most likely cluster solution: k=6
```

```
#Greenwood method
```

```
#PCP k=2
```

```
plot(y1_stand ~ x1_stand, type = "l", xlim = c(-.5, 7), ylim = c(0, 1),
```

```
  xaxt = "none", xlab = "", ylab = "", yaxt = "none",
```

```
  main = "PCP plot - circular, k = 2 Greenwood method")
```

```
labs <- c("Orientation", "Length", "Width")
```

```
axis(1, at = c(0, 3.5, 7), labels = labs, las = 1) #axis(2, at = c(0, 1), labels = c("Min", "Max"), las =
2)
```

```
points(cos(ori_rad)/2, sin(ori_rad)/2 + .5, cex = .75, col = cuts_2)
```

```
points(length_stand ~ length_vec, col = cuts_2)
```

```
points(Width_stand ~ Width_vec, col = cuts_2)
```

```
segments(seg_dat[,1], seg_dat[,2], seg_dat[,3], seg_dat[,4],
```

```
  col = adjustcolor(col = cuts_2, alpha.f = .1))
```

```
segments(seg_dat1[,1], seg_dat1[,2], seg_dat1[,3], seg_dat1[,4],
```

```
  col = adjustcolor(col = cuts_2, alpha.f = .1))
```

```

#group reps

points(cos(ori_rad[c(14, 76)])/2, sin(ori_rad[c(14, 76)])/2 + .5,
       cex = 1, col = c(1, 2))

points(length_stand[c(14, 76)] ~ length_vec[c(14, 76)], col = c(1, 2))
points(Width_stand[c(14, 76)] ~ Width_vec[c(14, 76)], col = c(1, 2))

segments(seg_dat[c(14, 76), 1], seg_dat[c(14, 76), 2],
         seg_dat[c(14, 76), 3], seg_dat[c(14, 76), 4],
         col = c(1, 2), lwd = 3)

segments(seg_dat1[c(14, 76), 1], seg_dat1[c(14, 76), 2],
         seg_dat1[c(14, 76), 3], seg_dat1[c(14, 76), 4],
         col = c(1, 2), lwd = 3)

#text(.65, .55, "E")
#text(-.65, .55, "W")

#Other approach

plot(y1_stand ~ x1_stand, type = "l", xlim = c(-.5, 7), ylim = c(0, 1),
     xaxt = "none", yaxt = "none", xlab = "", ylab = "",
     main = "PCP plot - circular, k = 2")

labs <- c("Orientation", "Length", "Width")

axis(2, at = c(0, 1), labels = c("Min", "Max"), las = 2)

axis(1, at = c(0, 3.5, 7), labels = labs, las = 1)

```

```

points(cos(ori_rad)/2, sin(ori_rad)/2 + .5, cex = .75, col = cuts_2)

points(length_stand ~ length_vec, col = cuts_2)

points(Width_stand ~ Width_vec, col = cuts_2)

segments(seg_dat[,1], seg_dat[,2], seg_dat[,3], seg_dat[,4],
         col = adjustcolor(col = cuts_2, alpha.f = .1))

segments(seg_dat1[,1], seg_dat1[,2], seg_dat1[,3], seg_dat1[,4],
         col = adjustcolor(col = cuts_2, alpha.f = .1))

#group reps

points(cos(ori_rad[meds_2])/2, sin(ori_rad[meds_2])/2 + .5,
       cex = .75, col = c(1, 2))

points(length_stand[meds_2] ~ length_vec[meds_2], col = c(1, 2))

points(Width_stand[meds_2] ~ Width_vec[meds_2], col = c(1, 2))

segments(seg_dat[meds_2,1], seg_dat[meds_2,2],
         seg_dat[meds_2,3], seg_dat[meds_2,4],
         col = adjustcolor(col = c(1, 2), alpha = 3), lwd = 2)

segments(seg_dat1[meds_2, 1], seg_dat1[meds_2, 2], seg_dat1[meds_2, 3],
         seg_dat1[meds_2, 4],
         col = adjustcolor(col = c(1, 2), alpha = 1), lwd = 2)

#Medoids can be overlapping. Graphic editor softwares are recommended.

#PCP k=3

```

```

plot(y1_stand ~ x1_stand, type = "l", xlim = c(-.5, 7), ylim = c(0, 1),
     xaxt = "none", yaxt = "none", xlab = "", ylab = "",
     main = "PCP plot - circular, k = 3")
labs <- c("Orientation", "Length", "Width")
axis(1, at = c(0, 3.5, 7), labels = labs, las = 1)
axis(2, at = c(0, 1), labels = c("Min", "Max"), las = 2)
points(cos(ori_rad)/2, sin(ori_rad)/2 + .5, cex = .75, col = cuts_3)
points(length_stand ~ length_vec, col = cuts_3)
points(Width_stand ~ Width_vec, col = cuts_3)
segments(seg_dat[,1], seg_dat[,2], seg_dat[,3], seg_dat[,4],
         col = adjustcolor(col = cuts_3, alpha.f = .1))
segments(seg_dat1[,1], seg_dat1[,2], seg_dat1[,3], seg_dat1[,4],
         col = adjustcolor(col = cuts_3, alpha.f = .1))
#group res

points(cos(ori_rad[meds_3])/2, sin(ori_rad[meds_3])/2 + .5,
       cex = .75, col = c(1, 2, 3))
points(length_stand[meds_3] ~ length_vec[meds_3], col = c(1, 2, 3))
points(Width_stand[meds_3] ~ Width_vec[meds_3], col = c(1, 2, 3))
segments(seg_dat[meds_3,1], seg_dat[meds_3,2],
         seg_dat[meds_3,3], seg_dat[meds_3,4],
         col = adjustcolor(col = c(1, 2, 3), alpha = 3), lwd = 2)
segments(seg_dat1[meds_3, 1], seg_dat1[meds_3, 2], seg_dat1[meds_3, 3],

```

```

seg_dat1[meds_3, 4],

col = adjustcolor(col = c(1, 2, 3), alpha = 1), lwd = 2)

#PCP k=4

plot(y1_stand ~ x1_stand, type = "l", xlim = c(-.5, 7), ylim = c(0, 1),
     xaxt = "none", yaxt = "none", xlab = "", ylab = "",
     main = "PCP plot - circular, k = 4")

labs <- c("Orientation", "Length", "Width")

axis(2, at = c(0, 1), labels = c("Min", "Max"), las = 2)

axis(1, at = c(0, 3.5, 7), labels = labs, las = 1)

points(cos(ori_rad)/2, sin(ori_rad)/2 + .5, cex = .75, col = cuts_4)

points(length_stand ~ length_vec, col = cuts_4)

points(Width_stand ~ Width_vec, col = cuts_4)

segments(seg_dat[,1], seg_dat[,2], seg_dat[,3], seg_dat[,4],
         col = adjustcolor(col = cuts_4, alpha.f = .1))

segments(seg_dat1[,1], seg_dat1[,2], seg_dat1[,3], seg_dat1[,4],
         col = adjustcolor(col = cuts_4, alpha.f = .1))

#group reps

points(cos(ori_rad[meds_4])/2, sin(ori_rad[meds_4])/2 + .5,
       cex = .75, col = c(1, 2, 3, 4))

points(length_stand[meds_4] ~ length_vec[meds_4], col = c(1, 2, 3, 4))

```

```

points(Width_stand[meds_4] ~ Width_vec[meds_4], col = c(1, 2, 3, 4))
segments(seg_dat[meds_4,1], seg_dat[meds_4,2],
         seg_dat[meds_4,3], seg_dat[meds_4,4],
         col = adjustcolor(col = c(1, 2, 3, 4), alpha = 3), lwd = 2)
segments(seg_dat1[meds_4, 1], seg_dat1[meds_4, 2], seg_dat1[meds_4, 3],
         seg_dat1[meds_4, 4],
         col = adjustcolor(col = c(1, 2, 3, 4), alpha = 1), lwd = 2)

```

```
#PCP k=5
```

```

plot(y1_stand ~ x1_stand, type = "l", xlim = c(-.5, 7), ylim = c(0, 1),
     xaxt = "none", yaxt = "none", xlab = "", ylab = "",
     main = "PCP plot - circular, k = 5")
labs <- c("Orientation", "Length", "Width")
axis(2, at = c(0, 1), labels = c("Min", "Max"), las = 2)
axis(1, at = c(0, 3.5, 7), labels = labs, las = 1)
points(cos(ori_rad)/2, sin(ori_rad)/2 + .5, cex = .75, col = cuts_5)
points(length_stand ~ length_vec, col = cuts_5)
points(Width_stand ~ Width_vec, col = cuts_5)
segments(seg_dat[,1], seg_dat[,2], seg_dat[,3], seg_dat[,4],
         col = adjustcolor(col = cuts_5, alpha.f = .1))
segments(seg_dat1[,1], seg_dat1[,2], seg_dat1[,3], seg_dat1[,4],
         col = adjustcolor(col = cuts_5, alpha.f = .1))

```

```

#group reps

points(cos(ori_rad[meds_5])/2, sin(ori_rad[meds_5])/2 + .5,
       cex = .75, col = c(1, 2, 3, 4,5))

points(length_stand[meds_5] ~ length_vec[meds_5], col = c(1, 2, 3, 4,5))
points(Width_stand[meds_5] ~ Width_vec[meds_5], col = c(1, 2, 3, 4,5))

segments(seg_dat[meds_5,1], seg_dat[meds_5,2],
         seg_dat[meds_5,3], seg_dat[meds_5,4],
         col = adjustcolor(col = c(1, 2, 3, 4, 5), alpha = 3), lwd = 2)

segments(seg_dat1[meds_5, 1], seg_dat1[meds_5, 2], seg_dat1[meds_5, 3],
         seg_dat1[meds_5, 4],
         col = adjustcolor(col = c(1, 2, 3, 4,5), alpha = 1), lwd = 2)

#The medoids are overlapping. We advise the use of graphic softwares to resolve this problem or
plot dashed lines.

#Get final data

#Example k=5

med5 <- Correlation[meds_5, c(1:3)]

rownames(med5) <- c("1st medoid", "2nd mediod", "3rd mediod", "4th mediod", "5th mediod")

med5 <- data.frame(meds_5, med5)

names(med5)[1] <- "Observation ID"

med5

```

```

summary(med5)

#Final solution k=4

med4 <- Correlation[meds_4, c(1:3)]
rownames(med4) <- c("A", "B", "C", "D")
med4 <- data.frame(meds_4, med4)
names(med4)[1] <- "Observation ID"
med4

summary(med4)

#----- UNDER 180° -----

xc <- Correlationunder180$ORIENTATION
xr <- data.frame(scale(Correlationunder180$WIDTH), scale(Correlationunder180$LENGTH))
xr <- data.frame(Correlationunder180$WIDTH, Correlationunder180$LENGTH)
#Calculate Gower's first and multiply by number of variables considered, excluding the #circular
variable.

library(cluster)

#Put variables that aren't circular one into xr
d1<-as.dist(as.matrix(daisy(xr,"gower")))*dim(xr)[2]
d1<-as.dist(as.matrix(daisy(xr,"gower")))*dim(xr)[2]

circd <- function(x){

```

```

#Assumes x is just a single variable

dist1<-matrix(0,nrow=length(x),ncol=length(x))

for (i in (1:(length(x)-1))) {
  for (j in i:length(x)) {
    dist1[j,i]=min(abs(x[i]-x[j]), (360 - abs(x[i]-x[j]))) / 180
  }
}

return(as.dist(dist1))
}

dc<-(d1+circd(xc))/(dim(xr)[2]+1)

#Divide by total number of variables (assumes no missing values)

#greenwood - circle only

circ_dist <- circd(Correlationunder180$ORIENTATION)

clust_circle <- hclust(circ_dist, method = 'ward.D2')

clust_circle

summary(clust_circle)

plot(clust_circle)

cuts_circle <- factor(cutree(clust_circle, k = 2))

summary(cuts_circle)

cuts_circle

plot(cuts_circle)

```

```

library(ade4)

length <- data.frame(scale(Correlationunder180$LENGTH))
width <- data.frame(scale(Correlationunder180$WIDTH))
direc <- data.frame(Correlationunder180$ORIENTATION)*(pi/180)
direc5 <- prep.circular(direc)
ktab1 <- ktab.list.df(list(length, width, direc5))
dist5 <- dist.ktab(ktab1, type = c("Q", "Q", "C"))
clust5 <- hclust(dist5, method = 'ward.D2') #plot(clust5)
cuts5 <- cutree(clust5, k = 2)

#Orientation only
ktab2 <- ktab.list.df(list(direc5))
dist2 <- dist.ktab(ktab2, type = 'C')
clus2 <- hclust(dist2, method = 'ward.D2')
cut2 <- cutree(clus2, k= 2)

clust_one <- hclust(dc, method = 'ward.D2')
plot(clust_one)
cuts_2 <- factor(cutree(clust_one, k = 2))
cuts_4 <- factor(cutree(clust_one, k = 4))
cuts_3 <- factor(cutree(clust_one, k = 3))
cuts_5 <- factor(cutree(clust_one, k = 5))

med <- function(members,Dist){
  if(length(members)==1){return(members)}

```

```

else{
  if(length(members)==0){return(0)}
  dists<-apply(Dist[members,members],1,sum)
  medoid<-members[which(dists==min(dists))]
  return(medoid[1])
}
}

ids <- 1:nrow(Correlationunder180)

#medoids 2 cluster solution
k_2_1 <- med(members = ids[cuts_2 == 1], Dist = as.matrix(dc)) #29
k_2_2 <-med(members = ids[cuts_2 == 2], Dist = as.matrix(dc)) #44
meds_2 <- c(k_2_1, k_2_2)

#medoids 3 cluster solution
k_3_1 <- med(members = ids[cuts_3 == 1], Dist = as.matrix(dc)) #51
k_3_2 <-med(members = ids[cuts_3 == 2], Dist = as.matrix(dc)) #44
k_3_3 <-med(members = ids[cuts_3 == 3], Dist = as.matrix(dc)) #26
meds_3 <- c(k_3_1, k_3_2, k_3_3)

#medoids 4 cluster solution
k_4_1 <- med(members = ids[cuts_4 == 1], Dist = as.matrix(dc)) #51
k_4_2 <- med(members = ids[cuts_4 == 2], Dist = as.matrix(dc)) #12
k_4_3 <- med(members = ids[cuts_4 == 3], Dist = as.matrix(dc)) #26
k_4_4 <- med(members = ids[cuts_4 == 4], Dist = as.matrix(dc)) #41

```

```

meds_4 <- c(k_4_1, k_4_2, k_4_3, k_4_4)

#medoids 5 cluster solution

k_5_1 <- med(members = ids[cuts_5 == 1], Dist = as.matrix(dc)) #51
k_5_2 <- med(members = ids[cuts_5 == 2], Dist = as.matrix(dc)) #44
k_5_3 <- med(members = ids[cuts_5 == 3], Dist = as.matrix(dc)) #26
k_5_4 <- med(members = ids[cuts_5 == 4], Dist = as.matrix(dc)) #41
k_5_5 <- med(members = ids[cuts_5 == 5], Dist = as.matrix(dc)) #38
meds_5 <- c(k_5_1, k_5_2, k_5_3, k_5_4, k_5_5)

par(mfrow = c(1,1))

old_par <- par(mar = c(5.1, 4.1, 4.1, 2.1))

par(mar= c(2, 4.1, 4.1, 2.1))

plot(clust_one, labels = F, xlab = "", sub = "", main= "Cluster Dendrogram under 180°")

#abline(h = 0.85, lwd = 2, col = 2)

#abline(h = 1.05, lwd = 2, col = 3)

par(mar = old_par)

scale_cape<- data.frame(apply(Correlationunder180[, c(1, 3)], 2, scale),
Correlationunder180$ORIENTATION) #names(cape_blanco2)

noscale_cape <- data.frame(Correlationunder180[,c(1,3)
Correlationunder180$ORIENTATION)

#package (clusterSim)

```

```
G1s <- numeric(0)
```

```
#Load the function from package clusterSim. I found it on CRAN
```

```
for(j in 1:6){
```

```
  G1s[j] <- index.G1(x = noscale_ape, cl = cutree(clust_one, k = j))
```

```
}
```

```
#If functions gives an error run:
```

```
.medoid<-function(x,d)
```

```
{
```

```
  minj<-0
```

```
  minsumdist<-sum(d)
```

```
  if(is.null(dim(x)) && is.null(dim(d))){
```

```
    dim(x)<-c(1,length(x))
```

```
    x
```

```
  }
```

```
  else{
```

```
    if(is.null(dim(d))){
```

```
      dim(d)<-c(1,1)
```

```
    }
```

```

if(is.null(dim(x))){
  dim(x)<-c(length(x),1)
}
for(j in 1:nrow(d)){
  if (sum(d[j,])<=minsumdist){
    #minj<-row.names(d)[j]
    minj<-j
    minsumdist<-sum(d[j,])
  }
}
resul<-as.matrix(x[minj,])
resul
}
}

index.G1<-function(x,cl,d=NULL,centrotypes="centroids")
{
  if(sum(c("centroids","medoids")==centrotypes)==0)
    stop("Wrong centrotypes argument")
  if("medoids"==centrotypes && is.null(d))
    stop("For argument centrotypes = 'medoids' d cannot be null")
  if(!is.null(d)){

```

```

if(!is.matrix(d)){
  d<-as.matrix(d)
}
row.names(d)<-row.names(x)
}

n <- length(cl)
k <- max(cl)
if(is.null(dim(x))){
  dim(x)<-c(length(x),1)
}
centers<-matrix(nrow=k,ncol=ncol(x))
for(i in 1:k)
{
  x.k = x[cl==i,]
  if(centrotypes=="centroids"){
    if(ncol(x)==1){
      centers[i,]<-mean(x.k)
    }
  }
  else{
    if (is.vector(x.k)){
      centers[i,]<-x.k
    }
  }
}

```

```

else{
  centers[i,]<-apply(x.k,2,mean)
}
}
}
else{
  centers[i,]<-medoid(x[cl==i,],d[cl==i,cl==i])
  #print(apply(x[cl==i,],2,mean))
  #print(centers[i,])
}
}
if (centrotypes=="centroids"){
  allmean <- apply(x,2,mean)
}
else{
  # print(apply(x,2,mean))
  allmean<-medoid(x,d)
  #print(allmean)
}
dmean <- sweep(x,2,allmean,"-")
allmeandist <- sum(dmean^2)
withins <- rep(0, k)
x <- (x - centers[cl,])^2

```

```

for(i in 1:k){
  within[i] <- sum(x[cl==i,])
}

wgss <- sum(withins)

bgss <- allmeandist - wgss

(bgss/(k-1))/(wgss/(n-k))

}

for(j in 1:10){
  G1s[j] <- index.G1(x = noscale_cape, cl = cutree(clust_one, k = j))
}

plot(1:10, G1s, type = 'l', xlab = "Number of clusters",
     main = "Calinski - Harabasz Pseudo F stat under 180°") #Gives k=2 as the most parsimonius
cluster solution. k=3 second most likely.

plot(clust_one, labels = F, xlab = "", sub = "", main= "Cluster Dendrogram under 180°; k=2")
abline(h = 0.795, lwd = 2, col = 2) #Indicate second most likely solution: k=3
abline(h = 1, lwd = 2, col = 3) #Indicate most likely cluster solution: k=2

#Greenwood method

#Required objects

```

```

theta <- seq(0, 360, .01)
x1 <- cos(pi*theta/180)
y1 <- sin(pi*theta/180)
y1_stand <- y1/2 + .5
x1_stand <- x1/2

#dont make data into circular object

Orientation2 <- Correlationunder180$ORIENTATION
ori_rad <- pi*(Orientation2)/180 + (3*pi/2)
Orientation2
ori_rad

Length2 <- Correlationunder180$LENGTH
length_stand <- Length2 / max(Length2)
length_vec <- rep(3.5, length(length_stand))
barom_vec <- rep(5, length(length_stand))
Width_vec <- rep(7, length(length_stand))
Width_stand <- (Correlationunder180$WIDTH - min(Correlationunder180$WIDTH)) /
  (max(Correlationunder180$WIDTH) - min(Correlationunder180$WIDTH))
seg_dat <- data.frame(cbind((cos(ori_rad)/2), (sin(ori_rad)/2 + .5),
  length_vec, length_stand))
seg_dat1 <- data.frame(cbind(length_vec, length_stand, Width_vec,
  Width_stand))

```

```

#PCP k=2

plot(y1_stand ~ x1_stand, type = "l", xlim = c(-.5, 7), ylim = c(0, 1),
     xaxt = "none", xlab = "", ylab = "", yaxt = "none",
     main = "PCP plot - circular, under 180°, k = 2 Greenwood method")

labs <- c("Orientation", "Length", "Width")

axis(1, at = c(0, 3.5, 7), labels = labs, las = 1) #axis(2, at = c(0, 1), labels = c("Min", "Max"), las =
2)

points(cos(ori_rad)/2, sin(ori_rad)/2 + .5, cex = .75, col = cuts_2)

points(length_stand ~ length_vec, col = cuts_2)

points(Width_stand ~ Width_vec, col = cuts_2)

segments(seg_dat[,1], seg_dat[,2], seg_dat[,3], seg_dat[,4],
         col = adjustcolor(col = cuts_2, alpha.f = .1))

segments(seg_dat1[,1], seg_dat1[,2], seg_dat1[,3], seg_dat1[,4],
         col = adjustcolor(col = cuts_2, alpha.f = .1))

#group reps

points(cos(ori_rad[c(29, 44)])/2, sin(ori_rad[c(29, 44)])/2 + .5,
       cex = 1, col = c(1, 2))

points(length_stand[c(29, 44)] ~ length_vec[c(29, 44)], col = c(1, 2))

points(Width_stand[c(29, 44)] ~ Width_vec[c(29, 44)], col = c(1, 2))

segments(seg_dat[c(29, 44), 1], seg_dat[c(29, 44), 2],
         seg_dat[c(29, 44), 3], seg_dat[c(29, 44), 4],

```

```

col = c(1, 2), lwd = 3)
segments(seg_dat1[c(29, 44), 1], seg_dat1[c(29, 44), 2],
         seg_dat1[c(29, 44), 3], seg_dat1[c(29, 44), 4],
         col = c(1, 2), lwd = 3)
#text( .65, .55, "E")
#text(-.65, .55, "W")

#Other approach

plot(y1_stand ~ x1_stand, type = "l", xlim = c(-.5, 7), ylim = c(0, 1),
     xaxt = "none", yaxt = "none", xlab = "", ylab = "",
     main = "PCP plot - circular, k = 2")
labs <- c("Orientation", "Length", "Width")
axis(2, at = c(0, 1), labels = c("Min", "Max"), las = 2)
axis(1, at = c(0, 3.5, 7), labels = labs, las = 1)
points(cos(ori_rad)/2, sin(ori_rad)/2 + .5, cex = .75, col = cuts_2, pch=19)
points(length_stand ~ length_vec, col = cuts_2, pch=19)
points(Width_stand ~ Width_vec, col = cuts_2, pch=19)
segments(seg_dat[,1], seg_dat[,2], seg_dat[,3], seg_dat[,4],
         col = adjustcolor(col = cuts_2, alpha.f = .1))
segments(seg_dat1[,1], seg_dat1[,2], seg_dat1[,3], seg_dat1[,4],
         col = adjustcolor(col = cuts_2, alpha.f = .1))

```

```

#group reps

points(cos(ori_rad[meds_2])/2, sin(ori_rad[meds_2])/2 + .5,
       cex = .75, col = c(1, 2), pch=19)

points(length_stand[meds_2] ~ length_vec[meds_2], col = c(1, 2), pch=19)
points(Width_stand[meds_2] ~ Width_vec[meds_2], col = c(1, 2), pch=19)

segments(seg_dat[meds_2,1], seg_dat[meds_2,2],
         seg_dat[meds_2,3], seg_dat[meds_2,4],
         col = adjustcolor(col = c(1, 2), alpha = 3), lwd = 2)

segments(seg_dat1[meds_2, 1], seg_dat1[meds_2, 2], seg_dat1[meds_2, 3],
         seg_dat1[meds_2, 4],
         col = adjustcolor(col = c(1, 2), alpha = 1), lwd = 2)

#Get final data

#Final solution k=2

med2 <- Correlationunder180[meds_2, c(1:3)]
rownames(med2) <- c("1st medoid", "2nd mediod")
med2 <- data.frame(meds_2, med2)
names(med2)[1] <- "Observation ID"

med2

summary(med2)

summary(Correlationunder180)

```

```

#----- OVER 180° -----

xc <- Correlationover180$ORIENTATION
xr <- data.frame(scale(Correlationover180$WIDTH), scale(Correlationover180$LENGTH))
xr <- data.frame(Correlationover180$WIDTH, Correlationover180$LENGTH)

#Calculate Gower's first and multiply by number of variables considered, excluding the #circular
variable.

library(cluster)

#Put variables that aren't circular one into xr
d1<-as.dist(as.matrix(daisy(xr,"gower")))*dim(xr)[2]
d1<-as.dist(as.matrix(daisy(xr,"gower")))*dim(xr)[2]

circd <- function(x){
  #Assumes x is just a single variable
  dist1<-matrix(0,nrow=length(x),ncol=length(x))
  for (i in (1:(length(x)-1))) {
    for (j in i:length(x)) {
      dist1[j,i]=min(abs(x[i]-x[j]), (360 - abs(x[i]-x[j]))) / 180
    }
  }
  return(as.dist(dist1))
}

```

```

dc<-(d1+circd(xc))/(dim(xr)[2]+1)

#Divide by total number of variables (assumes no missing values)

#greenwood - circle only

circ_dist <- circd(Correlationover180$ORIENTATION)

clust_circle <- hclust(circ_dist, method = 'ward.D2')

clust_circle

summary(clust_circle)

plot(clust_circle)

cuts_circle <- factor(cutree(clust_circle, k = 2))

summary(cuts_circle)

cuts_circle

plot(cuts_circle)

library(ade4)

length <- data.frame(scale(Correlationover180$LENGTH))

width <- data.frame(scale(Correlationover180$WIDTH))

direc <- data.frame(Correlationover180$ORIENTATION)*(pi/180)

direc5 <- prep.circular(direc)

ktab1 <- ktab.list.df(list(length, width, direc5))

dist5 <- dist.ktab(ktab1, type = c("Q", "Q", "C"))

clust5 <- hclust(dist5, method = 'ward.D2') #plot(clust5)

cuts5 <- cutree(clust5, k = 2)

#Orientation only

```

```

ktab2 <- ktab.list.df(list(direc5))
dist2 <- dist.ktab(ktab2, type = 'C')
clus2 <- hclust(dist2, method = 'ward.D2')
cut2 <- cutree(clus2, k= 2)
clust_one <- hclust(dc, method = 'ward.D2')
plot(clust_one)
cuts_2 <- factor(cutree(clust_one, k = 2))
cuts_4 <- factor(cutree(clust_one, k = 4))
cuts_3 <- factor(cutree(clust_one, k = 3))
cuts_5 <- factor(cutree(clust_one, k = 5))

med <- function(members,Dist){
  if(length(members)==1){return(members)}
  else{
    if(length(members)==0){return(0)}
    dists<-apply(Dist[members,members],1,sum)
    medoid<-members[which(dists==min(dists))]
    return(medoid[1])
  }
}

ids <- 1:nrow(Correlationover180)
#medoids 2 cluster solution

```

```

k_2_1 <- med(members = ids[cuts_2 == 1], Dist = as.matrix(dc)) #29
k_2_2 <- med(members = ids[cuts_2 == 2], Dist = as.matrix(dc)) #57
meds_2 <- c(k_2_1, k_2_2)

#medoids 3 cluster solution

k_3_1 <- med(members = ids[cuts_3 == 1], Dist = as.matrix(dc)) #36
k_3_2 <- med(members = ids[cuts_3 == 2], Dist = as.matrix(dc)) #57
k_3_3 <- med(members = ids[cuts_3 == 3], Dist = as.matrix(dc)) #26
meds_3 <- c(k_3_1, k_3_2, k_3_3)

#medoids 4 cluster solution

k_4_1 <- med(members = ids[cuts_4 == 1], Dist = as.matrix(dc)) #36
k_4_2 <- med(members = ids[cuts_4 == 2], Dist = as.matrix(dc)) #12
k_4_3 <- med(members = ids[cuts_4 == 3], Dist = as.matrix(dc)) #26
k_4_4 <- med(members = ids[cuts_4 == 4], Dist = as.matrix(dc)) #41
meds_4 <- c(k_4_1, k_4_2, k_4_3, k_4_4)

#medoids 5 cluster solution

k_5_1 <- med(members = ids[cuts_5 == 1], Dist = as.matrix(dc)) #36
k_5_2 <- med(members = ids[cuts_5 == 2], Dist = as.matrix(dc)) #48
k_5_3 <- med(members = ids[cuts_5 == 3], Dist = as.matrix(dc)) #26
k_5_4 <- med(members = ids[cuts_5 == 4], Dist = as.matrix(dc)) #41
k_5_5 <- med(members = ids[cuts_5 == 5], Dist = as.matrix(dc)) #38
meds_5 <- c(k_5_1, k_5_2, k_5_3, k_5_4, k_5_5)

```

```

par(mfrow = c(1,1))

old_par <- par(mar = c(5.1, 4.1, 4.1, 2.1))

par(mar= c(2, 4.1, 4.1, 2.1))

plot(clust_one, labels = F, xlab = "", sub = "", main= "Cluster Dendrogram over 180°")

#abline(h = 0.85, lwd = 2, col = 2)

#abline(h = 1.05, lwd = 2, col = 3)

par(mar = old_par)

scale_cape<- data.frame(apply(Correlationover180[, c(1, 3)], 2, scale),
Correlationover180$ORIENTATION) #names(cape_blanco2)

noscale_cape <- data.frame(Correlationover180[,c(1,3) ], Correlationover180$ORIENTATION)

#package (clusterSim)

G1s <- numeric(0)

#Load the function from package clusterSim. I found it on CRAN

for(j in 1:6){
  G1s[j] <- index.G1(x = noscale_cape, cl = cutree(clust_one, k = j))
}

#If functions gives an error run:

```

```

.medoid<-function(x,d)
{
  minj<-0
  minsumdist<-sum(d)
  if(is.null(dim(x)) && is.null(dim(d))){
    dim(x)<-c(1,length(x))
    x
  }
  else{
    if(is.null(dim(d))){
      dim(d)<-c(1,1)
    }
    if(is.null(dim(x))){
      dim(x)<-c(length(x),1)
    }
    for(j in 1:nrow(d)){
      if (sum(d[j,])<=minsumdist){
        #minj<-row.names(d)[j]
        minj<-j
        minsumdist<-sum(d[j,])
      }
    }
    resul<-as.matrix(x[minj,])
  }
}

```

```

    resul
  }
}

index.G1<-function(x,cl,d=NULL,centrotypes="centroids")
{
  if(sum(c("centroids","medoids")==centrotypes)==0)
    stop("Wrong centrotypes argument")
  if("medoids"==centrotypes && is.null(d))
    stop("For argument centrotypes = 'medoids' d cannot be null")
  if(!is.null(d)){
    if(!is.matrix(d)){
      d<-as.matrix(d)
    }
    row.names(d)<-row.names(x)
  }

  n <- length(cl)
  k <- max(cl)
  if(is.null(dim(x))){
    dim(x)<-c(length(x),1)
  }
}

```

```

centers<-matrix(nrow=k,ncol=ncol(x))
for(i in 1:k)
{
  x.k = x[cl==i,]
  if(centrotypes=="centroids"){
    if(ncol(x)==1){
      centers[i,]<-mean(x.k)
    }
    else{
      if (is.vector(x.k)){
        centers[i,]<-x.k
      }
      else{
        centers[i,]<-apply(x.k,2,mean)
      }
    }
  }
}
else{
  centers[i,]<-medoid(x[cl==i,],d[cl==i,cl==i])
  #print(apply(x[cl==i,],2,mean))
  #print(centers[i,])
}
}

```

```

if (centrotypes=="centroids"){
  allmean <- apply(x,2,mean)
}
else{
  # print(apply(x,2,mean))
  allmean<-.medoid(x,d)
  #print(allmean)
}
dmean <- sweep(x,2,allmean,"-")
allmeandist <- sum(dmean^2)
withins <- rep(0, k)
x <- (x - centers[cl,])^2
for(i in 1:k){
  withins[i] <- sum(x[cl==i,])
}
wgss <- sum(withins)
bgss <- allmeandist - wgss
(bgss/(k-1))/(wgss/(n-k))
}

for(j in 1:10){
  G1s[j] <- index.G1(x = noscale_cape, cl = cutree(clust_one, k = j))
}

```

```
}
```

```
plot(1:10, G1s, type = 'l', xlab = "Number of clusters",
```

```
    main = "Calinski - Harabasz Pseudo F stat over 180°") #Gives k=2 as the most parsimonius  
cluster solution. k=3 second most likely.
```

```
plot(clust_one, labels = F, xlab = "", sub = "", main= "Cluster Dendrogram over 180°; k=2")
```

```
abline(h = 0.795, lwd = 2, col = 2) #Indicate second most likely solution: k=3
```

```
abline(h = 1, lwd = 2, col = 3) #Indicate most likely cluster solution: k=2
```

```
#Greenwood method
```

```
#Required objects
```

```
theta <- seq(0, 360, .01)
```

```
x1 <- cos(pi*theta/180)
```

```
y1 <- sin(pi*theta/180)
```

```
y1_stand <- y1/2 + .5
```

```
x1_stand <- x1/2
```

```
#dont make data into circular object
```

```
Orientation2 <- Correlationover180$ORIENTATION
```

```
ori_rad <- pi*(Orientation2)/180 + (3*pi/2)
```

```
Orientation2
```

```
ori_rad
```

```

Length2 <- Correlationover180$LENGTH
length_stand <- Length2 / max(Length2)
length_vec <- rep(3.5, length(length_stand))
barom_vec <- rep(5, length(length_stand))
Width_vec <- rep(7, length(length_stand))
Width_stand <- (Correlationover180$WIDTH - min(Correlationover180$WIDTH)) /
  (max(Correlationover180$WIDTH) - min(Correlationover180$WIDTH))
seg_dat <- data.frame(cbind((cos(ori_rad)/2), (sin(ori_rad)/2 + .5),
  length_vec, length_stand))
seg_dat1 <- data.frame(cbind(length_vec, length_stand, Width_vec,
  Width_stand))

#PCP k=2
plot(y1_stand ~ x1_stand, type = "l", xlim = c(-.5, 7), ylim = c(0, 1),
  xaxt = "none", xlab = "", ylab = "", yaxt = "none",
  main = "PCP plot - circular, over 180°, k = 2 Greenwood method")
labs <- c("Orientation", "Length", "Width")
axis(1, at = c(0, 3.5, 7), labels = labs, las = 1) #axis(2, at = c(0, 1), labels = c("Min", "Max"), las =
2)

points(cos(ori_rad)/2, sin(ori_rad)/2 + .5, cex = .75, col = cuts_2, pch=19)
points(length_stand ~ length_vec, col = cuts_2, pch=19)
points(Width_stand ~ Width_vec, col = cuts_2, pch=19)

```

```

segments(seg_dat[,1], seg_dat[,2], seg_dat[,3], seg_dat[,4],
         col = adjustcolor(col = cuts_2, alpha.f = .1))
segments(seg_dat1[,1], seg_dat1[,2], seg_dat1[,3], seg_dat1[,4],
         col = adjustcolor(col = cuts_2, alpha.f = .1))

#group reps
points(cos(ori_rad[c(29, 57)])/2, sin(ori_rad[c(29, 57)])/2 + .5,
       cex = 1, col = c(1, 2), pch=19)
points(length_stand[c(29, 57)] ~ length_vec[c(29, 57)], col = c(1, 2), pch=19)
points(Width_stand[c(29, 57)] ~ Width_vec[c(29, 57)], col = c(1, 2), pch=19)
segments(seg_dat[c(29, 57), 1], seg_dat[c(29, 57), 2],
         seg_dat[c(29, 57), 3], seg_dat[c(29, 57), 4],
         col = c(1, 2), lwd = 3)
segments(seg_dat1[c(29, 57), 1], seg_dat1[c(29, 57), 2],
         seg_dat1[c(29, 57), 3], seg_dat1[c(29, 57), 4],
         col = c(1, 2), lwd = 3)

#text( .65, .55, "E")
#text(-.65, .55, "W")

#Other approach

plot(y1_stand ~ x1_stand, type = "l", xlim = c(-.5, 7), ylim = c(0, 1),
     xaxt = "none", yaxt = "none", xlab = "", ylab = "",

```

```

main = "PCP plot - circular, k = 2")
labs <- c("Orientation", "Length", "Width")
axis(2, at = c(0, 1), labels = c("Min", "Max"), las = 2)
axis(1, at = c(0, 3.5, 7), labels = labs, las = 1)
points(cos(ori_rad)/2, sin(ori_rad)/2 + .5, cex = .75, col = cuts_2, pch=19)
points(length_stand ~ length_vec, col = cuts_2, pch=19)
points(Width_stand ~ Width_vec, col = cuts_2, pch=19)
segments(seg_dat[,1], seg_dat[,2], seg_dat[,3], seg_dat[,4],
         col = adjustcolor(col = cuts_2, alpha.f = .1))
segments(seg_dat1[,1], seg_dat1[,2], seg_dat1[,3], seg_dat1[,4],
         col = adjustcolor(col = cuts_2, alpha.f = .1))

#group reps
points(cos(ori_rad[meds_2])/2, sin(ori_rad[meds_2])/2 + .5,
       cex = .75, col = c(1, 2), pch=19)
points(length_stand[meds_2] ~ length_vec[meds_2], col = c(1, 2), pch=19)
points(Width_stand[meds_2] ~ Width_vec[meds_2], col = c(1, 2), pch=19)
segments(seg_dat[meds_2,1], seg_dat[meds_2,2],
         seg_dat[meds_2,3], seg_dat[meds_2,4],
         col = adjustcolor(col = c(1, 2), alpha = 3), lwd = 2)
segments(seg_dat1[meds_2, 1], seg_dat1[meds_2, 2], seg_dat1[meds_2, 3],
         seg_dat1[meds_2, 4],
         col = adjustcolor(col = c(1, 2), alpha = 1), lwd = 2)

```

```

#Get final data

#Final solution k=2

med2 <- Correlationover180[meds_2, c(1:3)]
rownames(med2) <- c("1st medoid", "2nd medoid")

med2 <- data.frame(meds_2, med2)

names(med2)[1] <- "Observation ID"

med2

summary(med2)

summary(Correlationover180)

citation("mclust")

```

#3.4 Monothetic cluster analysis: M-cross-validation and and permutation-based hypothesis test

```

#Select the two variables with the greatest dissimilarity suspected to generate clusters under 180°
setwd("~/Desktop/MUN PHD/Our papers/Melrose paper/SUBMISSION FINAL/Datasets Pérez-
Pinedo et al., 2022/Orientation")

Correlationunder180$LENGTH <- NULL

Correlationunder1804c <- MonoClust(Correlationunder180, nclusters = 2, cir.var=2)

Correlationunder1804c

plot(Correlationunder1804c)

set.seed(12345)

cp.table <- cv.test(Correlationunder180, fold = 10, minnodes = 1, maxnodes = 10)

```

```
cp.table
```

```
ggcv(cp.table) +
```

```
#geom_hline(aes(yintercept = min(lower1SD)), color = "red", linetype = 2) +
```

```
#geom_hline(aes(yintercept = min(upper1SD)), color = "red", linetype = 2) +
```

```
geom_hline(aes(yintercept = 10000), color = "red", linetype = 2) +
```

```
geom_point(aes(x = ncluster[2], y = MSE[2]), color = "red", size = 2) +
```

```
geom_point(aes(x = ncluster[2], y = MSE[2]), color = "red", size = 5, shape = 4)
```

```
Correlationunder18010c <- MonoClust(Correlationunder180, nclusters = 10,cir.var=2)
```

```
Correlationunder18010c.pvalue <- perm.test(Correlationunder18010c, data =
```

```
Correlationunder180, method = "sw", rep = 1000)
```

```
plot(Correlationunder18010c.pvalue, branch = 1, uniform = TRUE)
```

```
#two cluster solution
```

```
Correlationunder1802c <- MonoClust(Correlationunder180, nclusters = 2,cir.var=2)
```

```
Correlationunder1802c.pvalue <- perm.test(Correlationunder1802c, data = Correlationunder180,
```

```
method = "sw", rep = 1000)
```

```
plot(Correlationunder1802c.pvalue, branch = 1, uniform = TRUE)
```

```
#Select the two variables with the greatest dissimilarity suspected to generate clusters over 180°
```

```
setwd("~/Desktop/MUN PHD/Our papers/Melrose paper/SUBMISSION FINAL/Datasets Pérez-  
Pinedo et al., 2022/Orientation")
```

```

Correlationover180$LENGTH <- NULL

Correlationover1804c <- MonoClust(Correlationover180, nclusters = 2,cir.var=2)

Correlationover1804c

plot(Correlationover1804c)

set.seed(12345)

cp.table <- cv.test(Correlationover180, fold = 10, minnodes = 1, maxnodes = 10)

cp.table

ggcv(cp.table) +
  #geom_hline(aes(yintercept = min(lower1SD)), color = "red", linetype = 2) +
  #geom_hline(aes(é = min(upper1SD)), color = "red", linetype = 2) +
  geom_hline(aes(yintercept = 10000), color = "red", linetype = 2) +
  geom_point(aes(x = ncluster[2], y = MSE[2]), color = "red", size = 2) +
  geom_point(aes(x = ncluster[2], y = MSE[2]), color = "red", size = 5, shape = 4)

Correlationover18010c <- MonoClust(Correlationover180, nclusters = 10,cir.var=2)

Correlationover18010c.pvalue <- perm.test(Correlationover18010c, data = Correlationover180,
method = "sw", rep = 1000)

plot(Correlationover18010c.pvalue, branch = 1, uniform = TRUE)

dev.off()

#-----

```

#[Pérez-Pinedo et al., 2022] Memorial University of Newfoundland, Canada.

## Appendix B – Supplementary material from Chapter 4

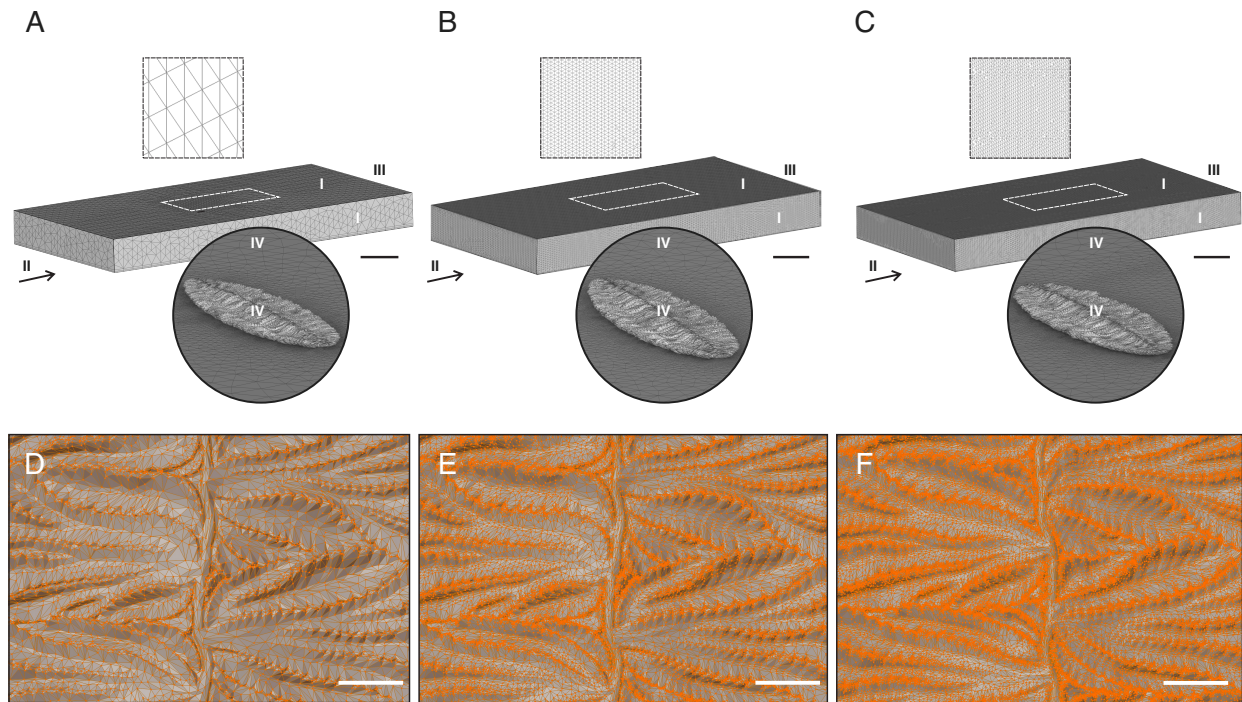


Figure 4.S1: Discretization and sensitivity tests for different meshing parameters for the computational domain (A-C) and the *Fractofusus misrai* geometry (D-F), related to Figure 3. A) Coarse FVR mesh. B) Medium FVR mesh. C) Fine FVR mesh. D) 100k polygon mesh. E) 300k polygon mesh. F) 500k polygon mesh. I) Slip-boundary condition. II) Velocity inlet. III) Pressure outlet. IV) No-slip boundary condition. Scale bars A-C 50 cm, and D-F 1 cm.

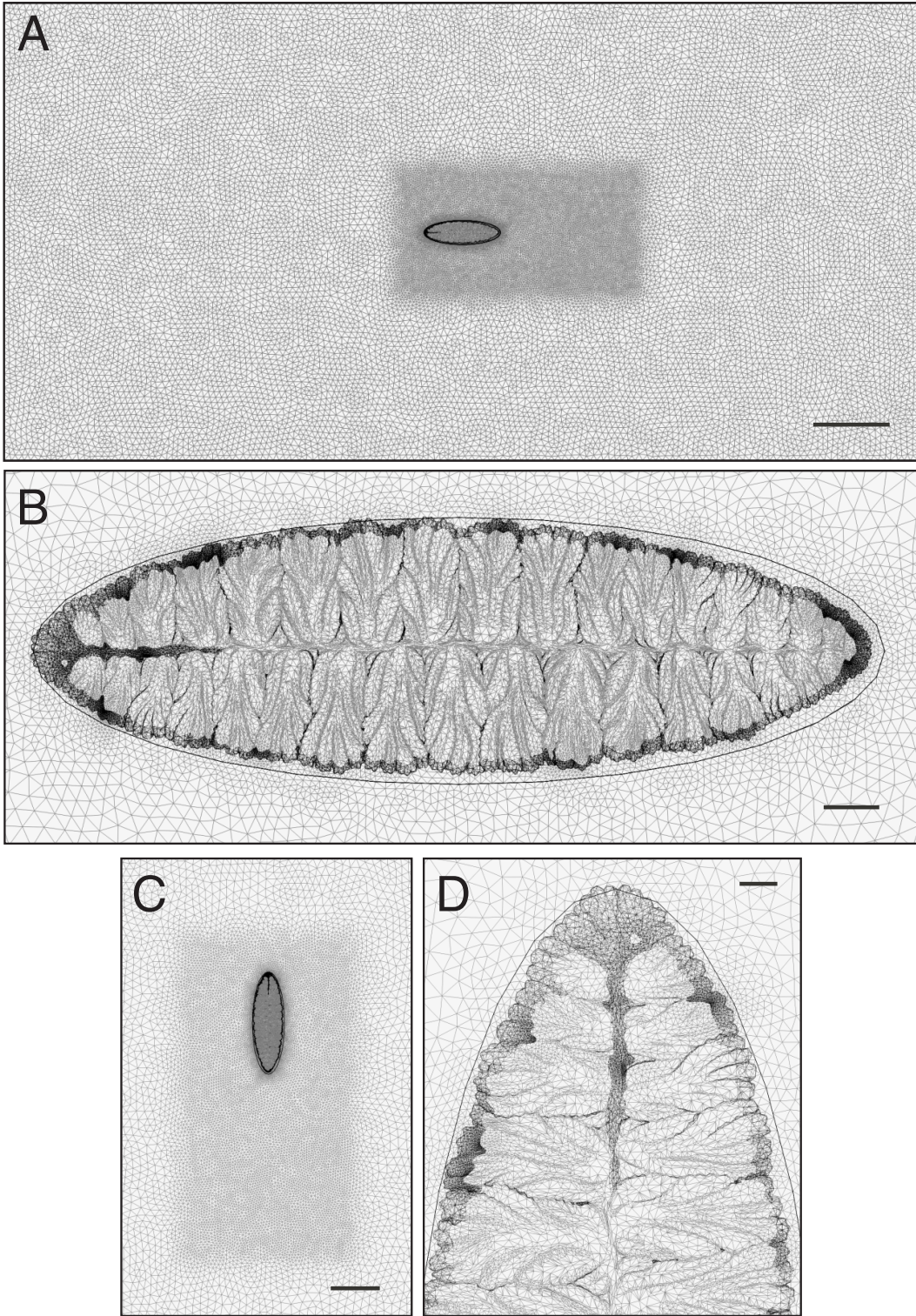


Figure 4.S2: Computational domain for CFD simulations, related to Figure 3. A) Entire flow volume region. B) General view of *Fractofusus misrai*. C) Cartesian box as region refinement. D)

Detail of primary branches of *Fractofusus misrai*. Scale bars A 30 cm, B 2 cm, C 15 cm, and D 1 cm.

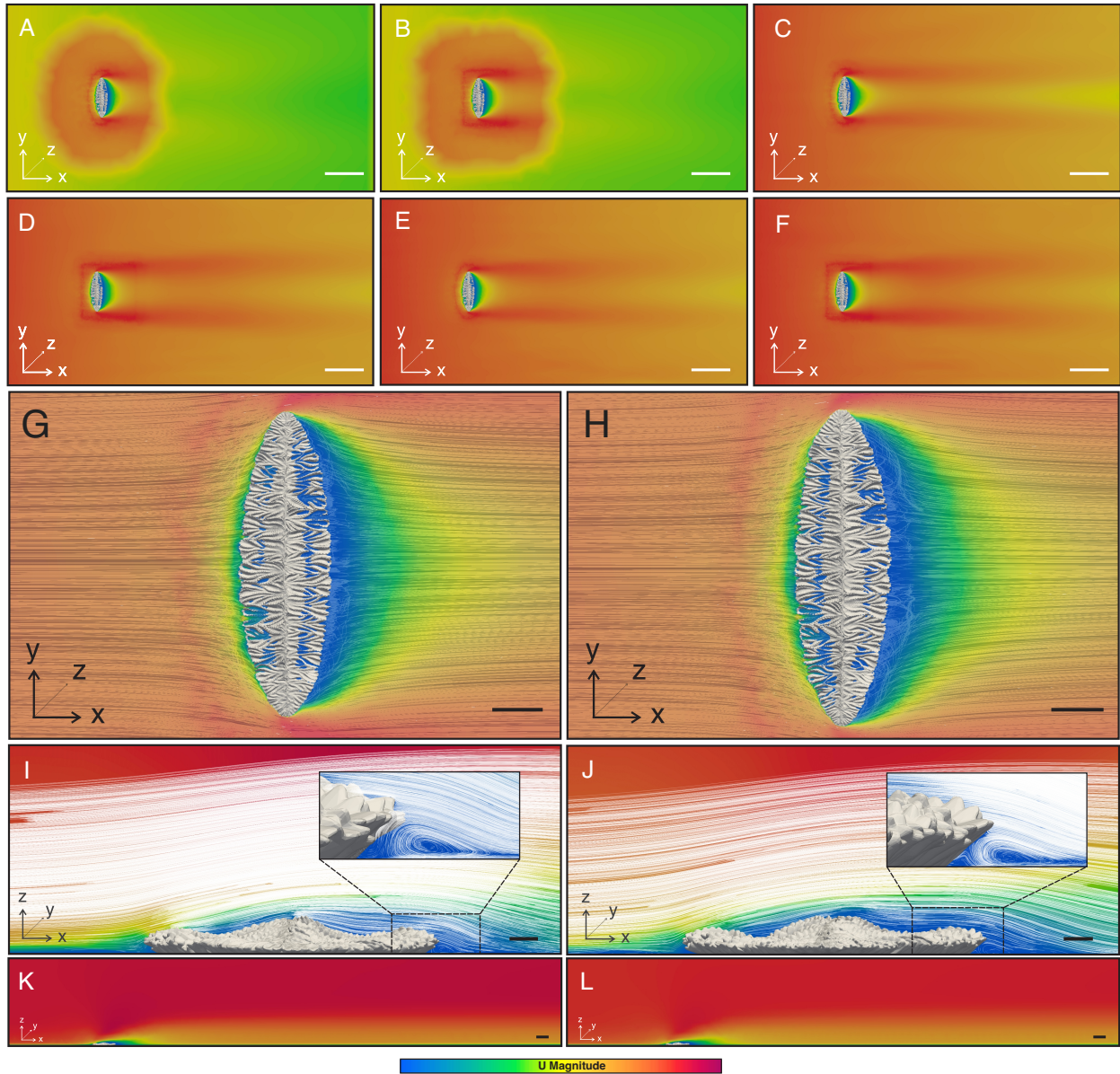


Figure 4.S3: CFD results of large *Fractofusus misrai* under  $U_x = 0.2$  m/s with different mesh discretization and cartesian box refinements, related to Figure 4. A) Coarse FVR mesh with no refinement. B) Coarse FVR mesh with refinement. C) Medium FVR mesh with no refinement. D) Medium FVR mesh with refinement. E) Fine FVR mesh with no refinement. F) Fine FVR mesh

with refinement. G-L) Two-dimensional horizontal and cross-sectional surface plots of streamlines and  $U_x$ . G,I,K) Perpendicular 300k polygon geometry, and (H,J,L) perpendicular 500k polygon geometry. Current flow from left to right. Velocity ranges from 0 to 0.2 m/s. Scale bars A-F 30 cm, G-H, K-L 5 cm, I-J 1 cm.

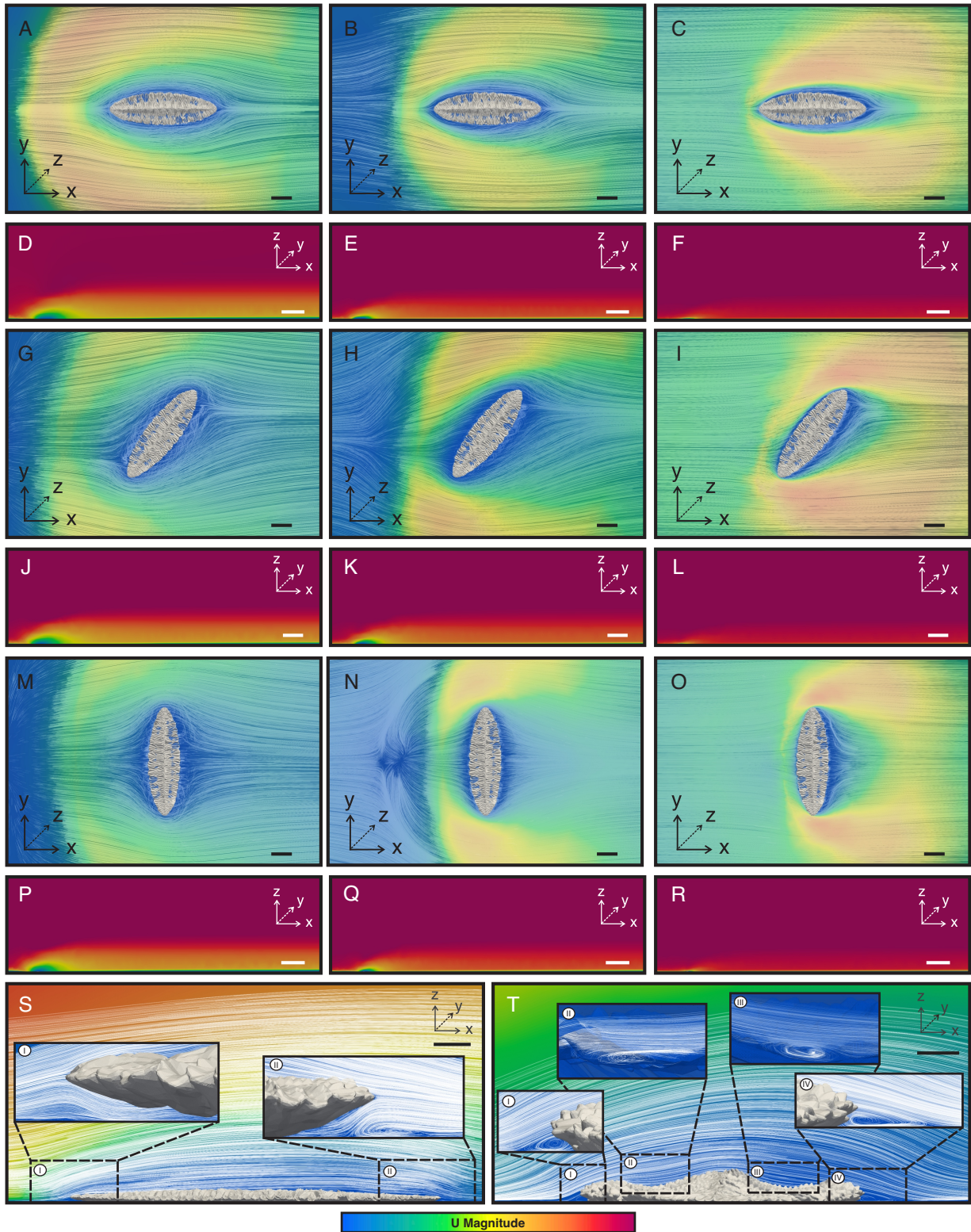


Figure 4.S4: CFD simulations of small *Fractofusus misrai* in different orientations relative to the simulated flow from (left to right), related to Figure 4. A-R) Two-dimensional horizontal and

cross-sectional surface plots of streamlines and different  $U_x$  regimes: first column (A,D,G,J M, and P) simulated flow of 0.05 m/s; second column (B,E,H,K,N, and Q) flows of 0.1 m/s; and third column (C,F,I,L,O, and R) 0.2 m/s. S-T) Detailed cross-sectional view of flow retention patterns and eddying of current-parallel (SI-SII) and current-perpendicular *Fractofusus misrai* (TI-TIV) in 0.1 m/s flow. Both orientations show the eddying at the frond margin (SI-SII; TI, TIV). Current perpendicular *F. misrai* also shows weak vortices on the upper surface of the frond both upcurrent of the axis of the frond (TII), and also in the lee of the axis (TIII). Velocity ranges from 0 to 0.05, 0.1, or 0.2 m/s as indicated in this caption. Scale bars top view 1 cm, side view 10 cm except S 0.5 cm, and T 0.1 cm.

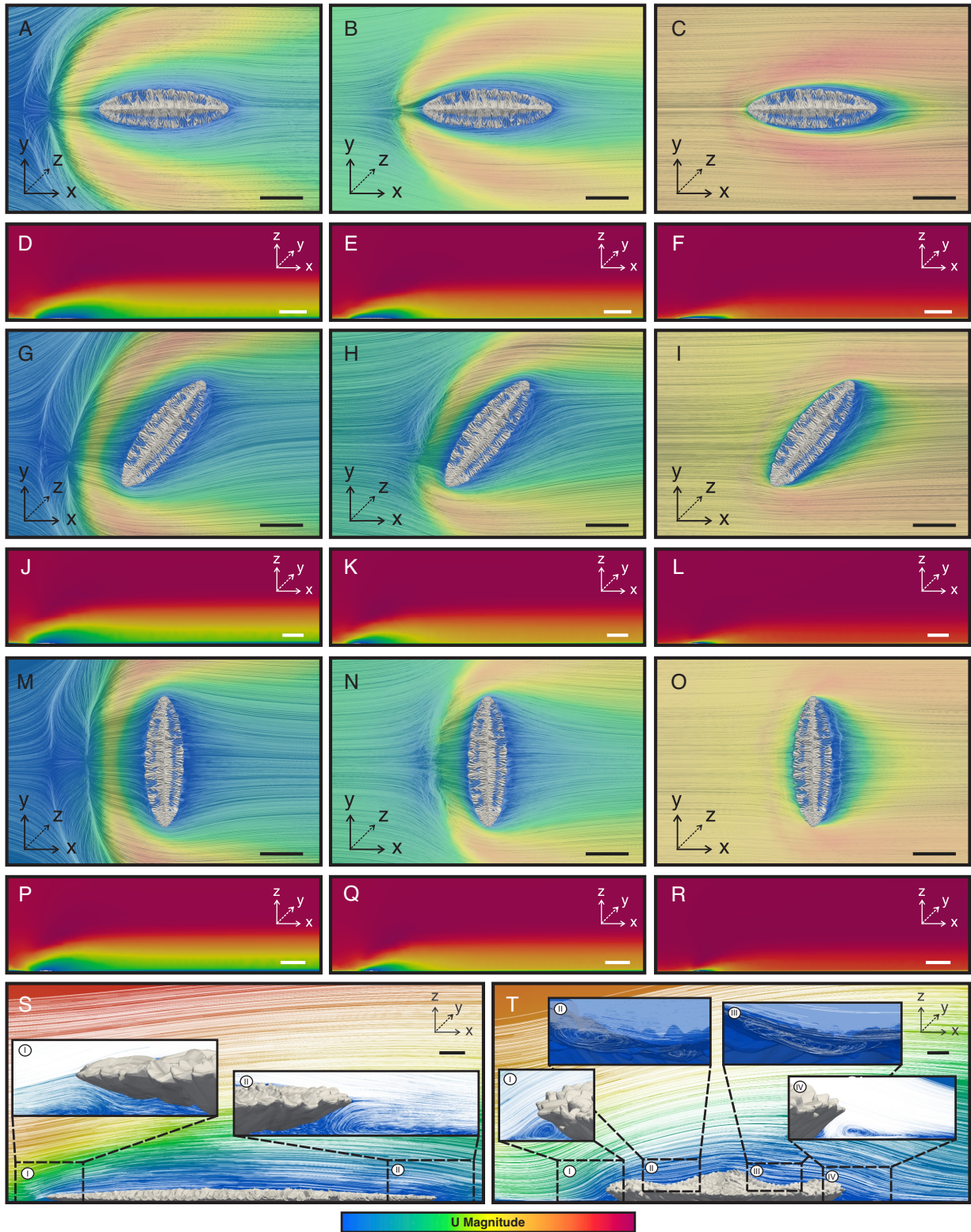


Figure 4.S5: CFD simulations of medium *Fractofusus misrai* in different orientations relative to the simulated flow from (left to right), related to Figure 4. First column (A,D,G,J M, and P)

simulated flow of 0.05 m/s; second column (B,E,H,K,N, and Q) flows of 0.1 m/s; and third column (C,F,I,L,O, and R) 0.2 m/ s. S-T) Detailed cross-sectional view of flow retention patterns and eddying of current-parallel (SI-SII) and current-perpendicular *Fractofusus misrai* (TI-TIV) in 0.1 m/s flow. Both orientations show the eddying at the frond margin (SI-SII; TI, TIV). Current perpendicular *F. misrai* also shows weak vortices on the upper surface of the frond both upcurrent of the axis of the frond (TII), and also in the lee of the axis (TIII). Velocity ranges from 0 to 0.05, 0.1, or 0.2 m/s as indicated in this caption. Scale bars top view 5 cm, cross-sectional view 10 cm except S 2 cm, and T 0.5 cm.

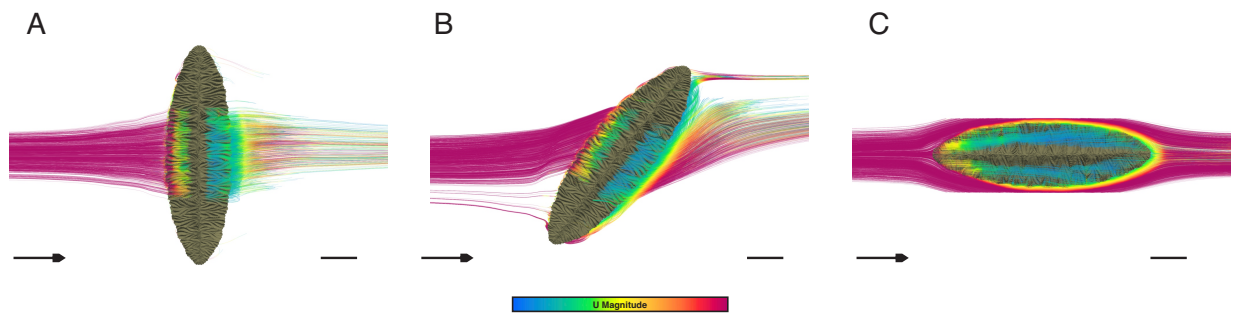


Figure 4.S6: General view of streamlines coloured according to  $U_x$  around different orientations of *Fractofusus misrai*, related to Figure 5. A) Perpendicular ( $90^\circ$ ), B) oblique ( $52^\circ$ ), and C) parallel ( $0^\circ$ ). Arrows indicate paleocurrent direction. Velocity ranges from 0 to 0.1 m/s. Scale bars 5 cm.

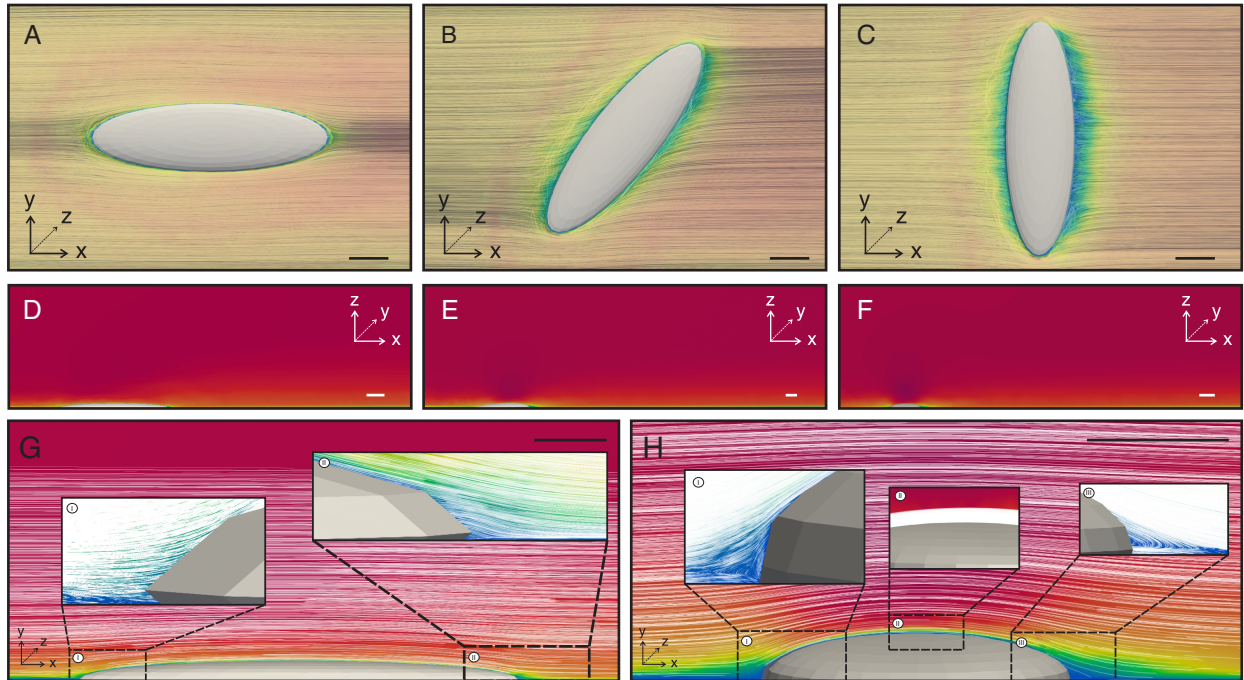


Figure 4.S7: CFD simulations of null models, related to Figure 4. A-H) Two-dimensional horizontal and cross-sectional surface plots of streamlines and  $U_x$ . G-H) Detailed cross-sectional view of flow patterns of parallel (GI-GII) and perpendicular (HI-HIII) null models under 0.1 m/s flow. Velocity ranges from 0 to 0.1 m/s. Current flow from left to right. Scale bars 5 cm.

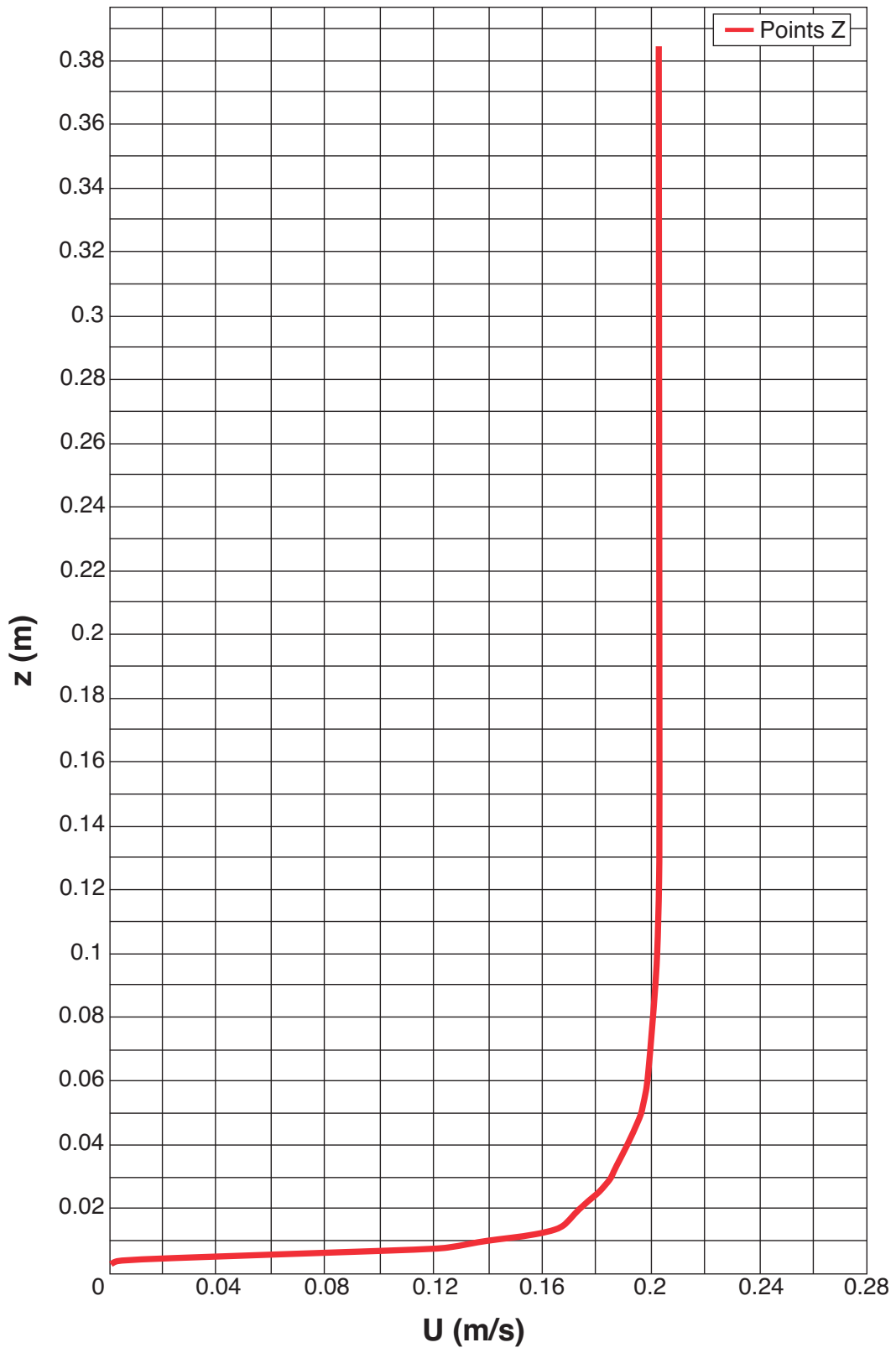


Figure 4.S8: Velocity profile ( $U_x$ ) along vertical axis ( $z$ ) from the bottom boundary of the fluid domain around *Fractofusus misrai*, related to Figure 4.

Table 4.S1: CFD simulations numeric results, related to Figure 6.

Size (cm)	Mesh finess	Orientation	Area ref (m <sup>2</sup> )	Ref (m)	U <sub>x</sub> (m/s)	Drag coefficient (Cd)	Drag force (Fd)	Reynold number (Re)	A/V (mm <sup>-1</sup> )	Convergence
0	edium 5	0°	.0013319	.33	.2	.31	.031	4411.2	.31	✓
0	edium 5	35°	.00273914	.28	.2	.67	.033	4411.2	.31	✓
0	edium 5	52°	.00357768	.22	.2	.58	.036	4411.2	.31	✓
0	edium 5	90°	.00441133	.1	.2	.57	.0455	4411.2	.31	✓
0	edium 5	0°	.0013319	.33	.1	.05	.012	2205.6	.31	✓
0	edium 5	35°	.00273914	.28	.1	.35	.017	2205.6	.31	✓
0	edium 5	52°	.00357768	.22	.1	.36	.022	2205.6	.31	✓
0	edium 5	90°	.00441133	.1	.1	.24	.024	2205.6	.31	✓
0	edium 5	0°	.0013319	.33	.05	.87	.0042	6102.8	.31	✓
0	edium 5	35°	.00273914	.28	.05	.93	.0059	6102.8	.31	✓
0	edium 5	52°	.00357768	.22	.05	.23	.0089	6102.8	.31	✓

0	edium 5	9 0°	0 .00441133	.1	.05	.95	0 .0097	6102.8	.31	✓
5	edium 5	0 °	0 .000386824	.16	.2	4.87	0 .01	2205.6	.62	✓
5	edium 5	3 5°	0 .000841123	.13	.2	.85	0 .012	2205.6	.62	✓
5	edium 5	5 2°	0 .00106621	.1	.2	.68	0 .0126	2205.6	.62	✓
5	edium 5	9 0°	0 .001303525	.05	.2	.63	0 .014	2205.6	.62	✓
5	edium 5	0 °	0 .000386824	.16	.1	.78	0 .0048	6102.8	.62	✓
5	edium 5	3 5°	0 .000841123	.13	.1	.82	0 .007	6102.8	.62	✓
5	edium 5	5 2°	0 .00106621	.1	.1	.66	0 .0081	6102.8	.62	✓
5	edium 5	9 0°	0 .001303525	.05	.1	.66	0 .0099	6102.8	.62	✓
5	edium 5	0 °	0 .000386824	.16	.05	.07	0 .0023	051.4	.62	✓
5	edium 5	3 5°	0 .000841123	.13	.05	.21	0 .0031	051.4	.62	✓
5	edium 5	5 2°	0 .00106621	.1	.05	.99	0 .0037	051.4	.62	✓
5	edium 5	9 0°	0 .001303525	.05	.05	.46	0 .0053	051.4	.62	✓
	edium 5	0 °	3 .41E-05	.05	.2	.03	0 .0005	0735.2	.06	✓
	edium 5	3 5°	5 .62E-05	.045	.2	.93	0 .00081	0735.2	.06	✓
	edium 5	5 2°	8 .11E-05	.036	.2	.7	0 .00088	0735.2	.06	✓

	edium 5	9 0°	0 .000100348	.017	.2	.76	0 .0012	0735.2	.06	✓
	edium 5	0 °	3 .41E-05	.05	.1	.07	0 .00044	367.6	.06	✓
	edium 5	3 5°	5 .62E-05	.045	.1	.64	0 .00064	367.6	.06	✓
	edium 5	5 2°	8 .11E-05	.036	.1	.04	0 .00072	367.6	.06	✓
	edium 5	9 0°	0 .000100348	.017	.1	.42	0 .0011	367.6	.06	✓
	edium 5	0 °	3 .41E-05	.05	.05	.2	0 .00028	683.8	.06	✓
	edium 5	3 5°	5 .62E-05	.045	.05	.7	0 .00043	683.8	.06	✓
	edium 5	5 2°	8 .11E-05	.036	.05	.7	0 .00053	683.8	.06	✓
	edium 5	9 0°	0 .000100348	.017	.05	.26	0 .00084	683.8	.06	✓
					<b>esh Calibrati on</b>					
0	ow 4	0 °	0 .0013319	.33	.05	.4	0 .005	6102.8	.31	✓
0	ow 4	0 °	0 .0013319	.33	.1	.31	0 .014	2205.6	.31	✓
0	ow 4	0 °	0 .0013319	.33	.2	.28	0 .021	4411.2	.31	✓
0	ow 4	3 5°	0 .00273914	.28	.05	.22	0 .0067	6102.8	.31	✓
0	ow 4	3 5°	0 .00273914	.28	.1	.42	0 .017	2205.6	.31	✓

0	ow 4	5 <sup>o</sup>	3 0 .00273914	.28	.2	.59	.022	4411.2	.31	✓
0	ow 4	2 <sup>o</sup>	5 0 .00357768	.22	.05	.2	.0089	6102.8	.31	✓
0	ow 4	2 <sup>o</sup>	5 0 .00357768	.22	.1	.31	.021	2205.6	.31	✓
0	ow 4	2 <sup>o</sup>	5 0 .00357768	.22	.2	.45	.029	4411.2	.31	✓
0	ow 4	0 <sup>o</sup>	9 0 .00441133	.1	.05	.96	.0098	6102.8	.31	✓
0	ow 4	0 <sup>o</sup>	9 0 .00441133	.1	.1	.24	.024	2205.6	.31	✓
0	ow 4	0 <sup>o</sup>	9 0 .00441133	.1	.2	.42	.034	4411.2	.31	✓
0	igh 6	°	0 0 .0013319	.33	.05	.88	.0041	6102.8	.31	✓
0	igh 6	°	0 0 .0013319	.33	.1	.91	.011	2205.6	.31	✓
0	igh 6	°	0 0 .0013319	.33	.2	.05	.018	4411.2	.31	✓
0	igh 6	5 <sup>o</sup>	3 0 .00273914	.28	.05	.85	.0055	6102.8	.31	✓
0	igh 6	5 <sup>o</sup>	3 0 .00273914	.28	.1	.18	.014	2205.6	.31	✓
0	igh 6	5 <sup>o</sup>	3 0 .00273914	.28	.2	.48	.023	4411.2	.31	✓
0	igh 6	2 <sup>o</sup>	5 0 .00357768	.22	.05	.72	.0067	6102.8	.31	✓
0	igh 6	2 <sup>o</sup>	5 0 .00357768	.22	.1	.04	.016	2205.6	.31	✓
0	igh 6	2 <sup>o</sup>	5 0 .00357768	.22	.2	.38	.024	4411.2	.31	✓

0	igh 6	9 0°	0 .00441133	.1	.05	.95	0 .0096	6102.8	.31	✓
0	igh 6	9 0°	0 .00441133	.1	.1	.09	0 .021	2205.6	.31	✓
0	igh 6	9 0°	0 .00441133	.1	.2	.39	0 .032	4411.2	.31	✓
0	edium 5 with ref	0 °	0 .0013319	.33	.05	.21	0 .0047	6102.8	.31	✓
0	edium 5 with ref	0 °	0 .0013319	.33	.1	.12	0 .013	2205.6	.31	✓
0	edium 5 with ref	0 °	0 .0013319	.33	.2	.15	0 .018	4411.2	.31	✓
0	edium 5 with ref	3 5°	0 .00273914	.28	.05	.85	0 .0056	6102.8	.31	✓
0	edium 5 with ref	3 5°	0 .00273914	.28	.1	.17	0 .014	2205.6	.31	✓
0	edium 5 with ref	3 5°	0 .00273914	.28	.2	.46	0 .022	4411.2	.31	✓
0	edium 5 with ref	5 2°	0 .00357768	.22	.05	.67	0 .0065	6102.8	.31	✓
0	edium 5 with ref	5 2°	0 .00357768	.22	.1	.07	0 .015	2205.6	.31	✓

0	edium 5 with ref	5 2°	0 .00357768	.22	.2	.36	0 .023	4411.2	.31	✓
0	edium 5 with ref	9 0°	0 .00441133	.1	.05	.56	0 .0075	6102.8	.31	✓
0	edium 5 with ref	9 0°	0 .00441133	.1	.1	.86	0 .017	2205.6	.31	✓
0	edium 5 with ref	9 0°	0 .00441133	.1	.2	.39	0 .032	4411.2	.31	✓
					<b>aminar flows</b>					
	edium 5	0 °	3 .41E-05	.05	.2	.25	0 .00011	0735.2	.06	✓
	edium 5	3 5°	5 .62E-05	.045	.2	.26	0 .00021	0735.2	.06	✓
	edium 5	5 2°	8 .11E-05	.036	.2	.23	0 .00028	0735.2	.06	✓
	edium 5	9 0°	0 .000100348	.017	.2	.33	0 .00056	0735.2	.06	✓
	edium 5	0 °	3 .41E-05	.05	.1	.28	0 .000028	367.6	.06	✓
	edium 5	3 5°	5 .62E-05	.045	.1	.26	0 .000048	367.6	.06	✓
	edium 5	5 2°	8 .11E-05	.036	.1	.23	0 .000062	367.6	.06	✓
	edium 5	9 0°	0 .000100348	.017	.1	.31	0 .00012	367.6	.06	✓

	edium 5	0 <sup>9</sup>	3 .41E-05	.05	.05	.34	0 .0000076	683.8	.06	✓
	edium 5	3 5 <sup>9</sup>	5 .62E-05	.045	.05	.29	0 .000012	683.8	.06	✓
	edium 5	5 2 <sup>9</sup>	8 .11E-05	.036	.05	.23	0 .000014	683.8	.06	✓
	edium 5	9 0 <sup>9</sup>	0 .000100348	.017	.05	.32	0 .000027	683.8	.06	✓
0	edium 5	0 9 <sup>9</sup>	0 .0013319	.33	.2	.37	0 .0085	4411.2	.31	✓
0	edium 5	9 0 <sup>9</sup>	0 .00441133	.1	.2	.43	0 .035	4411.2	.31	✓